FORMULATION OF INVARIANTS FOR DISCRETE ORTHOGONAL MOMENTS AND IMAGE CLASSIFICATION

PEE CHIH YANG

FACULTY OF SCIENCE
UNIVERSITY OF MALAYA
KUALA LUMPUR

2013

FORMULATION OF INVARIANTS FOR DISCRETE ORTHOGONAL MOMENTS AND IMAGE CLASSIFICATION

PEE CHIH YANG

THESIS SUBMITTED IN FULFILMENT OF THE REQUIREMENTS FOR THE DEGREE OF DOCTOR OF PHILOSOPHY

INSTITUTE OF MATHEMATICAL SCIENCES
FACULTY OF SCIENCE
UNIVERSITY OF MALAYA
KUALA LUMPUR

2013

UNIVERSITI MALAYA

ORIGINAL LITERARY WORK DECLARATION

Name of Candidate: **PEE CHIH YANG** (I.C./Passport No.: **700810015421**)

Registration/Matrix No.: **SHB030001**

Name of Degree: **Doctor of Philosophy**

Title of Project Paper/Research Report/Dissertation/Thesis ("this Work"):

Formulation of Invariants for Discrete Orthogonal Moments and Image Classification

Field of Study: **Statistical Image Analysis and Special Functions**

I do solemnly and sincerely declare that:

(1) I am the sole author/writer of this Work;
(2) This work is original;
(3) Any use of any work in which copyright exists was done by way of fair dealing and for permitted purposes and any excerpt or extract from, or reference to or reproduction of any copyright work has been disclosed expressly and sufficiently and the title of the Work and its authorship have been acknowledged in this Work;
(4) I do not have any actual knowledge nor do I ought reasonably to know that the making of this work constitutes an infringement of any copyright work;
(5) I hereby assign all and every rights in the copyright to this Work to the University of Malaya ("UM"), who henceforth shall be owner of the copyright in this Work and that any reproduction or use in any form or by any means whatsoever is prohibited without the written consent of UM having been first had and obtained;
(6) I am fully aware that if in the course of making this Work I have infringed any copyright whether intentionally or otherwise, I may be subject to legal action or any other action as may be determined by UM.

Candidate's Signature Date

Subscribed and solemnly declared before,

Witness's Signature Date

Name:
Designation:

ABSTRACT

The aim of this thesis is to study invariant algorithms for the domain of discrete orthogonal moments. The invariants are anisotropic scale and translation invariants, translation, rotation and scale invariants, and affine moment invariants. Due to the complexity of hypergeometric functions, existing invariant algorithms are slow. In addition, some of the features have poor classification performance and are highly sensitive to the noise. Therefore new sets of invariant algorithms have been proposed to resolve the above mentioned issues. Discrete Tchebichef moments are selected as the implementation platform of the proposed algorithms.To evaluate the performance of invariant algorithms, empirical studies have been carried out on large set of binary images which consist of numbers, English letters, symbols, Chinese characters and objects like animals, trees and company logos under noiseless and noisy conditions. The discriminative power of the features is studied using a set of very similar handwritten Chinese characters. Experimental results showed that the proposed invariant algorithms are superior in computational efficiency. The generated features from the proposed invariants in general, demonstrate improvements in classification performance in both noiseless and noisy conditions.

ABSTRAK

Tujuan tesis ini adalah untuk mengaji algoritma takubahan bagi domain momen ortogonal diskrit. Ketakubahan yang dikaji adalah ketakubahan skala anisotropik dan penterjemahan, ketakubahan skala, putaran and penterjemahan, dan ketakubahan afin. Atas sebab kerumitan fungsi hipergeometrik, algoritma takubahan yang sedia ada adalah perlahan. Sesetengah ciri yang dihasilkan oleh algoritma takubahan tersebut adalah lemah dalam keupayaan pengelasan dan terlalu peka terhadap hingar. Atas sebab itulah, set baru algoritma takubahan diperkenalkan untuk menyelesaikan masalah-masalah tersebut. Momen diskrit Tchebichef dijadikan asas perlaksanaan alogritma-algoritma yang dicadangkan. Bagi mengesahkan keupayaan algoritma-algoritma, kajian empirik telah dilaksanakan terhadap pelbagai imej termasuk nombor, huruf Inggeris, huruf Cina, dan objek-objek seperti binatang, pokok dan logo syarikat dibawah keadaan tanpa hingar dan keadaan yang hingar. Kuasa pembezalayan terhadap ciri-ciri yang dihasilkan telah dikaji dengan menggunakan set penulisan huruf Cina yang berdekataan. Keputusan eksperimen menunjukan algoritma takubahan yang diperkenalkan adalah unggul dalam kecekapan pengiraan. Ciri-ciri yang dihasilkan secara amnya menunjukan penambahbaikan dari aspek pengelasan dalam keadaan tanpa hingar dan keadaan hingar.

ACKNOWLEDGEMENTS

This thesis would never have been written without the contributions from a large number of people. In particular I want to thank the following persons:

I owe my greatest gratitude to my supervisor Professor Dr. Ong Seng Huat for his constant support and guidance throughout the course of this work. His patient, wisdom, and encouragement has made this thesis possible.

I am indebted to my co-supervisor Professor Dr. Raveendran Paramesran for his motivation, encouragement, guidance, and support especially during the most critical stage of my study.

For the examiners, I took to heart their perceptive and unsparing criticisms of the original manuscript, and the thesis has been benefited greatly from their insights.

I would like to extend my sincere gratitude to Associate Professor Dr. Ho Chin Kuan, Dean of Faculty of Computing and Informatics, Multimedia University, and Professor Dr. Mohd Bin Omar, Head of Institute of Mathematical Sciences, University of Malaya who have been instrumental in my pursuit.

The special thank goes to my old friend, Dr. Wong Wai Kuan who takes pain in proof reading this thesis.

I would like to express my appreciation to my friends and colleagues, especially Ms. Lim Siew Ling, Ms. Lim Lian Tze, Dr. Yap Pew Thian, Dr. Ting Choo Yee, Dr. Wong Chee Onn and Dr. Chua Kuan Chin for their help and encouragement.

My deepest gratitude goes to my family for their persistent love and support throughout my life. I am indebted to my wife Ms. Ng Chin Chin for her care, love and support. I am indebted to my parents for all the trouble they took to ensure we get the best in our life.

TABLE OF CONTENTS

LIST OF FIGURES

LIST OF TABLES

LIST OF SYMBOLS AND ACRONYMS

$I_{n,m}^{\langle \text{as-Z} \rangle}$	$(n+m)^{\text{th}}-$order of anisotropic scale Tchebichef moment invariant of Zhu et. al. (2007c).
$I_{n,m}^{\langle \text{ast-Z} \rangle}$	$(n+m)^{\text{th}}-$order of anisotropic scale and translation Tchebichef moment invariant of Zhu et. al. (2007c).
$I_{n,m}^{\langle \text{ast} \rangle}$	$(n+m)^{\text{th}}-$order of proposed anisotropic scale and translation Tchebichef moment invariant.
$I_{n,m}^{\langle \text{t-Z} \rangle}$	$(n+m)^{\text{th}}-$order of translation Tchebichef moment invariant of Zhu et. al. (2007c).
$I_{n,m}^{\langle \text{tr-Z} \rangle}$	$(n+m)^{\text{th}}-$order of translation and rotation Tchebichef moment invariant of Zhang et. al. (2010).
$I_{n,m}^{\langle \text{trs-H} \rangle}$	$(n+m)^{\text{th}}-$order of translation, rotation and scale geometric moment invariant of Hu (1962).
$I_{n,m}^{\langle \text{trs-Y} \rangle}$	$(n+m)^{\text{th}}-$order of translation, rotation and scale Tchebichef moment invariant of Yap et. al. (2003).
$I_{n,m}^{\langle \text{trs} \rangle}$	$(n+m)^{\text{th}}-$order of proposed translation, rotation and scale Tchebichef moment invariant.
AM	affine Tchebichef moments.
AS-Z	anisotropic scale Tchebichef moment invariants of Zhu et. al. (2007c).
AST	anisotropic scale and translation.
AST(1)	proposed anisotropic scale and translation Tchebichef moment invariants using first scale normalization scheme.
AST(2)	proposed anisotropic scale and translation Tchebichef moment invariants using the second scale normalization scheme.
AST(3)	proposed anisotropic scale and translation Tchebichef moments invariants using the third scale normalization scheme.
AST-G	anisotropic scale and translation Tchebichef moment invariants of Goh et. al. (2009).
AST-L	anisotropic scale and translation Tchebichef moment invariants of Liu et. al. (2011).
AST-P	anisotropic scale and translation geometric moment invariants of Palaniappan et. al. (2000).
AST-Z	anisotropic scale and translation Tchebichef moment invariants of Zhu et. al. (2007c).
LDA	linear discriminant analysis.
QDA	quadratic discriminant analysis.
SVM	support vector machine.
T-Z	translation Tchebichef moment invariants of Zhu et. al. (2007c).
TR-Z	translation and rotation Tchebichef moment invariants of Zhang et. al. (2010).
TRS	translation, rotation, and scale.
TRS-H	translation, rotation and scale Tchebichef moments invariants of Hu (1962).
TRS-Y	translation, rotation and scale Tchebichef moment invariants of Yap et. al. (2003).

LIST OF APPENDICES

CHAPTER 1

OBJECTIVES, SCOPES AND CONTRIBUTIONS

Moment invariants have a long history early before the era of computer. It probably originated from the theory of algebraic invariants studied by German mathematician David Hilbert in the nineteenth century (Hilbert & Sturmfels, 1993). The moment invariants were first introduced to the field of image analysis by Hu (1962). Since then numerous works have been devoted to the various improvements and generalizations of Hu's moments (Reiss, 1991; Li, 1992; Flusser & Suk, 1993; W.-H. Wong, Siu, & Lam, 1995). However the geometric moments suffered from a high degree of information redundancy and the higher order moments are sensitive to noise. Since then several approaches have been taken to overcome these problems. Flusser has proposed a method to derive the independent set of geometric moment invariants of any order (Flusser, 2000, 2002). However this does not solve the noise sensitivity issue of higher order moments. On the other hand, continuous orthogonal moments namely Legendre and Zernike moments were introduced to resolve the issue of information redundancy (Teague, 1980). This is followed by the introduction of discrete orthogonal moments to resolve the issue of continuous moment integration approximation (Mukundan, Ong, & Lee, 2001). Since then several invariant algorithms have been proposed for the family of discrete orthogonal moments (Yap, Raveendran, & Ong, 2003; Goh, Chong, Rosli, Fazli, & Sim, 2009; Zhu, Xia, Luo, & Coatrieux, 2007c; H. Zhang, Dai, Sun, Zhu, & Shu, 2010; H. Zhang et al., 2011). However the algorithms are numerically inefficient mainly due to the complexity of hypergeometric functions involved. From our study, several algorithms also suffered from the noise sensitivities and poor discriminative power in classification. Therefore new sets of algorithms are proposed in this thesis to resolve the above mentioned issues.

1.1 Objective

This thesis aims to solve problems related to invariant algorithms in the domain of discrete orthogonal moments. The invariant algorithms involved are anisotropic scale and

translation (AST) invariants, translation, rotation and scale (TRS) invariants, and affine invariants. Due to complexity of the hypergeometric functions, the invariant expressions are complicated and numerically inefficient. Thus new recurrence relations have been derived for fast computations of the invariant descriptors. Furthermore, the normalization parameters of existing invariants are commonly determined using moments like the geometric moments and complex moments. To do so, the moments need to be recalculated again from the given image, or converted from the discrete orthogonal moments. This has created additional overhead on numerical computations. More importantly, some of the parameters are inappropriately estimated which severely affected the classification performance. Therefore new sets of normalization schemes based on the discrete orthogonal moments have been derived. In this study, the proposed features are compared with current existing features in terms of classification performance under noiseless and noisy conditions. The discriminative power of the features is evaluated using a set of handwritten very similar Chinese characters. As the study focuses on invariant algorithms, Tchebichef moments are selected as the implementation platform for all the above mentioned invariants. This is mainly due to the popularity and simplicity of Tchebichef basis functions. In addition, being the global features descriptors, the kernel of Tchebichef moments has a unit weight function. The invariants can be accurately derived from the original Tchebichef moments without being affected by inverse transform problems of the weight function.

1.2 Scope and Organization

The study examines the invariants of discrete orthogonal moments, both in theory and applications in image classifications. Chapter 2 provides a brief overview on moments, invariants, and some classification algorithms that are used in experiments. Chapter 3 to Chapter 6 illustrate the invariant algorithms for various forms of deformations. As the invariant algorithms are rather independent, each of the chapters (Chapters 3-6) is almost self-contained and can be read separately. The following is the summary of the contents of the chapters.

- **Chapter 2: Introduction to Moment Invariants and Image Classification**

  In this chapter an overview is given on continuous and discrete moments. They are

geometric, Legendre, Tchebichef, Krawtchouk and Hahn moments. A brief introduction to the four main classifiers used in the experiments that is Euclidean distance algorithm, linear discriminant analysis, quadratic discriminant analysis and support vector machine are also provided.

- **Chapter 3: Fast Computation of Anisotropic Scale and Translation Invariants for Tchebichef Moments Using Algebraic Cancellation Approach**.

  In this chapter the anisotropic scale and translation invariants of Zhu et al. (2007c) is reviewed. This is followed by the proposal of two new algorithm for fast computation. The first algorithm uses an indirect approach in which the invariant descriptors are calculated indirectly from geometric moments. This method also indicates a strong correlation between invariant descriptors by Zhu et al. (2007c) and geometric moments. In the latter approach, the features are directly computed from Tchebichef moments using the newly proposed recurrence relations. Experimental results show both algorithms are numerically stable and exhibit high numerical efficiency when compared with the current methods.

- **Chapter 4: Anisotropic Scale and Translation Invariants for Tchebichef Moments using Image Normalization Technique**

  In this chapter the anisotropic scale and translation invariants proposed by Liu, Zhu, and Li (2011), and Goh et al. (2009) are reviewed. Both are based on methods of image normalization. However their approaches are found to be numerically inefficient. Furthermore, both of the normalization algorithms propose to use the origin as the centroid for their canonical forms which lead to ambiguities regarding the orthogonality of transformed moments. For that a new set of recurrence relations has been derived for fast computation of the invariant descriptors. To have features with better discriminative power, the centre of symmetry for the basis function is selected as centroid for the canonical image. To suit the requirements of different classification systems, three new normalization schemes based on Tchebichef moments have been proposed. The ambiguities of the transformation for the proposed normalization schemes have been solved theoretically. Empirical studies showed that the proposed algorithms are numerically efficient, and the generated features

are robust to noise and have better discriminative power.

- **Chapter 5: Translation, Rotation and Scale Invariants for Tchebichef Moments**

  In this chapter the translation, rotational and scale invariants proposed by Yap et al. (2003) and the translation and rotation invariants proposed by H. Zhang et al. (2010) have been reviewed. Yap et al. (2003) derived the invariant descriptors indirectly using modified geometric moments. In the event that the image is not available, the method is not usable. On the other hand invariants of H. Zhang et al. (2010) are highly numerically inefficient. Therefore a new set of recurrence relations has been derived for fast computation of the invariant moments. This comes together with a new set of normalization schemes based on Tchebichef moments for determination of normalization parameters. Empirical studies confirm the newly proposed algorithm is numerically efficient and provides better classification performance.

- **Chapter 6: Affine Tchebichef Moment Invariants using Image Normalization**

  In this chapter new affine Tchebichef moments invariants have been proposed by using the decomposition of seven single variable transformations proposed by Flusser, Suk, and Zitová (2009). These are simplified to four transformations: translation, rotation, and scale transformation, stretch transformation, second rotation transformation and reflective transformation. A new set of normalization scheme based on Tchebichef moments has been proposed to estimate the normalization parameters. Four distinct normalization schemes have been derived for second rotation transformation to handle symmetric patterns with 1-fold symmetry up to 4-fold symmetry, respectively. In an experiment, a set of non-symmetric patterns and a set of symmetric patterns (up to 4-fold symmetry) are used, all patterns have been accurately normalized to their canonical form without any ambiguity.

1.3 Contribution

In this section original and novel work in this thesis is listed:

- **Chapter 3**

  The main contribution of this chapter is the study on how a complicated algorithm

can be simplified by using the property of orthogonal moments. With this understanding, a new recurrence relation has been derived for fast computation on the current invariants. A connection between anisotropic scale and translation invariants of Zhu et al. (2007c) and geometric moments is an important finding indicating a strong correlation between the two features.

- **Chapter 4**

  The main contribution of this chapter is the implementation of the fast computation algorithms using recurrence relations. The use of the centre of symmetry as reference coordinate for the centroid of canonical images, is crucial in preserving the features' discriminative power. The derivation of three new scale normalization schemes for anisotropic scale and translation invariants and the uniqueness for the inverse transformation, enabled the Tchebichef moments based classification system to adopt new normalization scheme easily.

- **Chapter 5**

  The main contribution of this chapter is the generalization of the recurrence formula from anisotropic scale and translation invariants to much larger problems - the affine moments invariants. The new normalization schemes for translation, scale and rotation Tchebichef moments invariants are novel as they are capable of resolving the ambiguities arising from the normalization process. With that, the features will have better discriminative power and higher level of noise resistance.

- **Chapter 6**

  The main contribution of this chapter is the successful derivation of the affine Tchebichef moments invariants. It works accurately for non-symmetric patterns as well as symmetric patterns up to fourfold symmetry. In addition, all the normalized parameters are determined from Tchebichef moments accurately without ambiguity. Together with fast computation algorithms in Chapter 5, computationally fast and accurate affine Tchebichef moment invariants have been derived.

CHAPTER 2

INTRODUCTION TO MOMENT INVARIANTS AND IMAGE CLASSIFICATION

2.1 Moments

Moments are quantitative measures used to characterize a function and to capture its significant features. Mathematically, moments are simply projections of a function onto a set of polynomial basis. It has a long history and has been widely used in areas such as statistics and engineering. In statistics, it has been used for description of the shape of probability density function. In the field of image analysis, moments are used as shape descriptors of images. It has been successfully applied in various areas, like in aircraft and ship classification by Dudani, Breeding, and McGhee (1977), Belkasim (1991), Zvolanek (1981), characters recognition (Khotanzad & Yaw, 1990; Flusser & Suk, 1994a; Liao & Lu, 1997), data compression (Hsu & Tsai, 1993), template matching and registration of satellite images by Goshtasby R. Y. Wong and Hall (1978), (1985), Flusser and Suk(1994b).

Definition 2.1.1. In general, an $(m+n)^{\text{th}}-$order moment, $M_{n,m}(f)$ for an image $f(x,y)$, is defined as

$$M_{n,m}(f) = \iint_S b_{n,m}(x,y) f(x,y) dxdy, \quad m,n = 0,1,2,\cdots \tag{2.1}$$

where $b_{n,m}(x,y)$, is polynomial basis function defined on S. The parameter f at the left hand side of (2.1) is omitted if there is no danger of confusion.

2.1.1 Geometric Moments and Their Shape Representation

In the field of image analysis, the first significant paper on geometric moment invariants was by Hu (1962). In the paper, the affine geometric moment invariants based on the theory of algebraic invariants were introduced to the image processing community. Due to the simplicity of the geometric moments the proposed invariants are one of the most

popular and widely used features in the classification systems to date. The basis function of geometric moment is $b_{k,j}(x,y) = x^k y^j$, and this leads to

$$m_{k,j} = \int_{-\infty}^{\infty}\int_{-\infty}^{\infty} x^k y^j f(x,y)dxdy \tag{2.2}$$

Low order geometric moments represent different spatial characteristics of the image. $m_{0,0}$ is known as the mass of the image.

The first order moments $m_{1,0}$ and $m_{0,1}$ denote the intensity moment about the $x-$axis and $y-$axis of image, respectively. The center of gravity or centroid $(\bar{x},\bar{y})$ is

$$\bar{x} = \frac{m_{1,0}}{m_{0,0}}, \text{ and } \bar{y} = \frac{m_{0,1}}{m_{0,0}} \tag{2.3}$$

It is always convenient to evaluate the moments independent of the pattern position. This can be achieved by having the origin transformed to the centroid of the image. The moments computed with respect to the intensity centroid are called central moments

$$\mu_{n,m} = \int_{-\infty}^{\infty}\int_{-\infty}^{\infty} (x-\bar{x})^n (y-\bar{y})^m f(x,y)dxdy \tag{2.4}$$

The second order moments $\{m_{2,0}, m_{1,1} \text{ and } m_{0,2}\}$, are known as moments of inertia and they describe the “distribution of mass" with respect to the coordinate axes.

The radius of gyration with respect to $x-$axis and $y-$axis are respectively denoted as

$$\sqrt{\frac{m_{2,0}}{m_{0,0}}} \quad \text{and,} \quad \sqrt{\frac{m_{0,2}}{m_{0,0}}} \tag{2.5}$$

A principal axis of inertia of an image is defined as the two orthogonal axes, through the image centroid, having

$$m_{1,1} = 0. \tag{2.6}$$

Skewness is statistical measure of the degree of deviation from symmetry about the mean (Mukundan & Ramakrishnan, 1998). The coefficient of skewness of an image about the $x-$axis and $y-$axis are

$$S_x = \frac{\mu_{3,0}}{(\mu_{2,0})^{\frac{3}{2}}}, \tag{2.7}$$

$$S_y = \frac{\mu_{0,3}}{(\mu_{0,2})^{\frac{3}{2}}}. \tag{2.8}$$

However geometric moments suffer from a high degree of information redundancy, and the higher-order moments are sensitive to noise (Teh & Chin, 1988). To resolve the problems, the continuous orthogonal moments: Legendre moments and Zernike moments were later introduced by Teague (1980).

2.1.2 Continuous Orthogonal Moments

A set of basis polynomials $\{b_{n,m}(x,y)\}$ is said to be orthogonal if the elements satisfy the orthogonality condition (Szegö, 1939)

$$\iint_{\Omega} \omega(x,y) b_{n,m}(x,y) \cdot b_{p,q}(x,y) dxdy = \rho(m,n)\delta_{m,p}\delta_{n,q} \tag{2.9}$$

where $\omega(x,y)$ denotes the weight function (also called jump function), and $\rho(\cdot)$ is the squared norm. $\delta_{u,v}$ denotes the Kronecker delta, which equals to unity if $u = v$ and zero otherwise.

2.1.2 (a) Legendre Moments

From the Rodrigues representation, the $n-$degree Legendre polynomial (Koepf, 1998) is defined as

$$p_n(x) = \sum_{k=0}^{n} (-1)^{\frac{n-k}{2}} \frac{1}{2^n} \frac{(n+k)!x^k}{\left(\frac{n-k}{2}\right)!\left(\frac{n+k}{2}\right)!k!} \tag{2.10}$$

where $|x| \leq 1$ and $(n-k)$ is even.

The Legendre polynomials $\{p_n(x)\}$, is a complete orthogonal basis set on the interval $[-1,1]$

$$\int_{-1}^{1} p_n(x)p_m(x)dx = \frac{2}{2m+1}\delta_{n,m}. \tag{2.11}$$

Legendre polynomials have the three terms recurrence relation given by

$$p_{n+1}(x) = \frac{2n+1}{n+1}xp_n(x) - \frac{n}{n+1}p_{n-1}(x) \tag{2.12}$$

By having the basis $b_{n,m}(x,y) = p_n(x)p_m(y)$, the $(m+n)^{\text{th}}-$order Legendre moment of $f(x,y)$ defined in the continuous space $[-1,1] \times [-1,1]$ is

$$\begin{aligned} L_{n,m} &= \frac{(2n+1)(2m+1)}{4} \int_{-1}^{1}\int_{-1}^{1} p_n(x)p_m(y)f(x,y)dxdy, \\ & \qquad n,m = 0,1,\cdots. \end{aligned} \tag{2.13}$$

Continuous moments such as geometric moments, Legendre moments, complex moments, and Zernike moments (Teague, 1980; Khotanzad & Hong, 1990) have been extensively studied and successfully applied in the area of image analysis. However as pointed out by Mukundan et al. (2001), the implementation of the moments have the following weaknesses

(A1) Numerical approximation of continuous integrals

The integral of continuous moments as stated by (2.2) and (2.13) are approximated by discrete summations. This not only leads to numerical errors but also inaccuracy in analytical properties such as invariance and orthogonality.

(A2) Large variation in the dynamic range of values

The basis often involved large power function. For example geometric moments of order $(n+m)$ on an image of size $N \times N$ pixels, the basis function $x^n y^m$ will therefore have large variation in the dynamic range of values for different orders of moments. Applications involving such moment functions will have to additionally include scale normalization to maintain equal weight for all the components. Furthermore it may be necessary to develop methods for avoiding numerical instabilities when the image size is large.

(A3) Coordinate space transformation

In general, orthogonal moments' basis, has domain completely different from the image coordinate space. For example, the basis of Legendre polynomials have domain in range $[-1,1]$. The application of such orthogonal moments will require an appropriate transformation of the image coordinate space which will further increase the computational complexity.

2.2 Discrete Orthogonal Moments

To address the problems of continuous moments, different types of discrete orthogonal moments were proposed for image analysis. They are Tchebichef moments by Mukundan et al. (2001), Krawtchouk moments (Yap et al., 2003) , Hahn moments by Yap, Raveendran, and Ong (2007), Dual Hahn moments (Zhu, Shu, Zhou, Luo, & Coatrieux, 2007b) and Racah moments by Zhu, Shu, Liang, Luo, and Coatrieux (2007a).

Let $S_2(N)$ be the 2D space in discrete domain

$$S_2(N) = \{(x,y) | 0 \leq x,y \leq N-1, \quad x,y \in \mathbb{Z}\} \tag{2.14}$$

Suppose $\{b_n(x)\}$ denotes the discrete orthogonal polynomials (Erdelyi, Magnus, Oberhettinger, & Tricomi, 1953; Nikiforov, Suslov, & Uvarov, 1991) with weight $\omega(x)$, satisfying

the orthogonality condition

$$\sum_{x=0}^{N-1} \omega(x) b_n(x) b_p(x) = \rho(n,N)\delta_{n,p}$$
$$0 \leq n, p \leq N-1 \tag{2.15}$$

where $\rho(\cdot)$ denotes the squared-norm, then for any bounded function $f(x,y)$, in $S_2(N)$,

$$f(x,y) = \sqrt{\omega(x)\omega(y)} \sum_{n=0}^{N-1} \sum_{m=0}^{N-1} M_{n,m} b_n(x) b_m(y) \tag{2.16}$$

where the coefficients $M_{n,m}$ is given by

$$M_{n,m} = \frac{1}{\rho(n,N)\rho(m,N)} \sum_{x=0}^{N-1} \sum_{y=0}^{N-1} \sqrt{\omega(x)\omega(y)} b_n(x) b_m(y) f(x,y)$$
$$0 \leq n, m \leq N-1 \tag{2.17}$$

and the squared-norm $\rho(n,N)$ can be obtained by

$$\rho(n,N) = \sum_{x=0}^{N-1} \omega(x) \{b_n(x)\}^2. \tag{2.18}$$

The discrete moments given in (2.17) completely eliminates the need to approximate the continuous integrals and does not require coordinate space transformation.

Table 2.1 gives a summary of the polynomials, the weights by which, the polynomials can be derived from monomials using Gram-Schmidt orthogonalization (Erdelyi et al., 1953; Arfken, 1985).

Table 2.1: Some important discrete orthogonal polynomials and their weight functions for image analysis. n denotes the degree of polynomials and $(p, \alpha, \beta, \gamma)$ are parameters attached to the respective polynomials

Name	Notation	space of x and n	$\omega(x)$
Tchebichef	$t_n(x)$	$[0, N-1]$	1
Krawtchouk	$k_n(x; p, N-1)$	$[0, N-1]$	$\binom{N-1}{x} p^x (1-p)^{N--x}$
Hahn	$h_n(x; \alpha, \beta, \gamma, N-1)$	$[0, N-1]$	$\binom{\alpha+x}{x} \binom{\beta+N-1-x}{N-1-x}$

As shown in Table 2.1,Tchebichef polynomials have a unit weight function which makes it an ideal candidate for extracting global features of images. Krawtchouk polynomials and Hahn polynomials are weighted by the binomial distribution and hypergeometric distribution, respectively. These give additional capabilities to the descriptors in focusing on particular location of image, and extract the corresponding local-structure information (Yap et al., 2003, 2007).

2.2.1 Discrete Tchebichef Moments

Tchebichef polynomials are first introduced by Chebyshev (1864) and rediscovered by Gram (1883). The discrete Tchebicief polynomial $t_n(x)$ is defined as

$$\begin{aligned} t_n(x) &= (1-N)_n \, {}_3F_2(-n,-x,1+n\,;1,1-N\,;1) \\ & \qquad n,x = 0,\ 1,\ 2,\cdots,\ N-1 \end{aligned} \tag{2.19}$$

where ${}_pF_q$ is the generalized hypergeometric function (Andrews, Askey, & Roy, 2004) given by

$${}_pF_q\left(\left.\begin{matrix} a_1,a_2,\cdots,a_p \\ b_1,b_2,\cdots,b_q \end{matrix}\right| z\right) = \sum_{k=0}^{\infty} \frac{(a_1)_k (a_2)_k \cdots (a_p)_k}{(b_1)_k (b_2)_k \cdots (b_q)_k} \frac{z^k}{k!}. \tag{2.20}$$

$(a)_k$ is the Pochhammer symbol that represents the rising factorial:

$$(a)_k = a(a+1)(a+2)\ldots(a+k-1).$$

Tchebichef polynomials that satisfy the orthogonality condition (2.15) have squared-norm

$$\begin{aligned} \rho(n,N) &= (2n)! \begin{pmatrix} N+n \\ 2n+1 \end{pmatrix} \\ & \qquad n = 0,1,\cdots,N-1 \end{aligned} \tag{2.21}$$

where

$$\begin{pmatrix} n \\ r \end{pmatrix} = \frac{n!}{r!(n-r)!}. \tag{2.22}$$

The three terms recurrence relation is denoted as

$$\begin{aligned} & nt_n(x) - (2n-1)(2x-N+1)t_{n-1}(x) + (n-1)(N^2-(n-1)^2)t_{n-2}(x) = 0 \\ & \qquad n = 2,\ 3,\ \ldots,\ N-1. \end{aligned} \tag{2.23}$$

However the set of polynomials $t_n(x)$ grow by N^n, which have caused numerical instability in computation (Mukundan et al., 2001). To overcome the shortcoming, scaled Tchebichef polynomials are used to compute the feature moments:

$$\tilde{t}_n^N(x) = \frac{t_n(x)}{\beta(n,N)} \tag{2.24}$$

where $\beta(n,N)$ denotes the scale factor independent of x. Suppose that $\beta(n,N) = \sqrt{\rho(n,N)}$, we get

$$\beta(n,N) = \sqrt{\frac{N(N^2-1)(N^2-2^2)\cdots(N^2-n^2)}{2n+1}}. \tag{2.25}$$

With that, the scaled Tchebichef polynomials have unit squared-norm which make it orthonormal.

From now on, orthonormal Tchebichef polynomials defined on the space $[0,N-1]$, will be denoted as $\tilde{t}_n^N(x)$.

The $(n+m)^{\text{th}}-$order Tchebichef moment $T_{n,m}$ for image $f(x,y)$ on the space of $S_2(N)$, is defined as

$$T_{n,m} = \sum_{x=0}^{N-1}\sum_{y=0}^{N-1} \tilde{t}_n^N(x)\tilde{t}_m^N(y)f(x,y) \tag{2.26}$$

and the corresponding inverse moment transform is

$$f(x,y) = \sum_{n=0}^{N-1}\sum_{m=0}^{N-1} \tilde{t}_n^N(x)\tilde{t}_m^N(y)T_{n,m}. \tag{2.27}$$

The three-term recurrence relation for the Tchebichef polynomials, $\tilde{t}_n^N(x)$, can be expressed as

$$\begin{aligned} \tilde{t}_n^N(x) &= (x\tilde{A}_n^N + \tilde{B}_n^N)\tilde{t}_{n-1}^N(x) + \tilde{C}_n^N\tilde{t}_{n-2}^N(x), \\ &\qquad n = 2,3,\ldots,N-1, \quad x = 1,2,\cdots,N-1 \end{aligned} \tag{2.28}$$

and

$$\tilde{t}_0^N(x) = \frac{1}{\sqrt{N}} \tag{2.29}$$

$$\tilde{t}_1^N(x) = (x\tilde{A}_1^N + \tilde{B_1^N})\tilde{t}_0^N(x) \tag{2.30}$$

where

$$\tilde{A}_n^N = \frac{2}{n}\sqrt{\frac{4n^2-1}{N^2-n^2}} \tag{2.31}$$

$$\tilde{B}_n^N = \frac{(1-N)}{n}\sqrt{\frac{4n^2-1}{N^2-n^2}} \tag{2.32}$$

$$\tilde{C}_n^N = -\frac{(n-1)}{n}\sqrt{\frac{2n+1}{2n-3}}\sqrt{\frac{N^2-(n-1)^2}{N^2-n^2}}. \tag{2.33}$$

Both scaled and classical Tchebichef polynomials have symmetric property satisfying

$$\tilde{t}_n^N(x) = (-1)^n\tilde{t}_n^N(N-1-x). \tag{2.34}$$

From (2.34), the centre of symmetry for Tchebichef polynomials $\{\tilde{t}_n^N(x)\}$ is found to be at $\frac{N-1}{2}$.

Tchebichef moments can be effectively computed using (2.26) and (2.28) to (2.34). Due to discrete nature of the images, computation of Tchebichef moments are superior over continuous moments such as the Zernike and the Legendre moments. However computation of Tchebichef moments tends to exhibit numerical instabilities when the order of moments becomes large. This is mainly due to the cumulative errors caused by recursive computation of (2.28). The errors can be minimized by using the recurrence relation of Tchebichef polynomials $\tilde{t}_n^N(x)$ with respect to x (Mukundan, 2004)

$$\begin{aligned} \tilde{t}_n^N(x) &= \gamma_1 \tilde{t}_n^N(x-1) + \gamma_2 \tilde{t}_n^N(x-2) \\ & \qquad n = 1,2,\cdots,N-1; \quad x = 2,3,\cdots,N-1 \end{aligned} \tag{2.35}$$

where

$$\gamma_1 = \frac{-n(n+1)-(2x-1)(x-N-1)-x}{x(N-x)} \tag{2.36}$$

$$\gamma_2 = \frac{(x-1)(x-N-1)}{x(N-x)} \tag{2.37}$$

and

$$\tilde{t}_n^N(1) = \{1+\frac{n(1+n)}{1-N}\}\tilde{t}_n^N(0) \tag{2.38}$$

$$\begin{aligned} \tilde{t}_n^N(0) &= -\sqrt{\frac{N-1}{N+n}}\sqrt{\frac{2n+1}{2n-1}}\tilde{t}_{n-1}^N(0) \\ & \qquad n = 1,2,\cdots,N-1. \end{aligned} \tag{2.39}$$

2.2.2 Krawtchouk Moments

Krawtchouk polynomials are discrete orthogonal polynomials introduced by Mikhail Kravchuk (Krawtchouk, 1929a, 1929b). The polynomials are associated with binomial distribution. Following the definition given by Koekoek and Swarttouw (1998), the Krawtchouk polynomial $k_n(x;\alpha,\beta,N-1)$ is defined as

$$k_n(x;p,N-1) = {}_2F_1(-n,-x;-N+1;\frac{1}{p}) \tag{2.40}$$

where $n,x = 0,\ 1,\ 2,\cdots,\ N-1, N>1, p\in(0,1)$ and ${}_2F_1$ is the hypergeometric function as defined in (2.20).

Krawtchouk polynomials $\{k_n(x;p,N-1)\}$ form a complete set of discrete basis functions with weight function

$$\omega(x;p,N-1) = \binom{N-1}{x} p^x (1-p)^{N-1-x} \tag{2.41}$$

and satisfy the orthogonality condition

$$\sum_{x=0}^{N-1} \omega(x;p,N-1) k_n(x;p,N-1) k_m(x;p,N-1) = \rho(n;p,N-1)\delta_{n,m} \tag{2.42}$$

where $n,m = 0,1,\cdots,N-1$ and

$$\rho(n;p,N-1) = (-1)^n \left(\frac{1-p}{p}\right)^n \frac{n!}{(-N+1)_n}. \tag{2.43}$$

The orthonormalized Krawtchouk polynomial $\bar{k}_n(x;p,N-1)$ is defined as

$$\bar{k}_n(x;p,N-1) = k_n(x;p,N-1)\sqrt{\frac{\omega(x;p,N-1)}{\rho(n;p,N-1)}}. \tag{2.44}$$

For simplicity, the orthonormalized Krawtchouk polynomial is denoted as Krawtchouk polynomial with $\bar{k}_n(x)$.

The $(n+m)^{\text{th}}-$order Krawtchouk moment $Q_{n,m}$ for image intensity function $f(x,y)$ on space of $S_2(N)$, is defined as

$$Q_{n,m} = \sum_{x=0}^{N-1}\sum_{y=0}^{N-1} \bar{k}_n(x)\bar{k}_m(y) f(x,y) \tag{2.45}$$

and the corresponding inverse moment transform is

$$f(x,y) = \sum_{n=0}^{N-1}\sum_{m=0}^{N-1} \bar{k}_n(x)\bar{k}_m(y) Q_{n,m}. \tag{2.46}$$

The three-term recurrence relation of Krawtchouk polynomial, $\bar{k}_n(x)$, can be expressed as

$$\begin{aligned} \bar{k}_n(x) &= (x\bar{A}_n + \bar{B}_n)\bar{k}_{n-1}(x) + \bar{C}_n \bar{k}_{n-2}(x) \\ & \qquad n = 2,3,\ldots,N-1 \end{aligned} \tag{2.47}$$

and

$$\bar{k}_0(x) = \sqrt{\omega(x;p,N-1)} \tag{2.48}$$

$$\bar{k}_1(x) = \left[1 - \frac{x}{p(N-1)}\right]\sqrt{\frac{p(N-1)}{(1-p)}}\sqrt{\omega(x;p,N-1)} \tag{2.49}$$

where

$$\bar{A}_n = \frac{-1}{\sqrt{p(1-p)n(N-n)}} \tag{2.50}$$

$$\bar{B}_n = \frac{p(N-n)+(n-1)(1-p)}{\sqrt{p(1-p)n(N-n)}} \tag{2.51}$$

$$\bar{C}_n = -\sqrt{\frac{(n-1)(N-n+1)}{(N-n)n}}. \tag{2.52}$$

The symmetric property of Krawtchouk polynomial is

$$\bar{k}_n(x;p,N-1) = (-1)^n \left(\frac{1-p}{p}\right)^n \bar{k}_n(N-1-x;1-p,N-1). \tag{2.53}$$

Krawtchouk polynomials are self-dual

$$\bar{k}_n(x;p,N-1) = \bar{k}_x(n;p,N-1). \tag{2.54}$$

2.2.3 Hahn Moments

The Hahn faimly of orthogonal polynomials were introduced by Chebyshev(1907) and rediscovered by Hahn(1949). According to Koekoek and Swarttouw (1998), Hahn polynomial $h_n(x;\alpha,\beta,N-1)$ is defined as

$$h_n(x;\alpha,\beta,N-1) = {}_3F_2(-n,n+\alpha+\beta+1,-x;\alpha+1,-N;1)$$
$$n,x = 0,\ 1,\ 2,\cdots,\ N-1 \tag{2.55}$$

where $\alpha > -1$ & $\beta > -1$ or $\alpha < -N+1$ & $\beta < -N+1$, and ${}_3F_2$ is hypergeometric function as defined in (2.20).

Hahn polynomials $\{h_n(x;\alpha,\beta,N-1)\}$ form a complete set of discrete basis functions with weight function

$$\omega(x;\alpha,\beta,N-1) = \binom{\alpha+x}{x}\binom{\beta+N-1-x}{N-1-x} \tag{2.56}$$

and satisfy the orthogonality condition

$$\sum_{x=0}^{N-1} \omega(x;\alpha,\beta,N-1)h_n(x;\alpha,\beta,N-1)h_m(x;\alpha,\beta,N-1) = \rho(n;\alpha,\beta,N-1)\delta_{n,m} \tag{2.57}$$

where $n,m = 0,1,\cdots,N-1$ and

$$\rho(n;\alpha,\beta,N-1) = \frac{(-1)^n(n+\alpha+\beta+1)_N(\beta+1)_n n!}{(2n+\alpha+\beta+1)(\alpha+1)_n(-N+1)_n(N-1)!}. \tag{2.58}$$

The orthonormalized Hahn polynomial $\hat{h}_n(x;\alpha,\beta,N-1)$ is defined as

$$\hat{h}_n(x;\alpha,\beta,N-1) = h_n(x;\alpha,\beta,N-1)\sqrt{\frac{\omega(x;\alpha,\beta,N-1)}{\rho(n;\alpha,\beta,N-1)}} \tag{2.59}$$

For simplicity, the orthonormalized Hahn polynomial is denoted as $\hat{h}_n(x)$.

The $(n+m)^{\text{th}}-$order Hahn moments $H_{n,m}$ for image $f(x,y)$ in space of $S_2(N)$, is defined as

$$H_{n,m} = \sum_{x=0}^{N-1}\sum_{y=0}^{N-1} \hat{h}_n(x)\hat{h}_m(y)f(x,y) \tag{2.60}$$

and the corresponding inverse moment transform is

$$f(x,y) = \sum_{n=0}^{N-1}\sum_{m=0}^{N-1} \hat{h}_n(x)\hat{h}_m(y)H_{n,m}. \tag{2.61}$$

The three-term recurrence relation of Hahn polynomial, $\bar{h}_n(x)$, can be expressed as

$$\begin{aligned} \hat{h}_n(x) &= (x\hat{A}_n + \hat{B}_n)\hat{h}_{n-1}(x) + \hat{C}_n\hat{h}_{n-2}(x), \\ & \qquad n = 2,3,\ldots,N-1 \end{aligned} \tag{2.62}$$

where

$$\hat{A}_n = -\sqrt{\frac{(2n-1+\alpha+\beta)(2n+1+\alpha+\beta)(2n+\alpha+\beta)^2}{(n+\alpha+\beta)(n+\alpha)(n+\beta)(n+\alpha+\beta+N)(N-n)n}} \tag{2.63}$$

$$\begin{aligned} \hat{B}_n &= \left[1+\frac{(n-1+\alpha+\beta+N)(n-1+\beta)(2n+\alpha+\beta)(n-1)}{(2n-2+\alpha+\beta)(n+\alpha+\beta)(n+\alpha)(N-n)}\right] \\ &\quad \times\sqrt{\frac{(n+\alpha+\beta)(n+\alpha)(2n+1+\alpha+\beta)(N-n)}{(n+\alpha+\beta+N)(n+\beta)(2n-1+\alpha+\beta)n}} \end{aligned} \tag{2.64}$$

$$\begin{aligned} \hat{C}_n &= \sqrt{\frac{(n-1+\alpha+\beta+N)(n-1+\alpha)(n-1+\beta)(n-1+\alpha+\beta)}{(n+\alpha+\beta)(n+\alpha)(n+\beta)(n+\alpha+\beta+N)}} \\ &\quad \times\sqrt{\frac{(2n+1+\alpha+\beta)(2n+\alpha+\beta)^2(N+1-n)(n-1)}{(2n-3+\alpha+\beta)(2n-2+\alpha+\beta)^2(N-n)n}} \end{aligned} \tag{2.65}$$

and

$$\hat{h}_0(x) = \sqrt{\frac{(N-1)!}{(\alpha+\beta+2)_{N-1}}}\sqrt{\omega(x;\alpha,\beta,N-1)} \tag{2.66}$$

$$\begin{aligned} \hat{h}_1(x) &= \sqrt{\omega(x;\alpha,\beta,N-1)}\times\left[1-\frac{xn(n+\alpha+\beta+1)}{(\alpha+1)(N-1)}\right] \\ &\quad \times\sqrt{\frac{(3+\alpha+\beta)(\alpha+1)(N-1)(N-1)!}{(\beta+1)(2+\alpha+\beta)_N}}. \end{aligned} \tag{2.67}$$

2.3 Spatial Deformation and Moments Invariants

In the real world, images acquired by image systems in remote sensing, astronomy and medicine are imperfect. Various factors like imaging geometry, lens motion, systematic and random sensor errors etc can cause the acquired image to be unrecognisable. In this thesis we focus mainly on the following three spatial deformations which are defined as:

(B1) Anisotropic Scale and Translation Deformation

$$\begin{pmatrix} x' \\ y' \end{pmatrix} = \begin{pmatrix} a_1 & 0 \\ 0 & b_1 \end{pmatrix} \begin{pmatrix} x \\ y \end{pmatrix} + \begin{pmatrix} a_3 \\ b_3 \end{pmatrix} \tag{2.68}$$

where a_1, b_1 denote the scale coefficients, and a_3, b_3 are the spatial displacements of image in the direction of $x-$axis and $y-$axis, respectively.

(B2) Translation, rotation and scale Deformation

$$\begin{pmatrix} x' \\ y' \end{pmatrix} = a \begin{pmatrix} \cos\theta & \sin\theta \\ -\sin\theta & \cos\theta \end{pmatrix} \begin{pmatrix} x \\ y \end{pmatrix} + \begin{pmatrix} a_3 \\ b_3 \end{pmatrix}. \tag{2.69}$$

where the four-parameter transformation, has a as the positive scaling factor, θ as the angle of rotation, a_3 and b_3 are the spatial displacements of image in the direction of $x-$axis and $y-$axis, respectively.

(B3) Affine Deformation

$$\begin{pmatrix} x' \\ y' \end{pmatrix} = \begin{pmatrix} a_1 & a_2 \\ b_1 & b_2 \end{pmatrix} \begin{pmatrix} x \\ y \end{pmatrix} + \begin{pmatrix} a_3 \\ b_3 \end{pmatrix} \tag{2.70}$$

which denotes the general linear transformation of spatial coordinates.

Anisotropic scale and translation invariants are commonly encountered in character recognitions systems where characters printed in different type of fonts differ in scale and the spatial displacement. This also occurred in handwritten characters where the characters are written in different sizes and spatial displacements. On the other hand, translation, rotation and scale deformation are usually encountered in various type of biometric systems like face, finger print and iris recognition systems where the acquired images will tend to have different size, orientation and spatial displacement. Affine deformation is the

generalization of the above two transformations which represents wide spectrum of the spatial deformation of the images.

The ability to recognize patterns that have been deformed in various ways is an important process in classification systems. Basically, there are three major approaches to solve this problem - brute force, image normalization and invariant features (Flusser, 2007; Flusser et al., 2009). Brute-force approach appeared to be the simplest. However exhaustive search on parametric space of all possible patterns including the degraded ones, is practically inapplicable. In the normalization approach, the objects are transformed into a certain standard form known as canonical form before being classified. This is very efficient in the stage of classification. However in object normalization, it is usually not so easy to solve the inverse problems uniquely without ambiguities. The invariant features approach, on the other hand, uses a set of measurable quantities called invariants that are insensitive to particular deformations and that provide enough discriminative power to distinguish objects belonging to different classes. This is one of the most popular method. However invariants to a certain extent might also weaken the classification performance. Hence a trade off between invariance and discriminative power is a very important task in features based object recognition.

A function I is invariant of a particular deformation D on image f if

$$I(f) = I(D(f)) \tag{2.71}$$

On the other hand, a moment function $I_{n,m}$ is invariant of deformation D of image f if

$$I_{n,m}(f) = I_{n,m}(D(f)) \tag{2.72}$$

2.4 Image Classification

Models of data with a categorical response are called classification. A classifier is built from training data, for which classification is known. The classifier assigns new test data to one of the categorical levels of the response.

In this thesis the following classifiers will be used to evaluate the performance of invariant features:

(C1) Euclidean distance classifier,

(C2) Linear discriminant analysis (LDA),

(C3) Quadratic discriminant analysis (QDA), and

(C4) Support vector machine (SVM)

2.4.1 Euclidean Distance Classifier

The square of Euclidean distance classifier (Webb, Copsey, & Cawley, 2011) is defined as

$$d(\tilde{\mathbf{V}}_{\mathbf{s}}, \tilde{\mathbf{V}}_{\mathbf{t}}^{(\mathbf{k})}) = \sum_{j=1}^{J} (\tilde{v}_{s,j} - \tilde{v}_{t,j}^{(k)})^2 \tag{2.73}$$

where $\tilde{\mathbf{V}}_{\mathbf{s}} = \begin{pmatrix} \tilde{v}_{s,1} \\ \tilde{v}_{s,2} \\ \vdots \\ \tilde{v}_{s,T} \end{pmatrix}$ and $\tilde{\mathbf{V}}_{\mathbf{t}}^{(\mathbf{k})} = \begin{pmatrix} \tilde{v}_{s,1}^{(k)} \\ \tilde{v}_{s,2}^{(k)} \\ \vdots \\ \tilde{v}_{s,T}^{(k)} \end{pmatrix}$ are the $J-$dimensional scaled feature vectors of unknown sample and the scaled training vector of class k, respectively. The scaled feature vectors are used mainly to remove large dynamic range on moments values. The scaled formula is as follows:

$$\tilde{v}_{s,j} = \frac{v_{s,j} - \min\limits_{k} v_{t,j}^{(k)}}{\max\limits_{k} v_{t,j}^{(k)} - \min\limits_{k} v_{t,j}^{(k)}}. \tag{2.74}$$

The accuracy of a classifier is measured by

$$\eta = \frac{N_{\text{correct}}}{N_{\text{total}}} \tag{2.75}$$

where N_{correct} denotes the number of correctly classified images and N_{total} is the total number of images used in the testing set.

2.4.2 Discriminant Analysis

Discriminant analysis is a commonly used statistical technique for classification and to reduce the dimensionality of data (or known as feature selection process). The model is based on the assumption that the data is Gaussian mixture distributed (McLachlan & Wiley, 1992; Johnson & Wichern, 2002). Suppose for a $p-$dimensional feature data, conditional to be in class k, $\boldsymbol{X}|G = k \sim N_p(\mu_k, \Sigma_k)$. That is

$$f_k(x) \quad = \quad \frac{1}{(2\pi)^{p/2}|\Sigma_k|^{1/2}} \exp\left\{-\frac{1}{2}(\boldsymbol{x} - \mu_k)^T \Sigma_k^{-1} (\boldsymbol{x} - \mu_k)\right\}. \tag{2.76}$$

In the case of linear discriminant analysis (LDA), the covariance matrices are assumed to be equal, i.e. $\Sigma_k = \Sigma$.

Suppose R is an N by K class membership matrix:

$$\begin{aligned} R_{n,k} &= 1 \quad \text{if observation } n \text{ is from class } k, \\ R_{n,k} &= 0 \quad \text{otherwise.} \end{aligned}$$

The parameters of the Gaussian distribution are estimated as follow:

(D1) The priori probability $P(G = k) = \hat{\pi}_k = \frac{N_k}{N}$, where N_k is the number of sample of class k.

(D2) The estimate of the class mean for data is

$$\hat{\mu}_k = \frac{\sum_{n=1}^{N} R_{n,k} x_n}{\sum_{n=1}^{N} R_{n,k}}. \tag{2.77}$$

(D3) The unbiased estimate of the pool-in covariance matrix is

$$\hat{\Sigma} = \frac{\sum_{n=1}^{N} \sum_{k=1}^{K} R_{n,k} (x_n - \hat{\mu}_k)(x_n - \hat{\mu}_k)^T}{N - K}. \tag{2.78}$$

The linear discriminant function $d_k^L(x)$ is estimated by

$$\hat{d_k^L}(x) = \hat{\mu}_k^T \hat{\Sigma}^{-1} \boldsymbol{x} - \hat{\mu}_k^T \hat{\Sigma}^{-1} \hat{\mu}_k + \log(\hat{\pi}_k). \tag{2.79}$$

When the covariance matrices are not equal, we have the quadratic discriminant function $d_k^Q(x)$ estimated by

$$\hat{d_k^Q}(x) = \hat{\mu}_k^T \hat{\Sigma}_k^{-1} \boldsymbol{x} - \hat{\mu}_k^T \hat{\Sigma}_k^{-1} \hat{\mu}_k + \log(\hat{\pi}_k). \tag{2.80}$$

The classification rule for both LDA and QDA is given as follows

$$\hat{D}(x) = k^* \Leftrightarrow k^* = \arg\max_k \hat{d}_k(x). \tag{2.81}$$

2.4.3 Support Vector Machine

Support Vector Machine (SVM) is a duo classes classifier introduced by Vapnik (1995). The basic idea of SVM is to map non-linear input vectors to a very high dimension

feature space where in this feature space a linear decision surface can be constructed with maximum between class separation (Vapnik, 1995; Cortes & Vapnik, 1995). The term SVM was originated from the points in the training set in which, are closet to the decision surface that called as support vectors. For a training set with instance-label pairs $(\boldsymbol{x}_k, y_k), \quad k = 1, 2, \cdots l$, where $\boldsymbol{x}_k \in \Re^n$ and $\boldsymbol{y} \in \{1, -1\}^l$, the SVM requires the solution of the following optimization problem (Boser, Guyon, & V., 1992; Vapnik, 1995):

$$\begin{aligned} \min_{\boldsymbol{w},b,\xi} \quad & \frac{1}{2}\boldsymbol{w}^T\boldsymbol{w} + C\sum_{k=1}^{l}\xi_k \\ \text{subject to} \quad & y_k(\boldsymbol{w}^T\phi(\boldsymbol{x}_k) + b) \geq 1 - \xi_k, \\ & \xi_k \geq 0. \end{aligned} \tag{2.82}$$

The vectors $\boldsymbol{x}_k$ are mapped into higher (maybe infinite) dimensional space by the function ϕ. SVM will then find a linear separating hyperplane with maximum margin in this higher dimensional space. $C > 0$ is the penalty parameter of the error term. $K(\boldsymbol{x}_k, \boldsymbol{x}_j) = \phi(\boldsymbol{x}_k)\phi(\boldsymbol{x}_j)$ is called the kernel function. Below are the four commonly used basic kernels:

(E1) linear: $K(\boldsymbol{x}_k, \boldsymbol{x}_j) = \boldsymbol{x}_k^T\boldsymbol{x}_j$

(E2) polynomial: $K(\boldsymbol{x}_k, \boldsymbol{x}_j) = (\gamma\boldsymbol{x}_k^T\boldsymbol{x}_j + r)^d$, $\gamma > 0$

(E3) radial basis function (RBF): $K(\boldsymbol{x}_k, \boldsymbol{x}_j) = \exp(-\gamma||\boldsymbol{x}_k - \boldsymbol{x}_j||^2)$, $\gamma > 0$

(E4) sigmoid: $K(\boldsymbol{x}_k, \boldsymbol{x}_j) = \tanh(\gamma\boldsymbol{x}_k^T\boldsymbol{x}_j + r)$

where γ, r and d are kernel parameters.

In this thesis, LIBSVM (Chang & Lin, 2011) will be deployed as SVM classification tools for the experiments.

2.4.4 Design of Experiments

One of the aim of this thesis is to derive new invariant algorithms for fast computation and new invariant features with better discriminative power and robustness to noise. Series of experiments are conducted to validate the finding. Large amount of binary patterns are used in the experiments. These include numbers, English letters, symbols, printed Chinese characters, Chinese handwritten characters (HCL2000 database),

objects, companies logo, etc. The selected images consist of symmetric objects and non-symmetric objects in different complexities. The binary images are being used as it is commonly used to validate the accuracy of moment invariant algorithms (Khotanzad & Yaw, 1990; Belkasim, 1991; Yap et al., 2003; Chong, Raveendran, & Mukundan, 2004; Zhu et al., 2007c; Goh et al., 2009; H. Zhang et al., 2010, 2011). As each pixel of binary pattern can only contain a single bit of information, the errors and loss of information cause by spatial transformation are therefore very severe when compared with gray scale images. Therefore in general moment invariants work better for gray scale images and excluded from the experiments.

The Euclidean distance classifier is used to evaluate the robustness of invariant descriptors to noise. The classifier is selected mainly due to its simplicity and popularity (Yap et al., 2003; Yap, 2006; Zhu et al., 2007c), and effectiveness especially for small training data set. The discriminant functions LDA and QDA are widely used in dimensional reduction of feature sets. It also commonly used in statistical data analysis. Support vector machine on the other hand is one of the most popular classifiers in the area of data mining to date. In view that different classifiers might exhibit different classification performance, to ensure objectivity, all three classifiers (LDA, QDA and SVM) are used in the experiment to determine the discriminant power of features.

CHAPTER 3

FAST COMPUTATION OF ANISOTROPIC SCALE AND TRANSLATION TCHEBICHEF MOMENT INVARIANTS USING ALGEBRAIC CANCELLATION APPROACH

In this chapter, anisotropic scale and translation invariants for Tchebichef moments by Zhu et al. (2007c) have been studied. Due to complexity of the hypergeometric function, the invariants algorithm is numerically inefficient. Two new faster computation algorithms have been proposed to improve the numerical performance of current method. The first proposed algorithm uses indirect method based on geometric moments. In the second algorithm, the descriptors are computed directly from the original Tchebichef moments using a new set of recurrence formula. Empirical studies that determine the accuracy of the features and the computation performance have been performed. The results show significant improvement in computational performance with the new proposed algorithms.

3.1 Introduction

Algebraic cancellation is an effective and accurate technique used on deriving the anisotropic scale and translation (AST) invariants for moment functions. The algorithm first eliminates the spatial displacement deformations using the central moments transformation, the scale parameters are then separated from the moments, and then eliminated via the algebraic cancellation process. Algebraic cancellation techniques were first introduced for geometric moments. Several cancellation schemes have been proposed, they can be divided into two groups: cancellation scheme for uniformly scaled deformation, and cancellation scheme for non-uniformly scaled deformation. For a uniformly scale deformed image, the scale invariants can be achieved with any of the following cancellation

schemes: (Belkasim, 1991; Prokop & Reeves, 1992)

$$I_{n,m}^{\langle \text{st-1} \rangle} = \frac{\mu_{n,m}}{(\mu_{0,0})^{\frac{(n+m+2)}{2}}} \tag{3.1}$$

$$I_{n,m}^{\langle \text{st-2} \rangle} = \frac{\mu_{n,m}}{(\mu_{2,0}+\mu_{0,2})^{\frac{(n+m+2)}{4}}} \tag{3.2}$$

$$I_{n,m}^{\langle \text{st-3} \rangle} = \frac{\mu_{n,m}}{\mu_{0,0}} \left(\frac{\mu_{0,0}}{\mu_{2,0}+\mu_{0,2}} \right)^{\frac{(n+m)}{2}} \tag{3.3}$$

where $\mu_{n,m}$ denotes the central moments.

Similarly, for a non-uniformly scale deformed image, scale invariants can be achieved with any of the following cancellation schemes:

$$I_{n,m}^{\langle \text{ast-PK} \rangle} = \frac{\mu_{n,m}{\mu_{0,0}}^{\frac{(n+m+2)}{2}}}{(\mu_{2,0})^{\frac{(n+1)}{2}}(\mu_{0,2})^{\frac{(m+1)}{2}}} \tag{3.4}$$

$$I_{n,m}^{\langle \text{ast-P} \rangle} = \frac{\mu_{n,m}{\mu_{0,0}}^{(\gamma+1)}}{\mu_{n+\gamma,0}\mu_{0,m+\gamma}}, \quad \gamma = 1,2,\cdots \tag{3.5}$$

where (3.4) denotes the cancellation scheme proposed by Pan and Keane (1994), and (3.5) is the cancellation scheme proposed by Palaniappan, Raveendran, and Omatu (2000) (denoted as AST-P).

The method (in particular the cancellation scheme by Palaniappan et al.(2000)) is then extended to derive AST invariants for Legendre moments by Chong et al. (2004) and AST invariants for discrete Tchebichef moments by Zhu et al. (2007c).

In Section 3.2, a brief overview on anisotropic scale and translation invariants for Tchebichef moments by Zhu et al. (2007c) (denoted as AST-Z) is given. This followed by a discussion of computational efficiency issues in Section 3.3. In Section 3.4, two new fast computation algorithms are proposed. The first algorithm indirectly compute AST-Z using the geometric moments. The second algorithm uses a new recursive function on Tchebichef moments. In Section 3.5 some empirical studies on the proposed algorithm are given.

3.2 Review on Anisotropic Scale and Translation Tchebichef moment invariants of Zhu et. al.

According to Zhu et al. (2007c), translation invariants, and non-uniform scale invariants were proposed as two separate algorithms. They were combined to form AST

invariants for Tchebichef moments later. Here $I_{n,m}^{\langle \text{t-Z} \rangle}$ denotes the translated Tchebichef moment invariants by Zhu et al. (2007c) (T-Z), $I_{n,m}^{\langle \text{as-Z} \rangle}$ is the corresponding invariant descriptors for anisotropic scale invariants (AS-Z), and the invariant descriptors for AST-Z is represented by $I_{n,m}^{\langle \text{ast-Z} \rangle}$.

3.2.1 Translation Invariants of Tchebichef Moments

Consider Tchebichef polynomials $\{\tilde{t}_n^N(x)\}$ defined on $[0, N-1]$. $\tilde{t}_n^N(x)$ can be expressed as

$$\tilde{t}_n^N(x) = \sum_{k=0}^{n} \tilde{b}_{n,n-k} \langle x \rangle_k \tag{3.6}$$

where

$$\tilde{b}_{n,\,n-k} = \frac{1}{\sqrt{\rho(n,N)}} \frac{(n+k)!\,\langle n-N \rangle_{n-k}}{(n-k)!(k!)^2} \tag{3.7}$$

$\langle x \rangle_n$ denotes the falling factorial

$$\langle x \rangle_n = x \cdot (x-1) \cdots (x-n+1) \tag{3.8}$$

and $\rho(n,N)$ is the squared-norm given by

$$\rho(n,N) = \frac{N(N^2-1)(N^2-2^2)\cdots(N^2-n^2)}{2n+1}. \tag{3.9}$$

The translation invariant of Tchebichef moments, $I_{n,m}^{\langle \text{t-Z} \rangle}$, are defined by the Tchebichef central moments $T_{n,m}^{\langle \text{c} \rangle}$ as

$$\begin{aligned} I_{n,m}^{\langle \text{t-Z} \rangle} &= T_{n,m}^{\langle \text{c} \rangle} \\ &= \sum_{x=0}^{N-1} \sum_{y=0}^{N-1} \tilde{t}_n^N(x-\bar{x}) \tilde{t}_m^N(y-\bar{y}) f(x,y), \\ &\qquad n,m = 0,1,\cdots,N-1 \end{aligned} \tag{3.10}$$

where $(\bar{x}, \bar{y})$ denotes the centroid of the image.

As shown by Zhu et al. (2007c), spatial displacement coefficient is detachable from translated Tchebichef polynomial $\tilde{t}_n^N(x+a)$ such that

$$\tilde{t}_n^N(x+a) = \sum_{k=0}^{n} \tilde{\upsilon}_{n,n-k}(a) \tilde{t}_{n-k}^N(x). \tag{3.11}$$

Thus the Tchebichef central moments have the expression

$$\begin{aligned} T_{n,m}^{\langle \text{c} \rangle} &= \sum_{k=0}^{n} \sum_{j=0}^{m} \tilde{\upsilon}_{n,\,n-k}(-\bar{x})\, \tilde{\upsilon}_{m,\,m-j}(-\bar{y}) T_{n-k,m-j} \\ &\qquad n,m = 0,1,\cdots,N-1 \end{aligned} \tag{3.12}$$

where

$$\tilde{\upsilon}_{n,n-k}(a)\tilde{b}_{n-k,n-k} = \sum_{r=0}^{k}\binom{n-k+r}{r}\tilde{b}_{n,n-k+r}\langle a\rangle_r - \sum_{u=0}^{k-1}\tilde{b}_{n-u,n-k}\tilde{\upsilon}_{n,n-u}(a) \tag{3.13}$$

and $a = -\bar{x}$ or $-\bar{y}$.

Furthermore, the Tchebichef central moments can alternatively be expressed as

$$T_{n,m}^{\langle c\rangle} = \sum_{k=0}^{m}\sum_{j=0}^{n}\sum_{r=0}^{k-1}\sum_{s=0}^{j-1}\tilde{f}_r(n,k)\tilde{f}_s(m,j)\langle-\bar{x}\rangle_{k-r}\langle-\bar{y}\rangle_{j-s}T_{n-k,m-j} \tag{3.14}$$

with

$$\begin{aligned}\tilde{f}_u(n,\,k) = {} & \frac{(n-k)!}{(2n-2k)!}\left\{\frac{(2n-u)!}{u!(k-u)!(n-u)!}\frac{\beta(n-k,N)}{\beta(n,N)}\times\langle n-N\rangle_u\right.\\ & -\frac{1}{(n-k)!}\sum_{p=0}^{u-1}\frac{(2n-2k-p+u)!}{(u-p)!}\frac{\beta(n-k,N)}{\beta(n-p-k+u,N)}\\ & \left.\times\langle n-p-k+u-N\rangle_{u-p}\times\tilde{f}_p(n,\,k+p-u)\right\}\end{aligned} \tag{3.15}$$

and

$$\tilde{\upsilon}_{n,\,n-k}(a) = \sum_{u=0}^{k-1}\tilde{f}_u(n,k)\langle a\rangle_{k-u}. \tag{3.16}$$

3.2.2 Anisotropic Scale Invariant of Tchebichef Moments

Let the non-uniform scale transformed Tchebichef moments be defined as

$$\begin{aligned}T_{n,m}^{\langle as\rangle} = {} & |ab|\sum_{x=0}^{N-1}\sum_{y=0}^{N-1}\tilde{t}_n^N(ax)\tilde{t}_m^N(by)f(x,y)\\ & n,m = 0,1,\cdots,N-1\end{aligned} \tag{3.17}$$

where a and b denote the scale coefficients.

As shown by Comtet (1974),

$$\langle x\rangle_n = \sum_{k=0}^{n}s(n,k)x^k \tag{3.18}$$

with $s(n,k)$ denoting the Stirling numbers of the first kind having recurrence relations

$$s(n,k) = s(n-1,k-1) - (n-1)s(n-1,k) \tag{3.19}$$

and

$$\begin{aligned}s(0,0) &= 1\\ s(n,0) &= s(0,k) = 0, \qquad n\geq 1, k\geq 1.\end{aligned}$$

It can be easily deduced that

$$\tilde{t}_n^N(x) = \sum_{k=0}^{n} c_{n,k}^N x^k \tag{3.20}$$

where

$$c_{n,k}^N = \sum_{r=0}^{n-k} \tilde{b}_{n,n-r} s(n-r,k). \tag{3.21}$$

Similarly, the scaled Tchebichef polynomial, $\tilde{t}_n^N(ax)$, can be expressed as $n-$order polynomial of ax:

$$\tilde{t}_n^N(ax) = \sum_{k=0}^{n} c_{n,k}^N a^k x^k. \tag{3.22}$$

From (3.22), an expression that separates the scale coefficients from the original Tchebichef polynomials can be derived such that

$$\sum_{k=0}^{n} \kappa_{n,k} \tilde{t}_k(ax) = a^n \sum_{k=0}^{n} \kappa_{n,k} \tilde{t}_k(x) \tag{3.23}$$

where

$$\kappa_{n,k} = \begin{cases} 1, & k = n \\ \sum_{u=0}^{n-k-1} \frac{-c_{n-u,k}^N \kappa_{n,n-u}}{c_{k,k}^N}, & 0 \le k < n. \end{cases} \tag{3.24}$$

Consider

$$c_{n,k}^N = \sum_{r=0}^{n-k} c_{n,k}^N(r) \tag{3.25}$$

in which,

$$c_{n,k}^N(r) = \tilde{b}_{n,n-r} s(n-r,k). \tag{3.26}$$

The following recurrence relation has been derived to improve the computation efficiency

$$c_{n,k}^N(r-1) = \frac{r(2n-r+1)}{(n-N-r+1)(n-r+1)^2} \times \frac{s(n-r+1,k)}{s(n-r,k)} \times c_{n,k}^N(r) \quad k \le n-r, \quad 0 \le r \le n-1. \tag{3.27}$$

with

$$c_{n,0}^N(n) = \tilde{b}_{n,0}. \tag{3.28}$$

As shown by (3.23) and (3.24), the scale coefficients can be separated from the original Tchebichef polynomials. Let

$$\varphi_{n,m} = \sum_{k=0}^{n} \sum_{j=0}^{m} \kappa_{n,k} \kappa_{m,j} T_{n,m}. \tag{3.29}$$

The relation between the original and scaled Tchebichef moments are

$$\begin{aligned}\varphi_{n,m}^{'} &= |ab| \sum_{x=0}^{N-1}\sum_{y=0}^{N-1}\sum_{k=0}^{n}\sum_{j=0}^{m} \kappa_{n,k}\kappa_{m,j}\tilde{t}_k^N(ax)\tilde{t}_j^N(by)f(x,y) \\ &= a^{n+1}b^{m+1}\sum_{k=}^{n}\sum_{j=0}^{m}\kappa_{n,k}\kappa_{m,j}\sum_{x=0}^{N-1}\sum_{y=0}^{N-1}\tilde{t}_k^N(x)\tilde{t}_j^N(y)f(x,y) \\ &= a^{n+1}b^{m+1}\varphi_{n,m}. \end{aligned} \tag{3.30}$$

By using the cancellation scheme proposed by Palaniappan et al. (2000), the scale factors a and b can then be eliminated. Thus the invariant descriptors of AS-Z can be written as

$$\begin{aligned} I_{n,m}^{\langle \text{as-Z}\rangle} &= \frac{\varphi_{n,m}{\varphi_{0,0}}^{\gamma+1}}{\varphi_{n+\gamma,0}\varphi_{0,m+\gamma}}, \\ & \qquad n,m = 0,1,\cdots,N-1-\gamma, \quad \text{and} \quad \gamma = 1,2,\cdots. \end{aligned} \tag{3.31}$$

3.2.3 Anisotropic Scale and Translation Invariants of Tchebichef Moments

Let $T_{n,m}^{\langle \text{ast}\rangle}$ denote the AST transformed Tchebichef moments which are given by

$$\begin{aligned} T_{n,m}^{\langle \text{ast}\rangle} &= |a_1b_1| \sum_{x=0}^{N-1}\sum_{y=0}^{N-1}\tilde{t}_n^N(a_1x+a_2)\tilde{t}_m^N(b_1y+b_2)f(x,y), \\ & \qquad n,m = 0,1,\cdots,N-1 \end{aligned} \tag{3.32}$$

where a_1 and b_1 denote the scale coefficients, and a_2 and b_2 are the spatial displacement coefficients.

The coefficients a_2 and b_2 can be eliminated by using the Tchebichef central moments, (3.32) becomes

$$T_{n,m}^{\langle \text{c,ast}\rangle} = |a_1b_1| \sum_{x=0}^{N-1}\sum_{y=0}^{N-1}\tilde{t}_n^N(a_1(x-\bar{x}))\tilde{t}_m^N(b_1(y-\bar{y}))f(x,y). \tag{3.33}$$

Suppose

$$\phi_{n,m} = \sum_{k=0}^{n}\sum_{j=0}^{m}\kappa_{n,k}\kappa_{m,j}T_{k,j}^{\langle \text{c}\rangle} \tag{3.34}$$

where $\kappa_{n,k}$ denotes the coefficient of Tchebichef moments defined by (3.24).

The coefficient a_1 and b_1 can then be separated from the original central Tchebichef moments as

$$\begin{aligned} \phi_{n,m}^{'} &= |a_1b_1| \sum_{x=0}^{N-1}\sum_{y=0}^{N-1}\sum_{k=0}^{n}\sum_{j=0}^{m} \kappa_{n,k}\kappa_{m,j}\tilde{t}_k^N(a_1(x-\bar{x}))\tilde{t}_j^N(b_1(y-\bar{y}))f(x,y) \\ &= a_1^{n+1}b_1^{m+1}\sum_{k=}^{n}\sum_{j=0}^{m}\kappa_{n,k}\kappa_{m,j}\sum_{x=0}^{N-1}\sum_{y=0}^{N-1}\tilde{t}_k^N(x-\bar{x})\tilde{t}_j^N(y-\bar{y})f(x,y) \\ &= a_1^{n+1}b_1^{m+1}\phi_{n,m}. \end{aligned} \tag{3.35}$$

With the similar cancellation process used in (3.31), the invariant descriptors of AST-Z are

$$I_{n,m}^{\langle \text{ast-Z} \rangle} = \frac{\phi_{n,m}{\phi_{0,0}}^{\gamma+1}}{\phi_{n+\gamma,0}\phi_{0,m+\gamma}}, \quad n,m = 0,1,\cdots,N-1-\gamma, \quad \text{and} \quad \gamma = 1,2,\cdots. \tag{3.36}$$

3.3 Numerical Computations on Anisotropic Scale and Translation Invariants of Zhu et. al.

In this subsection we discuss the implementation of invariant algorithms of Zhu et al. (2007c).

3.3.1 Numerical Computations on Translation Invariants

The translation invariants T-Z can be computed by using (3.12) or (3.14). In the first approach, $\upsilon_{n,n-k}(\bar{x})$ is computed using (3.13), a recurrence relation on $\tilde{b}_{n,n-k}$ can be derived as

$$\tilde{b}_{n,n-k} = \frac{(k+1)^2(k+1-N)}{(n-k)(n+k+1)}\tilde{b}_{n,n-1-k}, \quad k = n-1,n-2,\cdots,0 \tag{3.37}$$

and

$$\begin{aligned} \tilde{b}_{n,0} &= \tilde{b}_{n-1,0}\frac{2}{n}\sqrt{\frac{(4n^2-1)}{(N^2-n^2)}}, \qquad n = 1,2,\cdots,N-1, \\ \tilde{b}_{0,0} &= \frac{1}{\sqrt{N}}. \end{aligned}$$

In the latter approach, the recurrence relation $\upsilon_{n,n-k}(\bar{x})$ is computed using (3.16) and (3.15) . However the expression of $f_u(n,k)$ is complicated. To simplify this, the function is decomposed into several sub-functions where each of them is expressible recursively. We have

$$\tilde{f}_u(n,k) = D(n,k,u,N) + \sum_{p=0}^{u-1} E(n,k,u,p,N)\tilde{f}_p(n,\ k+p-u) \tag{3.38}$$

where

$$\tilde{f}_0(n,k) = D(n,k,0,N) \tag{3.39}$$

and

$$D(n,k,u,N) = \frac{(n-k)!}{(2n-2k)!}\frac{(2n-u)!}{u!(k-u)!(n-u)!}\frac{\beta(n-k,N)}{\beta(n,N)} \times \langle n-N\rangle_u \quad (3.40)$$

$$E(n,k,u,p,N) = -\frac{(2n-2k-p+u)!}{(2n-2k)!(u-p)!}\frac{\beta(n-k,N)}{\beta(n-p-k+u,N)} \times \langle n-p-k+u-N\rangle_{u-p} \quad (3.41)$$

with

$$\beta(n,N) = \sqrt{\rho(n,N)}.$$

The recurrence relations of $D(n,k,u,N)$ and $E(n,k,i,m,N)$ can be derived as

$$D(n,k,u,N) = D(n,k,u-1,N)\frac{(k-u+1)(n-u+1)(n-N-u+1)}{u(2n-u+1)}$$

$$D(n,k,0,N) = D(n,k-1,0,N)\frac{2}{k}\sqrt{\frac{(2n-2k+3)(2n-2k+1)}{(N^2-(n-k+1)^2)}}$$

and

$$E(n,k,u,p,N) = E(n,k,u,p-1,N) \times \frac{(u-p+1)}{(2n-2k-p+u+1)(n-k-N+1+u-p)} \times \sqrt{\frac{[2(n-p-k+u)+1][N^2-(n-p-k+u+1)^2]}{[2(n-p-k+u)+3]}}$$

$$E(n,k,u,p,N) = E(n,k,u-1,p,N) \times \frac{(2n-2k-p+u)(n-k-N+u-p)}{(u-p)} \times \sqrt{\frac{[2(n-p-k+u-1)+1]}{[2(n-p-k+u)+1][N^2-(n-p-k+u)^2]}}.$$

3.3.2 Numerical Computations of Translation and Scale Invariants

As shown in (3.36), to get AST-Z, we first need to obtain Tchebichef central moments using (3.12) or (3.14). It is then followed by computation of expression $\phi_{n,m}$ using (3.34), and finally, the invariant descriptors are obtained by the cancellation process using (3.36). The complexity of the algorithms and the sequential computation on Tchebichef central moments followed by scale invariants appeared to be the bottleneck for AST-Z which will be resolved by new proposed algorithms.

3.4 Fast Computation for Translation and Scale Invariants

In this section two sets of fast computation algorithms are proposed. The first set of fast computation algorithms compute T-Z, AS-Z and AST-Z indirectly using geometric

moments. The latter approach computes the invariants from Tchebichef moments using the new set of recurrence relations.

3.4.1 Fast Computation on Translation Invariants using Indirect Approach

From (3.20), Tchebichef central moments can be deduced from geometric central moments $\mu_{k,j}$ to give

$$\begin{aligned} T_{n,m}^{\langle c \rangle} &= \sum_{x=0}^{N-1}\sum_{y=0}^{N-1} \tilde{t}_n^N(x-\bar{x})\tilde{t}_m^N(y-\bar{y})f(x,y) \\ &= \sum_{k=0}^{n}\sum_{j=0}^{m} c_{n,k}^N c_{m,j}^N \mu_{k,j}. \end{aligned} \tag{3.42}$$

Similar to the AS-Z invariants, for this method to be efficient, pre-computation on coefficients $c_{n,k}^N$ using (3.25) to (3.28) is required.

3.4.2 Fast Computation on Anisotropic Scale and Translation Invariants Using Indirect Approach

The indirect expression of AST-Z using geometric moments can be simplified with the following theorem.

Theorem 3.4.1. *Suppose that*

$$\xi_n(ax) = \sum_{k=0}^{n} \alpha_{n,k}\tilde{t}_k(ax) \tag{3.43}$$

where the coefficients $\alpha_{n,k}$ are constants, and $\alpha_{n,n} \neq 0$, then

$$\xi_n(ax) = a^n \xi_n(x) \tag{3.44}$$

if and only if

$$\xi_n(ax) = a^n \alpha_{n,n} c_{n,n}^N x^n. \tag{3.45}$$

Proof. It is obvious that $\xi_n(ax) = a^n\xi_n(x)$ if $\xi_n(ax) = a^n\alpha_{n,n}c_{n,n}^N x^n$.

As $\alpha_{n,n} \neq 0$, $\xi_n(ax)$ is an $n^{\text{th}}-$degree polynomial of x that is

$$\xi_n(ax) = \sum_{k=0}^{n} D_{n,k}a^k x^k \tag{3.46}$$

where $D_{n,k}$ is the constant coefficient for $(ax)^k$.

From (3.44), we have

$$\sum_{k=0}^{n} D_{n,k}x^k = \sum_{k=0}^{n} D_{n,k}a^{(k-n)}x^k. \tag{3.47}$$

By comparing the coefficient of x^k, we get

$$D_{n,k} = D_{n,k}a^{(k-n)} \tag{3.48}$$

As a can be any non-zero real constant, (3.48) will only be true if $D_{n,k} = 0$ when $k < n$. This proved the theorem. □

From Theorem 3.4.1, and the values $\kappa_{n,n} = 1$, the expression $\phi_{n,m}$ of (3.23) can be simplified as

$$\sum_{k=0}^{n} \kappa_{n,k}\tilde{t}_k^N(ax) = a^n c_{n,n}^N x^n. \tag{3.49}$$

Therefore $\phi_{n,m}$ of (3.34) can be written as

$$\phi_{n,m} = \sum_{k=0}^{n}\sum_{j=0}^{m} \kappa_{n,k}\kappa_{m,j}T_{k,j} = c_{n,n}^N c_{m,m}^N \mu_{n,m} \tag{3.50}$$

and the invariant descriptor of AST-Z has expression

$$\begin{aligned} I_{n,m}^{\langle \text{ast-Z}\rangle} &= \frac{c_{n,n}^N c_{m,m}^N (c_{0,0}^N)^{2\gamma}}{c_{n+\gamma,n+\gamma}^N c_{m+\gamma,m+\gamma}^N} \frac{\mu_{n,m}(\mu_{0,0})^{\gamma+1}}{\mu_{n+\gamma,0}\mu_{0,m+\gamma}} \\ &\qquad \gamma = 1,2,\cdots \end{aligned} \tag{3.51}$$

where $\mu_{n,m}$ denotes the geometric central moments.

The anisotropic scale invariants, AS-Z, on the other hand, can be derived using the same procedure with exception that the central moments $\mu_{p,q}$ of (3.50) is replaced by the geometric moments $m_{p,q}$.

The invariant descriptors (3.51), also show a strong correlation between AST-Z of Tchebichef moments and AST-P of Geometric moments which is given by

$$\begin{aligned} I_{n,m}^{\langle \text{ast-Z}\rangle} &= \frac{c_{n,n}^N c_{m,m}^N (c_{0,0}^N)^{2\gamma}}{c_{n+\gamma,n+\gamma}^N c_{m+\gamma,m+\gamma}^N} I_{n,m}^{\langle \text{ast-P}\rangle} \\ &\qquad n,m = 0,1,\cdots,N-1-\gamma, \quad \text{and} \quad \gamma = 1,2,\cdots. \end{aligned} \tag{3.52}$$

In the event when an image is not available, for example in image compression, only the selected orders of the Tchebichef moments are recorded, the indirect approach is not applicable. Therefore we propose an alternative approach that derives the invariants directly from the Tchebichef moments.

3.4.3 Fast Computation using New Recurrence Relation

In the process of generating the Tchebichef moments, the basis functions are not computed directly using its original definition. This is due to the complexity of the hypergeometric functions. In such case, the three terms recurrence relation is used extensively to speed-up the numerical computations. Following the same idea, the three terms recurrence relation will be deployed to simplify the expressions of invariant algorithms. The three terms recurrence relation of Tchebichef polynomial $\tilde{t}_n^N(x)$ is given by

$$\begin{aligned} \tilde{t}_n^N(x) &= (x\tilde{A}_n^N + \tilde{B}_n^N)\tilde{t}_{n-1}^N(x) + \tilde{C}_n^N\tilde{t}_{n-2}^N(x), \\ & \qquad n = 2,3,\ldots,N-1 \end{aligned} \tag{3.53}$$

and

$$\tilde{t}_0^N(x) = \frac{1}{\sqrt{N}} \tag{3.54}$$

$$\tilde{t}_1^N(x) = (x\tilde{A}_1^N + \tilde{B_1^N})\tilde{t}_0^N(x) \tag{3.55}$$

where

$$\tilde{A}_n^N = \frac{2}{n}\sqrt{\frac{4n^2-1}{N^2-n^2}} \tag{3.56}$$

$$\tilde{B}_n^N = \frac{(1-N)}{n}\sqrt{\frac{4n^2-1}{N^2-n^2}} \tag{3.57}$$

$$\tilde{C}_n^N = -\frac{(n-1)}{n}\sqrt{\frac{2n+1}{2n-3}}\sqrt{\frac{N^2-(n-1)^2}{N^2-n^2}}. \tag{3.58}$$

3.4.4 Fast Computation of Translation Invariants using Recurrence Relations Approach

The recurrence relation of Tchebichef central moments in (3.12) is given by the following theorem.

Theorem 3.4.2.

$$\begin{aligned} \tilde{t}_n^N(x+a) &= \sum_{k=0}^{n} \upsilon_{n,k}(a)\tilde{t}_k^N(x) \\ & \qquad n = 0,1,\cdots,N-1 \end{aligned} \tag{3.59}$$

if

$$\upsilon_{n,k}(a) = \begin{cases} 1, & \text{if} \quad n = k \\ \upsilon_{n-1,k-1}(a)K_{n,k}^{N,N} - \upsilon_{n-1,k}(a)a\tilde{A}_n^N + \upsilon_{n-2,k}(a)\tilde{C}_n^N & \\ \quad -\upsilon_{n-1,k+1}(a)K_{n,k+2}^{N,N}\tilde{C}_{k+2}^N, & \text{if} \quad n > k \end{cases} \tag{3.60}$$

and

$$K_{n,k}^{N,N} = \frac{\tilde{A}_n^N}{\tilde{A}_k^N}. \tag{3.61}$$

Proof. From (3.54) and (3.55), it is easily shown that

$$\tilde{t}_0^N(x+a) = \tilde{t}_0^N(x) \tag{3.62}$$

$$\tilde{t}_1^N(x+a) = \tilde{t}_1^N(x) + a\tilde{A}_1^N\tilde{t}_0^N(x) \tag{3.63}$$

where

$$\upsilon_{0,0}(a) = 1 \tag{3.64}$$

$$\upsilon_{1,1}(a) = 1 \quad \text{and,} \quad \upsilon_{1,0}(a) = a\tilde{A}_1^N. \tag{3.65}$$

By induction, suppose

$$\tilde{t}_p^N(x+a) = \sum_{k=0}^{p} \upsilon_{p,k}(a)\tilde{t}_k^N(x) \tag{3.66}$$

for $p \leq n$, we now consider $\tilde{t}_{n+1}^N(x+a)$.

From (3.53) the translated Tchebichef polynomial $\tilde{t}_{n+1}(x+a)$ has expression

$$\tilde{t}_{n+1}^N(x+a) = [(x+a)\tilde{A}_{n+1}^N + \tilde{B}_{n+1}^N]\tilde{t}_n^N(x+a) + \tilde{C}_{n+1}^N\tilde{t}_{n-1}^N(t+a). \tag{3.67}$$

By substituting with (3.66), we get

$$\begin{aligned} \tilde{t}_{n+1}^N(x+a) = {} & x\tilde{A}_{n+1}^N \sum_{k=0}^{n} \upsilon_{n,k}(a)\tilde{t}_k^N(x) + [a\tilde{A}_{n+1}^N + \tilde{B}_{n+1}^N] \sum_{k=0}^{n} \upsilon_{n,k}(a)\tilde{t}_k^N(x) + \\ & \tilde{C}_{n+1}^N \sum_{k=0}^{n-1} \upsilon_{n-1,k}(a)\tilde{t}_k^N(x). \end{aligned} \tag{3.68}$$

Consider the expression with x of (3.68), the variable x can be eliminated by reapplying the three terms recurrence relation as such

$$\begin{aligned} x\tilde{A}_{n+1}^N \sum_{k=0}^{n} \upsilon_{n,k}(a)\tilde{t}_k^N(x) = {} & \sum_{k=0}^{n} \upsilon_{n,k}(a)K_{n+1,k+1}^{N,N}[\tilde{t}_{k+1}^N(x) \\ & -\tilde{B}_{k+1}^N\tilde{t}_k^N(x) - \tilde{C}_{k+1}^N\tilde{t}_{k-1}^N(x)]. \end{aligned} \tag{3.69}$$

By substituting (3.69) back into (3.68), and some simplification steps, we thus have

$$\begin{aligned}\tilde{t}^N_{n+1}(x+a) &= \sum_{k=0}^{n+1}\Big\{\upsilon_{n,k-1}(a)K^{N,N}_{n+1,k} - a\tilde{A}^N_{n+1}\upsilon_{n,k}(a) \\ &\quad +\tilde{C}^N_{n+1}\upsilon_{n-1,k}(a) - \upsilon_{n,k+1}(a)K^{N,N}_{n+1,k+2}\tilde{C}^N_{k+2}\Big\}\tilde{t}^N_k(x). \quad (3.70)\end{aligned}$$

This proved the theorem. □

From Theorem 3.4.2, the Tchebichef central moments $T^{\langle c\rangle}_{n,m}$ can thus be effectively calculated by (3.12) and (3.60).

3.4.5 Fast Computation of Anisotropic Scale and Translation Invariants using Recurrence Relations Approach

In this subsection, recurrence relation of AST-Z and AS-Z is derived using the following theorem.

Theorem 3.4.3. *Suppose that*

$$\xi_n(x) = \sum_{k=0}^{n}\alpha_{n,k}(\bar{x})\tilde{t}^N_k(x) \quad (3.71)$$

where $\alpha_{n,k}(\bar{x})$ are functions with image centroid $\bar{x}$ as parameter and $\alpha_{n,n}(\bar{x}) \neq 0$. Then

$$\begin{aligned}\xi_n(a_1x+a_2) &= a_1^n\xi_n(x), \\ n &= 0,1,\cdots,N-1 \quad (3.72)\end{aligned}$$

if

$$\alpha_{n,k}(\bar{x}) = \begin{cases} 1, & \text{if} \quad n=k \\ \alpha_{n-1,k-1}(\bar{x})K^{N,N}_{n,k} - \alpha_{n-1,k}(\bar{x})\left[\bar{x}-\frac{(N-1)}{2}\right]\tilde{A}^N_n & \\ \quad -\alpha_{n-1,k+1}(\bar{x})K^{N,N}_{n,k+2}\tilde{C}^N_{k+2}, & \text{if} \quad n>k \end{cases} \quad (3.73)$$

and

$$K^{N,N}_{n,k} = \frac{\tilde{A}^N_n}{\tilde{A}^N_k}. \quad (3.74)$$

Proof. Suppose

$$x' = a_1x+a_2, \quad (3.75)$$

we found

$$x'-\bar{x}' = a_1(x-\bar{x}). \quad (3.76)$$

Suppose

$$\xi_0(x^{'}) = \tilde{t}_0^N(x^{'}) \tag{3.77}$$

From (3.54) we can easily deduce that

$$\xi_0(x^{'}) = \tilde{t}_0^N(x^{'}) = \frac{1}{\sqrt{N}} = \tilde{t}_0^N(x) = a_1^0 \xi_0(x) \tag{3.78}$$

which means

$$\alpha_{0,0}(\bar{x}^{'}) = \alpha_{0,0}(\bar{x}) = 1. \tag{3.79}$$

By multiplying (3.78), with $\left(x^{'} - \bar{x}^{'}\right)\tilde{A}_1^N$, and simplify the right hand side with (3.76), we get

$$\left(x^{'} - \bar{x}^{'}\right)\tilde{A}_1^N \xi_0(\bar{x}^{'}) \;\; = \;\; a\,(x-\bar{x})\tilde{A}_1^N \xi_0(x). \tag{3.80}$$

Consider the left hand side of (3.80), the variable $x^{'}$ can be eliminated using the three terms recurrence relation in (3.53). We get

$$\begin{aligned}
\left(x^{'} - \bar{x}^{'}\right)\tilde{A}_1^N \xi_0(x^{'}) &= \left(x^{'} - \bar{x}^{'}\right)\tilde{A}_1^N \alpha_{0,0}(\bar{x}^{'})\tilde{t}_0^N(x^{'}) \\
&= \alpha_{0,0}(\bar{x}^{'})\left[\left(x^{'}\tilde{A}_1^N + \tilde{B}_1^N\right)\tilde{t}_0^N(x^{'}) - \left(\bar{x}^{'}\tilde{A}_1^N + \tilde{B}_1^N\right)\tilde{t}_0^N(x^{'})\right] \\
&= \tilde{t}_1^N(x^{'}) - \left(\bar{x}^{'} - \frac{(N-1)}{2}\right)\tilde{A}_1^N \tilde{t}_0(x^{'}) \\
&= \xi_1(x^{'}).
\end{aligned} \tag{3.81}$$

From this we obtain,

$$\alpha_{1,1}(\bar{x}^{'}) = 1, \quad \text{and} \quad \alpha_{1,0}(\bar{x}^{'}) = -\left(\bar{x}^{'} - \frac{(N-1)}{2}\right)\tilde{A}_1^N. \tag{3.82}$$

When the similar procedure is applied to right hand side of (3.80) , we have

$$\begin{aligned}
a\,(x-\bar{x})\tilde{A}_1^N \xi_0(x) &= a\left[\tilde{t}_1^N(x) - \left(\bar{x}\tilde{A}_1^N + \tilde{B}_1^N\right)\tilde{t}_0^N(x)\right] \\
&= a\xi_1(x)
\end{aligned} \tag{3.83}$$

and

$$\alpha_{1,1}(\bar{x}) = 1 \quad \text{and} \quad \alpha_{1,0}(\bar{x}) = -\left(\bar{x} - \frac{(N-1)}{2}\right)\tilde{A}_1^N. \tag{3.84}$$

Suppose that $\xi_k(\bar{x}^{'}) = a^k \xi_k(x)$ for $k \leq n$, we now consider $\xi_{n+1}(\bar{x}^{'})$.

Assuming

$$\xi_{n+1}(\bar{x}^{'}) \;=\; \left(x^{'} - \bar{x}^{'}\right) \tilde{A}^N_{n+1} \xi_n(\bar{x}^{'}). \tag{3.85}$$

From the induction hypothesis, we have

$$\left(x^{'} - \bar{x}^{'}\right) \tilde{A}^N_{n+1} \xi_n(\bar{x}^{'}) \;=\; a^{n+1}\,(x - \bar{x})\, \tilde{A}^N_{n+1} \xi_n(\bar{x}). \tag{3.86}$$

Consider the left hand side of (3.86), we have

$$\begin{aligned}\left(x^{'} - \bar{x}^{'}\right) \tilde{A}^N_{n+1} \xi_n(\bar{x}^{'}) \;&=\; \sum_{k=0}^{n} \alpha_{n,k}(\bar{x}^{'}) K^{N,N}_{n+1,k+1} x^{'} \tilde{A}^N_{k+1} \tilde{t}_k(x^{'}) \\ &\quad - \sum_{k=0}^{n} \alpha_{n,k}(\bar{x}^{'}) \bar{x}^{'} \tilde{A}^N_{n+1} \tilde{t}_k(x^{'}).\end{aligned} \tag{3.87}$$

The variable $x^{'}$ can be eliminated by using (3.53). Therefore we get

$$\begin{aligned}\xi_{n+1}(\bar{x}^{'}) \;=\; \sum_{k=0}^{n+1} \Big[&\alpha_{n,k-1}(\bar{x}^{'}) K^{N,N}_{n+1,k} - \alpha_{n,k}(\bar{x}^{'}) K^{N,N}_{n+1,k+1} B^N_{k+1} \\ &- \alpha_{n,k+1}(\bar{x}^{'}) K^{N,N}_{n+1,k+2} \tilde{C}^N_{k+2} - \alpha_{n,k}(\bar{x}^{'}) \bar{x}^{'} \tilde{A}^N_{n+1} \Big] \tilde{t}_k(x^{'}).\end{aligned} \tag{3.88}$$

Similarly for the right hand side of (3.86),

$$\begin{aligned}a^{n+1}\,(x - \bar{x})\, \tilde{A}^N_{n+1} \xi_n(\bar{x}) \;=\; a^{n+1} \sum_{k=0}^{n+1} \Big[&\alpha_{n,k-1}(\bar{x}) K^{N,N}_{n+1,k} - \alpha_{n,k}(\bar{x}) K^{N,N}_{n+1,k+1} B^N_{k+1} \\ &- \alpha_{n,k+1}(\bar{x}) K^{N,N}_{n+1,k+2} \tilde{C}^N_{k+2} - \alpha_{n,k}(\bar{x}) \bar{x} \tilde{A}^N_{n+1} \Big] \tilde{t}_k(x)\end{aligned} \tag{3.89}$$

and this proved the recurrence relation (3.73). □

Suppose

$$\begin{aligned}\phi_{n,m} \;&=\; \sum_{x=0}^{N-1} \sum_{y=0}^{N-1} \xi_n(x) \xi_m(y) f(x,y), \\ &=\; \sum_{k=0}^{n} \sum_{j=0}^{m} \alpha_{n,k}(\bar{x}) \alpha_{m,j}(\bar{y}) T_{n,m}.\end{aligned} \tag{3.90}$$

The transformed moments and the original moments can be established as

$$\begin{aligned}\phi^{'}_{n,m} \;&=\; |a_1 b_1| \sum_{x=0}^{N-1} \sum_{y=0}^{N-1} \xi_n(a_1 x + a_2) \xi_m(b_1 y + b_2) f(x,y), \\ &=\; a_1^{n+1} b_1^{m+1} \sum_{x=0}^{N-1} \sum_{y=0}^{N-1} \xi_n(x) \xi_m(y) f(x,y), \\ &=\; a_1^{n+1} b_1^{m+1} \phi_{n,m}\end{aligned} \tag{3.91}$$

By the cancellation process using (3.36), we thus get AST-Z. On the other hand, when $\bar{x} = \bar{y} = 0$ in (3.90) , the features computed by (3.36) are AS-Z.

3.4.6 Invariants with Skew Parameters

As shown in (3.51), AST-Z works well for non-symmetric images. However for symmetric images, large portion of odd order AST-Z descriptors will have zero values which may cause difficulty in classification. To overcome this problem, additional skew parameters (denoted as w_x and w_y) are added to $\upsilon_{n,n-k}$ and $\upsilon_{m,m-j}$ of (3.12). In our implementation, we let

$$w_x = \text{sign}(\mu_{3,0})\varpi_x\sqrt{\frac{\mu_{2,0}}{\mu_{0,0}}}, \quad \text{and} \quad w_y = \text{sign}(\mu_{0,3})\varpi_y\sqrt{\frac{\mu_{0,2}}{\mu_{0,0}}}. \tag{3.92}$$

where $\mu_{k,j}$ denotes the central moment, ϖ_x and ϖ_y are skew factors in direction of $x-$axis and $y-$axis, respectively. The skew parameters w_x and w_y are designed such that (3.51) preserves the AST-invariance and gives non-zero values for all the odd-orders of AST-Z descriptors of symmetrical and non-symmetrical images.

3.5 Experimental Results

Several experiments were carried out to validate the accuracy and numerical performance of the proposed method on AST-Z. Binary patterns that consist of English letters, symbols, numbers and Chinese letters, varying from simple to complex patterns, with and without symmetries are used. Similar to Zhu et al. (2007c), and Chong et al. (2004), the accuracy of features are measured by relative standard deviation (RSD) with percentage spread i.e.

$$\text{RSD}(\%) = \frac{\sigma}{|\mu|}\% \tag{3.93}$$

where σ and μ denote the standard deviation and mean of the Tchebichef features, respectively.

3.5.1 Experiment on Accuracy of Invariant Descriptors

In this section we evaluate the accuracy of invariant descriptors T-Z, AS-Z and AST-Z using the proposed algorithms. Sets of patterns in different size, complexity, symmetric and non-symmetric, in different degree of deformations are used to evaluate the accuracy of new proposed algorithms. When large set of images exhibit similar performance, for simplicity, only selected images are shown to reflect the overall performance of the features. In addition, the proposed algorithms are just a new way to compute the invariants

descriptors by Zhu et al. (2007c). The result is therefore completely identical to original formulation. Thus only one set of result is shown in each experiment.

First of all, we evaluate the translation invariants (T-Z). As the accuracy performance on various images are identical, only the results of the following two patterns are shown: a Chinese character "和" and an English "A'. The Chinese letter represents group of non-symmetric images and the latter represents group of symmetric images, The Chinese character "和" is with size of 40×40 pixels, is shifted up and down, left and right arbitrary, as well as diagonally in relative to center of image space $S_2(50)$ by a single pixel value (note that $S_2(N) = \{(x,y) \mid x,y = 0,1,\cdots,N-1\}$). As shown in Table 3.1, Tchebichef central moments remain unchanged for all the translations and RSD is zero. On the other hand, the symmetric letter "A" of size 40×40 pixels is transformed under different translation factors relative to center of image space $S_2(80)$. As shown in Table 3.2, unlike the geometric central moments, Tchebichef central moments are non-zero for most of the odd order moments. This can be explained by the fact that Tchebichef polynomials are not symmetric at the centroid of image but at the middle of image space instead. By having image's centroid transformed to it origin, will move the image away from the middle of image space and the odd order translation descriptors will therefore be non-zero.

In testing the accuracy of AS-Z, the results shown in Table 3.3. In this experiment, translation descriptors are not involved. The scale factors are randomly selected between 0.6 to 2.6. As AS-Z and AST-Z are similar to AST-P, where the odd degree of central moments are usually small. Therefore the coefficient γ is set to 2 to ensure the numerical stability in cancellation process of (3.36). It is shown that, the values of invariants descriptors almost remain unchanged under different non-uniform scale transformation.

In the third experiment, the accuracy of AST-Z are evaluated using the patterns from the four distinct groups of characters i.e. numbers, alphabets, symbols and Chinese characters. For simplicity, one image is selected from each group to represent the overall performance on AST-Z. The patterns are 80×80 pixels in image space $S_2(250)$. As shown in Table 3.4, each character is non-uniformly expanded, contracted or reflected and then translated from the middle of domain. The results are shown in Table 3.5 and Table 3.6. In Table 3.5, the skew coefficient w_x and w_y are set to zero. There are large fluctuation

in accuracy of invariant features especially on the odd-order moments. This can be explained by the fact that the moments $\phi_{n,m}$ of (3.90) are equivalent to central moment of geometric moments. It is well known that the odd order central moments are usually small even for non-symmetric images. As a result, they are vulnerable to discretization errors. To overcome this problem, the skew parameters are introduced to shift the centroid away from the origin to avoid the errors caused by cancellation between small moment values. As shown in Table 3.6, the accuracy improved significantly when the skew parameters ϖ_x and ϖ_y are set to 13 and 10, respectively. Generally, the accuracy of AST-Z can be improved with other skew parameter values. The skew parameters above are selected so that the values of moment invariants are smaller than unity. However note that by shifting too much away from centroid, it will also reduce the within class separation. Thus compromise the discriminative power of the features in classification.

Table 3.1: Selected orders of translation invariant descriptors of Tchebichef moments for a Chinese character

Image	Translation	$I_{0,0}^{\langle \text{t-Z} \rangle}$	$I_{2,0}^{\langle \text{t-Z} \rangle}$	$I_{1,1}^{\langle \text{t-Z} \rangle}$	$I_{0,2}^{\langle \text{t-Z} \rangle}$	$I_{3,0}^{\langle \text{t-Z} \rangle}$	$I_{2,1}^{\langle \text{t-Z} \rangle}$	$I_{1,2}^{\langle \text{t-Z} \rangle}$	$I_{0,3}^{\langle \text{t-Z} \rangle}$
40×40	$(0,0)$	12.456	33.475	35.209	31.432	-69.450	-53.799	-51.861	-58.902
	$(1,1)$	12.456	33.475	35.209	31.432	-69.450	-53.799	-51.861	-58.902
	$(-1,1)$	12.456	33.475	35.209	31.432	-69.450	-53.799	-51.861	-58.902
	$(1,-1)$	12.456	33.475	35.209	31.432	-69.450	-53.799	-51.861	-58.902
RSD(%)		0	0	0	0	0	0	0	0

Table 3.2: Selected orders of translation invariant descriptors of Tchebichef moments for an English letter

Image	Translation	$I_{0,0}^{\langle \text{t-Z} \rangle}$	$I_{2,0}^{\langle \text{t-Z} \rangle}$	$I_{1,1}^{\langle \text{t-Z} \rangle}$	$I_{0,2}^{\langle \text{t-Z} \rangle}$	$I_{3,0}^{\langle \text{t-Z} \rangle}$	$I_{2,1}^{\langle \text{t-Z} \rangle}$	$I_{1,2}^{\langle \text{t-Z} \rangle}$	$I_{0,3}^{\langle \text{t-Z} \rangle}$
40×40	$(-2,1)$	7.290	17.203	21.330	17.471	-26.674	-28.934	-29.884	-28.437
	$(-7,13)$	7.290	17.203	21.331	17.471	-26.674	-28.934	-29.884	-28.437
	$(10,11)$	7.290	17.203	21.331	17.471	-26.674	-28.934	-29.884	-28.437
	$(12,-18)$	7.290	17.203	21.331	17.471	-26.674	-28.934	-29.884	-28.437
	$(-13,-14)$	7.290	17.203	21.331	17.471	-26.674	-28.934	-29.884	-28.437
	$(-15,3)$	7.290	17.203	21.331	17.471	-26.674	-28.934	-29.884	-28.437
RSD(%)		0	0	0	0	0	0	0	0

Table 3.3: The anisotropic scale invariant descriptors of Tchebichef moments for a non-uniformly scaled letter

Image 70×70	Scale	$I_{0,0}^{\text{as-Z}}$	$I_{2,0}^{\langle\text{as-Z}\rangle}$	$I_{1,1}^{\langle\text{as-Z}\rangle}$	$I_{0,2}^{\langle\text{as-Z}\rangle}$	$I_{3,0}^{\langle\text{as-Z}\rangle}$	$I_{2,1}^{\langle\text{as-Z}\rangle}$	$I_{1,2}^{\langle\text{as-Z}\rangle}$	$I_{0,3}^{\langle\text{as-Z}\rangle}$
	Original	538.788	274.951	166.342	216.581	225.835	110.087	125.261	187.903
	$a = 0.6, b = 1.1$	541.150	276.436	167.480	217.664	227.219	111.146	126.143	188.787
	$a = 1, b = 0.7$	545.470	278.311	167.359	218.291	228.988	110.644	125.853	189.309
	$a = 0.9, b = 2.3$	538.444	274.506	166.941	216.904	225.325	110.689	125.638	188.128
	$a = 1.2, b = 2.2$	537.398	274.103	166.648	216.494	224.983	110.477	125.423	187.794
	$a = 2.5, b = 0.9$	539.397	275.345	166.334	216.622	226.227	110.027	125.193	187.932
	$a = 0.8, b = 1.5$	540.173	275.446	167.102	217.253	226.219	110.754	125.750	188.408
	$a = 2.6, b = 2.4$	536.070	273.519	166.317	216.001	224.471	110.239	125.153	187.382
RSD(%)		0.527	0.544	0.284	0.337	0.629	0.342	0.282	0.325
Average RSD(%)		0.409							

Table 3.4: Image used in experiment of anisotropic scale and translation invariants (AST-Z)

(a_1, b_1)	Original	(2.4, -1.9)	(-1.9, 1.3)	(-1.6, -1.7)	(1.5, 2.2)	(1.1, -1.6)	(-0.7, 2.5)	(-0.5, 1.9)	(-0.6, -0.9)	(0.5, 0.5)
(a_2, b_2)	–	(-1, 2)	(5, -5)	(-4, 7)	(3, -4)	(6,-3)	(-3, 1)	(2, -1)	(5, -4)	(0,2)
	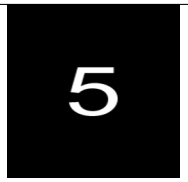		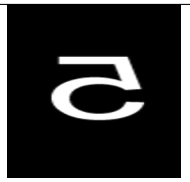				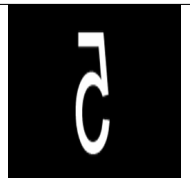	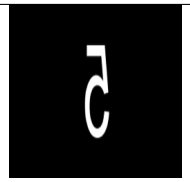	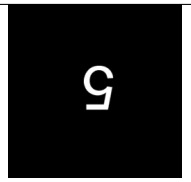	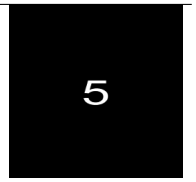
Image	im_5-1	im_5-2	im_5-3	im_5-4	im_5-5	im_5-6	im_5-7	im_5-8	im_5-9	im_5-10
	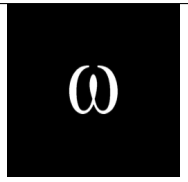		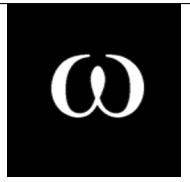	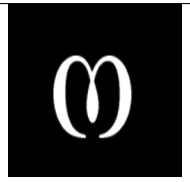	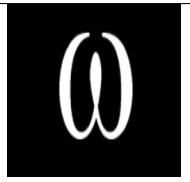	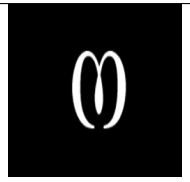	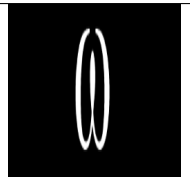	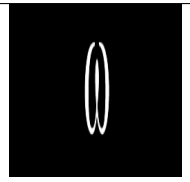	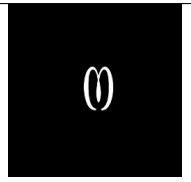	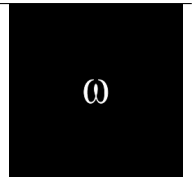
image	im_omega-1	im_omega-2	im_omega-3	im_omega-4	im_omega-5	im_omega-6	im_omega-7	im_omega-8	im_omega-9	im_omega-10
						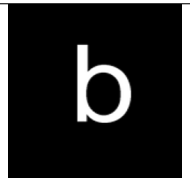	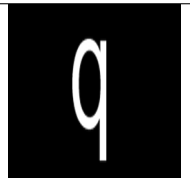	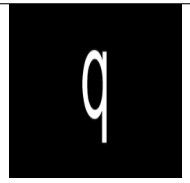	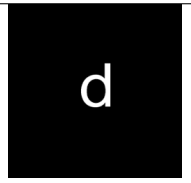	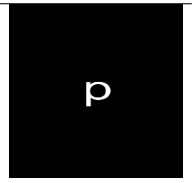
image	im_p-1	im_p-2	im_p-3	im_p-4	im_p-5	im_p-6	im_p-7	im_p-8	im_p-9	im_p-10
							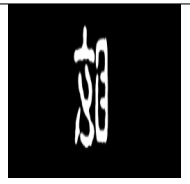	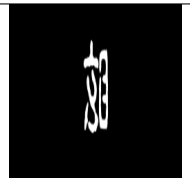		
image	im_xuan-1	im_xuan-2	im_xuan-3	im_xuan-4	im_xuan-5	im_xuan-6	im_xuan-7	im_xuan-8	im_xuan-9	im_xuan-10

Table 3.5: Selected orders of Tchebichef moments for anisotropic scale and translation invariants with skew factors $(\varpi_x, \varpi_y) = (0, 0)$

Image 70×70	$I_{0,0}^{\langle \text{ast-Z} \rangle}$	$I_{2,0}^{\langle \text{ast-Z} \rangle}$	$I_{1,1}^{\langle \text{ast-Z} \rangle}$	$I_{0,2}^{\langle \text{ast-Z} \rangle}$	$I_{3,0}^{\langle \text{ast-Z} \rangle}$	$I_{2,1}^{\langle \text{ast-Z} \rangle}$	$I_{1,2}^{\langle \text{ast-Z} \rangle}$	$I_{0,3}^{\langle \text{ast-Z} \rangle}$
im_5-1	7818	4225	498801	3942	1844	23548	−1965	6877
im_5-2	7846	4238	467228	3957	1857	22432	−1878	5742
im_5-3	7850	4239	462480	3959	1857	22343	−1857	5527
im_5-4	7845	4237	468190	3956	1859	22570	−1860	5799
im_5-5	7850	4239	463801	3959	1854	22318	−1873	5563
im_5-6	7847	4238	457405	3958	1859	22048	−1865	5440
im_5-7	7844	4237	455896	3956	1877	21917	−1819	5637
im_5-8	7832	4230	418475	3953	1886	20796	−1713	5210
im_5-9	7867	4248	524693	3967	1835	25355	−1930	6513
im_5-10	7914	4262	352538	4004	1891	17531	−1647	3666
RSD(%)	0.325	0.236	10.064	0.411	0.959	9.023	5.169	15.126
Average RSD(%) = 5.164								
im_omega-1	6265	3549	−93733	2803	1550	−476	1145	334
im_omega-2	6286	3560	−99234	2810	1552	−621	1039	346
im_omega-3	6286	3560	−100466	2810	1550	−671	1034	346
im_omega-4	6284	3558	−104863	2809	1539	−688	937	348
im_omega-5	6286	3560	−92176	2810	1560	−678	1093	348
im_omega-6	6298	3566	−110577	2813	1541	−611	989	350
im_omega-7	6241	3532	−159919	2796	1484	−890	619	321
im_omega-8	6281	3558	−159923	2811	1434	−521	419	349
im_omega-9	6330	3586	−65297	2819	1594	−899	1271	361
im_omega-10	6296	3563	−128184	2822	1412	0	358	374
RSD(%)	0.363	0.379	26.935	0.266	3.860	41.710	35.201	4.000
Average RSD(%) = 14.089								
im_p-1	7628	4267	−32386	3535	2009	−1013	−2235	884
im_p-2	7600	4259	−32602	3525	2004	−1011	−2237	878
im_p-3	7609	4261	−32492	3528	2006	−1006	−2233	880
im_p-4	7601	4259	−32533	3525	2005	−1015	−2237	879
im_p-5	7594	4258	−32649	3522	2003	−990	−2246	878
im_p-6	7606	4260	−32456	3526	2006	−1016	−2236	880
im_p-7	7667	4282	−32141	3554	2022	−1065	−2203	889
im_p-8	7417	4217	−33443	3434	1955	−702	−2439	858
im_p-9	7620	4270	−32525	3527	2007	−1026	−2259	881
im_p-10	7415	4204	−33057	3421	1956	−949	−2413	848
RSD(%)	1.146	0.565	1.125	1.265	1.134	10.391	3.596	1.432
Average RSD(%) = 2.582								
im_xuan-1	10336	5026	−126509	5239	−469	−141	−50852	1822
im_xuan-2	10414	5062	−148682	5274	−385	−155	−61908	1856
im_xuan-3	10411	5060	−158886	5273	−372	−150	−63474	1848
im_xuan-4	10415	5063	−162141	5274	−365	−181	−64907	1855
im_xuan-5	10414	5062	−158712	5274	−366	−146	−64470	1859
im_xuan-6	10416	5061	−138873	5276	−377	−142	−63050	1861
im_xuan-7	10415	5064	−224848	5276	−234	158	−93552	1857
im_xuan-8	10506	5103	−302429	5312	−224	−64	−105282	1910
im_xuan-9	10343	5017	−11384	5261	−687	58	−35650	1747
im_xuan-10	10540	5116	−262956	5327	−362	41	−67209	1890
RSD(%)	0.600	0.588	47.338	0.465	33.443	161.474	29.329	2.340
Average RSD(%) = 34.447								

Table 3.6: Selected orders of Tchebichef moments for anisotropic scale and translation invariants with skew factors $(\varpi_x, \varpi_y) = (13, 10)$

Image 70×70	$I_{0,0}^{\text{ast-Z}}$	$I_{2,0}^{\text{ast-Z}}$	$I_{1,1}^{\text{ast-Z}}$	$I_{0,2}^{\text{ast-Z}}$	$I_{3,0}^{\text{ast-Z}}$	$I_{2,1}^{\text{ast-Z}}$	$I_{1,2}^{\text{ast-Z}}$	$I_{0,3}^{\text{ast-Z}}$
im_5-1	0.455	0.381	0.341	0.375	0.374	0.329	0.326	0.365
im_5-2	0.457	0.383	0.342	0.377	0.375	0.330	0.327	0.367
im_5-3	0.457	0.383	0.342	0.377	0.375	0.330	0.328	0.367
im_5-4	0.457	0.383	0.342	0.377	0.375	0.330	0.327	0.367
im_5-5	0.457	0.383	0.342	0.377	0.375	0.330	0.328	0.367
im_5-6	0.457	0.383	0.342	0.377	0.375	0.330	0.328	0.367
im_5-7	0.457	0.383	0.342	0.377	0.375	0.330	0.327	0.367
im_5-8	0.456	0.382	0.341	0.376	0.374	0.329	0.327	0.366
im_5-9	0.458	0.384	0.343	0.378	0.376	0.331	0.328	0.368
im_5-10	0.461	0.386	0.345	0.380	0.378	0.333	0.330	0.37
RSD(%)	0.324	0.324	0.323	0.324	0.325	0.323	0.322	0.323
Average RSD(%) = 0.324								
im_omega-1	0.365	0.306	0.273	0.301	0.299	0.263	0.261	0.293
im_omega-2	0.366	0.307	0.274	0.302	0.300	0.264	0.262	0.294
im_omega-3	0.366	0.307	0.274	0.302	0.300	0.264	0.262	0.294
im_omega-4	0.366	0.306	0.274	0.302	0.300	0.264	0.262	0.294
im_omega-5	0.366	0.307	0.274	0.302	0.300	0.264	0.262	0.294
im_omega-6	0.367	0.307	0.274	0.302	0.301	0.265	0.263	0.294
im_omega-7	0.363	0.304	0.272	0.300	0.298	0.262	0.260	0.292
im_omega-8	0.366	0.306	0.273	0.302	0.300	0.264	0.262	0.293
im_omega-9	0.369	0.309	0.276	0.304	0.303	0.266	0.264	0.296
im_omega-10	0.367	0.307	0.274	0.302	0.301	0.264	0.262	0.294
RSD(%)	0.363	0.363	0.363	0.363	0.363	0.363	0.363	0.363
Average RSD(%) = 0.363								
im_p-1	0.444	0.372	0.331	0.366	0.364	0.319	0.317	0.356
im_p-2	0.443	0.370	0.330	0.365	0.363	0.318	0.316	0.355
im_p-3	0.443	0.371	0.331	0.365	0.363	0.318	0.316	0.355
im_p-4	0.443	0.370	0.330	0.365	0.363	0.318	0.316	0.355
im_p-5	0.442	0.370	0.330	0.365	0.362	0.318	0.315	0.355
im_p-6	0.443	0.371	0.330	0.365	0.363	0.318	0.316	0.355
im_p-7	0.447	0.374	0.333	0.368	0.366	0.321	0.318	0.358
im_p-8	0.432	0.362	0.322	0.356	0.354	0.310	0.308	0.346
im_p-9	0.444	0.371	0.331	0.366	0.364	0.319	0.316	0.356
im_p-10	0.432	0.361	0.322	0.356	0.354	0.310	0.308	0.346
RSD(%)	1.146	1.144	1.145	1.146	1.142	1.143	1.146	1.147
Average RSD(%) = 1.145								
im_xuan-1	0.602	0.504	0.450	0.496	0.494	0.434	0.431	0.483
im_xuan-2	0.607	0.508	0.453	0.500	0.498	0.437	0.434	0.487
im_xuan-3	0.606	0.508	0.453	0.500	0.498	0.437	0.434	0.486
im_xuan-4	0.607	0.508	0.453	0.500	0.498	0.437	0.434	0.487
im_xuan-5	0.607	0.508	0.453	0.500	0.498	0.437	0.434	0.487
im_xuan-6	0.607	0.508	0.453	0.500	0.498	0.437	0.434	0.487
im_xuan-7	0.607	0.508	0.453	0.500	0.498	0.437	0.434	0.487
im_xuan-8	0.612	0.512	0.457	0.505	0.502	0.441	0.438	0.491
im_xuan-9	0.602	0.504	0.450	0.497	0.494	0.434	0.431	0.483
im_xuan-10	0.614	0.514	0.459	0.506	0.504	0.443	0.439	0.492
RSD(%)	0.600	0.600	0.599	0.599	0.600	0.598	0.597	0.598
Average RSD(%) = 0.599								

3.5.2 Experiment on Numerical Efficiency

The computational efficiency on AST-Z and T-Z are shown in Table 3.7 and Table 3.8, respectively. Here AST-Z(1) and T-Z(1) denote the invariant descriptors with (3.12) to compute the translation invariants . AST-Z(2) and T-Z(2) denote the invariants descriptors with (3.14) for the translation invariants. AST-Z(R) and T-Z(R) denote the invariants descriptors computed by the proposed method using the new proposed recurrence relations. As the algorithms above are based on Tchebichef moments, extra time is required to generate the Tchebichef moments (see column 4). AST-Z(ID) and T-Z(ID) on the other hand denote the invariants of AST-Z and T-Z computed using the indirect approach, respectively. In this method the invariants are computed from geometric central moments. The generation time of Tchebichef moments is thus not required. The application was developed by using Matlab 2011b on a PC with Intel i3 550, 3GB of RAM and 3.2GHz processor. In this experiment, images with size 50×50, 100×100, 150×150, and 200×200 were used to generate invariant features with orders of 10, 20, 30 and 40. The experiment was repeated 200 times and the average CPU elapse times in units of millisecond were recorded.

With AST-Z(R), the invariants generation time of AST-Z improved by 37.8 and 38.2 times when compared with AST-Z(1) and AST-Z(2), respectively (see the average performance on column 5, 7 and 9 of Table 3.7). The significant improvement can be explained by the simplicity of the new proposed recurrence relations, and the complexity of algorithms, and the sequential computation of invariant descriptors by Zhu et al. (2007c). The algorithm AST-Z(R) also slightly faster than AST-Z(ID) (see column 3 and 6) despite the simplicity of the indirect expression. The performance of AST-Z(1) and AST-Z(2) are nearly identical. This indicate the complexity of the two approach are nearly identical.

The invariant generation times of AST-Z(R), AST-Z(1), and AST-Z(2), increase proportionally to the order of moment invariants and are less sensitive to the size of images. On the other hand moment generation times increase proportionally to both image size and the order of moments. This can be easily explained by the definition of discrete Tchebichef moments and the construction of the invariant functions.

Computation efficiency on translation invariant descriptors are showed in Table 3.8. As shown in the table, the proposed methods exhibit similar trends on preceding table

when they are compared with original algorithms by Zhu et al. (2007c).

3.6 Conclusion

In this chapter, two fast computation algorithms for the anisotropic scale and translation Tchebichef moment invariants of Zhu et al. (2007c) have been derived. The first algorithm indirectly computes the invariant descriptors using geometric moments. The second algorithm derives the invariants from Tchebichef moments using new set of recurrence relations. As the proposed recurrence relations are simplified using the properties of orthogonal moments, it is much simpler and able to outperform existing algorithms by large margin.

Table 3.7: Comparison of CPU elapse time (ms) for AST descriptors

Image Size	Order of descriptors	AST-Z(ID) (ms)	Moments generation time (ms)	AST-Z(R)		AST-Z(1)		AST-Z(2)	
				Invariant generation time (ms)	Total time (ms)	Invariant generation time (ms)	Total time (ms)	Invariant generation time (ms)	Total time (ms)
(50×50)	10	11.268	12.965	0.308	13.273	10.195	23.160	5.315	18.280
	20	30.755	29.982	1.236	31.218	53.380	83.362	34.651	64.634
	30	60.760	59.301	3.897	63.198	161.862	221.163	139.731	199.032
	40	102.506	100.225	9.569	109.795	365.742	465.967	416.400	516.625
(100×100)	10	42.843	36.620	0.295	36.915	10.246	46.866	5.340	41.960
	20	117.066	111.040	1.253	112.293	53.760	164.800	35.111	146.152
	30	233.137	225.079	3.896	228.975	162.109	387.188	139.277	364.356
	40	387.324	379.478	9.556	389.034	368.271	747.748	417.168	796.646
(150×150)	10	94.734	80.511	0.323	80.834	10.344	90.855	5.463	85.974
	20	261.233	243.899	1.281	245.180	53.978	297.877	36.315	280.214
	30	514.502	495.019	4.324	499.342	159.744	654.763	140.082	635.100
	40	859.382	915.599	9.618	925.218	366.359	1281.959	416.192	1331.792
(200×200)	10	169.721	141.876	0.736	142.612	11.336	153.212	6.006	147.882
	20	465.310	431.031	1.796	432.827	54.018	485.049	34.966	465.997
	30	915.908	881.486	4.446	885.931	159.814	1041.300	141.314	1022.800
	40	1527.950	1473.562	10.109	1483.671	365.268	1838.830	416.541	1890.103
Average		362.150	351.105	3.915	355.020	147.902	499.006	149.367	500.472

Table 3.8: Comparison of CPU elapse Time (ms) for translation descriptors

				T-Z(R)		T-Z(1)		T-Z(2)	
Image Size	Order of descriptors	T-Z(ID) (ms)	Moments generation time (ms)	Invariant generation time (ms)	Total time (ms)	Invariant generation time (ms)	Total time (ms)	Invariant generation time (ms)	Total time (ms)
(50×50)	10	8.791	10.46	0.191	10.651	6.49	16.95	3.196	13.657
	20	27.035	24.834	0.886	25.72	42.646	67.48	25.17	50.004
	30	59.142	51.467	2.995	54.462	136.756	188.224	106.772	158.24
	40	100.823	89.175	7.685	96.86	322.102	411.277	337.388	426.564
(100×100)	10	33.043	26.354	0.207	26.561	6.567	32.921	3.264	29.618
	20	101.682	91.244	0.9	92.144	43.811	135.055	24.398	115.642
	30	209.417	196.464	2.991	199.456	135.405	331.87	106.998	303.462
	40	361.62	339.511	7.691	347.202	322.039	661.55	336.435	675.947
(150×150)	10	74.106	57.897	0.236	58.132	6.696	64.592	3.403	61.3
	20	221.2	202.482	0.928	203.41	42.09	244.572	24.517	226.999
	30	462.907	434.498	3.022	437.519	137.489	571.987	107.241	541.738
	40	807.389	752.873	7.73	760.603	322.106	1074.979	337.747	1090.62
(200×200)	10	130.775	102.388	0.27	102.658	7.795	110.183	3.577	105.965
	20	392.912	411.664	0.959	412.623	42.699	454.363	24.736	436.4
	30	816.528	768.909	3.05	771.959	135.701	904.609	107.582	876.49
	40	1401.078	1389.016	8.194	1397.21	321.931	1710.947	338.117	1727.133
Average		325.528	309.327	2.996	312.323	127.02	436.347	118.159	427.486

CHAPTER 4

ANISOTROPIC SCALE AND TRANSLATION TCHEBICHEF MOMENT INVARIANTS USING IMAGE NORMALIZATION TECHNIQUE

Image normalization is an effective technique in deriving invariants for classification systems. In this chapter, AST invariants based on moment normalization is studied. A new set of recurrence relations is proposed for fast computation of AST invariants by this approach. To enhance the features discriminative power, the Tchebichef polynomials' centre of symmetry is selected as centroid of canonical images. In addition, three new scale normalization schemes based on Tchebichef moments have been proposed to further improve the classification performance. An empirical study showed significant improvement in the numerical computation and classification accuracy with proposed method.

4.1 Introduction

In image normalization, images are mapped to a standard form known as the canonical form that possess a set of predefined moment values. The first significant paper to use moment normalization on discrete orthogonal moments is proposed by Goh et al. (2009). In this paper, the AST-invariants were proposed for unweighted Hahn moments. The scale coefficients were derived based on radius of gyration from geometric moments. On the other hand, Liu et al. (2011) proposed anisotropic scale invariants for Tchebichef moments. Together with the Tchebichef central moments (Zhu et al., 2007c), we obtain the AST invariants. The latter approach uses second order Tchebichef moments to determine the scale coefficients. In Section 4.2 both of the above mentioned methods have been reviewed. In Section 4.3, new AST-invariants using image normalization approach have been proposed. The proposed invariants consist of recurrence relations for fast computation and new sets of normalization schemes for better classification performance. Section 4.4 gives empirical verification to support the theoretical frameworks. Section 4.5 concludes the chapter.

4.2 Preliminaries for the Proposed Invariants

We first review some expressions that will be used in the later sections.

Suppose $\tilde{t}_n^N(x)$ denotes the Tchebichef polynomial and $c_{n,k}^N$ are coefficients of the corresponding polynomials

$$t_n^N(x) = \sum_{k=0}^{n} c_{n,k}^N x^k, \tag{4.1}$$

and $d_{k,n}^N$ denote the coefficients of Tchebichef polynomials such that

$$\begin{aligned} x^n &= \sum_{j=0}^{n} d_{n,j}^N \tilde{t}_k^N(x), \\ & \qquad x, n = 0, 1, \cdots N-1. \end{aligned} \tag{4.2}$$

From the orthogonality property of Tchebichef polynomials $\tilde{t}_n^N(x)$, the coefficients $c_{n,k}^N$ and $d_{k,m}^N$ have the following relation

$$\sum_{k=m}^{n} c_{n,k}^N d_{k,m}^N = \delta_{n,m} \tag{4.3}$$

where $\delta_{n,m}$ denotes the Kronecker's delta that returns unity when $n = m$ and zero otherwise.

The three terms recurrence relation of Tchebichef polynomials, $\tilde{t}_n^N(x)$, can be expressed as

$$\begin{aligned} \tilde{t}_n^N(x) &= (x\tilde{A}_n^N + \tilde{B}_n^N)\tilde{t}_{n-1}^N(x) + \tilde{C}_n^N \tilde{t}_{n-2}^N(x), \\ & \qquad n = 2, 3, \ldots, N-1 \end{aligned} \tag{4.4}$$

and

$$\tilde{t}_0^N(x) = \frac{1}{\sqrt{N}} \tag{4.5}$$

$$\tilde{t}_1^N(x) = (x\tilde{A}_1^N + \tilde{B_1^N})\tilde{t}_0^N(x) \tag{4.6}$$

where

$$\tilde{A}_n^N = \frac{2}{n}\sqrt{\frac{4n^2-1}{N^2-n^2}} \tag{4.7}$$

$$\tilde{B}_n^N = \frac{(1-N)}{n}\sqrt{\frac{4n^2-1}{N^2-n^2}} \tag{4.8}$$

$$\tilde{C}_n^N = -\frac{(n-1)}{n}\sqrt{\frac{2n+1}{2n-3}}\sqrt{\frac{N^2-(n-1)^2}{N^2-n^2}}. \tag{4.9}$$

4.2.1 Anisotropic Scale and Translation Tchebichef Moment Invariants of Goh et. al.

Let the anisotropic scale and translation Tchebichef moment invariants of Goh et al. (2009) (AST-G) be defined as

$$I_{n,m}^{\langle \text{ast-G} \rangle} = |\hat{a}_1 \hat{b}_1| \sum_{x=0}^{N-1} \sum_{y=0}^{N-1} \tilde{t}_n^N(\hat{a}_1 x + \hat{a}_2) \tilde{t}_m^N(\hat{b}_1 y + \hat{b}_2) f(x,y). \tag{4.10}$$

From (4.1), we have

$$I_{n,m}^{\langle \text{ast-G} \rangle} = |\hat{a}_1 \hat{b}_1| \sum_{x=0}^{N-1} \sum_{y=0}^{N-1} \sum_{k=0}^{n} c_{n,n-k}^N (\hat{a}_1 x + \hat{a}_2)^{n-k} \sum_{j=0}^{m} c_{m,m-j}^N (\hat{b}_1 y + \hat{b}_2)^{m-j} f(x,y). \tag{4.11}$$

By performing binomial expansion, and grouping of the coefficients for x^{n-k} and y^{m-j}, the invariant moment becomes

$$I_{n,m}^{\langle \text{ast-G} \rangle} = |\hat{a}_1 \hat{b}_1| \sum_{x=0}^{N-1} \sum_{y=0}^{N-1} \sum_{k=0}^{n} \beta_{n,n-k}^{(1)} x^{n-k} \sum_{j=0}^{m} \beta_{m,m-j}^{(2)} y^{m-j} f(x,y) \tag{4.12}$$

where

$$\beta_{n,n-k}^{(1)} = \sum_{r=0}^{k} \binom{n-k+r}{r} c_{n,n-k+r}^N \hat{a}_2^r \hat{a}_1^{n-k} \tag{4.13}$$

$$\beta_{m,m-j}^{(2)} = \sum_{s=0}^{j} \binom{m-j+s}{s} c_{m,m-j+s}^N \hat{b}_2^s \hat{b}_1^{m-j}. \tag{4.14}$$

From (4.2), we have

$$x^n = \sum_{k=0}^{n} d_{n,n-k}^N \tilde{t}_{n-k}^N(x). \tag{4.15}$$

Thus the AST-G has the expression

$$I_{n,m}^{\langle \text{ast-G} \rangle} = |\hat{a}_1 \hat{b}_1| \sum_{k=0}^{n} \sum_{j=0}^{m} \tau_{n,n-k}^{(1)} \tau_{m,m-j}^{(2)} T_{n-k,m-j} \tag{4.16}$$

where

$$\tau_{n,n-k}^{(1)} = \sum_{r=0}^{k} \beta_{n,n-r}^{(1)} d_{n-r,n-k}^N \tag{4.17}$$

$$\tau_{m,m-j}^{(2)} = \sum_{s=0}^{j} \beta_{m,m-s}^{(2)} d_{m-s,m-j}^N. \tag{4.18}$$

4.2.2 Normalization Scheme for Anisotropic Scale and Translation Tchebichef Moment Invariants of Goh et. al.

The normalization of AST-G are determined by the radius of gyration of geometric moments (Goh et al., 2009). The normalization parameters are determined using any one of the following approach:

(A1) With a standard image or a set of standard moment values.

(A2) Without a set of standard moment values.

For the first approach, a set of moments including geometric moments up to first order, and central moments up to 3rd order are computed from the standard image. In case the standard moments are not provided, some prefixed values of $K_1^{'}$ and $K_2^{'}$ are required in the normalization process. This is summarized in Table 4.1.

Table 4.1: AST-G normalization for mapping function $x' = \hat{a}_1 x + \hat{a}_2$ and $y' = \hat{b}_1 y + \hat{b}_2$

	$x^{'}$		$y^{'}$	
	$\hat{a}_1$	$\hat{a}_2$	$\hat{b}_1$	$\hat{b}_2$
Translation only*	1	$\bar{x}^{'} - \bar{x}$	1	$\bar{y}^{'} - \bar{y}$
Scale only*	$\mathrm{sc}_x^{'}/\mathrm{sc}_x$	0	$\mathrm{sc}_y^{'}/\mathrm{sc}_y$	0
Translation and Scale*	$\mathrm{sc}_x^{'}/\mathrm{sc}_x$	$\bar{x}^{'} - (sc_x^{'}/sc_x)\bar{x}$	$\mathrm{sc}_y^{'}/\mathrm{sc}_y$	$\bar{y}^{'} - (\mathrm{sc}_y^{'}/\mathrm{sc}_y)\bar{y}$
Translation only▲	1	$K_1^{'} - \bar{x}$	1	$K_1^{'} - \bar{y}$
Scale only▲	$K_2^{'}/\mathrm{sc}_x$	0	$K_2^{'}/\mathrm{sc}_y$	0
Translation and Scale▲	$K_2^{'}/\mathrm{sc}_x$	$K_1^{'} - (K_2^{'}/\mathrm{sc}_x)\bar{x}$	$K_2^{'}/\mathrm{sc}_y$	$K_1^{'} - (K_2^{'}/\mathrm{sc}_y)\bar{y}$

* With standard moments

▲ Without standard moments

The radius of gyrations (with origin at image centroid):

$$|r_x| = \sqrt{\frac{\mu_{2,0}}{\mu_{0,0}}} \qquad \text{and} \qquad |r_y| = \sqrt{\frac{\mu_{0,2}}{\mu_{0,0}}}. \tag{4.19}$$

The skewness of image (with origin at image centroid):

$$s_x = \frac{\mu_{3,0}}{\mu_{2,0}^{\frac{3}{2}}} \qquad \text{and} \qquad s_y = \frac{\mu_{0,3}}{\mu_{0,2}^{\frac{3}{2}}}. \tag{4.20}$$

The scale factors are:

$$\mathrm{sc}_x = \mathrm{sign}(s_x)|r_x| \qquad \text{and} \qquad \mathrm{sc}_y = \mathrm{sign}(s_y)|r_y|. \tag{4.21}$$

The formulations for the radius of gyrations and the skewness of image, are equivalent to the definition stated in Chapter 2 with the condition that the origin is being shifted to the centroid of image.

In Goh et al. (2009), the coefficient values were recommended as

(B1) $K_2^{'} \in [0.5 \times N, 0.8 \times N]$, and

(B2) $K_1^{'} = 0$ which means the centroid of canonical forms are mapped to the origin.

4.2.3 Anisotropic Scale and Translation Tchebichef Moment Invariants of Liu et. al.

The second set of anisotropic scale and translation invariants was proposed by Liu et al. (2011) (denoted as AST-L). In the paper, the scale invariants were initially proposed to solve affine Tchebichef moment invariants using XYS and XSR decompositions. The method is an extension on H. Zhang et al. (2011) where affine Legendre moments are proposed to resolve the geometric distortion of watermarked images. As the method requires the image's centroid to be located at the origin, the expression is thus AST invariant. According to Liu et al. (2011), the centroid is

$$\bar{x} = \frac{c^N_{0,0}T_{1,0} - c^N_{1,0}T_{0,0}}{c^N_{1,1}T_{0,0}} \quad \text{and} \quad \bar{y} = \frac{c^N_{0,0}T_{0,1} - c^N_{1,0}T_{0,0}}{c^N_{1,1}T_{0,0}}. \tag{4.22}$$

The Tchebichef moment

$$I^{\langle \text{ast-L} \rangle}_{n,m} = \sum_{k=0}^{n}\sum_{j=0}^{m}\sum_{r=0}^{k}\sum_{s=0}^{j} \tilde{a}_1^{k+1}\tilde{b}_1^{j+1} c^N_{n,k}c^N_{m,j}d^N_{k,r}d^N_{j,s}T^{\langle c \rangle}_{r,s} \tag{4.23}$$

is AST-invariants if the scale parameters $\tilde{a}_1$ and $\tilde{b}_1$ satisfy the constraint

$$I^{\langle \text{ast-L} \rangle}_{2,0} = 1 = I^{\langle \text{ast-L} \rangle}_{0,2}$$

or the parameters, $\tilde{a}_1$ and $\tilde{b}_1$ are solutions of the system equations

$$\begin{aligned}(c^N_{2,2}d^N_{2,0}T^{\langle c \rangle}_{0,0} + c^N_{2,2}d^N_{2,1}T^{\langle c \rangle}_{1,0} + T^{\langle c \rangle}_{2,0})\tilde{a}_1^3 b_1 + (c^N_{2,1}d^N_{1,0}T^{\langle c \rangle}_{0,0} \\ + c^N_{2,1}d^N_{1,1}T^{\langle c \rangle}_{1,0})\tilde{a}_1^2\tilde{b}_1 + (c^N_{2,0}d^N_{0,0}T^{\langle c \rangle}_{0,0})\tilde{a}_1\tilde{b}_1 &= 1 \qquad (4.24)\\ (c^N_{2,2}d^N_{2,0}T^{\langle c \rangle}_{0,0} + c^N_{2,2}d^N_{2,1}T^{\langle c \rangle}_{0,1} + T^{\langle c \rangle}_{0,2})\tilde{a}_1\tilde{b}_1^3 + (c^N_{2,1}d^N_{1,0}T^{\langle c \rangle}_{0,0} \\ + c^N_{2,1}d^N_{1,1}T^{\langle c \rangle}_{0,1})\tilde{a}_1\tilde{b}_1^2 + (c^N_{2,0}d^N_{0,0}T^{\langle c \rangle}_{0,0})\tilde{a}_1\tilde{b}_1 &= 1. \qquad (4.25)\end{aligned}$$

By solving (4.24) and (4.25), the scale coefficients of $\tilde{a}$ and $\tilde{b}$ are found to be

$$\tilde{a}_1^2 = \frac{-A_3 \pm \sqrt{A_3^2 + 4\sqrt{A_1B_1}}}{2A_1}, \quad \text{and} \tag{4.26}$$

$$\tilde{b}_1^2 = \frac{-A_3 \pm \sqrt{A_3^2 + 4\sqrt{A_1B_1}}}{2B_1}. \tag{4.27}$$

where

$$\begin{aligned}
A_1 &= c^N_{2,2} d^N_{2,0} T^{\langle c \rangle}_{0,0} + c^N_{2,2} d^N_{2,1} T^{\langle c \rangle}_{1,0} + T^{\langle c \rangle}_{2,0}, \\
A_2 &= c^N_{2,1} d^N_{1,0} T^{\langle c \rangle}_{0,0} + c^N_{2,1} d^N_{1,1} T^{\langle c \rangle}_{1,0}, \\
A_3 &= c^N_{2,0} d^N_{0,0} T^{\langle c \rangle}_{0,0}, \\
B_1 &= c^N_{2,2} d^N_{2,0} T^{\langle c \rangle}_{0,0} + c^N_{2,2} d^N_{2,1} T^{\langle c \rangle}_{0,1} + T^{\langle c \rangle}_{0,2}, \\
B_2 &= c^N_{2,1} d^N_{1,0} T^{\langle c \rangle}_{0,0} + c^N_{2,1} d^N_{1,1} T^{\langle c \rangle}_{0,1}.
\end{aligned}$$

The scale normalization can be further generalized by

$$I^{\langle \text{ast-L} \rangle}_{2,0} = \Omega_L = I^{\langle \text{ast-L} \rangle}_{0,2} \quad \text{where} \quad \Omega_L \in \Re.$$

The full solution on solving this system of equations is given in Appendix A.

As shown above, despite the pre-computation on coefficients of $c^N_{n,k}$ and $d^N_{k,m}$, AST-L is inefficient. This is mainly due to the sequential computation of central Tchebichef moments and scale normalization descriptors. AST-G on the other hand is much faster as the expressions do not require sequential computation of translation invariants and scale invariants. However pre-computation of $c^N_{n,k}$ and $d^N_{k,m}$ are required and additional double precision memories in total of

$$4 \times \frac{(p+1)(p+2)}{2}.$$

are required to store variables $c^N_{n,k}$, $d^N_{k,m}$,$\beta^{(1)}_{n,n-k}$ and $\beta^{(2)}_{m,m-j}$. Here p denotes the order of the AST-G moments.

4.3 Proposed Anisotropic Scale and Translation Tchebichef Moment Invariants

In this section, a new anisotropic scale and translation Tchebichef moment invariant algorithms will be proposed. For convenience, it will be denoted as AST-invariants with invariant descriptors $\{I^{\langle \text{ast} \rangle}_{n,m}\}$. The AST-invariants come with a fast computation algorithm using recurrence relation, and new sets of normalization schemes purely based on Tchebichef moments. The fast computational algorithms are given in Section 4.3.1. Theoretical framework in determining the normalization parameters are given in Section 4.3.2.

Definition 4.3.1. Suppose an anisotropic scale and translation transformation is defined as

$$\begin{aligned} x' &= a_1 x + a_2 \qquad \text{and} \qquad y' = b_1 y + b_2 \\ (x,y) &\in S_2(N_0) \qquad \text{and} \qquad (x',y') \in S_2(N_s) \end{aligned} \tag{4.28}$$

while the AST-invariant descriptors are defined as

$$\begin{aligned} I_{n,m}^{\langle \text{ast} \rangle} &= |a_1 b_1| \sum_{x=0}^{N_0-1} \sum_{y=0}^{N_0-1} \tilde{t}_n^{N_s}(a_1 x + a_2) \tilde{t}_m^{N_s}(b_1 y + b_2) f(x,y) \\ & \qquad n,m = 0,1,\cdots,\min(N_0-1, N_s-1), \quad \text{and} \quad a_1,a_2,b_1,b_2 \in \Re. \end{aligned} \tag{4.29}$$

$S_2(N_0)$ and $S_2(N_s)$ denote the original and transformed image spaces, respectively. The two spaces are independent so that the invariant descriptors can be directly compute from original image without the need to re-mapped it to a prefixed space. This not only save the computer memory, it also speedup the calculation of image moments especially when large numbers of the images are small.

4.3.1 Recurrence Relation for Fast Computation of Anisotropic Scale and Translation Invariants

The recurrence relations for fast computation of AST-invariants are given by the following theorem.

Theorem 4.3.1.

$$I_{n,m}^{\langle \text{ast} \rangle} = |a_1 b_1| \sum_{k=0}^{n} \sum_{j=0}^{m} \lambda_{n,k}^{(1)} \lambda_{m,j}^{(2)} T_{k,j}. \tag{4.30}$$

if

$$\begin{aligned} \lambda_{n,k}^{(1)}(a_1,a_2;N_0,N_s) &= \lambda_{n-1,k-1}^{(1)} a_1 K_{n,k}^{N_s,N_0} + \lambda_{n-1,k}^{(1)} \tilde{A}_n^{N_s} \left(a_2 - \frac{(N_s-1)}{2} + \frac{a_1(N_0-1)}{2} \right) \\ &\quad - \lambda_{n-1,k+1}^{(1)} a_1 K_{n,k+2}^{N_s,N_0} \tilde{C}_{k+2}^{N_0} + \lambda_{n-2,k}^{(1)} \tilde{C}_n^{N_s} \end{aligned} \tag{4.31}$$

$$\begin{aligned} \lambda_{m,j}^{(2)}(b_1,b_2;N_0,N_s) &= \lambda_{m-1,j-1}^{(2)} b_1 K_{m,j}^{N_s,N_0} + \lambda_{m-1,j}^{(2)} \tilde{A}_m^{N_s} \left(b_2 - \frac{(N_s-1)}{2} + \frac{b_1(N_0-1)}{2} \right) \\ &\quad - \lambda_{m-1,j+1}^{(2)} b_1 K_{m,j+2}^{N_s,N_0} \tilde{C}_{j+2}^{N_0} + \lambda_{m-2,j}^{(2)} \tilde{C}_m^{N_s} \end{aligned} \tag{4.32}$$

where

$$K_{i,j}^{M,N} = \frac{\tilde{A}_i^M}{\tilde{A}_j^N} \tag{4.33}$$

and

$$\tilde{A}_n^{N_*} = \frac{2}{n}\sqrt{\frac{4n^2-1}{{N_*}^2-n^2}} \tag{4.34}$$

$$\tilde{B}_n^{N_*} = \frac{(1-N_*)}{n}\sqrt{\frac{4n^2-1}{{N_*}^2-n^2}} \tag{4.35}$$

$$\tilde{C}_n^{N_*} = -\frac{(n-1)}{n}\sqrt{\frac{2n+1}{2n-3}}\sqrt{\frac{{N_*}^2-(n-1)^2}{{N_*}^2-n^2}} \tag{4.36}$$

$$N_* = N_0 \text{ or } N_s.$$

Proof. For the zero and first degree normalized Tchebichef polynomials, $\tilde{t}_0^{N_s}(a_1x+a_2)$, and $\tilde{t}_1^{N_s}(a_1x+a_2)$, it is easy to show that

$$t_0^{N_s}(a_1x+a_2) = \sqrt{\frac{N_0}{N_s}}t_0^{N_0}(x) \tag{4.37}$$

and

$$\begin{aligned} t_1^{N_s}(a_1x+a_2) &= a_1K_{1,1}^{N_s,N_0}\sqrt{\frac{N_0}{N_s}}\tilde{t}_1^{N_0}(x) + \\ &\left(a_2-\frac{(N_s-1)}{2}+\frac{a_1(N_0-1)}{2}\right)\sqrt{\frac{N_0}{N_s}}\tilde{A}_1^{N_s}\tilde{t}_0^{N_0}(x) \end{aligned} \tag{4.38}$$

which are linear combinations of first $n-$degrees original Tchebichef polynomials $\tilde{t}_n^{N_0}(x)$. In this case, n has values 0 and 1.

By induction, suppose

$$\tilde{t}_p^{N_s}(a_1x+a_2) = \sum_{k=0}^{p}\lambda_{p,k}^{(1)}(a_1,a_2;N_0,N_s)\tilde{t}_k^{N_0}(x) \tag{4.39}$$

for $p=0,1,\cdots,n$, we now consider $\tilde{t}_{n+1}^{N_s}(a_1x+a_2)$.

From the three terms recurrence relation of (4.4), we have

$$\tilde{t}_{n+1}^{N_s}(a_1x+a_2) = [(a_1x+a_2)\tilde{A}_{n+1}^{N_s}+\tilde{B}_{n+1}^{N_s}]\tilde{t}_n^{N_s}(a_1x+a_2)+\tilde{C}_{n+1}^{N_s}\tilde{t}_{n-1}^{N_s}(a_1x+a_2). \tag{4.40}$$

By the induction hypothesis in (4.39), we get

$$\begin{aligned} \tilde{t}_{n+1}^{N_s}(a_1x+a_2) &= \sum_{k=0}^{n}\left\{\lambda_{n,k}^{(1)}\left[\tilde{A}_{n+1}^{N_s}a_2+\tilde{B}_{n+1}^{N_s}\right]+\lambda_{n-1,k}^{(1)}\tilde{C}_{n+1}^{N_s}\right\}\tilde{t}_k^{N_0}(x) \\ &\quad +a_1K_{n+1,i+1}^{N_s,N_0}\tilde{A}_{k+1}^{N_0}x\sum_{k=0}^{n}\lambda_{n,k}^{(1)}\tilde{t}_k^{N_0}(x). \end{aligned} \tag{4.41}$$

The variable "x" can be eliminated using the three terms recurrence relation in (4.4). Therefore we have

$$\begin{aligned} \tilde{t}_{n+1}^{N_s}(a_1x+a_2) &= \sum_{k=0}^{n+1}\left\{\lambda_{n,k-1}^{(1)}a_1K_{n+1,k}^{N_s,N_0}+\lambda_{n,k}^{(1)}\tilde{A}_{n+1}^{N_s}\left(a_2-\frac{(N_s-1)}{2}+\frac{a_1(N_0-1)}{2}\right)\right. \\ &\quad \left.-\lambda_{n,k+1}^{(1)}a_1K_{n+1,k+2}^{N_s,N_0}\tilde{C}_{k+2}^{N_0}+\lambda_{n-1,k}^{(1)}\tilde{C}_{n+1}^{N_s}\right\}\tilde{t}_k^{N_0}(x) \end{aligned} \tag{4.42}$$

which proved the recurrence relation (4.31).

The proof for (4.32) is similar. □

Theoretically, to preserve orthogonality, the domain of standard image function must be within the space of orthogonal basis - $S_2(N_s)$. Thus some of the current normalization schemes are not suitable. In next section the new normalization scheme of AST for spatial displacement deformations and scale deformations will be proposed.

4.3.2 Spatial Displacement Normalization of Anisotropic Scale and Translation Invariants

As mentioned by Goh et al. (2009) and Liu et al. (2011), for translation invariants, both of the algorithms recommend the use of origin as centroid for their canonical images. However from the definition of centrally transformed Tchebichef polynomials $\tilde{t}_n^N(x-\bar{x})$, at least half of the values of $x-\bar{x}$ are outside the domain of basis function. This thus caused ambiguity regarding the orthogonality of canonical form. In addition, since the Tchebichef polynomials are symmetric functions with centre of symmetry at $\frac{N-1}{2}$. To have features with good discriminative power, the centroid of images should be near to or at the point of $\frac{N-1}{2}$. For that, the following lemma and theorem are derived to identify the suitable centroid location of the standard images.

Lemma 4.3.2. *Suppose f is the image defined in space of $S_2(N)$, the image's centroid $(\bar{x},\bar{y})$ is*

$$\bar{x} = \frac{T_{0,1} - \tilde{B}_1^N T_{0,0}}{\tilde{A}_1^N T_{0,0}} \quad \textit{and} \quad \bar{y} = \frac{T_{1,0} - \tilde{B}_1^N T_{0,0}}{\tilde{A}_1^N T_{0,0}}. \tag{4.43}$$

Proof. From (4.5) and (4.6), we have

$$T_{1,0} = \frac{\tilde{A}_1^N}{N} m_{1,0} + \tilde{B}_1^N T_{0,0}, \tag{4.44}$$

$$T_{0,0} = \frac{m_{0,0}}{N} \tag{4.45}$$

where $m_{p,q} = \sum_{x=0}^{N-1} \sum_{y=0}^{N-1} x^p y^q f(x,y)$ is the geometric moment.
Thus we have

$$\bar{x} = \frac{m_{1,0}}{m_{0,0}} = \frac{T_{1,0} - \tilde{B}_1^N T_{0,0}}{\tilde{A}_1^N T_{0,0}} \tag{4.46}$$

The similar approach can be used to find $\bar{y}$. □

This Lemma 4.3.2 has the following important implication.

Theorem 4.3.3. *Suppose f denotes the image defined in the space of $S_2(N)$, the first order Tchebichef moments*

$$T_{1,0} = T_{0,1} = 0 \tag{4.47}$$

if and only if

$$\bar{x} = \bar{y} = \frac{(N-1)}{2}. \tag{4.48}$$

With this theorem, we may let the centroid of canonical images to be at the middle of $S_2(N_s)$, i.e. $\left(\frac{N_s-1}{2}, \frac{N_s-1}{2}\right)$. This is indeed the best location to ensure the canonical images are within the defined space. The constraint $T_{1,0} = T_{0,1} = 0$ is also useful to simplify the derivation of normalization expressions later.

4.3.3 Scale Normalization of Anisotropic Scale and Translation Invariants

As shown in Table 4.1, the scale normalization scheme proposed by Goh et al. (2009) is based on geometric moments which has incurred additional overhead in numerical computations. Liu et al. (2011) on the other hand uses the conditions of both the second order invariants $I_{0,2}^{\langle \text{ast-L} \rangle}$ and $I_{2,0}^{\langle \text{ast-L} \rangle}$ are equal to unity. However the method was derived with condition of canonical centroid at the origin. As such it is not compatible with our approach. Therefore we propose several normalization schemes based on Tchebichef moments. This gives flexibility in implementing the algorithms and eliminating the overhead caused by determining parameters from other domains.

Suppose the centroid of canonical image is at the middle of $S_2(N_s)$, the scale coefficient can be determined with one of the following conditions

(C1) Anisotropic scale normalization using second order Tchebichef moment invariants,

(C2) Anisotropic scale normalization using zero order and second order Tchebichef moment invariants,

(C3) Anisotropic scale normalization using ratio of second order and zero order Tchebichef moment invariants.

4.3.3 (a) *Anisotropic Scale Normalization using Second Order Tchebichef Moment Invariants*

In this normalization scheme, the second order invariants are equal to a constant Ω_1

$$I_{2,0}^{\langle \text{ast} \rangle} = \Omega_1 = I_{0,2}^{\langle \text{ast} \rangle}. \tag{4.49}$$

This is the generalization of the method proposed by Liu et al. (2011). However the two methods do not show the same result. This is mainly due to the spatial displacement normalization being not identical.

From Theorem 4.3.1, the normalized moment invariants $I_{2,0}^{\langle \text{ast} \rangle}$ and $I_{0,2}^{\langle \text{ast} \rangle}$ have the following expressions:

$$I_{2,0}^{\langle \text{ast} \rangle} = a_1^3 b_1 \left(\frac{N_0}{N_s}\right) P_1 + a_1 b_1 \left(\frac{N_0}{N_s}\right) \tilde{C}_2^{N_s} T_{0,0} \tag{4.50}$$

$$I_{0,2}^{\langle \text{ast} \rangle} = a_1 b_1^3 \left(\frac{N_0}{N_s}\right) P_2 + a_1 b_1 \left(\frac{N_0}{N_s}\right) \tilde{C}_2^{N_s} T_{0,0} \tag{4.51}$$

where

$$\begin{aligned} P_1 = & \left\{ K_{1,1}^{N_s,N_0} K_{2,2}^{N_s,N_0} T_{2,0} + 2\left(\frac{N_0-1}{2} - \bar{x}\right) \tilde{A}_1^{N_s} K_{2,1}^{N_s,N_0} T_{1,0} \right. \\ & \left. + \left[\tilde{A}_1^{N_s} \tilde{A}_2^{N_s} \left(\frac{N_0-1}{2} - \bar{x}\right)^2 - K_{1,1}^{N_s,N_0} K_{2,2}^{N_s,N_0} \tilde{C}_2^{N_0} \right] T_{0,0} \right\} \end{aligned} \tag{4.52}$$

$$\begin{aligned} P_2 = & \left\{ K_{1,1}^{N_s,N_0} K_{2,2}^{N_s,N_0} T_{0,2} + 2\left(\frac{N_0-1}{2} - \bar{y}\right) \tilde{A}_1^{N_s} K_{2,1}^{N_s,N_0} T_{0,1} \right. \\ & \left. + \left[\tilde{A}_1^{N_s} \tilde{A}_2^{N_s} \left(\frac{N_0-1}{2} - \bar{y}\right)^2 - K_{1,1}^{N_s,N_0} K_{2,2}^{N_s,N_0} \tilde{C}_2^{N_0} \right] T_{0,0} \right\}. \end{aligned} \tag{4.53}$$

The derivation of $I_{2,0}^{\langle \text{ast} \rangle}$ and $I_{0,2}^{\langle \text{ast} \rangle}$ are given in Appendix B.

From (4.50) and (4.51), using the constraints $I_{2,0}^{\langle \text{ast} \rangle} = I_{0,2}^{\langle \text{ast} \rangle}$, we get

$$a_1 = \pm b_1 \sqrt{\frac{P_2}{P_1}}. \tag{4.54}$$

From (4.54) and the constraint $I_{2,0}^{\langle \text{ast} \rangle} = \Omega_1$, we get

$$a_1^4 P_1^2 + P_1 \tilde{C}_2^{N_s} T_{0,0} a_1^2 - \Omega_1 \left(\frac{N_s}{N_0}\right) \sqrt{P_1 P_2} = 0 \tag{4.55}$$

which has solutions

$$a_1^2 = \frac{-\tilde{C}_2^{N_s} T_{0,0} \pm \sqrt{\left(\tilde{C}_2^{N_s} T_{0,0}\right)^2 + 4\Omega_1 \left(\frac{N_s}{N_0}\right) \sqrt{P_1 P_2}}}{2P_1} \tag{4.56}$$

and

$$b_1^2 = \frac{-\tilde{C}_2^{N_s} T_{0,0} \pm \sqrt{\left(\tilde{C}_2^{N_s} T_{0,0}\right)^2 + 4\Omega_1 \left(\frac{N_s}{N_0}\right) \sqrt{P_1 P_2}}}{2P_2}. \tag{4.57}$$

In order to have real solution, the following condition is required

$$\Omega_1 \geq -\frac{\left(\tilde{C}_2^{N_s} T_{0,0}\right)^2}{4\sqrt{P_1 P_2}} \left(\frac{N_0}{N_s}\right) = \hat{\Omega}_1. \tag{4.58}$$

In this normalization scheme, with a prefixed value on Ω_1, the canonical images are scaled proportional to the transformed space $S_2(N_s)$. This has been confirmed experimentally. With this, we can ensure that, the standard images will be consistently within the specific ranges of $S_2(N_s)$ regardless the variation of the transformed space.

4.3.3 (b) Anisotropic Scale Normalization using Zero Order and Second Orders Tchebichef Moment Invariants.

In this scheme, we use

$$I_{0,0}^{\langle \text{ast} \rangle} = \Omega_0 N_s \tag{4.59}$$

to control the size of normalized image while the second order moment invariants

$$I_{2,0}^{\langle \text{ast} \rangle} = I_{0,2}^{\langle \text{ast} \rangle}$$

is used to eliminate the anisotropic scale deformation.

From

$$I_{0,0}^{\langle \text{ast} \rangle} = |a_1 b_1| T_{0,0} \left(\frac{N_0}{N_s}\right) \tag{4.60}$$

we have

$$a_1 b_1 = \frac{\Omega_0}{T_{0,0}} \left(\frac{N_s^2}{N_0}\right). \tag{4.61}$$

From (4.61) and (4.54), we have

$$a_1^2 = \frac{\Omega_0}{T_{0,0}} \left(\frac{N_s^2}{N_0}\right) \times \sqrt{\frac{P_2}{P_1}} \tag{4.62}$$

$$b_1^2 = \frac{\Omega_0}{T_{0,0}} \left(\frac{N_s^2}{N_0}\right) \times \sqrt{\frac{P_1}{P_2}}. \tag{4.63}$$

As shown in (4.59), the scale coefficient Ω_0 is the ratio of canonical image's mass in relative to the transformed space $S_2(N_s)$. Therefore with a prefixed Ω_0, the canonical image will be scaled proportional to the transformed space automatically.

4.3.3 (c) *Anisotropic Scale Normalization using Ratio of Second Order and Zero Order Tchebichef Moment Invariants*

With the centroid of canonical image at the middle of the image space, the ratio of second order moment invariants $I_{2,0}^{\langle \text{ast} \rangle}$ with respect to $I_{0,0}^{\langle \text{ast} \rangle}$, and the ratio of $I_{0,2}^{\langle \text{ast} \rangle}$ with respect to $I_{0,0}^{\langle \text{ast} \rangle}$ are identical to the radius of gyration of geometric moments with centroid at the origin.

Suppose

$$\frac{I_{2,0}^{\langle \text{ast} \rangle}}{I_{0,0}^{\langle \text{ast} \rangle}} = \Omega_a \quad \text{and} \quad \frac{I_{0,2}^{\langle \text{ast} \rangle}}{I_{0,0}^{\langle \text{ast} \rangle}} = \Omega_b. \tag{4.64}$$

For $\frac{I_{2,0}^{\langle \text{ast} \rangle}}{I_{0,0}^{\langle \text{ast} \rangle}} = \Omega_a$, from (4.50) and (4.61), we get

$$\frac{a_1^3 b_1 \left(\frac{N_0}{N_s}\right) P_1 + a_1 b_1 \tilde{C}_2^{N_s} \left(\frac{N_0}{N_s}\right) T_{0,0}}{a_1 b_1 T_{0,0} \left(\frac{N_0}{N_s}\right)} = \Omega_a \tag{4.65}$$

which have

$$P_1 a_1^2 + \tilde{C}_2^{N_s} T_{0,0} = \Omega_a T_{0,0}. \tag{4.66}$$

For simplicity, suppose

$$\Omega_a = \tilde{\Omega}_a \tilde{C}_2^{N_s}, \qquad \tilde{\Omega}_a < 1 \tag{4.67}$$

we get

$$a_1 = \pm \sqrt{\frac{-T_{0,0} \tilde{C}_2^{N_s} (1 - \tilde{\Omega}_a)}{P_1}}. \tag{4.68}$$

Similarly for $\frac{I_{0,2}^{\langle \text{ast} \rangle}}{I_{0,0}^{\langle \text{ast} \rangle}} = \Omega_b$, by applying the same process, we can show that

$$b_1 = \pm \sqrt{\frac{-T_{0,0} \tilde{C}_2^{N_s} (1 - \tilde{\Omega}_b)}{P_2}} \tag{4.69}$$

and

$$\Omega_b = \tilde{\Omega}_b \tilde{C}_2^{N_s}, \qquad \tilde{\Omega}_b < 1. \tag{4.70}$$

Similar to first and second normalization schemes, with prefixed values of $\tilde{\Omega}_a$ and $\tilde{\Omega}_b$, the canonical image will be scaled proportional to transformed space $S_2(N_s)$ automatically.

4.3.4 Uniqueness Issue of Anisotropic Scale and Translation Invariants

As shown in the preceding section, solutions of scale coefficients a_1 and b_1 have ambiguities in the signs. These are mainly caused by the mirror reflection on $x-$axis and / or $y-$axis. To remove the ambiguities, the following lemma is required.

Lemma 4.3.4. *Suppose f, g_1 and g_2 are images in $S_2(N)$ with centroid at the middle of space and*

$$g_1\left(a(x-\bar{x})+\frac{N-1}{2},y\right) = f(x,y) \tag{4.71}$$

$$g_2\left(x,b(y-\bar{y})+\frac{N-1}{2}\right) = f(x,y), \qquad a,b\in\Re. \tag{4.72}$$

1. *If $T_{1,2}(f)\geq 0$, then*

$$T_{1,2}(g_1)\leq 0, \text{ if and only if } a<0. \tag{4.73}$$

2. *If $T_{2,1}(f)\geq 0$, then*

$$T_{2,1}(g_2)\leq 0, \text{ if and only if } b<0. \tag{4.74}$$

Proof. We first consider $T_{1,2}(g_1)$. From definition, we have

$$T_{1,2}(g_1)=|a|\sum_{x=0}^{N-1}\sum_{y=0}^{N-1}\tilde{t}_1^N\left(a(x-\bar{x})+\frac{N-1}{2}\right)\tilde{t}_2^N(y)f(x,y). \tag{4.75}$$

From (4.6) and the condition of $\bar{x}=\frac{N-1}{2}$ we can deduce that

$$\tilde{t}_1^N\left(a(x-\bar{x})+\frac{N-1}{2}\right)=a\tilde{t}_1^N(x). \tag{4.76}$$

By substituting (4.76) into (4.75),

$$T_{1,2}(g_1)=a|a|T_{1,2}(f). \tag{4.77}$$

As $T_{1,2}(f)\geq 0$, thus we have $T_{1,2}(g_1)\leq 0$ if and only if $a\leq 0$.
The proof is similar for (4.74). □

The image g_1 denotes the image f which is scaled by coefficient a relative to middle of space, in $x-$axis direction. g_2 on the other hand is the f scaled by coefficient b relative to middle of space, in $y-$axis direction. The above lemma provides us the theoretical basis to determine the direction of scale coefficients on f using the descriptors $I_{1,2}^{\langle \text{ast}\rangle}$ and $I_{2,1}^{\langle \text{ast}\rangle}$. By having

$$a=\text{sign}\left[I_{1,2}^{\langle \text{ast}\rangle}\right]|a| \tag{4.78}$$

$$b=\text{sign}\left[I_{2,1}^{\langle \text{ast}\rangle}\right]|b| \tag{4.79}$$

where sign(x) denotes function return value 1 if $x \geq 0$, and return -1 if otherwise. We therefore resolve the ambiguities caused by the mirror reflections.

We are now ready to solve the uniqueness issues of AST-invariants using the following theorem.

Theorem 4.3.5. *Suppose* $g(a_3x+a_4, b_3y+b_4) = f(x,y)$, *where* a_3, a_4, b_3, *and,* $b_4 \in \Re$, *then*

$$\begin{aligned} I_{n,m}^{\langle \text{ast} \rangle}(f) &= I_{n,m}^{\langle \text{ast} \rangle}(g), \\ & \quad n,m = 0,1,\cdots, min\,(N_0-1, N_s-1) \end{aligned} \tag{4.80}$$

if the invariants $I_{n,m}^{\langle \text{ast} \rangle}(f)$ *and* $I_{n,m}^{\langle \text{ast} \rangle}(g)$ *satisfy all the following conditions*

1. $I_{1,0}^{\langle \text{ast} \rangle}(*) = I_{0,1}^{\langle \text{ast} \rangle}(*)$
2. *One of the scale normalization schemes in Section 4.3.3*
3. $I_{1,2}^{\langle \text{ast} \rangle}(*) \geq 0$ *and* $I_{2,1}^{\langle \text{ast} \rangle}(*) \geq 0$

where $* \in \{f, g\}$.

Proof. Suppose

$$x_1 = a_3x + a_4 \quad \text{and} \quad y_1 = b_3y + b_4, \tag{4.81}$$

$f^{'}(x_f, y_f)$ denotes the AST transformed of image f, with

$$x_f = a_1x + a_2 \quad \text{and} \quad y_f = b_1y + b_2, \tag{4.82}$$

and $g^{'}(x_g, y_g)$ is the AST transformed of image g, with

$$x_g = a_1^{'}x_1 + a_2^{'} \quad \text{and} \quad y_g = b_1^{'}y_1 + b_2^{'}. \tag{4.83}$$

From (4.81), we get

$$x_g = a_1^{'}a_3x + a_1^{'}a_4 + a_2^{'} \quad \text{and} \quad y_g = b_1^{'}b_3y + b_1^{'}b_4 + b_2^{'}. \tag{4.84}$$

Thus AST-invariants of f and g have the following expressions

$$\begin{aligned} I_{n,m}^{\langle \text{ast} \rangle}(f) &= |a_1b_1| \sum_{k=0}^{n} \sum_{j=0}^{m} \lambda_{n,k}^{(1)_f}(a_1, a_2, ; N_0, N_s) \times \\ & \quad \lambda_{m,j}^{(2)_f}(b_1, b_2; N_0, N_s) T_{k,j}(f) \end{aligned} \tag{4.85}$$

and

$$I_{n,m}^{\langle \text{ast} \rangle}(g) = |a_1^{'} a_3 b_1^{'} b_3| \sum_{k=0}^{n} \sum_{j=0}^{m} \lambda_{n,k}^{(1)_g}(a_1^{'} a_3, a_1^{'} a_4 + a_2^{'}; N_0, N_s) \times \lambda_{m,j}^{(2)_g}(b_1^{'} b_3, b_1^{'} b_4 + b_2^{'}; N_0, N_s) T_{k,j}(f). \quad (4.86)$$

This means that $I_{n,m}^{\langle \text{ast} \rangle}(f) = I_{n,m}^{\langle \text{ast} \rangle}(g)$ if all the following conditions are satisfied

$$a_1 = a_1^{'} a_3 \quad (4.87)$$

$$a_2 = a_1^{'} a_4 + a_2^{'} \quad (4.88)$$

$$b_1 = b_1^{'} b_3 \quad (4.89)$$

$$b_2 = b_1^{'} b_4 + b_2^{'}. \quad (4.90)$$

Conditions (4.87) and (4.89) can be deduced by any of the scale normalization schemes in Sections 4.3.3 (a), 4.3.3 (b) and 4.3.3 (c), and the Lemma 4.3.4. From (4.87) and (4.89) and using the properties of $f^{'}$ and $g^{'}$ centred at the middle of $S_2(N_s)$, we can prove the conditions (4.88) and (4.90).

As conditions (4.87) to (4.90) are all satisfied, the theorem is proved. □

4.3.5 The Skewed Anisotropic Scale and Translated Tchebichef Moment Invariants

Skew coefficients (w_x, w_y) can be used to improve the feature accuracy and enhance classifications performance. Therefore the proposed AST-invariants finally have expression

$$I_{n,m}^{\langle \text{ast} \rangle} = |a_1 b_1| \sum_{k=0}^{n} \sum_{j=0}^{m} \lambda_{n,k}^{(1)}(s_x |a_1|, -s_x |a_1| \bar{x} + \frac{N_s - 1}{2} + w_x; N_0, N_s) \times \lambda_{m,j}^{(2)}(s_y |b_1|, -s_y |b_1| \bar{y} + \frac{N_s - 1}{2} + w_y; N_0, N_s) \times T_{k,j}$$
$$n, m = 0, 1, \cdots, \min\left\{ \frac{(N_0 - 1)}{2}, \frac{(N_s - 1)}{2} \right\}. \quad (4.91)$$

where the skew parameters (w_x, w_y) are some constant in unit of pixels, and $s_x = \text{sign}\left[I_{1,2}^{\langle \text{ast} \rangle} \right]$ and $s_y = \text{sign}\left[I_{2,1}^{\langle \text{ast} \rangle} \right]$.

4.4 Experimental Studies

In this section, empirical supports are given for the theoretical framework discussed in previous sections. In the first subsection, normalization parameters are estimated so

that orthogonality of the transformed images can be preserved whichever possible by using the proposed normalization scheme. In the second subsection, the accuracy of AST invariant descriptors are evaluated. This is followed by the evaluation of the numerical computational performance between the AST invariant algorithms. In the forth subsection, the robustness of AST-invariant features relative to noise have been studied. Finally sets of similar Chinese handwritten characters are used to evaluate the discriminative power of the features generated by different AST invariant algorithms.

4.4.1 Parameters Determination for Anisotropic Scale and Translation Invariants

In this experiment, a set of images with different complexities, representing groups of animals, company logos, characters, numbers, symbols and Chinese characters are used to determine the scale normalization parameters. The images are listed in Table 4.2. The size of each image is 70×70 pixels and both original space $S_2(N_0)$ and transformed space $S_2(N_s)$ are set to be equal to $S_2(200)$.

Table 4.2: Image used in the experiment of scale normalization

3	deer*	euro	h
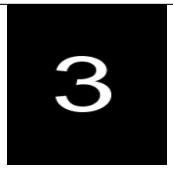	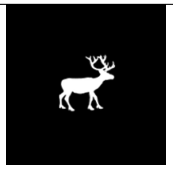		
mercedes**	**r**	**xiang**	**zeta**
			

*Original image of "deer" is courtesy of Professor Kimia, Brown University
**Original image of "mercedes" is courtesy of Flusser et al. (2009)

Table 4.3 gives the output of normalized images using the first scale normalization scheme. As shown in the table, when the scale coefficient $\Omega_1 < 0$, the size of the image is larger when Ω_1 is negative in decreasing magnitude. On the other hand, the image size is monotonically increasing for $\Omega_1 \geq 0$. Ideally, the best scale coefficients would be from $\Omega_1 < 0$. However as shown by (4.58), pre-computation is required to avoid imaginary solutions. Hence the best possible scale coefficient for the first normalization scheme

would be for

$$0 \leq \Omega_1 \leq 1. \tag{4.92}$$

Table 4.5 gives the output using the second scale normalization scheme. The size of the images in this case is determined by coefficient $\Omega_0 = \frac{I_{0,0}^{\langle \text{ast} \rangle}}{N_s}$ which is equivalent to the mass for binary images in relative to the area of $S_2(N_s)$. In this experiment, the suitable scale parameter values are found to be within the range of

$$0.05 \leq \Omega_0 \leq 0.2. \tag{4.93}$$

In the third normalization scheme, the scale coefficients are determined by the ratio between second order moments and zero order moment. As shown in Table 4.7, the range for suitable scale coefficients are

$$0.5 \leq \tilde{\Omega}_a, \tilde{\Omega}_b \leq 0.7. \tag{4.94}$$

Generally, the recommended parameter values will ensure a good classification performance. However it does not guarantee the best classification result. In the situation where centroid is near to the middle of transformed space $S_2(N_s)$, slight deviations of size might also bring better classification performance. Similarly, the use of smaller size canonical images does not imply a poor classification performance. This can be explained by the fact that the normalization process does not involve actual physical transformation and there is no loss of information. The process is just a transformation of original moments to match the moments of canonical form. As long as the major parts of canonical image is defined within the space of basis functions, the deviations with respect to classification performance is negligible. However in situations where the centroid of canonical image is deviated far from the middle of transformed space $S_2(N_s)$, the orthogonality property is no longer holds and the within class separation is degraded by skewing process which thus compromised the classification performance.

We next evaluate the performance of the normalization schemes from the aspect of size variations of the output images. As shown in Tables 4.4, 4.6 and 4.8, the average size deviations of the first, second and third scale normalization schemes, are 46.154% , 27.793% and 16.162%, respectively. This shows that the second order moments are not

suitable in controlling the size of the output images. The zero order moments appeared to be better than the second order moments. However size of canonical image is heavily affected by distribution of the image itself. This is showed by the images “mercedes", and “zeta" in Table 4.6. As the images are low in density distributions, it is unavoidable for the normalized images to take up wider space. Therefore the third normalization scheme is the best scale normalization scheme comparatively. This is mainly due to the zero order and second order moments to certain extent are correlated. Therefore the ratio between the second order and zero order Tchebichef moments can be effectively used to reduce the variations of size of output images.

4.4.2 Accuracy of Invariant Descriptors

In this section, we evaluate the accuracy of the proposed anisotropic scale and translation invariant. In the experiment, both original space $S_2(N_0)$ and transformed space $S_2(N_s)$ are equal to $S_2(250)$. A set of 80×80 pixels binary images in different complexity, symmetric and non-symmetric are selected for this experiment. As shown in Table 4.9, the images are non-uniformly expanded, contracted, or reflected, and arbitrary shifted from the middle of the domain. The invariants descriptors AST(1), AST(2), and AST(3), shown in Tables 4.10, 4.11 and 4.12 denote the AST-invariants features that use first, second and third scale normalization schemes, respectively to eliminate the size deformations. Accuracy of AST-G and AST-L are included in Tables 4.13 and 4.14 for the purpose of comparison. Overall the invariant descriptors exhibit high computational accuracy. Similar to algebraic cancellation approach, the odd order of moment invariats or the moments with relatively small values are more vulnerable to both re-sampling errors and discretization errors caused by the spatial deformations. This is due to anti-symmetric property of the basis function. When the image centroid is near to the center of symmetry, a small deviation on image values will significantly compromise the accuracy of the invariants descriptors. The accuracy of AST-L is far superior compared with others. The high precision of AST-L features can be explained by the deviation of the images from middle of space using Tchebichef central moments. Similar performance can be achieved by any of the AST algorithms when the centroid of images are shifted to the origin using skew parameters as shown in Table 4.15.

Table 4.3: Selected output images using the first scale normalization scheme

Image	Scale Coefficient (Ω_1)				
	-12	-1	0	10	100
mercedes					
xiang					
zeta					

Table 4.4: Size variations of the output images using the first scale normalization scheme with $\Omega_1 = -12$

Image	Mass ($m_{0,0}$)	M	N	Size ($= M \times N$)	$\hat{\Omega}_1$
3	2640.939	85	98	8330	-20.223
deer	2483.305	102	86	8772	-26.632
euro	2476.694	79	91	7189	-26.928
h	2609.198	100	72	7200	-21.01
mercedes	2910.521	123	123	15129	-15.744
r	2467.147	74	92	6808	-27.397
xiang	2680.538	107	97	10379	-19.419
zeta	4013.421	138	149	20562	-12.075
Min	2467.147	74	72	6808	-27.397
Max	4013.421	138	149	20562	-12.075
μ	2785.22	101	101	10546.125	-
σ	517.473	21.909	24.083	4867.495	-
RSD (%)	18.579	21.692	23.845	46.154	-

Table 4.5: Selected output images using the second scale normalization scheme

Image	Scale Coefficient, Ω_0				
	0.05	0.07	0.10	0.15	0.20
mercedes					
xiang					
zeta					

Table 4.6: Size variations of the output images using the second scale normalization scheme with $\Omega_0 = 0.10$

Image	Mass ($m_{0,0}$)	M	N	Size ($= M \times N$)
3	6077.685	128	148	18944
deer	6072.723	160	135	21600
euro	6073.272	123	142	17466
h	6068.301	153	110	16830
mercedes	6082.919	179	179	32041
r	6066.463	117	144	16848
xiang	6091.608	161	146	23506
zeta	6082.658	170	183	31110
Min	6066.463	117	110	16830
Max	6091.608	179	183	32041
μ	6076.954	148.875	148.375	22293.125
σ	8.45	23.185	23.464	6195.883
RSD (%)	0.139	15.574	15.814	27.793

Table 4.7: Selected output images using the third scale normalization scheme

Image	Scale Coefficient ($\tilde{\Omega}_a = \tilde{\Omega}_b$)				
	0.0	0.5	0.7	0.8	0.9
mercedes					
xiang					
zeta					

Table 4.8: Size variations of the output images using the third scale normalization scheme with $\tilde{\Omega}_a = \tilde{\Omega}_b = 0.7$

Image	Mass $m_{0,0}$	M	N	Size = $M \times N$
3	4374.667	108	125	13500
deer	5757.194	155	131	20305
euro	5822.373	119	139	16541
h	4539.712	132	95	12540
mercedes	3409.784	133	133	17689
r	5914.304	115	142	16330
xiang	4211.889	135	121	16335
zeta	2614.414	112	121	13552
Min	2614.414	108	95	12540
Max	5914.304	155	142	20305
μ	4580.542	126.125	125.875	15849
σ	1202.489	15.57	14.691	2561.569
RSD (%)	26.252	12.345	11.671	16.162

Table 4.9: Test images used by the experiment of accuracy on anisotropic scale and translation invariant descriptors

(a_1, b_1)	Original	(-2.4, 1.9)	(1.9, -1.3)	(1.6, 1.7)	(-1.5, -2.2)	(-1.1, 1.6)	(0.7, -2.5)	(0.5, -1.9)	(0.6, 0.9)	(-0.5, -0.5)
(a_2, b_2)	–	(1, -2)	(-5, 5)	(4, -7)	(-3, 4)	(-6,3)	(3, -1)	(-2, 1)	(-5, 4)	(0, -2)
		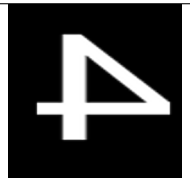			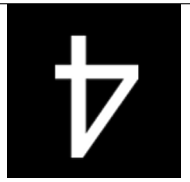	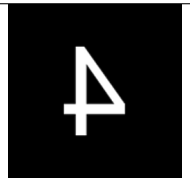	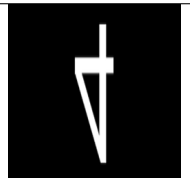	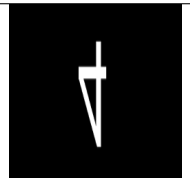		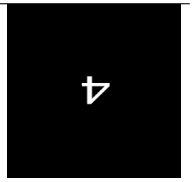
Image	im_4-1	im_4-2	im_4-3	im_4-4	im_4-5	im_4-6	im_4-7	im_4-8	im_4-9	im_4-10
			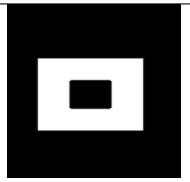	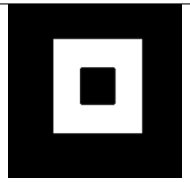	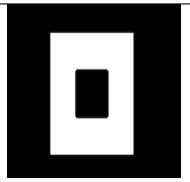	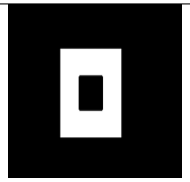	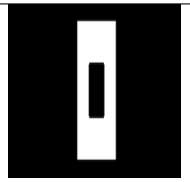	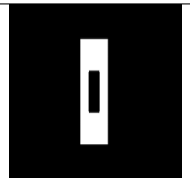	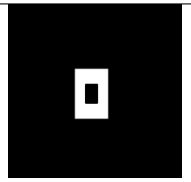	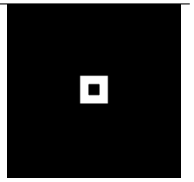
image	im_box-1	im_box-2	im_box-3	im_box-4	im_box-5	im_box-6	im_box-7	im_box-8	im_box-9	im_box-10
					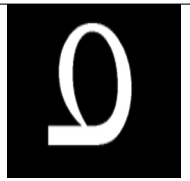	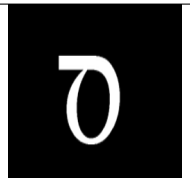	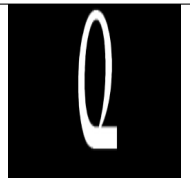	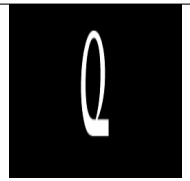	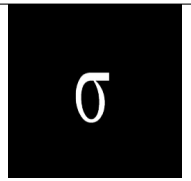	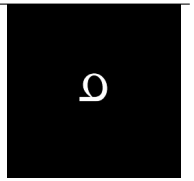
image	im_sigma-1	im_sigma-2	im_sigma-3	im_sigma-4	im_sigma-5	im_sigma-6	im_sigma-7	im_sigma-8	im_sigma-9	im_sigma-10
							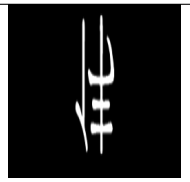	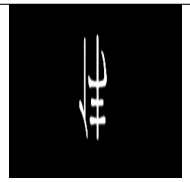		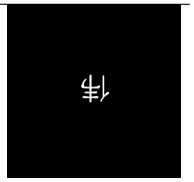
image	im_wei-1	im_wei-2	im_wei-3	im_wei-4	im_wei-5	im_wei-6	im_wei-7	im_wei-8	im_wei-9	im_wei-10

Table 4.10: Selected orders AST(1) with $\Omega_1 = -5$

Image	$I_{0,0}^{\langle ast \rangle}$	$I_{2,0}^{\langle ast \rangle}$	$I_{1,1}^{\langle ast \rangle}$	$I_{0,2}^{\langle ast \rangle}$	$I_{3,0}^{\langle ast \rangle}$	$I_{2,1}^{\langle ast \rangle}$	$I_{1,2}^{\langle ast \rangle}$	$I_{0,3}^{\langle ast \rangle}$
im_4-1	4.638	−5.000	−0.015	−5.000	−0.025	0.011	0.012	−0.012
im_4-2	4.638	−5.000	−0.015	−5.000	−0.025	0.011	0.012	−0.012
im_4-3	4.638	−5.000	−0.015	−5.000	−0.025	0.011	0.012	−0.012
im_4-4	4.638	−5.000	−0.015	−5.000	−0.025	0.011	0.012	−0.012
im_4-5	4.638	−5.000	−0.015	−5.000	−0.025	0.011	0.012	−0.012
im_4-6	4.638	−5.000	−0.015	−5.000	−0.025	0.011	0.012	−0.012
im_4-7	4.638	−5.000	−0.016	−5.000	−0.025	0.011	0.012	−0.012
im_4-8	4.638	−5.000	−0.016	−5.000	−0.025	0.011	0.013	−0.012
im_4-9	4.638	−5.000	−0.015	−5.000	−0.025	0.011	0.012	−0.012
im_4-10	4.638	−5.000	−0.016	−5.000	−0.025	0.011	0.013	−0.012
RSD(%)	0.000	0.000	3.157	0.000	0.000	0.000	3.456	0.000
Average RSD(%) = 0.827								
im_box-1	4.587	−5.000	0.000	−5.000	0.000	0.000	0.000	0.000
im_box-2	4.587	−5.000	0.000	−5.000	0.000	0.000	0.000	0.000
im_box-3	4.587	−5.000	0.000	−5.000	0.000	0.000	0.000	0.000
im_box-4	4.587	−5.000	0.000	−5.000	0.000	0.000	0.000	0.000
im_box-5	4.587	−5.000	0.000	−5.000	0.000	0.000	0.000	0.000
im_box-6	4.587	−5.000	0.000	−5.000	0.000	0.000	0.000	0.000
im_box-7	4.588	−5.000	0.000	−5.000	0.000	0.000	0.000	0.000
im_box-8	4.587	−5.000	0.000	−5.000	0.000	0.000	0.000	0.000
im_box-9	4.587	−5.000	0.000	−5.000	0.000	0.000	0.000	0.000
im_box-10	4.588	−5.000	0.000	−5.000	0.000	0.000	0.000	0.000
RSD(%)	0.009	0.000	0.000	0.000	0.000	0.000	0.000	0.000
Average RSD(%) = 0.001								
im_sigma-1	4.708	−5.000	0.028	−5.000	−0.005	0.002	0.007	−0.020
im_sigma-2	4.708	−5.000	0.028	−5.000	−0.005	0.002	0.007	−0.020
im_sigma-3	4.708	−5.000	0.028	−5.000	−0.005	0.002	0.007	−0.020
im_sigma-4	4.708	−5.000	0.028	−5.000	−0.005	0.002	0.007	−0.020
im_sigma-5	4.708	−5.000	0.028	−5.000	−0.005	0.002	0.007	−0.020
im_sigma-6	4.708	−5.000	0.028	−5.000	−0.005	0.002	0.007	−0.020
im_sigma-7	4.708	−5.000	0.028	−5.000	−0.005	0.002	0.007	−0.020
im_sigma-8	4.708	−5.000	0.028	−5.000	−0.005	0.002	0.007	−0.020
im_sigma-9	4.708	−5.000	0.028	−5.000	−0.005	0.002	0.007	−0.020
im_sigma-10	4.710	−5.000	0.026	−5.000	−0.004	0.002	0.007	−0.020
RSD(%)	0.013	0.000	2.275	0.000	6.454	0.000	0.000	0.000
Average RSD(%) = 1.093								
im_wei-1	4.731	−5.000	−0.017	−5.000	0.020	0.005	0.001	0.020
im_wei-2	4.730	−5.000	−0.016	−5.000	0.019	0.005	0.001	0.020
im_wei-3	4.730	−5.000	−0.016	−5.000	0.019	0.005	0.001	0.020
im_wei-4	4.730	−5.000	−0.017	−5.000	0.019	0.005	0.001	0.020
im_wei-5	4.730	−5.000	−0.017	−5.000	0.019	0.005	0.001	0.020
im_wei-6	4.730	−5.000	−0.016	−5.000	0.019	0.005	0.001	0.020
im_wei-7	4.733	−5.000	−0.017	−5.000	0.019	0.005	0.002	0.021
im_wei-8	4.726	−5.000	−0.020	−5.000	0.023	0.004	0.001	0.020
im_wei-9	4.730	−5.000	−0.017	−5.000	0.020	0.004	0.001	0.020
im_wei-10	4.726	−5.000	−0.021	−5.000	0.023	0.004	0.001	0.019
RSD(%)	0.045	0.000	9.843	0.000	8.165	10.278	28.748	2.357
Average RSD(%) = 7.430								

Table 4.11: Selected orders of AST(2) with $\Omega_0 = 0.09$

Image	$I_{0,0}^{\langle \mathrm{ast} \rangle}$	$I_{2,0}^{\langle \mathrm{ast} \rangle}$	$I_{1,1}^{\langle \mathrm{ast} \rangle}$	$I_{0,2}^{\langle \mathrm{ast} \rangle}$	$I_{3,0}^{\langle \mathrm{ast} \rangle}$	$I_{2,1}^{\langle \mathrm{ast} \rangle}$	$I_{1,2}^{\langle \mathrm{ast} \rangle}$	$I_{0,3}^{\langle \mathrm{ast} \rangle}$
im_4-1	22.590	−20.863	−0.362	−20.863	−1.299	0.570	0.650	−0.633
im_4-2	22.590	−20.857	−0.365	−20.857	−1.306	0.572	0.652	−0.632
im_4-3	22.590	−20.859	−0.365	−20.859	−1.303	0.572	0.651	−0.634
im_4-4	22.590	−20.859	−0.362	−20.859	−1.303	0.572	0.651	−0.632
im_4-5	22.590	−20.857	−0.364	−20.857	−1.305	0.572	0.652	−0.633
im_4-6	22.590	−20.858	−0.365	−20.858	−1.304	0.573	0.651	−0.634
im_4-7	22.590	−20.859	−0.373	−20.859	−1.317	0.571	0.654	−0.629
im_4-8	22.590	−20.857	−0.378	−20.857	−1.316	0.573	0.655	−0.635
im_4-9	22.590	−20.862	−0.347	−20.862	−1.285	0.569	0.647	−0.631
im_4-10	22.590	−20.852	−0.373	−20.852	−1.315	0.573	0.655	−0.630
RSD(%)	0.000	0.014	2.305	0.014	0.727	0.234	0.374	0.299
Average RSD(%) = 0.496								
im_box-1	22.590	−22.142	0.000	−22.142	0.000	0.000	0.000	0.000
im_box-2	22.590	−22.136	0.000	−22.136	0.000	0.000	0.000	0.000
im_box-3	22.590	−22.137	0.000	−22.137	0.000	0.000	0.000	0.000
im_box-4	22.590	−22.136	0.000	−22.136	0.000	0.000	0.000	0.000
im_box-5	22.590	−22.136	0.000	−22.136	0.000	0.000	0.000	0.000
im_box-6	22.590	−22.134	0.000	−22.134	0.000	0.000	0.000	0.000
im_box-7	22.590	−22.120	0.000	−22.120	0.000	0.000	0.000	0.000
im_box-8	22.590	−22.128	0.000	−22.128	0.000	0.000	0.000	0.000
im_box-9	22.590	−22.144	0.000	−22.144	0.000	0.000	0.000	0.000
im_box-10	22.590	−22.118	0.000	−22.118	0.000	0.000	0.000	0.000
RSD(%)	0.000	0.039	0.000	0.039	0.000	0.000	0.000	0.000
Average RSD(%) = 0.010								
im_sigma-1	22.590	−19.191	0.637	−19.191	−0.238	0.093	0.361	−1.014
im_sigma-2	22.590	−19.189	0.640	−19.189	−0.242	0.091	0.360	−1.020
im_sigma-3	22.590	−19.190	0.643	−19.190	−0.243	0.091	0.360	−1.021
im_sigma-4	22.590	−19.188	0.638	−19.188	−0.241	0.091	0.361	−1.019
im_sigma-5	22.590	−19.188	0.642	−19.188	−0.241	0.091	0.360	−1.021
im_sigma-6	22.590	−19.189	0.644	−19.189	−0.243	0.092	0.360	−1.022
im_sigma-7	22.590	−19.191	0.651	−19.191	−0.240	0.097	0.357	−1.025
im_sigma-8	22.590	−19.192	0.634	−19.192	−0.243	0.088	0.359	−1.015
im_sigma-9	22.590	−19.193	0.654	−19.193	−0.254	0.091	0.352	−1.030
im_sigma-10	22.590	−19.145	0.589	−19.145	−0.208	0.102	0.364	−0.988
RSD(%)	0.000	0.075	2.826	0.075	4.929	4.286	0.872	1.113
Average RSD(%) = 1.772								
im_wei-1	22.590	−18.657	−0.377	−18.657	0.973	0.225	0.072	1.007
im_wei-2	22.590	−18.673	−0.376	−18.673	0.965	0.227	0.072	0.999
im_wei-3	22.590	−18.674	−0.376	−18.674	0.964	0.228	0.072	0.998
im_wei-4	22.590	−18.668	−0.379	−18.668	0.968	0.227	0.073	1.000
im_wei-5	22.590	−18.676	−0.377	−18.676	0.967	0.227	0.072	0.999
im_wei-6	22.590	−18.675	−0.375	−18.675	0.958	0.228	0.073	0.995
im_wei-7	22.590	−18.604	−0.398	−18.604	0.962	0.226	0.076	1.031
im_wei-8	22.590	−18.780	−0.462	−18.780	1.158	0.179	0.048	0.981
im_wei-9	22.590	−18.685	−0.385	−18.685	0.988	0.216	0.070	0.993
im_wei-10	22.590	−18.769	−0.469	−18.769	1.151	0.189	0.043	0.962
RSD(%)	0.000	0.277	9.205	0.277	7.859	8.287	17.201	1.761
Average RSD(%) = 5.608								

Table 4.12: Selected orders of AST(3) with $\tilde{\Omega}_a = \tilde{\Omega}_b = 0.5$

Image	$I_{0,0}^{\langle \text{ast} \rangle}$	$I_{2,0}^{\langle \text{ast} \rangle}$	$I_{1,1}^{\langle \text{ast} \rangle}$	$I_{0,2}^{\langle \text{ast} \rangle}$	$I_{3,0}^{\langle \text{ast} \rangle}$	$I_{2,1}^{\langle \text{ast} \rangle}$	$I_{1,2}^{\langle \text{ast} \rangle}$	$I_{0,3}^{\langle \text{ast} \rangle}$
im_4-1	64.918	−36.291	−2.986	−36.291	−18.179	7.985	9.105	−8.861
im_4-2	64.840	−36.248	−3.004	−36.248	−18.227	7.986	9.102	−8.825
im_4-3	64.861	−36.259	−3.009	−36.259	−18.204	7.993	9.093	−8.851
im_4-4	64.866	−36.262	−2.989	−36.262	−18.209	7.985	9.100	−8.826
im_4-5	64.839	−36.247	−3.000	−36.247	−18.215	7.990	9.097	−8.830
im_4-6	64.856	−36.256	−3.006	−36.256	−18.207	7.996	9.096	−8.857
im_4-7	64.860	−36.259	−3.078	−36.259	−18.404	7.982	9.134	−8.791
im_4-8	64.829	−36.241	−3.111	−36.241	−18.356	7.994	9.144	−8.859
im_4-9	64.917	−36.290	−2.862	−36.290	−17.989	7.968	9.059	−8.835
im_4-10	64.764	−36.205	−3.065	−36.205	−18.304	7.976	9.123	−8.767
RSD(%)	0.068	0.068	2.239	0.068	0.618	0.108	0.262	0.349
Average RSD(%) = 0.473								
im_box-1	92.000	−51.000	0.000	−51.000	0.000	0.000	0.000	0.000
im_box-2	91.000	−51.000	0.000	−51.000	0.000	0.000	0.000	0.000
im_box-3	91.000	−51.000	0.000	−51.000	0.000	0.000	0.000	0.000
im_box-4	91.000	−51.000	0.000	−51.000	0.000	0.000	0.000	0.000
im_box-5	91.000	−51.000	0.000	−51.000	0.000	0.000	0.000	0.000
im_box-6	91.000	−51.000	0.000	−51.000	0.000	0.000	0.000	0.000
im_box-7	91.000	−51.000	0.000	−51.000	0.000	0.000	0.000	0.000
im_box-8	91.000	−51.000	0.000	−51.000	0.000	0.000	0.000	0.000
im_box-9	92.000	−51.000	0.000	−51.000	0.000	0.000	0.000	0.000
im_box-10	91.000	−51.000	0.000	−51.000	0.000	0.000	0.000	0.000
RSD(%)	0.462	0.000	0.000	0.000	0.000	0.000	0.000	0.000
Average RSD(%) = 0.058								
im_sigma-1	47.027	−26.290	2.761	−26.290	−1.489	0.585	2.256	−6.341
im_sigma-2	47.011	−26.280	2.771	−26.280	−1.510	0.567	2.251	−6.372
im_sigma-3	47.020	−26.285	2.785	−26.285	−1.517	0.570	2.251	−6.381
im_sigma-4	47.009	−26.279	2.763	−26.279	−1.503	0.571	2.254	−6.363
im_sigma-5	47.008	−26.279	2.778	−26.279	−1.508	0.570	2.251	−6.379
im_sigma-6	47.016	−26.284	2.789	−26.284	−1.520	0.573	2.249	−6.385
im_sigma-7	47.032	−26.292	2.824	−26.292	−1.503	0.606	2.235	−6.413
im_sigma-8	47.039	−26.296	2.751	−26.296	−1.518	0.549	2.246	−6.348
im_sigma-9	47.047	−26.300	2.837	−26.300	−1.587	0.572	2.206	−6.445
im_sigma-10	46.672	−26.091	2.516	−26.091	−1.275	0.626	2.232	−6.065
RSD(%)	0.238	0.238	3.232	0.238	5.424	3.788	0.678	1.643
Average RSD(%) = 1.935								
im_wei-1	43.222	−24.162	−1.380	−24.162	4.929	1.141	0.367	5.099
im_wei-2	43.331	−24.223	−1.384	−24.223	4.919	1.158	0.368	5.092
im_wei-3	43.338	−24.227	−1.384	−24.227	4.913	1.161	0.369	5.086
im_wei-4	43.296	−24.204	−1.391	−24.204	4.920	1.153	0.369	5.085
im_wei-5	43.348	−24.233	−1.388	−24.233	4.933	1.160	0.368	5.094
im_wei-6	43.342	−24.230	−1.380	−24.230	4.885	1.161	0.370	5.076
im_wei-7	42.882	−23.972	−1.433	−23.972	4.775	1.121	0.379	5.117
im_wei-8	44.045	−24.623	−1.757	−24.623	6.145	0.951	0.253	5.208
im_wei-9	43.408	−24.267	−1.422	−24.267	5.055	1.107	0.360	5.081
im_wei-10	43.968	−24.579	−1.777	−24.579	6.086	1.001	0.226	5.086
RSD(%)	0.791	0.791	10.741	0.791	9.898	6.712	16.056	0.760
Average RSD(%) = 5.818								

Table 4.13: Selected orders of AST-G with $K_2^{'} = 0.15 \times N_s$ and $K_1^{'} = \frac{(N_s-1)}{2}$

Image	$I_{0,0}^{\langle \text{ast-G} \rangle}$	$I_{2,0}^{\langle \text{ast-G} \rangle}$	$I_{1,1}^{\langle \text{ast-G} \rangle}$	$I_{0,2}^{\langle \text{ast-G} \rangle}$	$I_{3,0}^{\langle \text{ast-G} \rangle}$	$I_{2,1}^{\langle \text{ast-G} \rangle}$	$I_{1,2}^{\langle \text{ast-G} \rangle}$	$I_{0,3}^{\langle \text{ast-G} \rangle}$
im_4-1	35.056	−28.612	−0.871	−28.612	3.896	−1.711	−1.951	1.899
im_4-2	35.014	−28.578	−0.876	−28.578	3.906	−1.711	−1.95	1.891
im_4-3	35.025	−28.587	−0.878	−28.587	3.901	−1.713	−1.949	1.897
im_4-4	35.028	−28.589	−0.871	−28.589	3.902	−1.711	−1.950	1.891
im_4-5	35.014	−28.577	−0.875	−28.577	3.903	−1.712	−1.949	1.892
im_4-6	35.023	−28.585	−0.877	−28.585	3.902	−1.714	−1.949	1.898
im_4-7	35.025	−28.587	−0.897	−28.587	3.944	−1.710	−1.957	1.884
im_4-8	35.008	−28.573	−0.907	−28.573	3.933	−1.713	−1.959	1.898
im_4-9	35.056	−28.612	−0.835	−28.612	3.855	−1.708	−1.941	1.893
im_4-10	34.973	−28.544	−0.894	−28.544	3.922	−1.709	−1.955	1.879
RSD(%)	0.068	0.068	2.220	0.068	0.615	0.110	0.259	0.344
Average RSD(%) = 0.469								
im_box-1	49.459	−40.367	0.000	−40.367	0.000	0.000	0.000	0.000
im_box-2	49.363	−40.289	0.000	−40.289	0.000	0.000	0.000	0.000
im_box-3	49.372	−40.296	0.000	−40.296	0.000	0.000	0.000	0.000
im_box-4	49.366	−40.292	0.000	−40.292	0.000	0.000	0.000	0.000
im_box-5	49.358	−40.285	0.000	−40.285	0.000	0.000	0.000	0.000
im_box-6	49.327	−40.260	0.000	−40.260	0.000	0.000	0.000	0.000
im_box-7	49.110	−40.083	0.000	−40.083	0.000	0.000	0.000	0.000
im_box-8	49.233	−40.183	0.000	−40.183	0.000	0.000	0.000	0.000
im_box-9	49.483	−40.387	0.000	−40.387	0.000	0.000	0.000	0.000
im_box-10	49.079	−40.058	0.000	−40.058	0.000	0.000	0.000	0.000
RSD(%)	0.273	0.273	0.000	0.273	0.000	0.000	0.000	0.000
Average RSD(%) = 0.102								
im_sigma-1	25.395	−20.727	0.805	−20.727	0.319	−0.125	−0.483	1.359
im_sigma-2	25.386	−20.720	0.808	−20.720	0.324	−0.121	−0.482	1.365
im_sigma-3	25.391	−20.724	0.812	−20.724	0.325	−0.122	−0.482	1.367
im_sigma-4	25.385	−20.719	0.806	−20.719	0.322	−0.122	−0.483	1.364
im_sigma-5	25.385	−20.719	0.810	−20.719	0.323	−0.122	−0.482	1.367
im_sigma-6	25.389	−20.722	0.813	−20.722	0.326	−0.123	−0.482	1.368
im_sigma-7	25.398	−20.729	0.823	−20.729	0.322	−0.130	−0.479	1.374
im_sigma-8	25.402	−20.732	0.802	−20.732	0.325	−0.118	−0.481	1.360
im_sigma-9	25.406	−20.735	0.827	−20.735	0.340	−0.123	−0.473	1.381
im_sigma-10	25.203	−20.571	0.734	−20.571	0.273	−0.134	−0.478	1.300
RSD(%)	0.239	0.237	3.210	0.237	5.443	3.763	0.645	1.632
Average RSD(%) = 1.926								
im_wei-1	23.340	−19.050	−0.402	−19.050	1.056	0.244	0.079	1.093
im_wei-2	23.399	−19.098	−0.403	−19.098	1.054	0.248	0.079	1.091
im_wei-3	23.403	−19.101	−0.404	−19.101	1.053	0.249	0.079	1.090
im_wei-4	23.380	−19.083	−0.406	−19.083	1.054	0.247	0.079	1.090
im_wei-5	23.408	−19.105	−0.405	−19.105	1.057	0.249	0.079	1.092
im_wei-6	23.405	−19.103	−0.402	−19.103	1.047	0.249	0.079	1.088
im_wei-7	23.156	−18.900	−0.418	−18.900	1.023	0.240	0.081	1.097
im_wei-8	23.785	−19.413	−0.512	−19.413	1.317	0.204	0.054	1.116
im_wei-9	23.441	−19.132	−0.415	−19.132	1.083	0.237	0.077	1.089
im_wei-10	23.743	−19.379	−0.518	−19.379	1.304	0.215	0.048	1.090
RSD(%)	0.792	0.791	10.719	0.791	9.903	6.667	16.25	0.756
Average RSD(%) = 5.834								

Table 4.14: Selected orders of AST-L with $\Omega_L = -5$

Image	$I_{0,0}^{\langle \text{ast-L} \rangle}$	$I_{2,0}^{\langle \text{ast-L} \rangle}$	$I_{1,1}^{\langle \text{ast-L} \rangle}$	$I_{0,2}^{\langle \text{ast-L} \rangle}$	$I_{3,0}^{\langle \text{ast-L} \rangle}$	$I_{2,1}^{\langle \text{ast-L} \rangle}$	$I_{1,2}^{\langle \text{ast-L} \rangle}$	$I_{0,3}^{\langle \text{ast-L} \rangle}$
im_4-1	−2.283	−5.000	−6.799	−5.000	5.634	8.640	8.640	5.634
im_4-2	−2.283	−5.000	−6.792	−5.000	5.633	8.611	8.611	5.633
im_4-3	−2.283	−5.000	−6.792	−5.000	5.634	8.611	8.611	5.634
im_4-4	−2.283	−5.000	−6.799	−5.000	5.634	8.640	8.640	5.634
im_4-5	−2.283	−5.000	−6.799	−5.000	5.633	8.640	8.640	5.633
im_4-6	−2.283	−5.000	−6.792	−5.000	5.634	8.611	8.611	5.634
im_4-7	−2.283	−5.000	−6.792	−5.000	5.634	8.611	8.611	5.634
im_4-8	−2.283	−5.000	−6.792	−5.000	5.633	8.611	8.611	5.633
im_4-9	−2.283	−5.000	−6.799	−5.000	5.634	8.639	8.639	5.634
im_4-10	−2.283	−5.000	−6.799	−5.000	5.633	8.641	8.641	5.633
RSD (%)	0.000	0.000	0.054	0.000	0.009	0.177	0.177	0.009
Average RSD(%) = 0.053								
im_box-1	−2.277	−5.000	−6.778	−5.000	5.696	8.626	8.626	5.696
im_box-2	−2.277	−5.000	−6.778	−5.000	5.696	8.626	8.626	5.696
im_box-3	−2.277	−5.000	−6.778	−5.000	5.696	8.626	8.626	5.696
im_box-4	−2.277	−5.000	−6.778	−5.000	5.696	8.626	8.626	5.696
im_box-5	−2.277	−5.000	−6.778	−5.000	5.696	8.626	8.626	5.696
im_box-6	−2.277	−5.000	−6.778	−5.000	5.696	8.626	8.626	5.696
im_box-7	−2.277	−5.000	−6.778	−5.000	5.695	8.626	8.626	5.695
im_box-8	−2.277	−5.000	−6.778	−5.000	5.696	8.626	8.626	5.696
im_box-9	−2.277	−5.000	−6.778	−5.000	5.696	8.626	8.626	5.696
im_box-10	−2.277	−5.000	−6.778	−5.000	5.695	8.626	8.626	5.695
RSD (%)	0.000	0.000	0.000	0.000	0.007	0.000	0.000	0.007
Average RSD(%) = 0.002								
im_sigma-1	−2.291	−5.000	−6.826	−5.000	5.551	8.651	8.651	5.551
im_sigma-2	−2.291	−5.000	−6.812	−5.000	5.551	8.600	8.600	5.551
im_sigma-3	−2.291	−5.000	−6.812	−5.000	5.551	8.600	8.600	5.551
im_sigma-4	−2.291	−5.000	−6.826	−5.000	5.551	8.651	8.651	5.551
im_sigma-5	−2.291	−5.000	−6.826	−5.000	5.551	8.651	8.651	5.551
im_sigma-6	−2.291	−5.000	−6.812	−5.000	5.551	8.600	8.600	5.551
im_sigma-7	−2.291	−5.000	−6.812	−5.000	5.551	8.600	8.600	5.551
im_sigma-8	−2.291	−5.000	−6.812	−5.000	5.551	8.601	8.601	5.551
im_sigma-9	−2.291	−5.000	−6.826	−5.000	5.551	8.652	8.652	5.551
im_sigma-10	−2.291	−5.000	−6.826	−5.000	5.549	8.649	8.649	5.549
RSD (%)	0.000	0.000	0.108	0.000	0.011	0.309	0.309	0.011
Average RSD(%) = 0.094								
im_wei-1	−2.294	−5.000	−6.823	−5.000	5.524	8.611	8.611	5.524
im_wei-2	−2.294	−5.000	−6.830	−5.000	5.525	8.641	8.641	5.525
im_wei-3	−2.294	−5.000	−6.830	−5.000	5.525	8.641	8.641	5.525
im_wei-4	−2.294	−5.000	−6.823	−5.000	5.525	8.611	8.611	5.525
im_wei-5	−2.294	−5.000	−6.822	−5.000	5.525	8.611	8.611	5.525
im_wei-6	−2.294	−5.000	−6.830	−5.000	5.525	8.641	8.641	5.525
im_wei-7	−2.294	−5.000	−6.831	−5.000	5.522	8.642	8.642	5.522
im_wei-8	−2.293	−5.000	−6.830	−5.000	5.531	8.644	8.644	5.531
im_wei-9	−2.294	−5.000	−6.822	−5.000	5.526	8.611	8.611	5.526
im_wei-10	−2.293	−5.000	−6.820	−5.000	5.530	8.607	8.607	5.530
RSD (%)	0.018	0.000	0.065	0.000	0.049	0.194	0.194	0.049
Average RSD(%) = 0.071								

Table 4.15: Selected orders of AST(1) with $\Omega_1 = -5$, skew coefficients $(w_x, w_y) = (-\frac{(N_s-1)}{2}, -\frac{(N_s-1)}{2})$

Image	$I_{0,0}^{\langle ast \rangle}$	$I_{2,0}^{\langle ast \rangle}$	$I_{1,1}^{\langle ast \rangle}$	$I_{0,2}^{\langle ast \rangle}$	$I_{3,0}^{\langle ast \rangle}$	$I_{2,1}^{\langle ast \rangle}$	$I_{1,2}^{\langle ast \rangle}$	$I_{0,3}^{\langle ast \rangle}$
im_4-1	4.639	10.435	13.790	10.435	−13.106	−17.932	−17.930	−13.093
im_4-2	4.639	10.435	13.789	10.435	−13.104	−17.931	−17.929	−13.091
im_4-3	4.639	10.435	13.790	10.435	−13.105	−17.932	−17.930	−13.092
im_4-4	4.639	10.435	13.790	10.435	−13.105	−17.931	−17.929	−13.092
im_4-5	4.639	10.435	13.789	10.435	−13.104	−17.931	−17.929	−13.091
im_4-6	4.639	10.435	13.790	10.435	−13.104	−17.931	−17.930	−13.091
im_4-7	4.639	10.435	13.790	10.435	−13.104	−17.933	−17.931	−13.091
im_4-8	4.638	10.434	13.790	10.434	−13.102	−17.933	−17.931	−13.089
im_4-9	4.639	10.435	13.789	10.435	−13.105	−17.929	−17.927	−13.092
im_4-10	4.638	10.433	13.789	10.433	−13.099	−17.930	−17.929	−13.087
RSD(%)	0.009	0.006	0.004	0.006	0.015	0.007	0.007	0.013
Average RSD(%) = 0.008								
im_box-1	4.588	10.267	13.655	10.267	−12.616	−17.712	−17.712	−12.616
im_box-2	4.588	10.265	13.653	10.265	−12.612	−17.709	−17.709	−12.612
im_box-3	4.588	10.265	13.653	10.265	−12.612	−17.709	−17.709	−12.612
im_box-4	4.588	10.265	13.653	10.265	−12.611	−17.709	−17.709	−12.611
im_box-5	4.588	10.265	13.653	10.265	−12.611	−17.709	−17.709	−12.611
im_box-6	4.588	10.265	13.653	10.265	−12.611	−17.708	−17.708	−12.611
im_box-7	4.587	10.263	13.651	10.263	−12.605	−17.705	−17.705	−12.605
im_box-8	4.587	10.263	13.652	10.263	−12.606	−17.706	−17.706	−12.606
im_box-9	4.588	10.266	13.654	10.266	−12.614	−17.71	−17.71	−12.614
im_box-10	4.587	10.261	13.65	10.261	−12.601	−17.702	−17.702	−12.601
RSD(%)	0.011	0.017	0.010	0.017	0.036	0.016	0.016	0.036
Average RSD(%) = 0.020								
im_sigma-1	4.709	10.668	14.042	10.668	−13.728	−18.511	−18.506	−13.744
im_sigma-2	4.709	10.668	14.042	10.668	−13.727	−18.510	−18.505	−13.743
im_sigma-3	4.709	10.668	14.042	10.668	−13.727	−18.510	−18.505	−13.743
im_sigma-4	4.709	10.668	14.042	10.668	−13.727	−18.510	−18.505	−13.742
im_sigma-5	4.709	10.668	14.041	10.668	−13.727	−18.510	−18.504	−13.742
im_sigma-6	4.709	10.668	14.042	10.668	−13.727	−18.510	−18.504	−13.743
im_sigma-7	4.709	10.669	14.042	10.669	−13.728	−18.509	−18.504	−13.744
im_sigma-8	4.708	10.667	14.041	10.667	−13.723	−18.509	−18.503	−13.739
im_sigma-9	4.709	10.669	14.041	10.669	−13.728	−18.508	−18.503	−13.744
im_sigma-10	4.707	10.661	14.037	10.661	−13.708	−18.505	−18.499	−13.724
RSD(%)	0.014	0.022	0.011	0.022	0.045	0.009	0.010	0.044
Average RSD(%) = 0.022								
im_wei-1	4.731	10.741	14.063	10.741	−13.905	−18.462	−18.465	−13.904
im_wei-2	4.731	10.743	14.064	10.743	−13.910	−18.465	−18.468	−13.910
im_wei-3	4.731	10.743	14.064	10.743	−13.910	−18.465	−18.469	−13.910
im_wei-4	4.731	10.743	14.064	10.743	−13.908	−18.464	−18.468	−13.908
im_wei-5	4.732	10.744	14.065	10.744	−13.912	−18.466	−18.469	−13.911
im_wei-6	4.731	10.743	14.064	10.743	−13.910	−18.465	−18.468	−13.909
im_wei-7	4.728	10.733	14.056	10.733	−13.883	−18.452	−18.455	−13.882
im_wei-8	4.737	10.762	14.085	10.762	−13.966	−18.512	−18.515	−13.961
im_wei-9	4.732	10.744	14.065	10.744	−13.912	−18.468	−18.471	−13.911
im_wei-10	4.737	10.763	14.086	10.763	−13.968	−18.514	−18.517	−13.963
RSD(%)	0.059	0.087	0.070	0.087	0.194	0.116	0.115	0.182
Average RSD(%) = 0.114								

4.4.3 Numerical Efficiency

In this section, the computational efficiency of the proposed method in comparison with AST-G, AST-L and AST-Z has been evaluated. The program was implemented in Matlab 2011b, on Intel i3 550 processor with 3.2GHz, 3GB of RAM. In this experiment, images with size 50×50, 100×100, 150×150, and 200×200 pixels were used to generate invariant features with orders of 10, 20, 30 and 40. The experiment was repeated 200 times and the average CPU elapse times in millisecond were recorded. From Table 4.16, excluding the moment generation time, on average, the efficiency of the proposed method is about 5.44 times and 91.88 times faster than AST-G and AST-L, respectively. The significant improvement in performance are mainly due to the simplicity of the new recurrence relations. AST-L and AST-Z are inefficient mainly due to complexity of hypergeometric functions involved. The sequential computation on translation invariants followed by anisotropic scale invariants further slowdown the calculation of the invariant descriptors.

Table 4.16: Comparison of CPU elapse time (ms) for AST invariants algorithms

			Proposed Method		AST-G		AST-L		AST-Z(1)	
Image Size	Order of descriptors	Moments generation times (ms)	Invariant generation times (ms)	Total time (ms)	Invariant generation times (ms)	Total time (ms)	Invariant generation times (ms)	Total time (ms)	Invariant generation times (ms)	Total time (ms)
(50×50)	10	12.921	0.376	13.297	1.318	14.239	7.685	20.605	10.419	23.340
	20	29.623	0.984	30.606	5.819	35.442	62.421	92.044	56.114	85.737
	30	58.477	3.125	61.601	17.737	76.213	262.046	320.522	162.442	220.919
	40	98.555	7.898	106.452	40.907	139.462	796.051	894.606	367.224	465.779
(100×100)	10	28.167	0.267	36.586	1.271	37.591	7.644	43.964	10.334	46.653
	20	95.368	0.981	109.978	5.883	114.881	62.326	171.323	54.157	163.154
	30	205.950	3.124	225.195	17.771	239.842	262.796	484.867	161.750	383.821
	40	353.170	7.873	381.514	42.230	415.871	794.557	1,168.198	368.488	742.129
(150×150)	10	80.049	0.266	80.315	1.397	81.446	7.768	87.816	10.437	90.485
	20	242.386	0.980	243.366	6.008	248.395	64.719	307.105	54.024	296.411
	30	493.040	3.122	496.161	17.891	510.931	262.934	755.974	161.333	654.372
	40	878.077	7.876	885.953	40.910	918.987	793.619	1,671.696	367.583	1,245.66
(200×200)	10	141.172	0.267	141.439	1.561	142.733	7.943	149.115	10.615	151.787
	20	427.373	0.981	428.354	6.155	433.528	62.694	490.067	54.247	481.620
	30	933.857	3.111	936.968	17.956	951.812	263.281	1197.137	161.354	1,095.211
	40	1,464.211	7.886	1,472.097	42.522	1,506.733	794.216	2,258.427	367.713	1,831.924
Average		346.400	3.070	353.118	16.709	366.757	282.044	632.092	148.640	498.688

4.4.4 Robustness to Noise

Noise has an adverse effect on the invariance of moments. This is due to the difficulty in determining the accurate normalizing parameters such as the centroid $(\bar{x}, \bar{y})$, and the scale coefficients a_1 and a_2 under noisy condition. Since the normalizing parameters are important for mapping the transformed image to a standard normalized form, the invariance of the moments is directly affected in the presence of noise. In this experiment, the performance of AST is tested. For the purpose of comparison, AST-G, AST-L, AST-Z, and AST-P are also shown. The following features are used for the recognition task

$$\mathbf{V} = [I_{0,0}, I_{2,0}, I_{0,2}, I_{3,0}, I_{1,2}, I_{2,1}, I_{0,3}]^T \tag{4.95}$$

where $I_{n,m}$ denotes the AST-Invariants defined in the previous section. In this experiment, the square of Euclidean distance is utilized as the classification measures.

$$d(\tilde{\mathbf{V}}_\mathbf{s}, \tilde{\mathbf{V}}_\mathbf{t}^{(\mathbf{k})}) = \sum_{j=1}^{J} (\tilde{v}_{s,j} - \tilde{v}_{t,j}^{(k)})^2, \tag{4.96}$$

where $\tilde{\mathbf{V}}_\mathbf{s}$ is the $J-$dimensional scaled feature vectors of unknown sample, and $\tilde{\mathbf{V}}_\mathbf{t}^{(\mathbf{k})}$ is the scaled training vector of class k. The scaled feature vectors are used mainly to remove large dynamic range on moments values. The scaled formula is as follows:

$$\tilde{v}_{s,j} = \frac{v_{s,j} - \min\limits_k v_{t,j}^{(k)}}{\max\limits_k v_{t,j}^{(k)} - \min\limits_k v_{t,j}^{(k)}}. \tag{4.97}$$

The recognition accuracy, η, is defined as

$$\eta = \frac{\text{Number of correctly classified images}}{\text{Total number of images used in the test}}. \tag{4.98}$$

The numbers and upper case letters “0", “5", “B", “F", “I", “J", “O", and “S" from Figure 4.1 are used as the training set. The size of each training image is 80×80 pixels. Both of the original space $S_2(N_0)$ and transformed space $S_2(N_s)$ are equal to $S_2(251)$. The testing set is generated by scaling and translating the training set with scale factors $a_1, b_1 \in \{-1.5, -1, -0.5, 0.5, 1, 1.5\}$ and translation parameters $a_2, b_2 \in \{-1, 0, 1\}$. The transformation forms a testing set of 2,592 images. This is followed by adding salt-and-pepper noise with different noise densities. Figure 4.2 shows some of the testing images contaminated by 1% to 4% of salt-and-pepper noise.

Figure 4.1: Binary images as training set for experiment on character recognition.

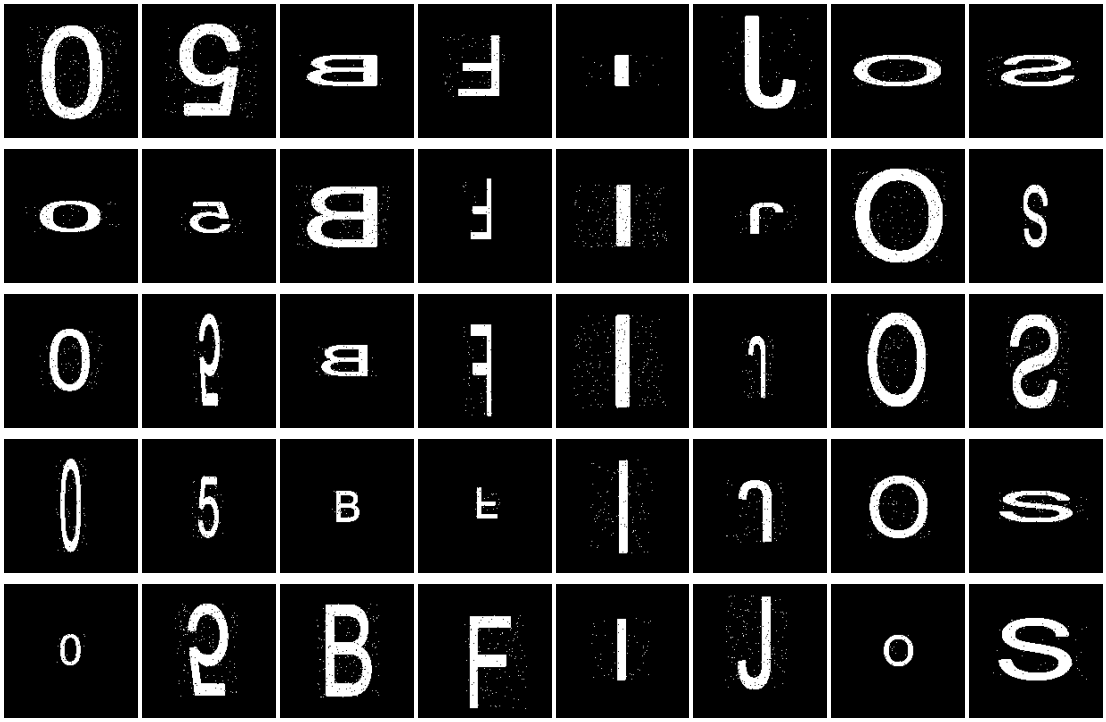

Figure 4.2: Part of the images in the testing set.

Table 4.17: Classification Result of image with translation and scale transformation

Salt & pepper	AST(3)*	AST(3)-W*	AST-G	AST-Z	AST-P	AST-L
No noise	100.00%	100.00%	98.61%	100.00%	100.00%	75.00%
1%	75.89%	26.89%	35.80%	71.61%	71.61%	30.25%
2%	72.99%	26.42%	35.29%	65.09%	65.09%	20.87%
3%	71.91%	27.74%	35.15%	60.84%	60.84%	19.60%
4%	69.95%	27.01%	36.30%	58.91%	58.91%	19.33%

AST(3)* denotes AST using the $3^{rd}-$scale normazation scheme
AST(3)-W* denotes AST(3) with centroid at the origin.

Table 4.17 shows the feature vectors are used to classify these images and recognition accuracy is compared with others AST-invariant algorithms.

In this experiment, AST(3) denotes the AST-invariants using the third scaling normalization scheme with scale coefficients $\tilde{\Omega}_a = \tilde{\Omega}_b = 0$, and skew parameters set to $(w_x, w_y) = (-10, 0)$. As follow the recommendation of Goh et al. (2009), the scale coefficient of AST-G is set to $K_2^{'} = 0.6 \times N_s$ (to compliant with the recommended range $[0.5N_s, 0.8N_s]$), and $K_1^{'} = 0$. As shown in Table 4.17, AST-L, AST-W and AST-G have the three lowest in classification performance. The poor performance is mainly due to ambiguity caused by shifting of centroid away from the middle of transformed space $S_2(N_s)$. The explanation is supported by the poor performance shown by AST(3)-W, from which, in this case the scale parameter is identical to AST(3), however the image centroid is shifted to origin by the skew parameters. AST-Z which have the identical performance when compared with AST-P confirmed the strong correlation between the two algorithms.

4.4.5 Recognition of Similar Chinese Handwritten Characters

In this subsection, the discriminative power of AST-invariants features are evaluated using Chinese handwritten characters. For this purpose, the HCL2000 database (H. Zhang, Guo, Chen, & Li, 2009) is selected; this database consists of large amount of very similar Chinese handwritten characters written by 1,000 different writers. As shown in Figure 4.3, nine pairs of very similar Chinese handwritten characters each differing by one stroke in nine different zones are selected for this experiment. Figures 4.4 and 4.5 show some of the randomly selected images that are used in the experiment. The database is separated into two groups. The group with label of “hh" consists of character sets written by 300 writers. The second group with label of “xx", consists of character sets written by another 700 writers. The images with label “xx” are used as training set and the images with “hh" are used for testing. The images are scaled to size 70×70 pixels. The original space $S_2(N_0)$ and transformed space $S_2(N_s)$ are both equal to $S_2(150)$. The AST-invariants descriptors: AST(3), AST(3)-W, AST-G, AST-L, AST-Z and AST-P are selected as feature extractors. The scale parameters for AST(3) are $\tilde{\Omega}_a = \tilde{\Omega}_b = 0.7$. AST(3)-W uses the same scale coefficients as AST(3), but the images' centroid are shifted to the origin by skew parameters $(w_x, w_y) = (-\frac{(N_s-1)}{2}, -\frac{(N_s-1)}{2})$. AST-G on the other hand, are made

compliant with proposed normalization conditions. We let the scale coefficient $K_2^{'}$ be $0.187 \times N_s$ and translation coefficient $K_1^{'} = \frac{N_s - 1}{2}$, which indicate the centroid of canonical forms of AST-G are now at the middle of transformed space $S_2(N_s)$.

For each AST invariant, moments up to order 10 are generated. This would make up a total of 66 feature vectors. The features generated from the training set are used by forward sequential search algorithm for dimensional reduction. Two sets of feature vectors each with 15 variables are selected by the search algorithm using the linear discriminant analysis (LDA), and quadratic discriminant analysis (QDA) as the classifiers, respectively. In the process of classification, LDA , QDA and support vector machine (SVM) are used as the classifiers. The three classifiers are used to ensure the objectiveness of the experiment in determining the discriminative power of proposed features. For classification using SVM, the radial basis function (RBF) kernel are deployed. A grid search on the penalty parameter C and kernel parameter γ using five-fold cross-validation has been executed to find the best parameter values (C, γ), for range $C = 2^{-3}, 2^{-2}, \cdots, 2^3$ and $\gamma = 2^{-5}, 2^{-2}, \cdots, 2^1$.

Each pair of Chinese characters is evaluated separately. For each case, a total of 1400 Chinese handwritten characters from the two groups are used for feature selection and training, another 600 images are used for testing. The average misclassification rate (mcr) for all the pairs of characters are recorded. Figures 4.6 to 4.9 show the outcome of the experiments. Figure 4.6 indicates the classification performance of the LDA used in the process of dimension reduction, training and testing. Figure 4.7 shows the outcome of experiment with LDA used in the search algorithm, and SVM is used in training and testing. Figure 4.8 indicates the performance of the QDA algorithm in process of dimension reduction, training and testing. Finally Figure 4.9 shows the performance of using QDA in dimension reduction, and the SVM is used in training and testing. Unlike the previous experiment, AST-G in this case shows identical performance when compared to AST(3). The two features outperform other features by a margin ranging from 8% to 15%. The improvement on AST-G can be explained by the fact that AST-G is now using the similar normalization strategy as AST(3). The classification performance of AST-Z and AST-P are nearly identical, this indicates the strong correlation between the two algorithms. The performance of AST-L is relatively poor when compare with the others. This mainly due

to ambiguity caused by deviation of canonical images from the middle of space.

As shown in Figures 4.6 to 4.9, classification performance of the propose AST consistently outperform AST-L, AST-Z and AST-P in different type of classifiers. We therefore conclude that the discriminative power of proposed features is better with the new normalization schemes.

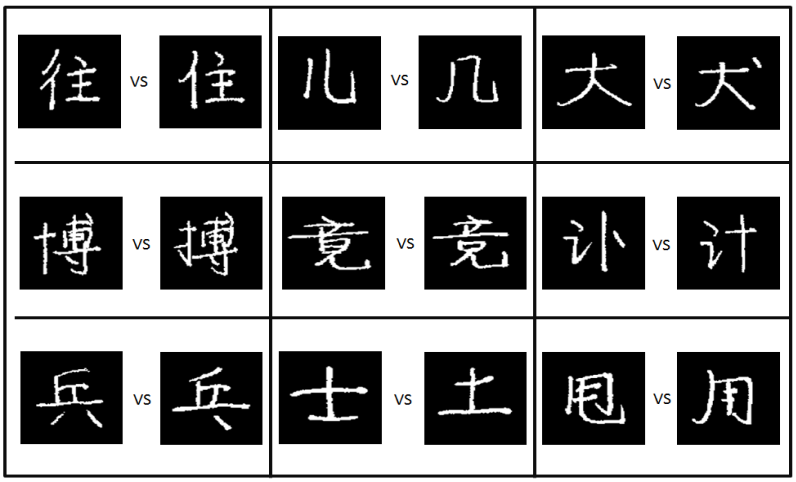

Figure 4.3: Very similar Chinese characters that differ by one stroke in nine different zones.

4.5 Conclusion

In this chapter the anisotropic scale and translation Tchebichef moment invariants using the method of image normalization has been reviewed. A new set of recurrence relations is proposed for fast computation on AST-invariants. Three new scale normalization schemes based on Tchebichef moments and the new spatial displacement normalization have been proposed to further improve the features discriminative power and classification performance. The performance of the proposed algorithm is supported by series of experiments conducted in this chapter.

Set	Index	Training Set (xx001-xx700)	Testing Set (hh001-hh300)
1	2816		
	3668		
2	654		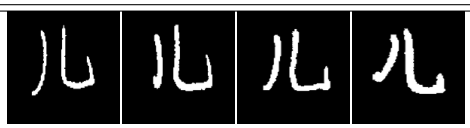
	1153	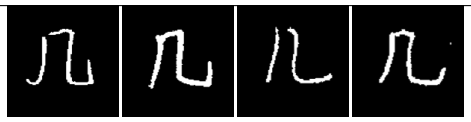	
3	460		
	2271		
4	198		
	200		
5	1342		
	1343		

Figure 4.4: Some randomly selected images from the training and testing.

Set	Index	Training Set (xx001-xx700)	Testing Set (hh001-hh300)
6	781		
	1167		
7	183		
	2025		
8	2476		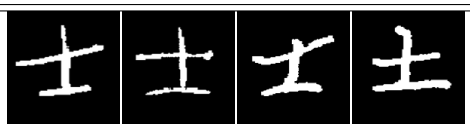
	2760		
9	2545		
	3326		

Figure 4.5: Some randomly selected images from training and testing.

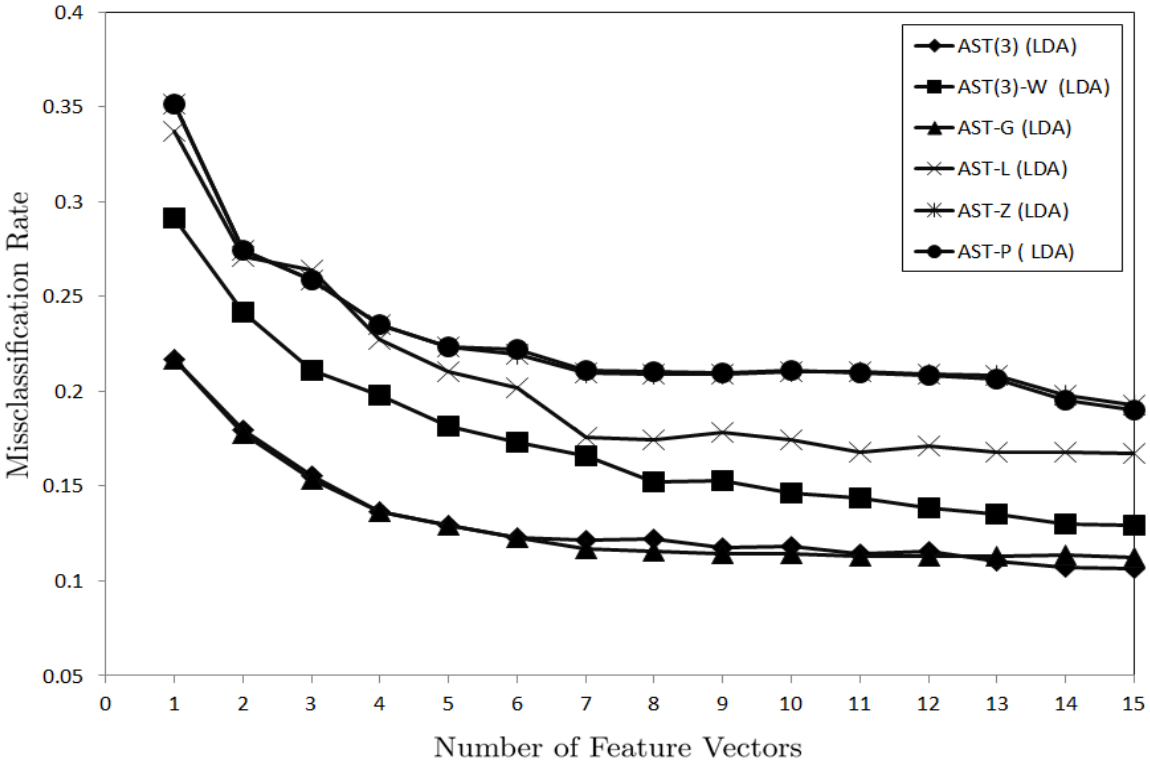

Figure 4.6: Comparison of discriminative power for AST algorithms using linear discriminative classifier on Chinese handwritten characters.

n_f	AST(3)	AST(3)-W	AST-G	AST-L	AST-Z	AST-P
1	0.217	0.292	0.217	0.337	0.351	0.351
2	0.180	0.242	0.178	0.271	0.274	0.274
3	0.155	0.211	0.154	0.264	0.259	0.259
4	0.136	0.198	0.137	0.227	0.236	0.235
5	0.130	0.181	0.129	0.211	0.223	0.223
6	0.123	0.173	0.123	0.202	0.220	0.222
7	0.121	0.166	0.117	0.176	0.210	0.211
8	0.122	0.152	0.116	0.175	0.209	0.210
9	0.118	0.153	0.114	0.178	0.209	0.210
10	0.118	0.147	0.114	0.174	0.210	0.211
11	0.114	0.144	0.113	0.168	0.210	0.210
12	0.116	0.138	0.113	0.171	0.209	0.208
13	0.111	0.136	0.113	0.168	0.209	0.207
14	0.107	0.130	0.114	0.168	0.198	0.195
15	0.106	0.129	0.112	0.167	0.193	0.190

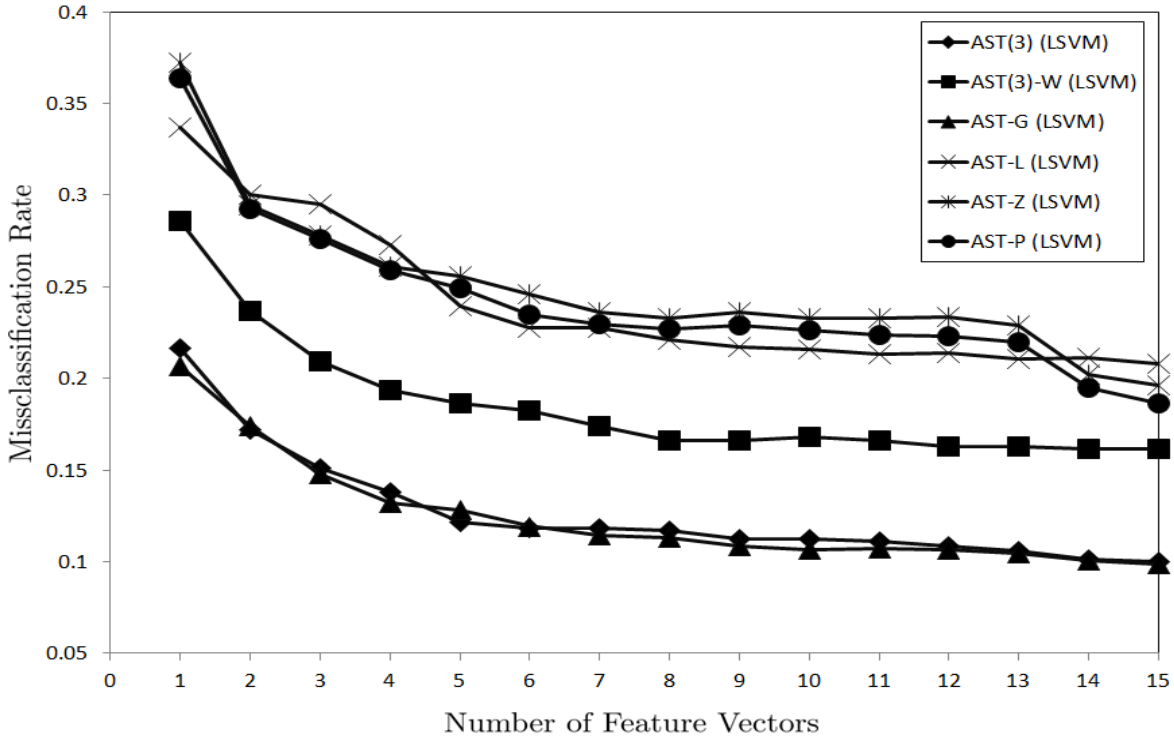

Figure 4.7: Comparison of discriminative power for AST algorithms using support vector machine classifier on Chinese handwritten characters.

n_f	AST(3)	AST(3)-W	AST-G	AST-L	AST-Z	AST-P
1	0.216	0.286	0.207	0.337	0.372	0.364
2	0.172	0.237	0.174	0.300	0.294	0.293
3	0.151	0.209	0.148	0.295	0.278	0.276
4	0.138	0.194	0.132	0.273	0.261	0.259
5	0.121	0.187	0.128	0.239	0.256	0.249
6	0.118	0.182	0.119	0.228	0.246	0.235
7	0.119	0.174	0.115	0.228	0.236	0.230
8	0.117	0.166	0.113	0.221	0.233	0.227
9	0.112	0.166	0.108	0.217	0.236	0.229
10	0.113	0.168	0.107	0.216	0.233	0.227
11	0.111	0.166	0.107	0.213	0.233	0.224
12	0.108	0.163	0.106	0.214	0.233	0.223
13	0.106	0.163	0.104	0.211	0.229	0.220
14	0.101	0.162	0.100	0.211	0.202	0.195
15	0.100	0.161	0.099	0.208	0.196	0.186

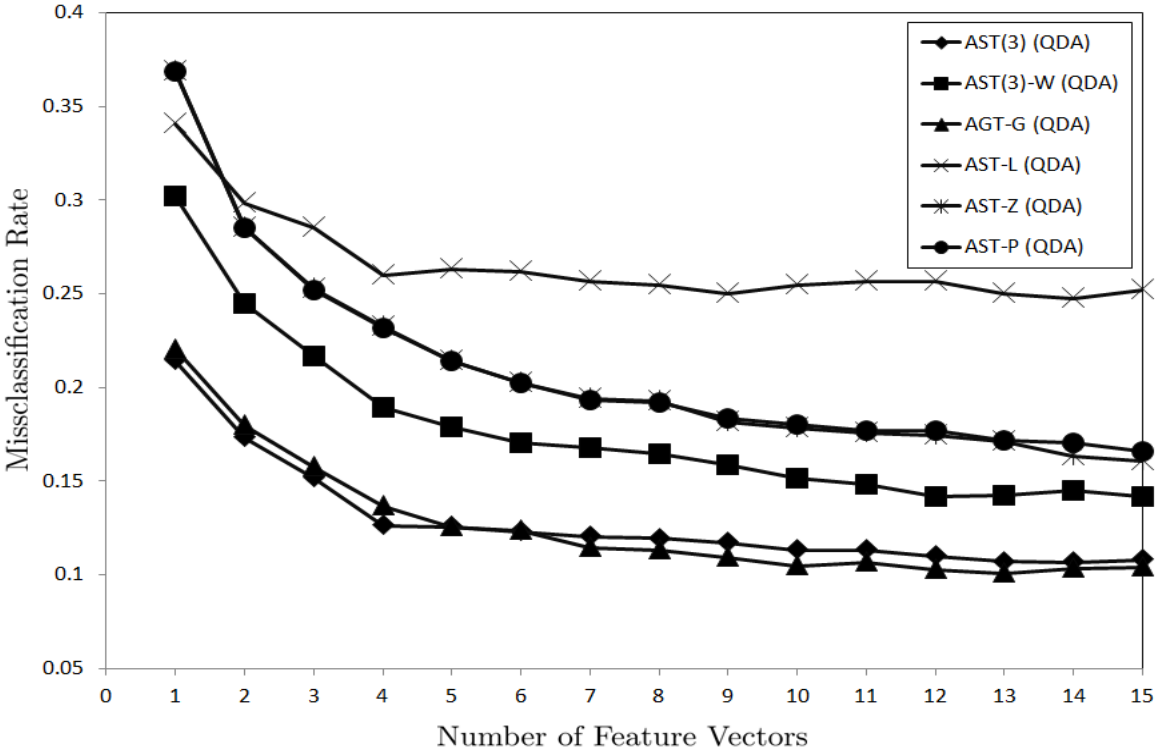

Figure 4.8: Comparison of discriminative power for AST algorithms using quadratic discriminative classifier on Chinese handwritten characters.

n_f	AST(3)	AST(3)-W	AST-G	AST-L	AST-Z	AST-P
1	0.214	0.302	0.220	0.341	0.369	0.369
2	0.173	0.245	0.179	0.299	0.286	0.285
3	0.151	0.217	0.157	0.286	0.253	0.252
4	0.126	0.190	0.137	0.260	0.232	0.232
5	0.125	0.179	0.126	0.263	0.214	0.214
6	0.123	0.171	0.123	0.261	0.202	0.202
7	0.120	0.168	0.115	0.257	0.194	0.193
8	0.119	0.165	0.113	0.255	0.193	0.192
9	0.117	0.159	0.109	0.250	0.182	0.183
10	0.113	0.152	0.105	0.255	0.178	0.180
11	0.113	0.148	0.106	0.256	0.176	0.177
12	0.110	0.141	0.103	0.256	0.175	0.177
13	0.107	0.142	0.101	0.250	0.171	0.172
14	0.106	0.145	0.103	0.248	0.164	0.171
15	0.108	0.142	0.104	0.252	0.161	0.166

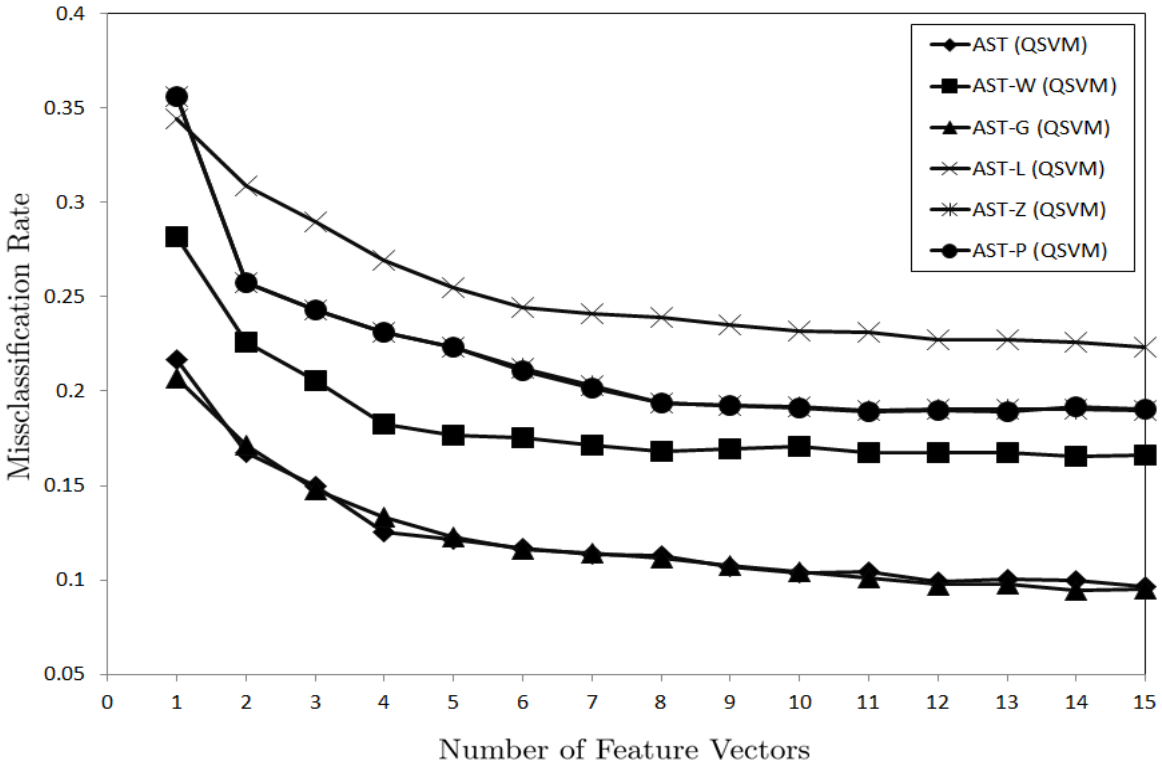

Figure 4.9: Comparison of discriminative power for AST algorithms using support vector machine classifier on Chinese handwritten characters.

n_f	AST(3)	AST(3)-W	AST-G	AST-L	AST-Z	AST-P
1	0.217	0.282	0.207	0.344	0.356	0.356
2	0.167	0.226	0.172	0.309	0.258	0.258
3	0.149	0.206	0.148	0.290	0.243	0.243
4	0.126	0.183	0.133	0.269	0.231	0.231
5	0.121	0.176	0.123	0.255	0.223	0.223
6	0.117	0.175	0.116	0.244	0.212	0.211
7	0.114	0.171	0.114	0.241	0.203	0.202
8	0.113	0.168	0.112	0.239	0.194	0.194
9	0.107	0.169	0.107	0.235	0.192	0.193
10	0.104	0.171	0.104	0.232	0.192	0.191
11	0.104	0.168	0.101	0.231	0.190	0.189
12	0.099	0.167	0.097	0.227	0.191	0.190
13	0.100	0.167	0.098	0.227	0.190	0.189
14	0.100	0.165	0.094	0.226	0.190	0.192
15	0.097	0.166	0.095	0.223	0.190	0.191

CHAPTER 5

TRANSLATION, ROTATION AND SCALE TCHEBICHEF MOMENT INVARIANTS

In this chapter, translation, rotation, and scale (TRS) invariants for the discrete orthogonal moments are reviewed. The first TRS invariants of discrete orthogonal moments are proposed by Yap et al. (2007). In (Yap et al., 2007), the TRS Krawtchouk moment invariants are calculated indirectly using modified geometric moments. This is followed by translation and rotational Tchebichef moment invariants of H. Zhang et al. (2010) for Tchebichef moments using the image normalization approach. However the method is slow mainly due to the complexity of the hypergeometric functions involved. On the other hand, the algorithm proposed by Yap et al. (2007) is relatively faster. However the invariants are computed from the modified geometric moments. In the situation where the image is not present, this method is not usable. Thus a new set of TRS invariants have been proposed for discrete Tchebichef moments. The algorithms use new recursive formulae of the functions involved for fast computation. On top of that, a new set of normalization scheme based on Tchebichef moments has been proposed to improve the classification accuracy and to avoid the computational overhead caused by determining the parameters from other domains. An empirical study has confirmed that the proposed algorithms showed significant improvement in terms of numerical performance and classification accuracy.

5.1 Introduction

Translation, rotation and scale (TRS) is the spatial coordinate transformation defined by

$$\begin{pmatrix} x' \\ y' \end{pmatrix} = a \begin{pmatrix} \cos\theta & \sin\theta \\ -\sin\theta & \cos\theta \end{pmatrix} \begin{pmatrix} x \\ y \end{pmatrix} + \begin{pmatrix} a_3 \\ b_3 \end{pmatrix}. \tag{5.1}$$

It is a four-parameter transformation, in which, a denotes the positive scaling factor, θ is the angle of rotation, a_3 and b_3 are the spatial displacements of image in the direction of $x-$axis and $y-$axis, respectively.

Invariants to translation, rotation and scale were first introduced by Hu (1962) for geometric moments (TRS-H). According to Hu, the translation invariance was achieved by shifting the image centroid to the origin using the central moments. The scale factor a was eliminated by the cancellation process using zero order moment. The rotation invariance was achieved by using the principal axis normalization. The $(n+m)^{\text{th}}-$order of translation, rotation and scale geometric moment invariant, $I_{n,m}^{\langle \text{trs-H} \rangle}$, can be computed by

$$I_{n,m}^{\langle \text{trs-H} \rangle} = \frac{\left[\int_{-\infty}^{\infty} \int_{-\infty}^{\infty} ((x-\bar{x})\cos\theta_h + (y-\bar{y})\sin\theta_h)^n \times (-(x-\bar{x})\sin\theta_h + (y-\bar{y})\cos\theta_h)^m f(x,y)dxdy \right]}{m_{0,0}^{\frac{n+m}{2}+1}} \tag{5.2}$$

where

$$\bar{x} = \frac{m_{1,0}}{m_{0,0}}, \text{ and } \bar{y} = \frac{m_{0,1}}{m_{0,0}} \tag{5.3}$$

and $m_{p,q}$ denotes the geometric moment.

The angle θ_h is derived based on principal axis normalization given in Table 5.1 (Yap, 2006). The formula of θ_h is in fact equivalent to normalization of

$$\mu_{2,0}^{'} \geq \mu_{0,2}^{'} \tag{5.4}$$

where $\mu_{n,m}^{'}$ is the central moment after the process of normalization.

The normalization however failed to resolve the ambiguity of object being rotated by 180^{o} apart. Therefore additional normalization conditions is required as follows

$$\mu_{3,0}^{'} \geq 0 \tag{5.5}$$

In Section 4.2, translation, rotation and scale Tchebichef moment invariants of Yap et. al. (2003) (TRS-Y) and translation and rotation Tchebichef moment invariants of Zhang et. al. (2010) (TR-Z), have been reviewed. In Section 4.3, a new set of TRS invariant algorithms is proposed for Tchebichef moments. Section 4.4 gives an empirical verification to support the theoretical frameworks. Section 4.5 concludes the topic.

5.2 Preliminaries for the Proposed Invariants

We first review some expressions that will be used in the latter sections.

Table 5.1: Values of θ_h

$\mu_{2,0}-\mu_{0,2}$	$\mu_{1,1}$	θ_h
0	0	0
0	+	$\pi/4$
0	−	$-\pi/4$
+	0	0
+	+	θ_b
+	−	$\theta_b+\pi$
−	0	$\pi/2$
−	+	$\theta_b+\pi/2$
−	−	$\theta_b+\pi/2$
$\theta_b=\frac{1}{2}\tan^{-1}\left(\frac{2\mu_{1,1}}{(\mu_{2,0}-\mu_{0,2})}\right)$		

Suppose $\tilde{t}_n^N(x)$ denotes the Tchebichef polynomial and $c_{n,k}^N$ are coefficients of the polynomials

$$t_n^N(x)=\sum_{k=0}^{n} c_{n,k}^N x^k \tag{5.6}$$

and $d_{k,n}^N$ denote the coefficients of Tchebichef polynomials such that

$$\begin{aligned} x^n &= \sum_{j=0}^{n} d_{n,j}^N \tilde{t}_k^N(x), \\ & \qquad x,n=0,1,\cdots N-1. \end{aligned} \tag{5.7}$$

From the orthogonality property of Tchebichef polynomial $\tilde{t}_n^N(x)$, the coefficients $c_{n,k}^N$ and $d_{k,m}^N$ have the following relation

$$\sum_{k=m}^{n} c_{n,k}^N d_{k,m}^N=\delta_{n,m} \tag{5.8}$$

where $\delta_{n,m}$ denotes the Kronecker's delta that returns unity when $n=m$ and zero otherwise.

The three terms recurrence relation of Tchebichef polynomial, $\tilde{t}_n^N(x)$, can be expressed as

$$\begin{aligned} \tilde{t}_n^N(x) &= (x\tilde{A}_n^N+\tilde{B}_n^N)\tilde{t}_{n-1}^N(x)+\tilde{C}_n^N\tilde{t}_{n-2}^N(x), \\ & \qquad n=2,3,\ldots,N-1 \end{aligned} \tag{5.9}$$

and

$$\tilde{t}_0^N(x) = \frac{1}{\sqrt{N}} \tag{5.10}$$

$$\tilde{t}_1^N(x) = (x\tilde{A}_1^N+\tilde{B_1^N})\tilde{t}_0^N(x) \tag{5.11}$$

where

$$\tilde{A}_n^N = \frac{2}{n}\sqrt{\frac{4n^2-1}{N^2-n^2}} \tag{5.12}$$

$$\tilde{B}_n^N = \frac{(1-N)}{n}\sqrt{\frac{4n^2-1}{N^2-n^2}} \tag{5.13}$$

$$\tilde{C}_n^N = -\frac{(n-1)}{n}\sqrt{\frac{2n+1}{2n-3}}\sqrt{\frac{N^2-(n-1)^2}{N^2-n^2}}. \tag{5.14}$$

5.2.1 Translation, Rotation and Scale Tchebichef Moment Invariants using Indirect Approach

In this section the invariance proposed by Yap et al. (2003) was implemented for the Tchebichef moments. The $(n+m)^{\text{th}}-$order of TRS-Y $I_{n,m}^{\langle\text{trs-Y}\rangle}$, is expressed in the form of modified geometric moments

$$\begin{aligned} I_{n,m}^{\langle\text{trs-Y}\rangle} &= \frac{N^2}{2m_{0,0}}\sum_{x=0}^{N-1}\sum_{y=0}^{N-1}\tilde{t}_n^N\left\{[(x-\bar{x})\cos(\theta_h)+(y-\bar{y})\sin(\theta_h)]\sqrt{\frac{N^2}{2m_{0,0}}}+\frac{N}{2}\right\} \\ &\quad\times\tilde{t}_m^N\left\{[-(x-\bar{x})\sin(\theta_h)+(y-\bar{y})\cos(\theta_h)]\sqrt{\frac{N^2}{2m_{0,0}}}+\frac{N}{2}\right\}\times f(x,y) \\ &= \sum_{k=0}^{n}\sum_{j=0}^{m}c_{n,k}^N c_{m,j}^N \dot{m}_{k,j} \end{aligned} \tag{5.15}$$

where

$$\begin{aligned} \dot{m}_{p,q} &= \frac{N^2}{2m_{0,0}}\sum_{x=0}^{N-1}\sum_{y=0}^{N-1}f(x,y)\times\left\{[(x-\bar{x})\cos(\theta_h)+(y-\bar{y})\sin(\theta_h)]\sqrt{\frac{N^2}{2m_{0,0}}}+\frac{N}{2}\right\}^p \\ &\quad\times\left\{[-(x-\bar{x})\sin(\theta_h)+(y-\bar{y})\cos(\theta_h)]\sqrt{\frac{N^2}{2m_{0,0}}}+\frac{N}{2}\right\}^q \end{aligned} \tag{5.16}$$

and

$$\begin{aligned} \theta_h &= \frac{1}{2}\tan^{-1}\left(\frac{2\mu_{1,1}}{\mu_{2,0}-\mu_{0,2}}\right) \\ \bar{x} &= \frac{m_{1,0}}{m_{0,0}} \text{ and } \bar{y} = \frac{m_{0,1}}{m_{0,0}} \end{aligned} \tag{5.17}$$

$m_{p,q}$ denotes the geometric moment, and $\mu_{p,q}$ denotes the central moment.

The angle of θ_h is implemented following the values in Table 5.1, and the conditions (5.4) and (5.5) are used to resolve the ambiguities caused by principal axis normalization.

5.2.2 Translation and Rotation Tchebichef Moment Invariants of Zhang et. al.

TR-Z was initially proposed to provide rotational invariants for symmetric images (H. Zhang et al., 2010). It consists of the combination of two invariant algorithms, i.e. the translation invariants and rotation invariants to form the translation and rotational invariants.

5.2.2 (a) Translation Tchebichef Moment Invariants

Similar to Zhu et al. (2007c), the translation invariant is obtained via transforming the image's centroid to the origin using Tchebichef central moment

$$T_{n,m}^{\langle \mathrm{c} \rangle} = \sum_{x=0}^{N-1} \sum_{y=0}^{N-1} \tilde{t}_n^N(x-\bar{x}) \tilde{t}_m^N(y-\bar{y}) f(x,y) \tag{5.18}$$

where $(\bar{x}, \bar{y})$ denotes the image centroid coordinate given by

$$\bar{x} = \frac{c_{0,0}^N T_{1,0} - c_{1,0}^N T_{0,0}}{c_{1,1}^N T_{0,0}}, \text{ and } \bar{y} = \frac{c_{0,0}^N T_{0,1} - c_{1,0}^N T_{0,0}}{c_{1,1}^N T_{0,0}}. \tag{5.19}$$

By using (5.6), the translated Tchebichef polynomial $\tilde{t}_n^N(x-\bar{x})$ is decomposed into polynomials of x

$$\tilde{t}_n^N(x-\bar{x}) = \sum_{k=0}^{n} \sum_{r=0}^{k} \binom{k}{r} c_{n,k}^N x^r (-\bar{x})^{k-r}. \tag{5.20}$$

With the help of (5.7), we get

$$\tilde{t}_n^N(x-\bar{x}) = \sum_{k=0}^{n} \sum_{r=0}^{k} \sum_{u=0}^{r} \binom{k}{r} c_{n,k}^N d_{r,u}^N (-\bar{x})^{k-r} \tilde{t}_u^N(x). \tag{5.21}$$

Similarly for $\tilde{t}_m^N(y-\bar{y})$, we have

$$\tilde{t}_m^N(y-\bar{y}) = \sum_{j=0}^{m} \sum_{s=0}^{j} \sum_{v=0}^{s} \binom{j}{s} c_{m,j}^N d_{s,v}^N (-\bar{y})^{j-s} \tilde{t}_v^N(y). \tag{5.22}$$

By substituting (5.21) and (5.22) into (5.18), we get

$$T_{n,m}^{\langle \mathrm{c} \rangle} = \sum_{k=0}^{n} \sum_{j=0}^{m} \sum_{r=0}^{k} \sum_{u=0}^{r} \sum_{s=0}^{j} \sum_{v=0}^{s} \binom{k}{r} \binom{j}{s} c_{n,k}^N c_{m,j}^N d_{r,u}^N d_{s,v}^N \times (-\bar{x})^{k-r} (-\bar{y})^{j-s} T_{u,v}. \tag{5.23}$$

5.2.2 (b) Rotation Tchebichef Moment Invariants

As the derivation of the rotational invariant by H. Zhang et al.(2010) requires the image's centroid to be at the origin, the following invariants are therefore translation and rotational invariants. The moment invariants, $I_{n,m}^{\langle \text{tr-Z} \rangle}$, are derived from the following expressions

$$I_{n,m}^{\langle \text{tr-Z} \rangle} = \sum_{k=0}^{n} \sum_{j=0}^{m} \sum_{s=0}^{k} \sum_{t=0}^{m} \sum_{u=0}^{s+t} \sum_{v=0}^{k+j-s-t} \binom{k}{s} \binom{j}{t} (-1)^t \times (\cos\theta_z)^{j+s-t} (\sin\theta_z)^{k+t-s} c_{n,k}^N c_{m,j}^N d_{s+t,u}^N d_{j+k-s-t,v}^N T_{u,v}^{\langle \text{c} \rangle} \quad (5.24)$$

where

$$\theta_z = \frac{1}{2} \tan^{-1} \left(\frac{pT_{1,1}^{\langle \text{c} \rangle} - qT_{0,0}^{\langle \text{c} \rangle}}{T_{2,0}^{\langle \text{c} \rangle} - T_{0,2}^{\langle \text{c} \rangle}} \right), \qquad p = \frac{2c_{2,2}^N c_{0,0}^N}{(c_{1,1}^N)^2}, \quad q = \frac{2c_{2,2}^N (c_{1,0}^N)^2}{c_{0,0}^N (c_{1,1}^N)^2}. \quad (5.25)$$

According to our study, the derivation of TR-Z is indeed equivalent to normalization of

$$I_{1,1}^{\langle \text{tr-Z} \rangle} = \left(\frac{c_{1,0}^N}{c_{0,0}^N} \right)^2 I_{0,0}^{\langle \text{tr-Z} \rangle}. \quad (5.26)$$

The proof is given in Appendix C.

TR-Z has several weaknesses

(A1) Inability to resolve principal axis normalization ambiguities.

From our study, the rotation invariant algorithm has failed to resolved the ambiguities caused by principal axis normalization. This will be discussed in Section 5.4.

(A2) Slow in numerical computation

The formation of the invariant descriptor $I_{n,m}^{\langle \text{tr-Z} \rangle}$ involved the decomposition of the transformed Tchebichef polynomials to polynomials in x and y, followed by consolidating the expressions of x and y back to the original Tchebichef polynomials (see (5.20) to (5.22)). As a result, the invariant formulae have long nested iterations which significantly slow down the numerical computation. On top of that the sequential computation of translation invariants followed by the rotational invariants further slowed down the speed of computation.

(A3) Lack of scale invariants.

The algorithms were unable to handle patterns having variation in size.

Comparatively, the algorithm of TRS-Y is simpler and faster. The complicated expressions are simplified by the modified geometric moments. However in the event where the image is not available, for example in image compression and only the selected orders of the Tchebichef moments are recorded, the indirect approach is not applicable. In addition, as shown by (5.15), the complexity of TRS-Y is proportional to the size of images. Thus the method is less efficient especially for large size images.

5.3 Proposed Translation, Rotation and Scale Tchebichef Moment Invariants

In this subsection the new TRS invariants are derived via image normalization. For convenience, TRS-invariants represent the new proposed TRS Tchebichef moment invariants with invariant descriptors denoted as $\{I_{n,m}^{\langle \text{trs} \rangle}\}$.

5.3.1 Fast Computation using Recurrence Relations

Mathematically, TRS transformation is a special case of affine transformation. Therefore we introduce a recurrence relation for the affine Tchebichef moments (AM), so that it can later be used in derivation of the TRS transformed Tchebichef moments.

Suppose $f(x,y)$ is an image in the original space $S_2(N_0)$ and $g(x',y') = f(x,y)$ is the correspondent affine transformed images in the transformed space $S_2(N_s)$ such that

$$\begin{pmatrix} x' \\ y' \end{pmatrix} = \begin{pmatrix} a_1 & a_2 \\ b_1 & b_2 \end{pmatrix} \begin{pmatrix} x \\ y \end{pmatrix} + \begin{pmatrix} a_3 \\ b_3 \end{pmatrix} \tag{5.27}$$

where $S_2(N) = \{(x,y) \mid x,y = 0,1,\cdots,N-1\}$.

$S_2(N_0)$ and $S_2(N_s)$ are original and transformed spaces, respectively. The two spaces are independent so that the invariant descriptors can be directly computed from original images. This eliminate the need to re-mapped the original image into a prefixed space thus save numerous amount of computation resources in calculating the image moments.

Definition 5.3.1. The affine transformed Tchebichef moments $\{T_{n,m}^{\langle \text{am} \rangle}\}$ are defined as

$$\begin{aligned} T_{n,m}^{\langle \text{am} \rangle} &= |J| \sum_{x=0}^{N_0-1} \sum_{y=0}^{N_0-1} \tilde{t}_n^{N_s}(a_1x + a_2y + a_3)\tilde{t}_m^{N_s}(b_1x + b_2y + b_3) f(x,y) \\ & \quad a_1, a_2, a_3, b_1, b_2, \text{ and, } b_3 \in \Re, \\ & \quad n,m = 0,1,\cdots,\min(N_s - 1, N_0, -1) \end{aligned} \tag{5.28}$$

where J denotes the Jacobian of the transformation satisfying

$$J = \begin{vmatrix} a_1 & a_2 \\ b_1 & b_2 \end{vmatrix} \neq 0. \tag{5.29}$$

Theorem 5.3.1. *The affine transformed Tchebichef moment $T_{n,m}^{\langle \mathrm{am} \rangle}$ is given by*

$$T_{n,m}^{\langle \mathrm{am} \rangle} = |J| \sum_{k=0}^{n+m} \sum_{j=0}^{n+m-k} \lambda_{n,m,k,j} T_{k,j} \tag{5.30}$$

where $J = \begin{vmatrix} a_1 & a_2 \\ b_1 & b_2 \end{vmatrix}$, and the coefficients $\lambda_{n,m,k,j}$ have two recurrence relations respective to row and column. They are

$$\begin{aligned} \lambda_{n,m,k,j}\left(\begin{array}{c} a_1, a_2, a_3 \\ b_1, b_2, b_3 \end{array} \middle| N_0, N_s \right) &= -\lambda_{n-1,m,k+1,j} a_1 K_{n,k+2}^{N_s,N_0} \tilde{C}_{k+2}^{N_0} - \lambda_{n-1,m,k,j+1} a_2 K_{n,j+2}^{N_s,N_0} \tilde{C}_{j+2}^{N_0} \\ &\quad + \lambda_{n-1,m,k,j} \tilde{A}_n^{N_s} \left[a_3 + \left(\frac{N_0 - 1}{2} \right) (a_1 + a_2) - \left(\frac{N_s - 1}{2} \right) \right] \\ &\quad + \lambda_{n-1,m,k-1,j} a_1 K_{n,k}^{N_s,N_0} + \lambda_{n-1,m,k,j-1} a_2 K_{n,j}^{N_s,N_0} \\ &\quad + \lambda_{n-2,m,k,j} \tilde{C}_n^{N_s} \end{aligned} \tag{5.31}$$

and

$$\begin{aligned} \lambda_{n,m,k,j}\left(\begin{array}{c} a_1, a_2, a_3 \\ b_1, b_2, b_3 \end{array} \middle| N_0, N_s \right) &= -\lambda_{n,m-1,k+1,j} b_1 K_{m,k+2}^{N_s,N_0} \tilde{C}_{k+2}^{N_0} - \lambda_{n,m-1,k,j+1} b_2 K_{m,j+2}^{N_s,N_0} \tilde{C}_{j+2}^{N_0} \\ &\quad + \lambda_{n,m-1,k,j} \tilde{A}_m^{N_s} \left[b_3 + \left(\frac{N_0 - 1}{2} \right) (b_1 + b_2) - \left(\frac{N_s - 1}{2} \right) \right] \\ &\quad + \lambda_{n,m-1,k-1,j} b_1 K_{m,k}^{N_s,N_0} + \lambda_{n,m-1,k,j-1} b_2 K_{m,j}^{N_s,N_0} \\ &\quad + \lambda_{n,m-2,k,j} \tilde{C}_m^{N_s}. \end{aligned} \tag{5.32}$$

Proof. Suppose

$$x' = a_1 x + a_2 y + a_3 \tag{5.33}$$

$$y' = b_1 x + b_2 y + b_3 \tag{5.34}$$

where $a_1, a_2, a_3, b_1, b_2, b_3 \in \Re$, $(x, y) \in S_2(N_0)$ and $(x', y') \in S_2(N_s)$.

Consider

$$\tilde{t}_0^{N_s}(x') \tilde{t}_0^{N_s}(y') = \left(\frac{N_0}{N_s} \right) \tilde{t}_0^{N_0}(x) \tilde{t}_0^{N_0}(y), \tag{5.35}$$

we get

$$\lambda_{0,0,0,0} = \left(\frac{N_0}{N_s}\right). \tag{5.36}$$

For $\tilde{t}_1^{N_s}(x')\tilde{t}_0^{N_s}(y')$, we have

$$\begin{aligned}
\tilde{t}_1^{N_s}(x')\tilde{t}_0^{N_s}(y') &= \left[(a_1x+a_2y+a_3)\tilde{A}_1^{N_s}+\tilde{B}_1^{N_s}\right]\tilde{t}_0^{N_s}(a_1x+a_2y+a_3) \\
&= a_1K_{1,1}^{N_s,N_0}\left(\frac{N_0}{N_s}\right)\left[x\tilde{A}_1^{N_0}\tilde{t}_0^{N_0}(x)\tilde{t}_0^{N_0}(y)\right] \\
&\quad +a_2K_{1,1}^{N_s,N_0}\left(\frac{N_0}{N_s}\right)\left[y\tilde{A}_1^{N_0}\tilde{t}_0^{N_0}(x)\tilde{t}_0^{N_0}(y)\right] \\
&\quad +K_{1,1}^{N_s,N_0}\left(\frac{N_0}{N_s}\right)\left[a_3\tilde{A}_1^{N_0}-\frac{(N_s-1)}{2}\tilde{A}_1^{N_0}\right]\tilde{t}_0^{N_0}(x)\tilde{t}_0^{N_0}(y) \\
&= \cdots \\
&= a_1K_{1,1}^{N_s,N_0}\left(\frac{N_0}{N_s}\right)\tilde{t}_1^{N_0}(x)\tilde{t}_0^{N_0}(y)+a_2K_{1,1}^{N_s,N_0}\left(\frac{N_0}{N_s}\right)\tilde{t}_0^{N_0}(x)\tilde{t}_1^{N_0}(y) \\
&\quad +\tilde{A}_1^{N_s}\left(\frac{N_0}{N_s}\right)\left[a_3+\frac{(N_0-1)}{2}(a_1+a_2)-\frac{(N_s-1)}{2}\right] \\
&\quad \times\tilde{t}_0^{N_0}(x)\tilde{t}_0^{N_0}(y)
\end{aligned} \tag{5.37}$$

which imply that

$$\lambda_{1,0,1,0} = a_1K_{1,1}^{N_s,N_0}\left(\frac{N_0}{N_s}\right) \tag{5.38}$$

$$\lambda_{1,0,0,1} = a_2K_{1,1}^{N_s,N_0}\left(\frac{N_0}{N_s}\right) \tag{5.39}$$

$$\lambda_{1,0,0,0} = \tilde{A}_1^{N_s}\left(\frac{N_0}{N_s}\right)\left[a_3+\frac{(N_0-1)}{2}(a_1+a_2)-\frac{(N_s-1)}{2}\right]. \tag{5.40}$$

Similarly, for $\tilde{t}_0^{N_s}(x')\tilde{t}_1^{N_s}(y')$

$$\begin{aligned}
\tilde{t}_0^{N_s}(x')\tilde{t}_1^{N_s}(y') &= b_1K_{1,1}^{N_s,N_0}\left(\frac{N_0}{N_s}\right)\tilde{t}_1^{N_0}(x)\tilde{t}_0^{N_0}(y)+b_2K_{1,1}^{N_s,N_0}\left(\frac{N_0}{N_s}\right)\tilde{t}_0^{N_0}(x)\tilde{t}_1^{N_0}(y) \\
&\quad +\tilde{A}_1^{N_s}\left(\frac{N_0}{N_s}\right)\left[b_3+\frac{(N_0-1)}{2}(b_1+b_2)-\frac{(N_s-1)}{2}\right] \\
&\quad \times\tilde{t}_0^{N_0}(x)\tilde{t}_0^{N_0}(y).
\end{aligned} \tag{5.41}$$

we get

$$\lambda_{0,1,1,0} = b_1K_{1,1}^{N_s,N_0}\left(\frac{N_0}{N_s}\right) \tag{5.42}$$

$$\lambda_{0,1,0,1} = b_2K_{1,1}^{N_s,N_0}\left(\frac{N_0}{N_s}\right) \tag{5.43}$$

$$\lambda_{0,1,0,0} = \tilde{A}_1^{N_s}\left(\frac{N_0}{N_s}\right)\left[b_3+\frac{(N_0-1)}{2}(b_1+b_2)-\frac{(N_s-1)}{2}\right]. \tag{5.44}$$

Suppose

$$\tilde{t}_p^{N_s}(a_1x+a_2y+a_3)\tilde{t}_q^{N_s}(b_1x+b_2y+b_3)=\sum_{k=0}^{p+q}\sum_{j=0}^{p+q-k}\lambda_{p,q,k,j}\tilde{t}_k^{N_0}(x)\tilde{t}_j^{N_0}(y) \tag{5.45}$$

is true for $p\leq n, q\leq m$.

We now consider $\tilde{t}_{n+1}^{N_s}(a_1x+a_2y+a_3)\tilde{t}_m^{N_s}(b_1x+b_2y+b_3)$.

From the three terms recurrence relation of the Tchebichef polynomials (5.9), we have

$$\begin{aligned}
\tilde{t}_{n+1}^{N_s}(x^{'})\tilde{t}_m^{N_s}(y^{'}) &= \left\{\left(x^{'}\tilde{A}_{n+1}^{N_s}+\tilde{B}_{n+1}^{N_s}\right)\tilde{t}_n^{N_s}(x^{'})+\tilde{C}_{n+1}^{N_s}\tilde{t}_{n-1}^{N_s}(x^{'})\right\}\tilde{t}_m^{N_s}(y^{'}) \\
&= \left\{(a_1x+a_2y)\tilde{A}_{n+1}^{N_s}\right\}\tilde{t}_n^{N_s}(a_1x+a_2y+a_3)\tilde{t}_m^{N_s}(b_1x+b_2y+b_3) \\
&\quad+\left\{a_3\tilde{A}_{n+1}^{N_s}+\tilde{B}_{n+1}^{N_s}\right\}\tilde{t}_n^{N_s}(a_1x+a_2y+a_3)\tilde{t}_m^{N_s}(b_1x+b_2y+b_3) \\
&\quad+\tilde{C}_{n+1}^{N_s}\tilde{t}_{n-1}^{N_s}(a_1x+a_2y+a_3)\tilde{t}_m^{N_s}(b_1x+b_2y+b_3).
\end{aligned} \tag{5.46}$$

By using the induction hypothesis (5.45), we get

$$\begin{aligned}
\tilde{t}_{n+1}^{N_s}(x^{'})\tilde{t}_m^{N_s}(y^{'}) &= \sum_{k=0}^{n+m+1}\sum_{j=0}^{n+m+1-k}\Big\{\lambda_{n,m,k-1,j}a_1K_{n+1,k}^{N_s,N_0}-\lambda_{n,m,k,j}a_1K_{n+1,k+1}^{N_s,N_0}\tilde{B}_{k+1}^{N_0} \\
&\qquad-\lambda_{n,m,k+1,j}a_1K_{n+1,k+1}^{N_s,N_0}\tilde{C}_{k+2}^{N_0}+\lambda_{n,m,k,j-1}a_2K_{n+1,j}^{N_s,N_0} \\
&\qquad-\lambda_{n,m,k,j}a_2K_{n+1,j+1}^{N_s,N_0}\tilde{B}_{j+1}^{N_0}-\lambda_{n,m,k,j+1}a_2K_{n+1,j+2}^{N_s,N_0}\tilde{C}_{k+2}^{N_0}\Big\} \\
&\qquad\times\tilde{t}_k^{N_0}(x)\tilde{t}_j^{N_0}(y) \\
&\quad+\sum_{k=0}^{n+m}\sum_{j=0}^{n+m-k}\left\{\tilde{A}_{n+1}^{N_s}a_3+\tilde{B}_{n+1}^{N_s}\right\}\lambda_{n,m,k,j}\tilde{t}_k^{N_0}(x)\tilde{t}_j^{N_0}(y) \\
&\quad+\sum_{k=0}^{n+m-1}\sum_{j=0}^{n+m-1-k}\tilde{C}_{n+1}^{N_s}\lambda_{n-1,m,k,j}\tilde{t}_k^{N_0}(x)\tilde{t}_j^{N_0}(y) \\
&= \cdots \\
&= \sum_{k=0}^{n+m+1}\sum_{j=0}^{n+m+1-k}\Big\{-\lambda_{n,m,k+1,j}a_1K_{n+1,k+2}^{N_s,N_0}\tilde{C}_{k+2}^{N_0}-\lambda_{n,m,k,j+1}a_2K_{n+1,j+2}^{N_s,N_0}\tilde{C}_{j+2}^{N_0} \\
&\qquad+\lambda_{n,m,k,j}\tilde{A}_{n+1}^{N_s}\left[a_3+\left(\frac{N_0-1}{2}\right)(a_1+a_2)-\left(\frac{N_s-1}{2}\right)\right] \\
&\qquad+\lambda_{n,m,k-1,j}a_1K_{n+1,k}^{N_s,N_0}+\lambda_{n,m,k,j-1}a_2K_{n+1,k}^{N_s,N_0} \\
&\qquad+\lambda_{n-1,m,k,j}\tilde{C}_{n+1}^{N_s}\Big\}\tilde{t}_k^{N_0}(x)\tilde{t}_j^{N_0}(y).
\end{aligned} \tag{5.47}$$

Similarly, by applying the same procedures, we obtain

$$\begin{aligned}\tilde{t}_n^{N_s}(x')\tilde{t}_{m+1}^{N_s}(y') &= \sum_{k=0}^{n+m+1}\sum_{j=0}^{n+m+1-k}\Big\{-\lambda_{n,m,k+1,j}b_1K_{m+1,k+2}^{N_s,N_0}\tilde{C}_{k+2}^{N_0} \\ &\quad -\lambda_{n,m,k,j+1}b_2K_{m+1,j+2}^{N_s,N_0}\tilde{C}_{j+2}^{N_0} \\ &\quad +\lambda_{n,m,k,j}\tilde{A}_{m+1}^{N_s}\left[b_3+\left(\frac{N_0-1}{2}\right)(b_1+b_2)-\left(\frac{N_s-1}{2}\right)\right] \\ &\quad +\lambda_{n,m,k-1,j}b_1K_{m,k}^{N_s,N_0}+\lambda_{n,m,k,j-1}b_2K_{m+1,j}^{N_s,N_0} \\ &\quad +\lambda_{n,m-1,k,j}\tilde{C}_{m+1}^{N_s}\Big\}\tilde{t}_k^{N_0}(x)\tilde{t}_j^{N_0}(y). \end{aligned} \tag{5.48}$$

The theorem is now proved. □

5.3.2 Normalization Schemes of Translation, Rotation and Scale Tchebichef Moment Invariants

In this section, we consider the normalization conditions that determine the parameter values for the proposed TRS invariants, and the uniqueness issues arising from the process of normalization.

Theorem 5.3.2. *Suppose $I_{n,m}^{\langle\mathrm{trs}\rangle}$ denote the proposed translation, rotation and scale Tchebichef moment invariants satisfying the following normalization conditions*

$$I_{0,0}^{\langle\mathrm{trs}\rangle} = \Omega_0 N_s \tag{5.49}$$

$$I_{1,0}^{\langle\mathrm{trs}\rangle} = 0 = I_{0,1}^{\langle\mathrm{trs}\rangle} \tag{5.50}$$

$$I_{1,1}^{\langle\mathrm{trs}\rangle} = 0 \tag{5.51}$$

then

$$\begin{aligned} I_{n,m}^{\langle\mathrm{trs}\rangle} &= \omega^2\sum_{x=0}^{N_0-1}\sum_{y=0}^{N_0-1}\tilde{t}_n^{N_s}\begin{pmatrix}\omega\cos(\theta)(x-\bar{x}) \\ +\omega\sin(\theta)(y-\bar{y})+\frac{N_s-1}{2}\end{pmatrix}\times \\ &\quad \tilde{t}_m^{N_s}\begin{pmatrix}-\omega\sin(\theta)(x-\bar{x}) \\ +\omega\cos(\theta)(y-\bar{y})+\frac{N_s-1}{2}\end{pmatrix}f(x,y) \\ &\quad n,m=0,1,\cdots,\min\{N_0-1,N_s-1\} \end{aligned} \tag{5.52}$$

where

$$\omega=\sqrt{\frac{\Omega_0N_s^2}{T_{0,0}N_0}} \tag{5.53}$$

and

$$\theta = \frac{1}{2}tan^{-1}\left\{ \frac{\begin{array}{c} 2\left(\frac{N_0-1}{2}-\bar{x}\right)\left(\frac{N_0-1}{2}-\bar{y}\right)\tilde{A}_1^{N_0}T_{0,0}+2\left(\frac{N_0-1}{2}-\bar{x}\right)T_{0,1} \\ +2\left(\frac{N_0-1}{2}-\bar{y}\right)T_{1,0}+\frac{2T_{1,1}}{\tilde{A}_1^{N_0}} \end{array}}{\begin{array}{c} \tilde{A}_1^{N_0}\left[\left(\frac{N_0-1}{2}-\bar{x}\right)^2-\left(\frac{N_0-1}{2}-\bar{y}\right)^2\right]T_{0,0}-2\left(\frac{N_0-1}{2}-\bar{x}\right)T_{1,0} \\ +2\left(\frac{N_0-1}{2}-\bar{y}\right)T_{0,1}+\frac{T_{2,0}}{\tilde{A}_2^{N_0}}-\frac{T_{0,2}}{\tilde{A}_2^{N_0}} \end{array}} \right\}. \quad (5.54)$$

Proof. Suppose $f^{'}(x^{'},y^{'}) = f(x,y)$ with

$$\begin{pmatrix} x' \\ y' \end{pmatrix} = \omega \begin{pmatrix} \cos\theta & \sin\theta \\ -\sin\theta & \cos\theta \end{pmatrix} \begin{pmatrix} x \\ y \end{pmatrix} + \begin{pmatrix} a_3 \\ b_3 \end{pmatrix}. \quad (5.55)$$

From (5.1), the transformed TRS has expression

$$\begin{aligned} I_{n,m}^{\langle \text{trs} \rangle} &= \omega^2 \sum_{x=0}^{N_0-1}\sum_{y=0}^{N_0-1} \tilde{t}_n^{N_s}(\omega\cos(\theta)x+\omega\sin(\theta)y+a_3)\times \\ &\qquad \tilde{t}_m^{N_s}(-\omega\sin(\theta)x+\omega\cos(\theta)y+b_3)f(x,y) \\ &\qquad n,m = 0,1,\cdots,\min\{N_0-1,N_s-1\}. \end{aligned} \quad (5.56)$$

Consider the zero order moment, and the first normalization condition given by (5.49),

$$I_{0,0}^{\langle \text{trs} \rangle} = \omega^2 \frac{N_0}{N_s} T_{0,0} = \Omega_0 N_s, \quad (5.57)$$

we get

$$\omega = \sqrt{\frac{\Omega_0 N_s^2}{T_{0,0}N_0}}. \quad (5.58)$$

From (5.55), we can deduce that

$$\bar{x}^{'} = \bar{x}\omega\cos(\theta)+\bar{y}\omega\sin(\theta)+a_3 \quad (5.59)$$

$$\bar{y}^{'} = -\bar{x}\omega\sin(\theta)+\bar{y}\omega\cos(\theta)+b_3 \quad (5.60)$$

where $(\bar{x},\bar{y})$ and $(\bar{x}^{'},\bar{y}^{'})$ denote the centroid for f and $f^{'}$, respectively.

According to Theorem 4.3.3 the images with first order moments equal to zero will have centroid at middle of $S_2(N_s)$. Therefore we have

$$a_3 = -\bar{x}\omega\cos(\theta)-\bar{y}\omega\sin(\theta)+\frac{N_s-1}{2}, \quad (5.61)$$

$$b_3 = \bar{x}\omega\sin(\theta)-\bar{y}\omega\cos(\theta)+\frac{N_s-1}{2}. \quad (5.62)$$

By using (5.61) and (5.62), the expression (5.52) is proved.

We find the angle θ.

From Theorem 5.3.1 and the definition of $I_{n,m}^{\langle \text{trs} \rangle}$ given in (5.52), we have

$$I_{n,m}^{\langle \text{trs} \rangle} = \omega^2 \sum_{k=0}^{n+m} \sum_{j=0}^{n+m-k} \lambda_{n,m,k,j}^{\langle \text{trs} \rangle} T_{k,j} \tag{5.63}$$

where

$$\lambda_{n,m,k,j}^{\langle \text{trs} \rangle} = \lambda_{n,m,k,j} \left(\begin{array}{l} \omega\cos\theta, \quad \omega\sin\theta, \\ -\bar{x}\omega\cos\theta - \bar{y}\omega\sin\theta + \frac{N_s-1}{2}; \\ -\omega\sin\theta, \quad \omega\cos\theta, \\ \bar{x}\omega\sin\theta - \bar{y}\omega\cos\theta + \frac{N_s-1}{2} \end{array} \middle| N_0, N_s \right). \tag{5.64}$$

By using (5.63), we can deduce that

$$I_{1,1}^{\langle \text{trs} \rangle} = \sum_{k=0}^{2} \sum_{j=0}^{2-k} \lambda_{1,1,k,j}^{\langle \text{trs} \rangle} T_{k,j} \tag{5.65}$$

$$\begin{aligned} &= \left\{ \begin{array}{l} \frac{1}{2}\sin(2\theta)\left[-\left(\frac{N_0-1}{2} - \bar{x}\right)^2 + \left(\frac{N_0-1}{2} - \bar{y}\right)^2 \right] \\ +\cos(2\theta)\left(\frac{N_0-1}{2} - \bar{x}\right)\left(\frac{N_0-1}{2} - \bar{y}\right) \end{array} \right\} \times \omega^2 \left(\tilde{A}_1^{N_s}\right)^2 \left(\frac{N_0}{N_s}\right) T_{0,0} \\ &\quad + K_{1,1}^{N_s,N_0} \omega^2 \tilde{A}_1^{N_s} \left(\frac{N_0}{N_s}\right) \left\{ \begin{array}{l} -\sin(2\theta)\left(\frac{(N_0-1)}{2} - \bar{x}\right) \\ +\cos(2\theta)\left(\frac{(N_0-1)}{2} - \bar{y}\right) \end{array} \right\} T_{1,0} \\ &\quad + K_{1,1}^{N_s,N_0} \omega^2 \tilde{A}_1^{N_s} \left(\frac{N_0}{N_s}\right) \left\{ \begin{array}{l} \sin(2\theta)\left(\frac{(N_0-1)}{2} - \bar{y}\right) \\ +\cos(2\theta)\left(\frac{(N_0-1)}{2} - \bar{x}\right) \end{array} \right\} T_{0,1} \\ &\quad + \cos(2\theta)\left(K_{1,1}^{N_s,N_0}\right)^2 \omega^2 T_{1,1} - \frac{1}{2}\sin(2\theta) K_{1,1}^{N_s,N_0} K_{1,2}^{N_s,N_0} \omega^2 \left(\frac{N_0}{N_s}\right) T_{2,0} \\ &\quad + \frac{1}{2}\sin(2\theta) K_{1,1}^{N_s,N_0} K_{1,2}^{N_s,N_0} \omega^2 \left(\frac{N_0}{N_s}\right) T_{0,2}. \end{aligned} \tag{5.66}$$

The derivation of $I_{1,1}^{\langle \text{trs} \rangle}$ are shown in Appendix D.

By using the third normalization condition as stated in (5.51), we get (5.54). □

The first normalization condition (5.49) eliminates the variation of the image size. The scale coefficient Ω_0 is defined so that the canonical forms are scaled proportional to transformed space $S_2(N_s)$. The second condition (5.50) achieves the translation invariants by shifting the images centroid to the middle of the transformed space. The third normalization condition (5.51) is for the rotation invariants using the principal axis normalization. However the solutions are not unique and require the additional constraints to resolve the ambiguities.

5.3.3 Uniqueness Issues of Translation, Rotational and Scaled Tchebichef Moment Invariants

In the principal axis normalization of geometric moments, there arises multiple ambiguities with each 90^{o} apart respective to the image's centroid. For that, the constraints (5.4) and (5.5) are used in resolving the ambiguities. (5.4) rotates the image's principal axis so that it is parallel to the $x-$axis. This reduced the four ambiguities down to two with each 180^{o} apart. By applying (5.5), the normalization will thus be unique.
In this chapter, despite the above mentioned method, we proposed an alternative way to deal with the ambiguities using the Tchebichef moments. For that, the following lemma is required.

Lemma 5.3.3. *Suppose g_1 and g_2 are two identical images with centroid at the middle of $S_2(N_s)$.*

1. *If g_1 and g_2 are separated by a 90^{o} rotation about their image centroid then*

$$T_{2,0}(g_1) - T_{0,2}(g_1) = -\left[T_{2,0}(g_2) - T_{0,2}(g_2)\right]. \tag{5.67}$$

2. *If g_1 and g_2 are separated by a 180^{o} rotation about their image centroid, then*

$$T_{3,0}(g_2) = -T_{3,0}(g_1). \tag{5.68}$$

Proof. From the given conditions, Tchebichef moments of g_2 are expressible as TRS transform on g_1. We have

$$\begin{aligned} T_{2,0}(g_2) &= \sum_{x=0}^{N_s-1}\sum_{y=0}^{N_s-1} \tilde{t}_2^{N_s}\begin{pmatrix} \cos\left(\frac{\pi}{2}\right)x + \sin\left(\frac{\pi}{2}\right)y \\ -\cos\left(\frac{\pi}{2}\right)\bar{x} - \sin\left(\frac{\pi}{2}\right)\bar{y} + \frac{N_s-1}{2} \end{pmatrix} \\ &\quad \times \tilde{t}_0^{N_s}\begin{pmatrix} -\sin\left(\frac{\pi}{2}\right)x + \cos\left(\frac{\pi}{2}\right)y \\ +\sin\left(\frac{\pi}{2}\right)\bar{x} - \cos\left(\frac{\pi}{2}\right)\bar{y} + \frac{N_s-1}{2} \end{pmatrix} g_1(x,y) \\ &= \sum_{x=0}^{N_s-1}\sum_{y=0}^{N_s-1} \tilde{t}_2^{N_s}(y)\tilde{t}_0^{N_s}(N_s-1-x)g_1(x,y) \\ &= T_{0,2}(g_1). \end{aligned} \tag{5.69}$$

Similarly, for

$$\begin{aligned} T_{0,2}(g_2) &= \sum_{x=0}^{N_s-1}\sum_{y=0}^{N_s-1} \tilde{t}_0^{N_s}\left(\begin{array}{l}\cos\left(\frac{\pi}{2}\right)x+\sin\left(\frac{\pi}{2}\right)y \\ -\cos\left(\frac{\pi}{2}\right)\bar{x}-\sin\left(\frac{\pi}{2}\right)\bar{y}+\frac{N_s-1}{2}\end{array}\right) \\ &\quad \times\tilde{t}_2^{N_s}\left(\begin{array}{l}-\sin\left(\frac{\pi}{2}\right)x+\cos\left(\frac{\pi}{2}\right)y \\ +\sin\left(\frac{\pi}{2}\right)\bar{x}-\cos\left(\frac{\pi}{2}\right)\bar{y}+\frac{N_s-1}{2}\end{array}\right) g_1(x,y) \\ &= \sum_{x=0}^{N_s-1}\sum_{y=0}^{N_s-1} \tilde{t}_0^{N_s}(y)\tilde{t}_2^{N_s}(N_s-1-x)g_1(x,y) \\ &= T_{2,0}(g_1). \end{aligned} \tag{5.70}$$

Thus we have

$$T_{2,0}(g_2)-T_{0,2}(g_2) = -\left[T_{2,0}(g_1)-T_{0,2}(g_1)\right] \tag{5.71}$$

Now, we consider the condition of g_1 and g_2 which are 180^{o} apart. We have

$$\begin{aligned} T_{3,0}(g_2) &= \sum_{x=0}^{N_s-1}\sum_{y=0}^{N_s-1} \tilde{t}_3^{N_s}\left(\begin{array}{l}\cos(\pi)x+\sin(\pi)y \\ -\cos(\pi)\bar{x}-\sin(\pi)\bar{y}+\frac{N_s-1}{2}\end{array}\right) \\ &\quad \times\tilde{t}_0^{N_s}\left(\begin{array}{l}-\sin(\pi)x+\cos(\pi)y \\ +\sin(\pi)\bar{x}-\cos(\pi)\bar{y}+\frac{N_s-1}{2}\end{array}\right) g_1(x,y) \\ &= \sum_{x=0}^{N_s-1}\sum_{y=0}^{N_s-1} \tilde{t}_3^{N_s}(N_s-1-y)\tilde{t}_0^{N_s}(y)g_1(x,y) \\ &= -T_{3,0}(g_1) \end{aligned} \tag{5.72}$$

□

Lemma 5.3.3 gives the theoretical basis of using the following constraints to resolve ambiguities caused by principal axis normalization on Tchebichef moments:

$$I_{2,0}^{\langle\text{trs}\rangle} \geq I_{0,2}^{\langle\text{trs}\rangle}, \text{ and} \tag{5.73}$$

$$I_{3,0}^{\langle\text{trs}\rangle} \geq 0. \tag{5.74}$$

With that, we are now ready to solve the uniqueness issues of the proposed TRS-invariants.

Theorem 5.3.4. *Suppose g is the corresponding image of f distorted by translation, rotation and scale deformation, then*

$$I_{n,m}^{\langle \mathrm{trs} \rangle}(f) = I_{n,m}^{\langle \mathrm{trs} \rangle}(g) \tag{5.75}$$

if the invariants $I_{n,m}^{\langle \mathrm{trs} \rangle}(f)$ and $I_{n,m}^{\langle \mathrm{trs} \rangle}(g)$ satisfy all the following normalization criteria

(B1) $I_{0,0}^{\langle \mathrm{trs} \rangle}(*) = \Omega_0 N_s$

(B2) $I_{1,0}^{\langle \mathrm{trs} \rangle}(*) = 0 \; = \; I_{0,1}^{\langle \mathrm{trs} \rangle}(*)$

(B3) $I_{1,1}^{\langle \mathrm{trs} \rangle}(*) = 0$

(B4) $I_{2,0}^{\langle \mathrm{trs} \rangle}(*) \geq I_{0,2}^{\langle \mathrm{trs} \rangle}(*)$

(B5) $I_{3,0}^{\langle \mathrm{trs} \rangle}(*) \geq 0$

Note: $* \in \{f, g\}$

Proof. Suppose g is TRS transformed to f such that $g(x_1, y_1) = f(x, y)$ and

$$\begin{pmatrix} x_1 \\ y_1 \end{pmatrix} = \omega_1 \begin{pmatrix} \cos\theta_1 & \sin\theta_1 \\ -\sin\theta_1 & \cos\theta_1 \end{pmatrix} \begin{pmatrix} x \\ y \end{pmatrix} + \begin{pmatrix} a_3 \\ b_3 \end{pmatrix}. \tag{5.76}$$

Let $f^{'}$ and $g^{'}$ denote the TRS normalized images of f and g, respectively, so that

$$f^{'}(x_f, y_f) = f(x, y) \quad \text{and} \quad g^{'}(x_g, y_g) = g(x_1, y_1) \tag{5.77}$$

with

$$x_f = \omega_f \cos\theta_f (x - \bar{x}) + \omega_f \sin\theta_f (y - \bar{y}) + \frac{N_s - 1}{2} \tag{5.78}$$

$$y_f = -\omega_f \sin\theta_f (x - \bar{x}) + \omega_f \cos\theta_f (y - \bar{y}) + \frac{N_s - 1}{2} \tag{5.79}$$

and

$$x_g = \omega_g \cos\theta_g (x_1 - \bar{x}_1) + \omega_g \sin\theta_g (y_1 - \bar{y}_1) + \frac{N_s - 1}{2} \tag{5.80}$$

$$y_g = -\omega_g \sin\theta_g (x_1 - \bar{x}_1) + \omega_g \cos\theta_g (y_1 - \bar{y}_1) + \frac{N_s - 1}{2}. \tag{5.81}$$

In the above transformation, the centroid of f and g are mapped to the middle of the space following the second normalization condition.

By using (5.76), x_g and y_g can be expressed as functions of x and y . We get

$$\begin{aligned} x_g &= \omega_g\omega_1(x-\bar{x})\left[\cos\theta_g\cos\theta_1-\sin\theta_g\sin\theta_1\right] \\ &\quad +\omega_g\omega_1(y-\bar{y})\left[\cos\theta_g\sin\theta_1+\sin\theta_g\cos\theta_1\right]+\frac{N_s-1}{2} \\ &= \omega_g\omega_1(x-\bar{x})\cos(\theta_g+\theta_1)+\omega_g\omega_1(y-\bar{y})\sin(\theta_g+\theta_1)+\frac{N_s-1}{2} \end{aligned} \tag{5.82}$$

and

$$\begin{aligned} y_g &= -\omega_g\omega_1(x-\bar{x})\left[\sin\theta_g\cos\theta_1+\cos\theta_g\sin\theta_1\right] \\ &\quad +\omega_g\omega_1(y-\bar{y})\left[-\sin\theta_g\sin\theta_1+\cos\theta_g\cos\theta_1\right]+\frac{N_s-1}{2} \\ &= \omega_g\omega_1(x-\bar{x})\sin(\theta_g+\theta_1)+\omega_g\omega_1(y-\bar{y})\cos(\theta_g+\theta_1)+\frac{N_s-1}{2}. \end{aligned} \tag{5.83}$$

From (5.78) and (5.79) and Theorem 5.3.2, we have

$$\begin{aligned} I_{n,m}^{\langle\mathrm{trs}\rangle}(f) &= \omega_f^2\sum_{x=0}^{N_0-1}\sum_{y=0}^{N_0-1}\tilde{t}_n^{N_s}\left(\begin{array}{l}(x-\bar{x})\omega_f\cos(\theta_f)\\ +(y-\bar{y})\omega_f\sin(\theta_f)+\frac{N_s-1}{2}\end{array}\right)\times \\ &\qquad \tilde{t}_m^{N_s}\left(\begin{array}{l}-(x-\bar{x})\omega_f\sin(\theta_f)\\ +(y-\bar{y})\omega_f\cos(\theta_f)+\frac{N_s-1}{2}\end{array}\right)f(x,y), \\ &\qquad n,m=0,1,\cdots,\min\{N_0-1,N_s-1\} \end{aligned} \tag{5.84}$$

where

$$\omega_f=\sqrt{\frac{\Omega_0 N_s^2}{T_{0,0}N_0}} \tag{5.85}$$

and

$$\tan(2\theta_f)=\left\{\frac{\begin{array}{c}2\left(\frac{N_0-1}{2}-\bar{x}\right)\left(\frac{N_0-1}{2}-\bar{y}\right)\tilde{A}_1^{N_0}T_{0,0}\\ +2\left(\frac{N_0-1}{2}-\bar{x}\right)T_{0,1}\\ +2\left(\frac{N_0-1}{2}-\bar{y}\right)T_{1,0}+\frac{2T_{1,1}}{\tilde{A}_1^{N_0}}\end{array}}{\begin{array}{c}\tilde{A}_1^{N_0}\left[\left(\frac{N_0-1}{2}-\bar{x}\right)^2-\left(\frac{N_0-1}{2}-\bar{y}\right)^2\right]T_{0,0}\\ -2\left(\frac{N_0-1}{2}-\bar{x}\right)T_{1,0}\\ +2\left(\frac{N_0-1}{2}-\bar{y}\right)T_{0,1}+\frac{T_{2,0}}{\tilde{A}_2^{N_0}}-\frac{T_{0,2}}{\tilde{A}_2^{N_0}}\end{array}}\right\}. \tag{5.86}$$

Similarly for g, from (5.82 & 5.83), and Theorem 5.3.2, we have

$$\begin{aligned} I_{n,m}^{\langle \mathrm{trs} \rangle}(g) &= (\omega_g \omega_1)^2 \sum_{x=0}^{N_0-1} \sum_{y=0}^{N_0-1} f(x,y) \\ &\quad \times \tilde{t}_n^{N_s} \left(\begin{array}{l} (x-\bar{x})\omega_g\omega_1 \cos(\theta_g+\theta_1) \\ +(y-\bar{y})\omega_g\omega_1 \sin(\theta_g+\theta_1) + \frac{N_s-1}{2} \end{array} \right) \\ &\quad \times \tilde{t}_m^{N_s} \left(\begin{array}{l} -(x-\bar{x})\omega_g\omega_1 \sin(\theta_g+\theta_1) \\ +(y-\bar{y})\omega_g\omega_1 \cos(\theta_g+\theta_1) + \frac{N_s-1}{2} \end{array} \right), \\ &\quad n,m = 0,1,\cdots,\min\{N_0-1, N_s-1\} \end{aligned} \tag{5.87}$$

where

$$\omega_g \omega_1 = \sqrt{\frac{\Omega_0 N_s^2}{T_{0,0} N_0}} \tag{5.88}$$

and

$$\tan(2(\theta_g+\theta_1)) = \left\{ \begin{array}{c} 2\left(\frac{N_0-1}{2}-\bar{x}\right)\left(\frac{N_0-1}{2}-\bar{y}\right)\tilde{A}_1^{N_0} T_{0,0} \\ +2\left(\frac{N_0-1}{2}-\bar{x}\right) T_{0,1} \\ +2\left(\frac{N_0-1}{2}-\bar{y}\right) T_{1,0} + \frac{2T_{1,1}}{\tilde{A}_1^{N_0}} \\ \hline \tilde{A}_1^{N_0}\left[\left(\frac{N_0-1}{2}-\bar{x}\right)^2 - \left(\frac{N_0-1}{2}-\bar{y}\right)^2\right] T_{0,0} \\ -2\left(\frac{N_0-1}{2}-\bar{x}\right) T_{1,0} \\ +2\left(\frac{N_0-1}{2}-\bar{y}\right) T_{0,1} + \frac{T_{2,0}}{\tilde{A}_2^{N_0}} - \frac{T_{0,2}}{\tilde{A}_2^{N_0}} \end{array} \right\}. \tag{5.89}$$

From (5.85) and (5.88), we get

$$\omega_g \omega_1 = \pm \omega_f. \tag{5.90}$$

The negative sign of (5.90) can be treated as change of phase by angle of π, which can later be resolved together using the forth and fifth normalization criteria. Without loss of generality, we may therefore let

$$\omega_g \omega_1 = \omega_f. \tag{5.91}$$

From (5.86) and (5.89), we have

$$\tan(2\theta_f) = \tan[2(\theta_g+\theta_1)] \tag{5.92}$$

that will give us solutions

$$\begin{aligned} \theta_f - \theta_g &= \theta_1 + n\pi \\ & n = 0, \pm 1, \cdots \end{aligned} \tag{5.93}$$

By using the forth and fifth conditions on normalization criteria, the ambiguities are resolved. Thus we get

$$\theta_f - \theta_g \quad = \quad \theta_1. \tag{5.94}$$

By substituting (5.91) and (5.94) into (5.87), we therefore have

$$I_{n,m}^{\langle \mathrm{trs} \rangle}(g) = I_{n,m}^{\langle \mathrm{trs} \rangle}(f).$$

□

It is important to note that the solution fails if both $I_{1,1}^{\langle \mathrm{trs} \rangle}(f) = 0$ and $I_{2,0}^{\langle \mathrm{trs} \rangle}(f) - I_{0,2}^{\langle \mathrm{trs} \rangle}(f) = 0$. To resolve the issue, higher order TRS moments are needed to determine the rotation angle. This will be discussed in Chapter 6.

5.3.4 Skewed Translation, Rotation and Scaled Tchebichef Moment Invariants

Similar to previous chapters, skewed parameters for TRS are introduced to enhance the discriminative power of the moment invariants.

$$I_{n,m}^{\langle \mathrm{trs} \rangle} = \omega^2 \sum_{k=0}^{n+m} \sum_{j=0}^{n+m-k} \lambda_{n,m,k,j}^{\langle \mathrm{trs} \rangle} T_{k,j} \tag{5.95}$$

where

$$\lambda_{n,m,k,j}^{\langle \mathrm{trs} \rangle} \quad = \quad \lambda_{n,m,k,j} \left(\begin{array}{l} \quad \omega\cos\theta, \quad \omega\sin\theta, \\ -\omega\bar{x}\cos\theta - \omega\bar{y}\sin\theta + \frac{N_s-1}{2} + w_x; \\ \quad -\omega\sin\theta, \quad \omega\cos\theta, \\ \omega\bar{x}\sin\theta - \omega\bar{y}\cos\theta + \frac{N_s-1}{2} + w_y \end{array} \middle| N_0, N_s \right). \tag{5.96}$$

Here skew parameters (w_x, w_y) are denoted as the spatial displacements transformation in units of pixel from the middle of space.

5.4 Experimental Results

In this section, experimental results of the TRS algorithms are provided. The first experiment evaluates the accuracy of the rotation invariants of the proposed algorithm. In the second experiment, the accuracy of the proposed translation, rotation and scale invariants algorithm is reviewed. The third experiment valuates the computational performance of TRS algorithms. Finally, the classification performance of the proposed algorithm is evaluated in non-noisy and noisy environments.

5.4.1 Accuracy on Rotation Invariants

In this subsection, we evaluate the accuracy of the rotation invariant algorithms. For this experiment, the original space $S_2(N_0)$ and transformed space $S_2(N_s)$ are both equal to $S_2(120)$. A set of binary images with size 60×60 in original space, are used in this experiment. The images shown in Figure 5.1 are rotated by angles $\theta : 0^o, 5, 10^o, \cdots, 355^o$. The relative standard deviations of the percentage spread RSD$(\%)$, are used in the experiment to measure the accuracy of TRS algorithms. The selected feature values for proposed TRS, TR-Z and TRS-Y are recorded in Tables 5.2, 5.3 and 5.4, respectively. As shown in the tables, the three features exhibit good accuracy for rotational invariants. Comparatively, TR-Z is found to be better in terms of the accuracy. However when we analyze the normalized images, ambiguities have been detected for TR-Z. A pair of normalized images for each pattern of "7"and "shen" and their feature values are shown in Tables 5.5 and 5.6 for TR-Z and TRS, respectively. In Table 5.6 where the proposed TRS algorithms are used as rotation descriptor. No ambiguity has been detected and the features were accurately computed. In Table 5.5, for display purpose, the output of canonical images of TR-Z are translated from the origin to middle of transformed space $S_2(N_s)$. The output of the canonical forms is found to be separated by an angle of 180^o rotation relative to images' centroid. The feature values of TR-Z however are found to be nearly identical despite the ambiguities. This can be due to the "skew" effect of images from the middle of transformed space. As a result, the translation and rotation invariants of Zhang et. al. can be considered as accurate numerically. However from the perspective of classification, the TR-Z algorithm has failed to discriminate the two very distinctive forms implies that the features set has poor within classes separation. Therefore TR-Z invariants could be poor in classification performance. The statement has been confirmed by experiments.

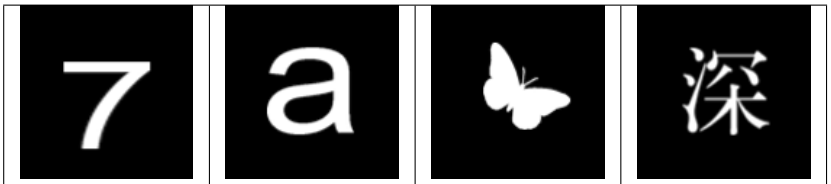

7	a	butterfly	shen

Figure 5.1: Images used for evaluation of rotation invariants. Original image of "butterfly" is courtesy of Professor Kimia, Brown University.

Table 5.2: Selected orders of proposed TRS invariants for experiment on translation and rotational deformations

image(θ)	$I_{0,0}^{\langle \text{trs} \rangle}$	$I_{2,0}^{\langle \text{trs} \rangle}$	$I_{1,1}^{\langle \text{trs} \rangle}$	$I_{0,2}^{\langle \text{trs} \rangle}$	$I_{3,0}^{\langle \text{trs} \rangle}$	$I_{2,1}^{\langle \text{trs} \rangle}$	$I_{1,2}^{\langle \text{trs} \rangle}$	$I_{0,3}^{\langle \text{trs} \rangle}$
7(30)	12.000	−7.718	0.000	−11.203	2.242	−0.651	−0.757	1.131
7(70)	12.000	−7.718	0.000	−11.203	2.242	−0.652	−0.757	1.131
7(130)	12.000	−7.717	0.000	−11.204	2.243	−0.650	−0.757	1.130
7(170)	12.000	−7.718	0.000	−11.203	2.242	−0.651	−0.757	1.131
7(190)	12.000	−7.718	0.000	−11.203	2.243	−0.651	−0.757	1.131
7(260)	12.000	−7.718	0.000	−11.203	2.242	−0.651	−0.757	1.131
7(290)	12.000	−7.717	0.000	−11.204	2.242	−0.652	−0.757	1.130
7(330)	12.000	−7.717	0.000	−11.203	2.243	−0.651	−0.757	1.131
RSD (%)	0.000	0.007	0.000	0.004	0.023	0.098	0.000	0.041
Average RSD(%) = 0.022								
a(30)	12.000	−10.587	0.000	−10.848	0.068	0.199	0.046	0.004
a(70)	12.000	−10.588	0.000	−10.848	0.068	0.199	0.046	0.004
a(130)	12.000	−10.589	0.000	−10.847	0.066	0.199	0.047	0.004
a(170)	12.000	−10.588	0.000	−10.848	0.068	0.199	0.046	0.004
a(190)	12.000	−10.588	0.000	−10.848	0.068	0.199	0.046	0.004
a(260)	12.000	−10.588	0.000	−10.848	0.068	0.199	0.046	0.004
a(290)	12.000	−10.588	0.000	−10.848	0.068	0.199	0.046	0.004
a(330)	12.000	−10.588	0.000	−10.848	0.068	0.199	0.046	0.004
RSD (%)	0.000	0.005	0.000	0.003	1.044	0.000	0.767	0.000
Average RSD(%) = 0.227								
butterfly(30)	12.000	−10.565	0.000	−12.456	0.152	0.349	−0.031	−0.018
butterfly(70)	12.000	−10.566	0.000	−12.456	0.152	0.348	−0.031	−0.018
butterfly(130)	12.000	−10.564	0.000	−12.456	0.153	0.349	−0.031	−0.018
butterfly(170)	12.000	−10.566	0.000	−12.456	0.152	0.348	−0.031	−0.018
butterfly(190)	12.000	−10.566	0.000	−12.456	0.152	0.348	−0.031	−0.018
butterfly(260)	12.000	−10.566	0.000	−12.456	0.152	0.348	−0.031	−0.018
butterfly(290)	12.000	−10.566	0.000	−12.456	0.152	0.349	−0.031	−0.018
butterfly(330)	12.000	−10.566	0.000	−12.456	0.152	0.348	−0.031	−0.018
RSD (%)	0.000	0.007	0.000	0.000	0.232	0.149	0.000	0.000
Average RSD(%) = 0.049								
shen(30)	12.000	−8.707	0.000	−9.035	0.364	−0.172	−0.012	−0.014
shen(70)	12.000	−8.706	0.000	−9.038	0.362	−0.173	−0.011	−0.013
shen(130)	12.000	−8.707	0.000	−9.035	0.372	−0.168	−0.019	−0.012
shen(170)	12.000	−8.704	0.000	−9.036	0.364	−0.173	−0.013	−0.013
shen(190)	12.000	−8.704	0.000	−9.037	0.364	−0.173	−0.012	−0.013
shen(260)	12.000	−8.704	0.000	−9.036	0.364	−0.173	−0.013	−0.013
shen(290)	12.000	−8.707	0.000	−9.036	0.361	−0.174	−0.011	−0.013
shen(330)	12.000	−8.703	0.000	−9.034	0.362	−0.174	−0.012	−0.013
RSD (%)	0.000	0.019	0.000	0.014	0.933	1.117	20.099	4.112
Average RSD(%) = 3.287								

Table 5.3: Selected orders of TR-Z Invariants Moments for experiment on translation and rotation deformations

image(θ)	$I_{0,0}^{\langle \text{tr-Z} \rangle}$	$I_{2,0}^{\langle \text{tr-Z} \rangle}$	$I_{1,1}^{\langle \text{tr-Z} \rangle}$	$I_{0,2}^{\langle \text{tr-Z} \rangle}$	$I_{3,0}^{\langle \text{tr-Z} \rangle}$	$I_{2,1}^{\langle \text{tr-Z} \rangle}$	$I_{1,2}^{\langle \text{tr-Z} \rangle}$	$I_{0,3}^{\langle \text{tr-Z} \rangle}$
7(30)	9.020	22.891	26.612	20.922	−40.502	−39.639	−36.309	−29.491
7(70)	9.020	22.892	26.613	20.923	−40.503	−39.641	−36.310	−29.492
7(130)	9.019	22.890	26.610	20.920	−40.499	−39.636	−36.305	−29.485
7(170)	9.020	22.891	26.612	20.922	−42.698	−39.001	−35.567	−30.598
7(190)	9.020	22.892	26.613	20.923	−42.698	−39.001	−35.567	−30.598
7(260)	9.020	22.891	26.612	20.922	−42.698	−39.001	−35.567	−30.598
7(290)	9.020	22.891	26.612	20.922	−42.699	−39.001	−35.566	−30.595
7(330)	9.020	22.891	26.611	20.922	−42.698	−39.000	−35.566	−30.597
RSD (%)	0.004	0.003	0.004	0.004	2.715	0.841	1.070	1.900
Average RSD(%) = 0.818								
a(30)	15.495	38.510	45.715	38.076	−66.561	−65.771	−65.316	−64.133
a(70)	15.496	38.514	45.720	38.080	−66.566	−65.777	−65.323	−64.141
a(130)	15.498	38.517	45.725	38.086	−66.567	−65.782	−65.331	−64.159
a(170)	15.496	38.513	45.719	38.079	−66.820	−66.531	−65.494	−64.152
a(190)	15.496	38.513	45.719	38.079	−66.820	−66.530	−65.494	−64.151
a(260)	15.496	38.513	45.719	38.079	−66.820	−66.531	−65.494	−64.152
a(290)	15.494	38.509	45.714	38.075	−66.812	−66.523	−65.487	−64.146
a(330)	15.496	38.514	45.720	38.08	−66.824	−66.533	−65.497	−64.157
RSD (%)	0.007	0.006	0.007	0.009	0.198	0.588	0.135	0.013
Average RSD(%) = 0.120								
butterfly(30)	13.276	32.443	39.168	30.129	−54.095	−56.176	−51.713	−40.296
butterfly(70)	13.275	32.442	39.168	30.129	−54.088	−56.173	−51.712	−40.297
butterfly(130)	13.275	32.444	39.168	30.128	−53.707	−55.279	−51.791	−40.339
butterfly(170)	13.275	32.442	39.168	30.129	−53.698	−55.276	−51.791	−40.343
butterfly(190)	13.275	32.442	39.168	30.129	−53.698	−55.277	−51.793	−40.344
butterfly(260)	13.275	32.442	39.168	30.129	−53.698	−55.276	−51.791	−40.343
butterfly(290)	13.275	32.441	39.167	30.128	−54.089	−56.173	−51.711	−40.295
butterfly(330)	13.275	32.440	39.166	30.127	−54.086	−56.17	−51.709	−40.292
RSD (%)	0.003	0.004	0.002	0.003	0.386	0.859	0.083	0.063
Average RSD(%) = 0.175								
shen(30)	8.124	19.876	23.969	19.726	−33.253	−34.076	−33.879	−32.230
shen(70)	8.125	19.880	23.973	19.728	−33.263	−34.082	−33.882	−32.228
shen(130)	8.121	19.868	23.960	19.718	−33.239	−34.064	−33.862	−32.213
shen(170)	8.122	19.873	23.964	19.721	−32.978	−34.201	−33.879	−32.228
shen(190)	8.123	19.874	23.966	19.722	−32.980	−34.203	−33.881	−32.229
shen(260)	8.122	19.873	23.964	19.721	−32.978	−34.201	−33.879	−32.228
shen(290)	8.124	19.877	23.970	19.726	−32.983	−34.208	−33.887	−32.237
shen(330)	8.122	19.873	23.963	19.721	−32.980	−34.200	−33.879	−32.231
RSD (%)	0.017	0.018	0.018	0.017	0.426	0.196	0.021	0.021
Average RSD(%) = 0.092								

Table 5.4: Selected orders of TRS-Y for experiment on translation and rotation deformations

image(θ)	$I_{0,0}^{\langle\text{trs-Y}\rangle}$	$I_{2,0}^{\langle\text{trs-Y}\rangle}$	$I_{1,1}^{\langle\text{trs-Y}\rangle}$	$I_{0,2}^{\langle\text{trs-Y}\rangle}$	$I_{3,0}^{\langle\text{trs-Y}\rangle}$	$I_{2,1}^{\langle\text{trs-Y}\rangle}$	$I_{1,2}^{\langle\text{trs-Y}\rangle}$	$I_{0,3}^{\langle\text{trs-Y}\rangle}$
7(30)	60.000	75.431	0.013	−11.695	130.383	−35.321	−42.500	63.956
7(70)	60.000	75.426	0.013	−11.696	130.399	−35.346	−42.487	63.967
7(130)	60.000	75.445	0.013	−11.724	130.432	−35.264	−42.492	63.909
7(170)	60.000	75.422	0.013	−11.704	130.391	−35.328	−42.483	63.950
7(190)	60.000	75.423	0.013	−11.701	130.408	−35.327	−42.491	63.949
7(260)	60.000	75.422	0.013	−11.704	130.391	−35.328	−42.483	63.950
7(290)	60.000	75.434	0.013	−11.719	130.372	−35.358	−42.464	63.929
7(330)	60.000	75.441	0.013	−11.701	130.413	−35.326	−42.494	63.946
RSD (%)	0.000	0.012	0.000	0.085	0.015	0.076	0.026	0.028
Average RSD(%) = 0.030								
a(30)	60.000	3.685	0.013	−2.826	5.291	11.203	2.514	1.408
a(70)	60.000	3.679	0.013	−2.828	5.309	11.198	2.508	1.401
a(130)	60.000	3.642	0.013	−2.811	5.186	11.189	2.568	1.393
a(170)	60.000	3.674	0.013	−2.835	5.287	11.200	2.524	1.411
a(190)	60.000	3.677	0.013	−2.835	5.285	11.197	2.522	1.408
a(260)	60.000	3.674	0.013	−2.835	5.287	11.200	2.524	1.411
a(290)	60.000	3.678	0.013	−2.824	5.294	11.202	2.524	1.418
a(330)	60.000	3.678	0.013	−2.828	5.284	11.201	2.532	1.408
RSD (%)	0.000	0.354	0.000	0.283	0.720	0.036	0.712	0.498
Average RSD(%) = 0.325								
butterfly(30)	60.000	4.237	0.013	−43.027	10.039	19.551	−2.356	−1.814
butterfly(70)	60.000	4.217	0.013	−43.023	10.033	19.539	−2.358	−1.814
butterfly(130)	60.000	4.263	0.013	−43.038	10.108	19.559	−2.376	−1.812
butterfly(170)	60.000	4.224	0.013	−43.025	10.031	19.542	−2.356	−1.815
butterfly(190)	60.000	4.220	0.013	−43.022	10.032	19.542	−2.355	−1.816
butterfly(260)	60.000	4.224	0.013	−43.025	10.031	19.542	−2.356	−1.815
butterfly(290)	60.000	4.229	0.013	−43.025	10.036	19.544	−2.358	−1.815
butterfly(330)	60.000	4.223	0.013	−43.031	10.044	19.532	−2.357	−1.822
RSD (%)	0.000	0.355	0.000	0.012	0.259	0.041	0.297	0.165
Average RSD(%) = 0.141								
shen(30)	60.000	50.687	0.013	42.506	24.144	−8.872	−0.031	2.635
shen(70)	60.000	50.727	0.013	42.424	24.040	−8.967	−0.018	2.684
shen(130)	60.000	50.690	0.013	42.488	24.637	−8.661	−0.441	2.731
shen(170)	60.000	50.767	0.013	42.469	24.166	−8.918	−0.088	2.684
shen(190)	60.000	50.760	0.013	42.457	24.156	−8.924	−0.060	2.675
shen(260)	60.000	50.767	0.013	42.469	24.166	−8.918	−0.088	2.684
shen(290)	60.000	50.705	0.013	42.462	24.016	−9.014	−0.021	2.688
shen(330)	60.000	50.803	0.013	42.528	24.075	−8.989	−0.079	2.722
RSD (%)	0.000	0.083	0.000	0.075	0.811	1.235	135.922	1.079
Average RSD(%) = 17.401								

Table 5.5: Selected Output images of rotation invariants by Zhang et. al.

Input	Output	θ_z	$I_{0,0}^{\langle \text{tr-Z} \rangle}$	$I_{2,0}^{\langle \text{tr-Z} \rangle}$	$I_{1,1}^{\langle \text{tr-Z} \rangle}$	$I_{0,2}^{\langle \text{tr-Z} \rangle}$	$I_{3,0}^{\langle \text{tr-Z} \rangle}$	$I_{2,1}^{\langle \text{tr-Z} \rangle}$	$I_{1,2}^{\langle \text{tr-Z} \rangle}$	$I_{0,3}^{\langle \text{tr-Z} \rangle}$
		52.7°	9.020	22.891	26.611	20.922	−40.501	−39.638	−36.308	−29.489
		12.7°	9.020	22.892	26.613	20.923	−42.698	−39.001	−35.567	−30.598
		48.8°	8.122	19.873	23.963	19.721	−33.253	−34.069	−33.870	−32.222
		8.8°	8.123	19.874	23.966	19.722	−32.980	−34.203	−33.881	−32.229

Table 5.6: Selected output image of rotation invariants by TRS

Input	Output	θ_1	$I_{0,0}^{\langle \text{trs} \rangle}$	$I_{2,0}^{\langle \text{trs} \rangle}$	$I_{1,1}^{\langle \text{trs} \rangle}$	$I_{0,2}^{\langle \text{trs} \rangle}$	$I_{3,0}^{\langle \text{trs} \rangle}$	$I_{2,1}^{\langle \text{trs} \rangle}$	$I_{1,2}^{\langle \text{trs} \rangle}$	$I_{0,3}^{\langle \text{trs} \rangle}$
		52.7°	12.000	−7.717	0.000	−11.203	2.243	−0.651	−0.757	1.131
		192.7°	12.000	−7.718	0.000	−11.203	2.243	−0.651	−0.757	1.131
		228.8°	12.000	−8.703	0.000	−9.034	0.362	−0.174	−0.012	−0.013
		8.8°	12.000	−8.704	0.000	−9.037	0.364	−0.173	−0.012	−0.013

5.4.2 Experiment on Accuracy of Translation, Rotation, and Scale Invariants

In this subsection the computational accuracy of the proposed algorithms has been reviewed. A set of images of different complexities representing groups of numbers, letters, Chinese characters and symbols are used in this experiment. Here the original space $S_2(N_0)$ and the transformed space $S_2(N_s)$ are both equal to $S_2(200)$. In Table 5.7, images with size 90×90 pixels, are scaled uniformly by factors of $\{0.5, 0.6, \cdots, 1.5\}$, rotated by angles between 0^o to 359^o and translated by $\{-5, 0, 5\}$ from the centre. The selected output of TRS invariants are listed in Tables 5.8 and 5.9 for proposed TRS-invariants and TRS-Y, respectively. TR-Z was not evaluated as the features did not have the scale invariants. As shown in the tables, the performance of proposed TRS and TRS-Y are nearly identical. This is mainly due to both algorithms are using nearly similar normalization strategy. The methods are accurate for the even order invariants or invariants with relatively large values. The odd order invariants and the invariants with relatively small values are less accurate. This is mainly due to the cancellation process of the invariant transformation functions which is vulnerable to discretization errors. The problems can be easily overcome by incorporating suitable skew parameter values.

Table 5.7: Test images used by the experiment of translation, rotation and scale deformations

(ω, θ^{o})	Original	(1.2, 30)	(0.9, 57)	(0.6, 112)	(1.5, 145)	(1.3, 193)	(0.7, 204)	(1.1, 242)	(0.8, 281)	(0.5, 349)
(a_3, b_3)	–	(-5, -5)	(-5, 5)	(0, 5)	(5, 0)	(0,-5)	(0,0)	(-5, 0)	(5, -5)	(5, 5)
										
Image	im_3-1	im_3-2	im_3-3	im_3-4	im_3-5	im_3-6	im_3-7	im_3-8	im_3-9	im_3-10
			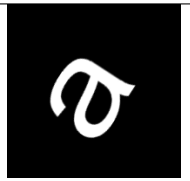	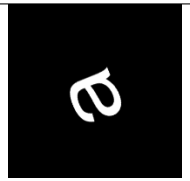						
image	im_a-1	im_a-2	im_a-3	im_a-4	im_a-5	im_a-6	im_a-7	im_a-8	im_a-9	im_a-10
				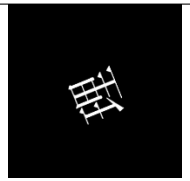			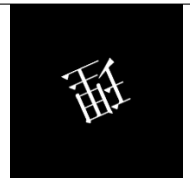			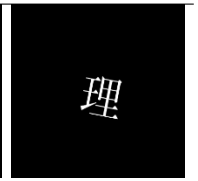
image	im_li-1	im_li-2	im_li-3	im_li-4	im_li-5	im_li-6	im_li-7	im_li-8	im_li-9	im_li-10
										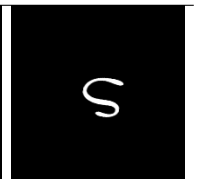
image	im_sigma-1	im_sigma-2	im_sigma-3	im_sigma-4	im_sigma-5	im_sigma-6	im_sigma-7	im_sigma-8	im_sigma-9	im_sigma-10

Table 5.8: Selected orders of propose TRS-Invariants for experiment on translation, rotation and scale deformation

Image	$I_{0,0}^{\langle trs \rangle}$	$I_{2,0}^{\langle trs \rangle}$	$I_{1,1}^{\langle trs \rangle}$	$I_{0,2}^{\langle trs \rangle}$	$I_{3,0}^{\langle trs \rangle}$	$I_{2,1}^{\langle trs \rangle}$	$I_{1,2}^{\langle trs \rangle}$	$I_{0,3}^{\langle trs \rangle}$
im_3-1	20.000	−15.131	0.000	−17.002	0.531	−0.745	−0.325	−1.319
im_3-2	20.000	−15.132	0.000	−17.003	0.530	−0.746	−0.326	−1.319
im_3-3	20.000	−15.132	0.000	−17.003	0.530	−0.746	−0.326	−1.319
im_3-4	20.000	−15.136	0.000	−17.008	0.533	−0.744	−0.323	−1.314
im_3-5	20.000	−15.132	0.000	−17.003	0.530	−0.746	−0.325	−1.319
im_3-6	20.000	−15.130	0.000	−17.002	0.530	−0.746	−0.326	−1.319
im_3-7	20.000	−15.130	0.000	−17.002	0.532	−0.746	−0.325	−1.319
im_3-8	20.000	−15.132	0.000	−17.002	0.530	−0.745	−0.326	−1.319
im_3-9	20.000	−15.133	0.000	−17.002	0.525	−0.748	−0.325	−1.317
im_3-10	20.000	−15.135	0.000	−16.987	0.535	−0.750	−0.325	−1.335
RSD(%)	0.000	0.013	0.000	0.032	0.488	0.226	0.283	0.42
Average RSD(%) = 0.183								
im_a-1	20.000	−17.632	0.000	−18.071	0.126	0.336	0.071	0.008
im_a-2	20.000	−17.633	0.000	−18.071	0.126	0.336	0.071	0.008
im_a-3	20.000	−17.633	0.000	−18.071	0.125	0.336	0.071	0.008
im_a-4	20.000	−17.633	0.000	−18.073	0.124	0.334	0.072	0.008
im_a-5	20.000	−17.633	0.000	−18.071	0.126	0.336	0.071	0.008
im_a-6	20.000	−17.633	0.000	−18.071	0.126	0.336	0.071	0.008
im_a-7	20.000	−17.636	0.000	−18.071	0.122	0.335	0.072	0.008
im_a-8	20.000	−17.632	0.000	−18.071	0.126	0.336	0.071	0.008
im_a-9	20.000	−17.632	0.000	−18.074	0.131	0.336	0.067	0.007
im_a-10	20.000	−17.645	0.000	−18.084	0.129	0.333	0.069	0.007
RSD(%)	0.000	0.022	0.000	0.023	1.959	0.321	2.133	5.406
Average RSD(%) = 1.233								
im_li-1	20.000	−15.100	0.000	−16.094	0.657	−0.286	0.561	0.160
im_li-2	20.000	−15.101	0.000	−16.095	0.658	−0.287	0.561	0.162
im_li-3	20.000	−15.099	0.000	−16.097	0.654	−0.285	0.563	0.151
im_li-4	20.000	−15.104	0.000	−16.093	0.655	−0.280	0.563	0.156
im_li-5	20.000	−15.101	0.000	−16.095	0.657	−0.287	0.561	0.160
im_li-6	20.000	−15.101	0.000	−16.093	0.657	−0.287	0.561	0.161
im_li-7	20.000	−15.091	0.000	−16.090	0.654	−0.283	0.567	0.151
im_li-8	20.000	−15.100	0.000	−16.095	0.656	−0.286	0.562	0.159
im_li-9	20.000	−15.095	0.000	−16.086	0.666	−0.291	0.562	0.174
im_li-10	20.000	−15.092	0.000	−16.086	0.648	−0.289	0.564	0.156
RSD(%)	0.000	0.028	0.000	0.024	0.681	1.061	0.338	4.119
Average RSD(%) = 0.781								
im_sigma-1	20.000	−12.385	0.000	−15.331	0.910	−0.061	−1.807	−1.756
im_sigma-2	20.000	−12.386	0.000	−15.330	0.909	−0.060	−1.807	−1.757
im_sigma-3	20.000	−12.384	0.000	−15.331	0.909	−0.058	−1.807	−1.760
im_sigma-4	20.000	−12.387	0.000	−15.333	0.907	−0.060	−1.806	−1.755
im_sigma-5	20.000	−12.385	0.000	−15.331	0.910	−0.060	−1.807	−1.757
im_sigma-6	20.000	−12.386	0.000	−15.330	0.910	−0.061	−1.807	−1.756
im_sigma-7	20.000	−12.391	0.000	−15.331	0.908	−0.061	−1.807	−1.754
im_sigma-8	20.000	−12.386	0.000	−15.330	0.911	−0.061	−1.807	−1.756
im_sigma-9	20.000	−12.380	0.000	−15.339	0.905	−0.058	−1.805	−1.756
im_sigma-10	20.000	−12.346	0.000	−15.341	0.902	−0.035	−1.804	−1.774
RSD(%)	0.000	0.103	0.000	0.026	0.305	13.895	0.060	0.330
Average RSD(%) = 1.840								

Table 5.9: Selected orders of TRS-Y for experiment on translation, rotation and scale deformation

Image	$I_{0,0}^{\langle \text{trs-Y} \rangle}$	$I_{2,0}^{\langle \text{trs-Y} \rangle}$	$I_{1,1}^{\langle \text{trs-Y} \rangle}$	$I_{0,2}^{\langle \text{trs-Y} \rangle}$	$I_{3,0}^{\langle \text{trs-Y} \rangle}$	$I_{2,1}^{\langle \text{trs-Y} \rangle}$	$I_{1,2}^{\langle \text{trs-Y} \rangle}$	$I_{0,3}^{\langle \text{trs-Y} \rangle}$
im_3-1	100.000	68.959	0.008	22.183	33.019	−41.075	−18.001	−71.741
im_3-2	100.000	68.940	0.008	22.165	32.982	−41.083	−18.008	−71.737
im_3-3	100.000	68.929	0.008	22.175	33.002	−41.084	−18.033	−71.758
im_3-4	100.000	68.828	0.008	22.037	33.133	−40.999	−17.883	−71.502
im_3-5	100.000	68.950	0.008	22.167	33.003	−41.078	−18.002	−71.730
im_3-6	100.000	68.976	0.008	22.186	33.005	−41.090	−18.005	−71.742
im_3-7	100.000	68.991	0.008	22.198	33.129	−41.100	−17.989	−71.750
im_3-8	100.000	68.948	0.008	22.186	33.014	−41.070	−18.021	−71.737
im_3-9	100.000	68.904	0.008	22.177	32.730	−41.213	−17.984	−71.658
im_3-10	100.000	68.861	0.008	22.557	33.276	−41.308	−17.951	−72.633
RSD(%)	0.000	0.074	0.000	0.597	0.423	0.211	0.239	0.422
Average RSD(%) = 0.246								
im_a-1	100.000	6.428	0.008	−4.541	8.531	18.819	3.924	1.625
im_a-2	100.000	6.423	0.008	−4.541	8.542	18.817	3.919	1.624
im_a-3	100.000	6.424	0.008	−4.527	8.501	18.816	3.942	1.652
im_a-4	100.000	6.410	0.008	−4.594	8.468	18.746	3.990	1.626
im_a-5	100.000	6.424	0.008	−4.541	8.540	18.820	3.920	1.622
im_a-6	100.000	6.417	0.008	−4.542	8.532	18.823	3.925	1.646
im_a-7	100.000	6.339	0.008	−4.537	8.318	18.788	4.010	1.639
im_a-8	100.000	6.441	0.008	−4.533	8.538	18.829	3.918	1.628
im_a-9	100.000	6.451	0.008	−4.613	8.839	18.821	3.706	1.581
im_a-10	100.000	6.112	0.008	−4.869	8.702	18.660	3.809	1.591
RSD(%)	0.000	1.584	0.000	2.271	1.610	0.283	2.254	1.370
Average RSD(%) = 1.172								
im_li-1	100.000	69.736	0.008	44.886	40.107	−15.401	31.759	11.601
im_li-2	100.000	69.723	0.008	44.869	40.156	−15.456	31.723	11.688
im_li-3	100.000	69.766	0.008	44.816	39.934	−15.306	31.881	11.090
im_li-4	100.000	69.633	0.008	44.919	40.024	−15.056	31.881	11.395
im_li-5	100.000	69.723	0.008	44.873	40.110	−15.412	31.751	11.613
im_li-6	100.000	69.718	0.008	44.917	40.120	−15.432	31.757	11.663
im_li-7	100.000	69.957	0.008	45.000	39.975	−15.200	32.067	11.087
im_li-8	100.000	69.729	0.008	44.875	40.079	−15.388	31.799	11.545
im_li-9	100.000	69.872	0.008	45.094	40.630	−15.676	31.823	12.381
im_li-10	100.000	69.947	0.008	45.091	39.629	−15.539	31.925	11.372
RSD(%)	0.000	0.154	0.000	0.213	0.617	1.116	0.329	3.177
Average RSD(%) = 0.701								
im_sigma-1	100.000	137.618	0.008	63.963	56.249	−2.213	−100.470	−94.924
im_sigma-2	100.000	137.590	0.008	63.985	56.231	−2.168	−100.475	−95.001
im_sigma-3	100.000	137.644	0.008	63.972	56.233	−2.038	−100.435	−95.183
im_sigma-4	100.000	137.554	0.008	63.920	56.091	−2.164	−100.399	−94.904
im_sigma-5	100.000	137.612	0.008	63.963	56.258	−2.171	−100.457	−94.980
im_sigma-6	100.000	137.600	0.008	63.982	56.255	−2.195	−100.454	−94.972
im_sigma-7	100.000	137.461	0.008	63.969	56.142	−2.200	−100.460	−94.851
im_sigma-8	100.000	137.588	0.008	63.999	56.307	−2.199	−100.475	−94.924
im_sigma-9	100.000	137.744	0.008	63.774	56.016	−2.035	−100.323	−94.953
im_sigma-10	100.000	138.577	0.008	63.722	55.855	−0.739	−100.318	−95.969
RSD(%)	0.000	0.230	0.000	0.151	0.250	22.462	0.060	0.346
Average RSD(%) = 2.937								

5.4.3 Numerical Computational Efficiency

In this subsection, the computational efficiency of the proposed algorithms has been evaluated. The program was implemented in Matlab 2011b, on Intel i3 550 processor with 3.2GHz, 3GB of RAM. In this experiment, images with size 50×50, 100×100, 150×150, and 200×200 pixels were used to generate invariants with orders of 10, 20, and 30. The experiment was repeated 200 times and the average CPU elapse times in millisecond are recorded. From Table 5.10, on average (excluding the moment generation time), the proposed method is about 1,930 times faster than TR-Z. This shows significant amount of overhead due to the expression in the TR-Z algorithm and the effectiveness of recurrence relations in simplifying the numerical computations. In terms of total computation time, the proposed method is superior when compared with TR-Z and TRS-Y. On average the propose method is 5.2 times faster than TRS-Y.

Table 5.10: Comparison of CPU elapse time (ms) for translation, rotational and scale descriptors

				Proposed TRS		TR-Z	
Image Size	Order of descriptors	TRS-Y (ms)	Moments generation times (ms)	Invariant generation times (ms)	Total time (ms)	Invariant generation times (ms)	Total time (ms)
(50×50)	10	54.121	10.308	1.607	11.915	60.007	70.315
	20	137.500	25.337	9.940	35.277	5,151.538	5,176.875
	30	312.279	52.836	37.452	90.288	89,207.182	89,260.018
(100×100)	10	229.861	26.595	1.582	28.177	59.913	86.508
	20	537.152	93.267	9.957	103.223	5,177.623	5,270.89
	30	1,060.712	199.316	37.385	236.701	89,308.026	89,507.342
(150×150)	10	495.126	58.638	1.577	60.215	59.818	118.456
	20	1,212.572	205.791	9.898	215.689	5,265.398	5,471.188
	30	2,377.346	441.696	37.594	479.290	89,328.581	89,770.276
(200×200)	10	858.131	103.563	1.591	105.154	59.891	163.455
	20	2,159.725	417.853	9.915	427.769	5,168.708	5,586.561
	30	4,221.422	774.458	37.420	811.878	89,323.500	90,097.958
Average		1,137.996	200.805	16.327	217.131	31,514.182	31,714.987

5.4.4 Experiment on Object Classification

In this experiment, the classification performance of the proposed TRS have been tested. For the purpose of comparison, TRS-Y, TR-Z are included. The following feature vectors are used to classify the images

$$\mathbf{V} = [I_{2,0}, I_{0,2}, I_{3,0}, I_{1,2}, I_{2,1}, I_{0,3}]^T \tag{5.97}$$

where $I_{n,m}$ denote the TRS-invariants defined in previous section. In this experiment, Euclidean distance is utilized as the classification measure. The formula given below is similar to (2.73).

$$d(\tilde{\mathbf{V}}_\mathbf{s}, \tilde{\mathbf{V}}_\mathbf{t}^{(\mathbf{k})}) = \sum_{j=1}^{J} (\tilde{v}_{s,j} - \tilde{v}_{t,j}^{(k)})^2 \tag{5.98}$$

where $\tilde{\mathbf{V}}_\mathbf{s}$ is the $J-$dimensional scaled feature vector of unknown sample, and $\tilde{\mathbf{V}}_\mathbf{t}^{(\mathbf{k})}$ is the scaled training vector of class k.

The recognition accuracy,η, is defined as follows

$$\eta = \frac{\text{Number of correctly classified images}}{\text{Total number of images used in the test}}. \tag{5.99}$$

A set of Chinese characters as listed in Figure 5.2 are used as training set. The size of each training image is 100×100 pixels. The original space$S_2(N_0)$ and transformed space $S_2(N_s)$ are equal to $S_2(150)$. The testing set is generated by rotating with angles of $\theta \in \{0^o, 20^o, \cdots 340^o\}$ and translation t_x and $t_y \in \{-5, 0, 5\}$. Due to TR-Z being not scale invariant, scale deformations are not applicable to the test images. Excluding those similar to the original images, the transformation forms a testing set of 12,940 images. This is followed by adding salt-and-pepper noise with different noise densities. Figure 5.3 shows some of the testing images contaminated by 4% of salt-and-pepper noise.

Figure 5.2: Binary images as training set for experiment on character recognition.

The classification performance of the proposed TRS is compared with the other TRS-invariants algorithms shown in Table **??**. As shown in the table, the proposed TRS has identical performance when compared with TRS-Y. This is mainly due to both algorithms using the identical normalization strategy. On the other hand, TR-Z is lowest in the classification performance. This is mainly caused by the skew effect that compromised the within class separation. As such, adding of noise will wipe out the slim separation between those classes. Therefore TR-Z is found to be extremely sensitive to noise. The argument is supported by the poor performance shown by TRS-W where the centroid of the image has been shifted to the origin.

Classification result of images with translation and rotation transformation

	Accuracy (%)			
Salt & pepper	TRS	TRS-W*	TRS-Y	TR-Z
No noise	100	100	100	100
0.01	95.750	76.121	95.696	31.221
0.02	89.845	41.213	89.737	19.985
0.03	78.601	26.275	78.408	14.830
0.04	67.473	20.363	67.403	5.587

TRS-W* denotes TRS with centroid at the origin.

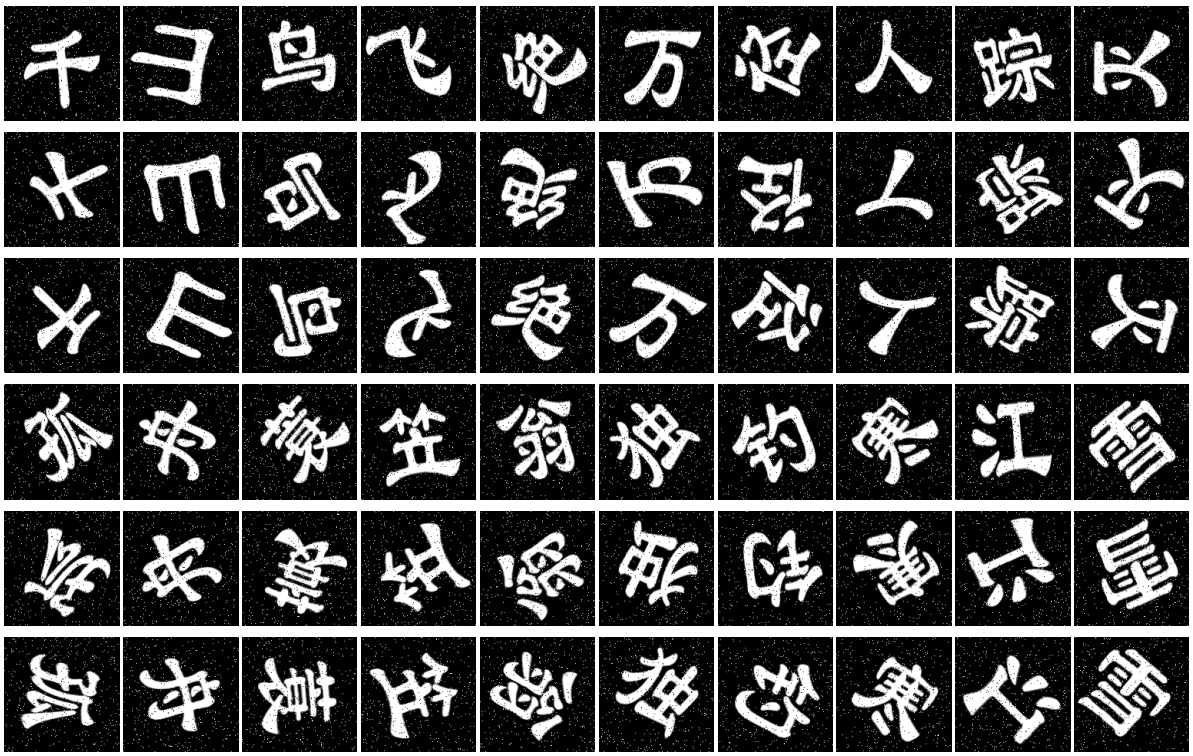

Figure 5.3: Part of the images in the testing set.

5.5 Conclusion

In this chapter, the translation, rotation and scale Tchebichef moment invariants of Yap et al.(2003) and translation rotation Tchebichef moment invariants of H. Zhang et al. (2011) have been reviewed. Both methods are slow in the computational speed. In addition, the classification performance of TR-Z is highly sensitive to noise. Thus a new TRS invariants has been proposed to resolve the above mentioned issues. A new set of recurrence relations has been derived for the fast computation of affine Tchebichef moments which can then be applied to derive the TRS invariant descriptors. A new set of normalization scheme using Tchebichef moments have been defined so that the computation overhead caused by determination of the normalization parameters from other domain can be avoided. Empirical studies showed significant improvement in numerical performance with the proposed algorithm. The features of proposed invariants are also found to have equivalent or better classification performance when compared with existing TRS invariants.

CHAPTER 6

AFFINE TCHEBICHEF MOMENT INVARIANTS USING IMAGE NORMALIZATION

In this chapter a new affine Tchebichef moment invariants has been proposed. The invariants consists of recurrence relations for fast computation, and a new set of normalization schemes based on Tchebichef moments. An experiment has been carried out to verify the correctness of the proposed algorithms.

6.1 Introduction

Affine transformation is a general linear transformation of spatial coordinates which can be defined as

$$\begin{pmatrix} x' \\ y' \end{pmatrix} = \begin{pmatrix} a_1 & a_2 \\ b_1 & b_2 \end{pmatrix} \begin{pmatrix} x \\ y \end{pmatrix} + \begin{pmatrix} a_3 \\ b_3 \end{pmatrix}$$
$$(x,y) \in S_2(N_0), \text{ and } (x^{'},y^{'}) \in S_2(N_s). \tag{6.1}$$

The affine transformed Tchebichef moments $T_{n,m}^{\langle \mathrm{am} \rangle}$ are defined as

$$T_{n,m}^{\langle \mathrm{am} \rangle} = |J| \sum_{x=0}^{N_0-1} \sum_{y=0}^{N_0-1} \tilde{t}_n^{N_s}(a_1x+a_2y+a_3)\tilde{t}_m^{N_s}(b_1x+b_2y+b_3)f(x,y)$$
$$a_1,a_2,a_3,b_1,b_2, \text{ and, } b_3 \in \Re,$$
$$n,m = 0,1,\cdots, \min\{N_s-1, N_0-1\} \tag{6.2}$$

where Jacobian of the transformation J satisfies

$$J = \begin{vmatrix} a_1 & a_2 \\ b_1 & b_2 \end{vmatrix} \neq 0. \tag{6.3}$$

Image normalization to affine transformation is based on proper decomposition of an affine transformation into several simpler transformations. Several decomposition schemes have been proposed. Pei and Lin (1995) proposed a decomposition of two rotations and a nonuniform scaling between them. Their method used eigenvalues of the covariance matrix and tensors for computation of normalization coefficients. However

the method failed to work on symmetric objects. Shen and Ip (1997) derived the invariants using generalized complex moments and Fourier transformation in polar coordinates. The method worked for symmetric objects but is exceedingly complicated. Rothe, Susse, and Voss (1996) proposed two different decomposition schemes known as XSR, (the decomposition to skew, nonuniform scaling and rotation), and XYS (the decomposition to two skews and a nonuinform scaling). However the approaches lead to some ambiguities, which were later studied in detail by Y. Zhang, Wen, Zhang, and Soh (2003). For discrete domain, affine Tchebichef moments has been proposed by Liu et al. (2011) based on the decomposition of XSR and XYS by Rothe et al. (1996). However the invariant algorithms are numerically inefficient mainly due to complexity of hypergeometric moments involved. Furthermore, as pointed out in Chapter 5, some ambiguities have been detected for the rotation algorithm used by Liu et al. (2011) in XSR. Therefore we propose an alternative approach that follow the decomposition technique by Flusser et al. (2009). The method is selected mainly due to its ability to accurately discriminate both non-symmetric and symmetric patterns. In Section 6.2, the proposed affine Tchebichef moment invariants has been derived. This is followed by an experiment to verify the accuracy of the proposed method in Section 6.3. Section 6.4 concludes this topic.

6.2 Proposed Affine Tchebichef Moment Invariants

6.2.1 Fast Computation of Affine Tchebichef Moment Invariants

Fast computation algorithms has been derived in Chapter 5 by using Theorem 5.3.1. We list it here for the purpose of completeness.

The $(n+m)^{\text{th}}-$order of affine transformed Tchebichef moment $T_{n,m}^{\langle \text{am} \rangle}$ has expression

$$T_{n,m}^{\langle \text{am} \rangle} = |J| \sum_{k=0}^{n+m} \sum_{j=0}^{n+m-k} \lambda_{n,m,k,j} T_{k,j} \tag{6.4}$$

where $J = \begin{vmatrix} a_1 & a_2 \\ b_1 & b_2 \end{vmatrix}$, and the coefficients $\lambda_{n,m,k,j}$, have recurrence relations

$$\begin{aligned}
\lambda_{n,m,k,j}\left(\begin{array}{c} a_1,a_2,a_3 \\ b_1,b_2,b_3 \end{array}\middle| N_0,N_s\right) &= -\lambda_{n-1,m,k+1,j}a_1K^{N_s,N_0}_{n,k+2}\tilde{C}^{N_0}_{k+2} - \lambda_{n-1,m,k,j+1}a_2K^{N_s,N_0}_{n,j+2}\tilde{C}^{N_0}_{j+2} \\
&\quad +\lambda_{n-1,m,k,j}\tilde{A}^{N_s}_{n}\left[a_3+\left(\frac{N_0-1}{2}\right)(a_1+a_2)-\left(\frac{N_s-1}{2}\right)\right] \\
&\quad +\lambda_{n-1,m,k-1,j}a_1K^{N_s,N_0}_{n,k} + \lambda_{n-1,m,k,j-1}a_2K^{N_s,N_0}_{n,j} \\
&\quad +\lambda_{n-2,m,k,j}\tilde{C}^{N_s}_{n} \qquad (6.5)
\end{aligned}$$

and

$$\begin{aligned}
\lambda_{n,m,k,j}\left(\begin{array}{c} a_1,a_2,a_3 \\ b_1,b_2,b_3 \end{array}\middle| N_0,N_s\right) &= -\lambda_{n,m-1,k+1,j}b_1K^{N_s,N_0}_{m,k+2}\tilde{C}^{N_0}_{k+2} - \lambda_{n,m-1,k,j+1}b_2K^{N_s,N_0}_{m,j+2}\tilde{C}^{N_0}_{j+2} \\
&\quad +\lambda_{n,m-1,k,j}\tilde{A}^{N_s}_{m}\left[b_3+\left(\frac{N_0-1}{2}\right)(b_1+b_2)-\left(\frac{N_s-1}{2}\right)\right] \\
&\quad +\lambda_{n,m-1,k-1,j}b_1K^{N_s,N_0}_{n,k} + \lambda_{n,m-1,k,j-1}b_2K^{N_s,N_0}_{m,j} \\
&\quad +\lambda_{n,m-2,k,j}\tilde{C}^{N_s}_{m}. \qquad (6.6)
\end{aligned}$$

6.2.2 Normalization Scheme for Affine Tchebichef Moment Invariants

Suppose $f(x,y)$ denotes the original image in space $S_2(N_0)$ and $f^{'}(x^{'},y^{'})$ denotes the corresponding affine transformed image in space $S_2(N_s)$. According to Flusser et al. (2009), the affine normalization with the 7 decompositions, each with a single transformation variable, is given as follows:

(A1) Horizontal translation:

$$x^{'} = x+\alpha \qquad (6.7)$$

$$y^{'} = y. \qquad (6.8)$$

(A2) Vertical translation:

$$x^{'} = x \qquad (6.9)$$

$$y^{'} = y+\beta. \qquad (6.10)$$

(A3) Uniform scaling:

$$x' = \omega x \tag{6.11}$$

$$y' = \omega y. \tag{6.12}$$

(A4) First Rotation

$$x' = x\cos\theta_1 + y\sin\theta_1 \tag{6.13}$$

$$y' = -x\sin\theta_1 + y\cos\theta_1. \tag{6.14}$$

(A5) Stretching:

$$x' = \delta x \tag{6.15}$$

$$y' = \frac{1}{\delta} y. \tag{6.16}$$

(A6) Second rotation

$$x' = x\cos\theta_2 + y\sin\theta_2 \tag{6.17}$$

$$y' = -x\sin\theta_2 + y\cos\theta_2. \tag{6.18}$$

(A7) Mirror reflection

$$x' = x \tag{6.19}$$

$$y' = \pm y. \tag{6.20}$$

As shown in Chapters 3 to 5, a new set of normalization schemes is required for the above transformations, so that, better classification performance can be assured, and the numerical computation overhead caused by determining parameters from other domain can be avoided.

6.2.3 Translation, Rotation and Scale Invariants

As the first four transformations are the decomposition of translation, rotation and scale (TRS) transformation we may combine them into a single TRS transform following the normalization scheme proposed by Theorem 5.3.2:

$$x^{'} = \omega\cos\theta_1(x-\bar{x}) + \omega\sin\theta_1(y-\bar{y}) + \frac{N_s-1}{2} \tag{6.21}$$

$$y^{'} = -\omega\sin\theta_1(x-\bar{x}) + \omega\cos\theta_1(y-\bar{y}) + \frac{N_s-1}{2}. \tag{6.22}$$

In this case the transformed image's centroid is at the middle of $S_2(N_s)$. The scale coefficient ω is determined so that the canonical image is proportionally to the transformed space $S_2(N_s)$.

$$\omega = \sqrt{\frac{\Omega_0 N_s^2}{T_{0,0}\times N_0}} \tag{6.23}$$

where Ω_0 denotes the scale coefficients.

The first rotation angle θ_1 is

$$\theta_1 = \frac{1}{2}tan^{-1}\left\{\frac{\begin{array}{c}2\left(\frac{N_0-1}{2}-\bar{x}\right)\left(\frac{N_0-1}{2}-\bar{y}\right)\tilde{A}_1^{N_0}T_{0,0}+2\left(\frac{N_0-1}{2}-\bar{x}\right)T_{0,1}\\ +2\left(\frac{N_0-1}{2}-\bar{y}\right)T_{1,0}+\frac{2T_{1,1}}{\tilde{A}_1^{N_0}}\end{array}}{\begin{array}{c}\tilde{A}_1^{N_0}\left[\left(\frac{N_0-1}{2}-\bar{x}\right)^2-\left(\frac{N_0-1}{2}-\bar{y}\right)^2\right]T_{0,0}-2\left(\frac{N_0-1}{2}-\bar{x}\right)T_{1,0}\\ +2\left(\frac{N_0-1}{2}-\bar{y}\right)T_{0,1}+\frac{T_{2,0}}{\tilde{A}_2^{N_0}}-\frac{T_{0,2}}{\tilde{A}_2^{N_0}}\end{array}}\right\}. \tag{6.24}$$

Ambiguities of principal axis normalization are then resolved by Theorem 5.3.4 with constraints

$$I_{2,0}^{\langle\text{trs}\rangle} \geq I_{0,2}^{\langle\text{trs}\rangle}, \text{ and} \tag{6.25}$$

$$I_{3,0}^{\langle\text{trs}\rangle} \geq 0. \tag{6.26}$$

6.2.4 Normalization on Stretching

The stretch normalization of (6.15) and (6.16) is proposed to eliminate the non-reflective anisotropic scale deformation. It is given by the following theorem.

Theorem 6.2.1. *Suppose $I_{n,m}^{\langle \text{trs} \rangle}$ denotes the TRS Tchebichef moment invariant, then a non-reflective anisotropic scaled deformation can be resolved by stretch normalization with constraint*

$$I_{2,0}^{\langle \text{s,trs} \rangle} = I_{0,2}^{\langle \text{s,trs} \rangle} \tag{6.27}$$

and stretch coefficient

$$\delta = \left(\frac{I_{0,2}^{\langle \text{trs} \rangle} - \tilde{C}_2^{N_s} I_{0,0}^{\langle \text{trs} \rangle}}{I_{2,0}^{\langle \text{trs} \rangle} - \tilde{C}_2^{N_s} I_{0,0}^{\langle \text{trs} \rangle}} \right)^{\frac{1}{4}} \tag{6.28}$$

where $I_{n,m}^{\langle \text{s, trs} \rangle}$ denotes the Tchebichef moment after the normalizations of TRS transformation and stretch transformation.

Proof. From Theorem 5.3.1, we get

$$I_{2,0}^{\langle \text{s, trs} \rangle} = \delta^2 I_{2,0}^{\langle \text{s, trs} \rangle} + \tilde{C}_2^{N_s} \left(1 - \delta^2\right) I_{0,0}^{\langle \text{s, trs} \rangle} \qquad \text{and} \tag{6.29}$$

$$I_{0,2}^{\langle \text{s, trs} \rangle} = \left(\frac{1}{\delta^2} \right) I_{0,2}^{\langle \text{s, trs} \rangle} + \tilde{C}_2^{N_s} \left[1 - \left(\frac{1}{\delta^2} \right) \right] I_{0,0}^{\langle \text{s, trs} \rangle}. \tag{6.30}$$

The derivation of $I_{2,0}^{\langle \text{s, trs} \rangle}$ and $I_{0,2}^{\langle \text{s, trs} \rangle}$ are given by Appendix E.
By using the constraint $I_{2,0}^{\langle \text{s, trs} \rangle} = I_{0,2}^{\langle \text{s, trs} \rangle}$ we can show that

$$\delta = \left(\frac{I_{0,2}^{\langle \text{s, trs} \rangle} - \tilde{C}_2^{N_s} I_{0,0}^{\langle \text{s, trs} \rangle}}{I_{2,0}^{\langle \text{s, trs} \rangle} - \tilde{C}_2^{N_s} I_{0,0}^{\langle \text{s, trs} \rangle}} \right)^{\frac{1}{4}}. \tag{6.31}$$

□

6.2.5 Normalization on Second Rotation

After the process of TRS and stretch normalizations, Tchebichef moments of order two and below are no longer usable. This is mainly due to the dependency in the process of normalization. For example, it is found that $I_{0,0}^{\langle \text{s, trs} \rangle} = \Omega_0 N_s$, $I_{1,0}^{\langle \text{s, trs} \rangle} = I_{0,1}^{\langle \text{s, trs} \rangle} = I_{1,1}^{\langle \text{s, trs} \rangle} = 0$, and $I_{2,0}^{\langle \text{s, trs} \rangle} = I_{0,2}^{\langle \text{s, trs} \rangle}$. Thus higher order Tchebichef moments are required to determine the second rotation. It is also important to note that, with all the prescribed normalization, non-symmetric image might end up to be symmetric. Hence the capability of second rotational algorithm to deal with symmetric image is curtailed for the accuracy of

AMI. For the second rotation, the normalization scheme proposed by Abu-Mostafa and Psaltis (1985) which is based on complex moments is usually used. This can also be accomplished based on Tchebichef moments. The theorem is given as follows

Theorem 6.2.2. *Suppose $I_{n,m}^{\langle \mathrm{s,\ trs}\rangle}$ are the Tchebichef moments after TRS and stretch normalizations, and $R_2(\theta_2)$ denotes the second rotation normalization about the centre of transformed space with angle θ_2. The second rotation on the normalized moment, $I_{n,m}^{\langle \mathrm{r_2,\ s,\ trs}\rangle}$, is rotational invariant if it satisfies one of the following normalization criteria*

(B1) Second rotation normalization for non-symmetric, 1-fold symmetric images,

$$\theta_2 = \tan^{-1}\left[\frac{I_{2,1}^{\langle \mathrm{s,\ trs}\rangle} + K_{1,3}^{N_s,N_s} I_{0,3}^{\langle \mathrm{s,\ trs}\rangle}}{I_{1,2}^{\langle \mathrm{s,\ trs}\rangle} + K_{1,3}^{N_s,N_s} I_{3,0}^{\langle \mathrm{s,\ trs}\rangle}}\right] \tag{6.32}$$

and

$$I_{1,2}^{\langle \mathrm{r_2,\ s,\ trs}\rangle} + K_{1,3}^{N_s,N_s} I_{3,0}^{\langle \mathrm{r_2,\ s,\ trs}\rangle} > 0. \tag{6.33}$$

(B2) Second rotation normalization for 2-fold symmetric images,

$$\theta_2 = \frac{1}{2}\tan^{-1}\frac{I_{3,1}^{\langle \mathrm{s,\ trs}\rangle} + I_{1,3}^{\langle \mathrm{s,\ trs}\rangle}}{\left\{\begin{array}{l} \frac{1}{2}\left[K_{1,4}^{N_s,N_s}\tilde{C}_4^{N_s} - K_{1,2}^{N_s,N_s}\tilde{C}_3^{N_s} - K_{3,2}^{N_s,N_s}\tilde{C}_2^{N_s}\right] \\ \quad \times (I_{0,2}^{\langle \mathrm{s,\ trs}\rangle} - I_{2,0}^{\langle \mathrm{s,\ trs}\rangle}) - \frac{1}{2}K_{1,4}^{N_s,N_s}(I_{0,4}^{\langle \mathrm{s,\ trs}\rangle} - I_{4,0}^{\langle \mathrm{s,\ trs}\rangle}) \end{array}\right\}} \tag{6.34}$$

and

$$\begin{aligned} \frac{1}{2}\left[K_{1,4}^{N_s,N_s}\tilde{C}_4^{N_s} - K_{1,2}^{N_s,N_s}\tilde{C}_3^{N_s} - K_{3,2}^{N_s,N_s}\tilde{C}_2^{N_s}\right] \times (I_{0,2}^{\langle \mathrm{r_2,\ s,\ trs}\rangle} - I_{2,0}^{\langle \mathrm{r_2,\ s,\ trs}\rangle}) \\ -\frac{1}{2}K_{1,4}^{N_s,N_s}(I_{0,4}^{\langle \mathrm{r_2,\ s,\ trs}\rangle} - I_{4,0}^{\langle \mathrm{r_2,\ s,\ trs}\rangle}) > 0. \end{aligned} \tag{6.35}$$

(B3) Second rotation normalization for 3-fold symmetric images,

$$\theta_2 = \frac{1}{3}\tan^{-1}\left\{\frac{\tilde{A}_1^{N_s} I_{0,3}^{\langle \mathrm{s,\ trs}\rangle} - 3\tilde{A}_3^{N_s} I_{2,1}^{\langle \mathrm{s,\ trs}\rangle}}{3\tilde{A}_3^{N_s} I_{1,2}^{\langle \mathrm{s,\ trs}\rangle} - \tilde{A}_1^{N_s} I_{3,0}^{\langle \mathrm{s,\ trs}\rangle}}\right\} \tag{6.36}$$

and

$$3\tilde{A}_3^{N_s} I_{1,2}^{\langle \mathrm{r_2,\ s,\ trs}\rangle} - \tilde{A}_1^{N_s} T_{3,0}^{\langle \mathrm{r_2,\ s,\ trs}\rangle} > 0. \tag{6.37}$$

(B4) Second rotation of normalization for 4-fold symmetric images,

$$\theta_2 = \frac{1}{4}\tan^{-1}\frac{I_{3,1}^{\langle \mathrm{s,\,trs}\rangle} - I_{1,3}^{\langle \mathrm{s,\,trs}\rangle}}{\left\{\begin{array}{l}\left[\frac{1}{2}K_{1,2}^{N_s,N_s}\tilde{C}_2^{N_s}\tilde{C}_3^{N_s} - K_{3,2}^{N_s,N_s}(\tilde{C}_2^{N_s})^2\right] I_{0,0}^{\langle \mathrm{s,\,trs}\rangle} \\ +\left[\frac{5}{4}K_{3,2}^{N_s,N_s}\tilde{C}_2^{N_s} - \frac{1}{4}K_{1,2}^{N_s,N_s}\tilde{C}_3^{N_s} - \frac{1}{4}K_{1,4}^{N_s,N_s}\tilde{C}_4^{N_s}\right] \\ \qquad \times (I_{2,0}^{\langle \mathrm{s,\,trs}\rangle} + I_{0,2}^{\langle \mathrm{s,\,trs}\rangle}) \\ +\frac{1}{4}K_{1,4}^{N_s,N_s} \times (I_{4,0}^{\langle \mathrm{s,\,trs}\rangle} + I_{0,4}^{\langle \mathrm{s,\,trs}\rangle}) - \frac{3}{2}K_{3,2}^{N_s,N_s} I_{2,2}^{\langle \mathrm{s,\,trs}\rangle}\end{array}\right\}} \tag{6.38}$$

and

$$\begin{aligned}&\left[\frac{1}{2}K_{1,2}^{N_s,N_s}\tilde{C}_2^{N_s}\tilde{C}_3^{N_s} - K_{3,2}^{N_s,N_s}(\tilde{C}_2^{N_s})^2\right] I_{0,0}^{\langle \mathrm{r_2,\,s,\,trs}\rangle} \\ &+\left[\frac{5}{4}K_{3,2}^{N_s,N_s}\tilde{C}_2^{N_s} - \frac{1}{4}K_{1,2}^{N_s,N_s}\tilde{C}_3^{N_s} - \frac{1}{4}K_{1,4}^{N_s,N_s}\tilde{C}_4^{N_s}\right] \\ &\qquad \times (I_{2,0}^{\langle \mathrm{r_2,\,s,\,trs}\rangle} + I_{0,2}^{\langle \mathrm{r_2,\,s,\,trs}\rangle}) \\ &+\frac{1}{4}K_{1,4}^{N_s,N_s}(I_{4,0}^{\langle \mathrm{r_2,\,s,\,trs}\rangle} + I_{0,4}^{\langle \mathrm{r_2,\,s,\,trs}\rangle}) - \frac{3}{2}K_{3,2}^{N_s,N_s} I_{2,2}^{\langle \mathrm{r_2,\,s,\,trs}\rangle} > 0.\end{aligned} \tag{6.39}$$

Proof. From Theorem 5.3.1, we can deduce the following invariant moments:

$$\begin{aligned}I_{2,1}^{\langle \mathrm{r_2,\,s,\,trs}\rangle} &= -\frac{1}{2}\sin(2\theta_2)\cos\theta_2 K_{1,3}^{N_s,N_s} I_{3,0}^{\langle \mathrm{s,\,trs}\rangle} \\ &\quad +\frac{1}{2}\sin(2\theta_2)\sin\theta_2 K_{1,3}^{N_s,N_s} I_{0,3}^{\langle \mathrm{s,\,trs}\rangle} \\ &\quad +\left\{\cos(2\theta_2)\cos\theta_2 - \frac{1}{2}\sin(2\theta_2)\sin\theta_2\right\} I_{2,1}^{\langle \mathrm{s,\,trs}\rangle} \\ &\quad +\left\{\cos(2\theta_2)\sin\theta_2 + \frac{1}{2}\sin(2\theta_2)\cos\theta_2\right\} I_{1,2}^{\langle \mathrm{s,\,trs}\rangle}\end{aligned} \tag{6.40}$$

$$\begin{aligned}I_{0,3}^{\langle \mathrm{r_2,\,s,\,trs}\rangle} &= -\sin^3\theta_2 I_{3,0}^{\langle \mathrm{s,\,trs}\rangle} + \cos^3\theta_2 I_{0,3}^{\langle \mathrm{s,\,trs}\rangle} \\ &\quad +\frac{3}{2}\sin(2\theta_2)\sin\theta_2 K_{3,1}^{N_s,N_s} I_{2,1}^{\langle \mathrm{s,\,trs}\rangle} \\ &\quad -\frac{3}{2}\sin(2\theta_2)\cos\theta_2 K_{3,1}^{N_s,N_s} I_{1,2}^{\langle \mathrm{s,\,trs}\rangle}\end{aligned} \tag{6.41}$$

$$
\begin{aligned}
I_{3,1}^{\langle \mathrm{r}_2,\,\mathrm{s},\,\mathrm{trs}\rangle} &= -\cos^3\theta_2\sin\theta_2 K_{1,4}^{N_s,N_s} I_{4,0}^{\langle \mathrm{s},\,\mathrm{trs}\rangle} + \sin^3\theta_2\cos\theta_2 K_{1,4}^{N_s,N_s} I_{0,4}^{\langle \mathrm{s},\,\mathrm{trs}\rangle} \\
&\quad + \cos(3\theta_2)\cos\theta_2 I_{3,1}^{\langle \mathrm{s},\,\mathrm{trs}\rangle} + \sin(3\theta_2)\sin\theta_2 I_{1,3}^{\langle \mathrm{s},\,\mathrm{trs}\rangle} \\
&\quad + \frac{3}{4}\sin(4\theta_2) K_{3,2}^{N_s,N_s} I_{2,2}^{\langle \mathrm{s},\,\mathrm{trs}\rangle} \\
&\quad + \left\{ \cos^3\theta_2\sin\theta_2 K_{1,4}^{N_s,N_s}\tilde{C}_4^{N_s} - \tilde{C}_3^{N_s} K_{1,2}^{N_s,N_s}\sin^3\theta_2\cos\theta_2 \right. \\
&\qquad \left. + K_{3,2}^{N_s,N_s}\tilde{C}_2^{N_s}\sin(2\theta_2)\left[-\frac{3}{2}\cos^2\theta_2 + \sin^2\theta_2 \right] \right\} I_{2,0}^{\langle \mathrm{s},\,\mathrm{trs}\rangle} \\
&\quad + \left\{ -\sin^3\theta_2\cos\theta_2 K_{1,4}^{N_s,N_s}\tilde{C}_4^{N_s} + \tilde{C}_3^{N_s} K_{1,2}^{N_s,N_s}\sin\theta_2\cos^3\theta_2 \right. \\
&\qquad \left. + K_{3,2}^{N_s,N_s}\tilde{C}_2^{N_s}\sin(2\theta_2)\left[\frac{3}{2}\sin^2\theta_2 - \cos^2\theta_2 \right] \right\} I_{0,2}^{\langle \mathrm{s},\,\mathrm{trs}\rangle} \\
&\quad + \sin(4\theta_2)\left\{ -\frac{1}{4} K_{1,2}^{N_s,N_s}\tilde{C}_2^{N_s}\tilde{C}_3^{N_s} + \frac{1}{2} K_{3,2}^{N_s,N_s}(\tilde{C}_2^{N_s})^2 \right\} I_{0,0}^{\langle \mathrm{s},\,\mathrm{trs}\rangle}
\end{aligned} \tag{6.42}
$$

and

$$
\begin{aligned}
I_{1,3}^{\langle \mathrm{r}_2,\,\mathrm{s},\,\mathrm{trs}\rangle} &= -\sin^3\theta_2\cos\theta_2 K_{1,4}^{N_s,N_s} I_{4,0}^{\langle \mathrm{s},\,\mathrm{trs}\rangle} + \cos^3\theta_2\sin\theta_2 K_{1,4}^{N_s,N_s} I_{0,4}^{\langle \mathrm{s},\,\mathrm{trs}\rangle} \\
&\quad + \sin(3\theta_2)\sin\theta_2 I_{3,1}^{\langle \mathrm{s},\,\mathrm{trs}\rangle} + \cos(3\theta_2)\cos\theta_2 I_{1,3}^{\langle \mathrm{s},\,\mathrm{trs}\rangle} \\
&\quad + \frac{3}{4} K_{3,2}^{N_s,N_s}\sin(4\theta_2) I_{2,2}^{\langle \mathrm{s},\,\mathrm{trs}\rangle} \\
&\quad + \left\{ \sin^3\theta_2\cos\theta_2 K_{1,4}^{N_s,N_s}\tilde{C}_4^{N_s} - \frac{1}{2}\tilde{C}_3^{N_s} K_{1,2}^{N_s,N_s}\sin(2\theta_2)\cos^2\theta_2 \right. \\
&\qquad \left. + K_{3,2}^{N_s,N_s}\tilde{C}_2^{N_s}\sin(2\theta_2)\left[-\frac{3}{2}\sin^2\theta_2 + \cos^2\theta_2 \right] \right\} I_{2,0}^{\langle \mathrm{s},\,\mathrm{trs}\rangle} \\
&\quad + \left\{ -\cos^3\theta_2\sin\theta_2 K_{1,4}^{N_s,N_s}\tilde{C}_4^{N_s} + \frac{1}{2}\sin(2\theta_2)\sin^2\theta_2 K_{1,2}^{N_s,N_s}\tilde{C}_3^{N_s} \right. \\
&\qquad \left. + K_{3,2}^{N_s,N_s}\tilde{C}_2^{N_s}\sin(2\theta_2)\left[\frac{3}{2}\cos^2\theta_2 - \sin^2\theta_2 \right] \right\} I_{0,2}^{\langle \mathrm{s},\,\mathrm{trs}\rangle} \\
&\quad + \sin(4\theta_2)\left\{ \frac{1}{4} K_{1,2}^{N_s,N_s}\tilde{C}_2^{N_s}\tilde{C}_3^{N_s} - \frac{1}{2} K_{3,2}^{N_s,N_s}(\tilde{C}_2^{N_s})^2 \right\} I_{0,0}^{\langle \mathrm{s},\,\mathrm{trs}\rangle}.
\end{aligned} \tag{6.43}
$$

Consider

$$
\begin{aligned}
I_{2,1}^{\langle \mathrm{r}_2,\,\mathrm{s},\,\mathrm{trs}\rangle} + K_{1,3}^{N_s,N_s} I_{0,3}^{\langle \mathrm{r}_2,\,\mathrm{s},\,\mathrm{trs}\rangle} &= -\sin\theta_2\left[I_{1,2}^{\langle \mathrm{s},\,\mathrm{trs}\rangle} + K_{1,3}^{N_s,N_s} I_{3,0}^{\langle \mathrm{s},\,\mathrm{trs}\rangle} \right] \\
&\quad + \cos\theta_2\left[I_{2,1}^{\langle \mathrm{s},\,\mathrm{trs}\rangle} + K_{1,3}^{N_s,N_s} I_{0,3}^{\langle \mathrm{s},\,\mathrm{trs}\rangle} \right].
\end{aligned} \tag{6.44}
$$

Suppose

$$
I_{2,1}^{\langle \mathrm{r}_2,\,\mathrm{s},\,\mathrm{trs}\rangle} + K_{1,3}^{N_s,N_s} I_{0,3}^{\langle \mathrm{r}_2,\,\mathrm{s},\,\mathrm{trs}\rangle} = 0 \tag{6.45}
$$

we get

$$
\theta_2 = \tan^{-1}\left\{ \frac{I_{2,1}^{\langle \mathrm{s},\,\mathrm{trs}\rangle} + K_{1,3}^{N_s,N_s} I_{0,3}^{\langle \mathrm{s},\,\mathrm{trs}\rangle}}{I_{1,2}^{\langle \mathrm{s},\mathrm{trs}\rangle} + K_{1,3}^{N_s,N_s} I_{3,0}^{\langle \mathrm{s},\,\mathrm{trs}\rangle}} \right\}. \tag{6.46}
$$

Similar to the principal axis normalization, ambiguity of the normalization can be resolved by restricting the expression of the denominator after transformation to be a positive number, i.e.

$$I_{1,2}^{\langle \mathrm{r}_2,\,\mathrm{s},\,\mathrm{trs}\rangle} + K_{1,3}^{N_s,N_s} I_{3,0}^{\langle \mathrm{r}_2,\,\mathrm{s},\,\mathrm{trs}\rangle} > 0. \tag{6.47}$$

Experimental results show that the expression is accurate for non-symmetric and 1-fold symmetric images. However in general, this rotation normalization scheme is applicable to any image provided that the numerator and denominator of (6.46) are both non-zero, or both not smaller than a preassigned threshold value.

For the second rotation normalization of 2-fold symmetric images, we consider

$$\begin{aligned} I_{3,1}^{\langle \mathrm{r}_2,\,\mathrm{s},\,\mathrm{trs}\rangle} + I_{1,3}^{\langle \mathrm{r}_2,\,\mathrm{s},\,\mathrm{trs}\rangle} &= \sin(2\theta_2)\left\{\frac{1}{2}\left[-K_{1,4}^{N_s,N_s}\tilde{C}_4^{N_s} + K_{1,2}^{N_s,N_s}\tilde{C}_3^{N_s} + K_{3,2}^{N_s,N_s}\tilde{C}_2^{N_s}\right]\right. \\ &\qquad \times \left(I_{0,2}^{\langle\,\mathrm{s},\,\mathrm{trs}\rangle} - I_{2,0}^{\langle \mathrm{s},\,\mathrm{trs}\rangle}\right) \\ &\qquad \left. + \frac{1}{2}K_{1,4}^{N_s,N_s}\left(I_{0,4}^{\langle \mathrm{s},\,\mathrm{trs}\rangle} - I_{4,0}^{\langle \mathrm{s},\,\mathrm{trs}\rangle}\right)\right\} \\ &\quad + \cos(2\theta_2)\left\{I_{3,1}^{\langle \mathrm{s},\,\mathrm{trs}\rangle} + I_{1,3}^{\langle \mathrm{s},\,\mathrm{trs}\rangle}\right\} \end{aligned} \tag{6.48}$$

By having

$$I_{3,1}^{\langle \mathrm{r}_2,\,\mathrm{s},\,\mathrm{trs}\rangle} + I_{1,3}^{\langle \mathrm{r}_2,\,\mathrm{s},\,\mathrm{trs}\rangle} = 0, \tag{6.49}$$

we get

$$\theta_2 = \frac{1}{2}\tan^{-1}\frac{I_{3,1}^{\langle \mathrm{s},\,\mathrm{trs}\rangle} + I_{1,3}^{\langle \mathrm{s},\,\mathrm{trs}\rangle}}{\left\{\begin{array}{l} \frac{1}{2}\left[K_{1,4}^{N_s,N_s}\tilde{C}_4^{N_s} - K_{1,2}^{N_s,N_s}\tilde{C}_3^{N_s} - K_{3,2}^{N_s,N_s}\tilde{C}_2^{N_s}\right] \\ \quad \times (I_{0,2}^{\langle \mathrm{s},\,\mathrm{trs}\rangle} - I_{2,0}^{\langle \mathrm{s},\,\mathrm{trs}\rangle}) - \frac{1}{2}K_{1,4}^{N_s,N_s}(I_{0,4}^{\langle \mathrm{s},\,\mathrm{trs}\rangle} - I_{4,0}^{\langle \mathrm{s},\,\mathrm{trs}\rangle}) \end{array}\right\}} \tag{6.50}$$

with the constraint

$$\begin{aligned} \frac{1}{2}\left[K_{1,4}^{N_s,N_s}\tilde{C}_4^{N_s} - K_{1,2}^{N_s,N_s}\tilde{C}_3^{N_s} - K_{3,2}^{N_s,N_s}\tilde{C}_2^{N_s}\right] \times (I_{0,2}^{\langle \mathrm{r}_2,\,\mathrm{s},\,\mathrm{trs}\rangle} - I_{2,0}^{\langle \mathrm{r}_2,\,\mathrm{s},\,\mathrm{trs}\rangle}) \\ - \frac{1}{2}K_{1,4}^{N_s,N_s}(I_{0,4}^{\langle \mathrm{r}_2,\,\mathrm{s},\,\mathrm{trs}\rangle} - I_{4,0}^{\langle \mathrm{r}_2,\,\mathrm{s},\,\mathrm{trs}\rangle}) > 0. \end{aligned} \tag{6.51}$$

The second rotation normalization for 3-fold symmetric images is based on the following expression

$$\begin{aligned} I_{2,1}^{\langle \mathrm{r}_2,\,\mathrm{s},\,\mathrm{trs}\rangle} - \frac{1}{3}K_{1,3}^{N_s,N_s} I_{0,3}^{\langle \mathrm{r}_2,\,\mathrm{s},\,\mathrm{trs}\rangle} &= \sin(3\theta_2)\left(I_{1,2}^{\langle \mathrm{s},\,\mathrm{trs}\rangle} - \frac{1}{3}K_{1,3}^{N_s,N_s} I_{3,0}^{\langle \mathrm{s},\,\mathrm{trs}\rangle}\right) \\ &\quad + \cos(3\theta_2)\left(I_{2,1}^{\langle \mathrm{s},\,\mathrm{trs}\rangle} - \frac{1}{3}K_{1,3}^{N_s,N_s} I_{0,3}^{\langle \mathrm{s},\,\mathrm{trs}\rangle}\right). \end{aligned} \tag{6.52}$$

By having

$$I_{2,1}^{\langle \mathrm{r}_2,\,\mathrm{s},\,\mathrm{trs}\rangle} - \frac{1}{3} K_{1,2}^{N_s,N_s} I_{0,3}^{\langle \mathrm{r}_2,\,\mathrm{s},\,\mathrm{trs}\rangle} = 0, \tag{6.53}$$

we have

$$\theta_2 = \frac{1}{3}\tan^{-1}\left\{ \frac{\tilde{A}_1^{N_s} I_{0,3}^{\langle \mathrm{s},\,\mathrm{trs}\rangle} - 3\tilde{A}_3^{N_s} I_{2,1}^{\langle \mathrm{s},\,\mathrm{trs}\rangle}}{3\tilde{A}_3^{N_s} I_{1,2}^{\langle \mathrm{s},\,\mathrm{trs}\rangle} - \tilde{A}_1^{N_s} I_{3,0}^{\langle \mathrm{s},\,\mathrm{trs}\rangle}} \right\} \tag{6.54}$$

and the constraint

$$3\tilde{A}_3^{N_s} I_{1,2}^{\langle \mathrm{r}_2,\,\mathrm{s},\,\mathrm{trs}\rangle} - \tilde{A}_1^{N_s} I_{3,0}^{\langle \mathrm{r}_2,\,\mathrm{s},\,\mathrm{trs}\rangle} > 0. \tag{6.55}$$

Finally, we consider the second rotation normalization for 4-fold symmetric images

$$\begin{aligned} I_{3,1}^{\langle \mathrm{r}_2,\,\mathrm{s},\,\mathrm{trs}\rangle} - I_{1,3}^{\langle \mathrm{r}_2,\,\mathrm{s},\,\mathrm{trs}\rangle} = & \\ \sin(4\theta_2) & \left\{ \begin{array}{l} \left[-\frac{1}{2} K_{1,2}^{N_s,N_s} \tilde{C}_2^{N_s} \tilde{C}_3^{N_s} + K_{3,2}^{N_s,N_s} (\tilde{C}_2^{N_s})^2 \right] I_{0,0}^{\langle \mathrm{s},\,\mathrm{trs}\rangle} \\ + \left[\frac{1}{4} K_{1,4}^{N_s,N_s} \tilde{C}_4^{N_s} + \frac{1}{4} K_{1,2}^{N_s,N_s} \tilde{C}_3^{N_s} - \frac{5}{4} K_{3,2}^{N_s,N_s} \tilde{C}_2^{N_s} \right] \\ \qquad \times (I_{0,2}^{\langle \mathrm{s},\,\mathrm{trs}\rangle} + I_{2,0}^{\langle \mathrm{s},\,\mathrm{trs}\rangle}) + \frac{3}{2} K_{3,2}^{N_s,N_s} I_{2,2}^{\langle \mathrm{s},\,\mathrm{trs}\rangle} \\ -\frac{1}{4} K_{1,4}^{N_s,N_s} (I_{4,0}^{\langle \mathrm{s},\,\mathrm{trs}\rangle} + I_{0,4}^{\langle \mathrm{s},\,\mathrm{trs}\rangle}) \end{array} \right\} \qquad (6.56) \\ + \cos(4\theta_2) & \left[I_{3,1}^{\langle \mathrm{s},\,\mathrm{trs}\rangle} - I_{1,3}^{\langle \mathrm{s},\,\mathrm{trs}\rangle} \right] \qquad (6.57) \end{aligned}$$

By having

$$I_{3,1}^{\langle \mathrm{r}_2,\,\mathrm{s},\,\mathrm{trs}\rangle} - I_{1,3}^{\langle \mathrm{r}_2,\,\mathrm{s},\,\mathrm{trs}\rangle} = 0, \tag{6.58}$$

we get

$$\theta_2 = \frac{1}{4}\tan^{-1} \frac{I_{3,1}^{\langle \mathrm{s},\,\mathrm{trs}\rangle} - I_{1,3}^{\langle \mathrm{s},\,\mathrm{trs}\rangle}}{\left\{ \begin{array}{l} \left[\frac{1}{2} K_{1,2}^{N_s,N_s} \tilde{C}_2^{N_s} \tilde{C}_3^{N_s} - K_{3,2}^{N_s,N_s} (\tilde{C}_2^{N_s})^2 \right] I_{0,0}^{\langle \mathrm{s},\,\mathrm{trs}\rangle} \\ + \left[\frac{5}{4} K_{3,2}^{N_s,N_s} \tilde{C}_2^{N_s} - \frac{1}{4} K_{1,2}^{N_s,N_s} \tilde{C}_3^{N_s} - \frac{1}{4} K_{1,4}^{N_s,N_s} \tilde{C}_4^{N_s} \right] \\ \qquad \times (I_{2,0}^{\langle \mathrm{s},\,\mathrm{trs}\rangle} + I_{0,2}^{\langle \mathrm{s},\,\mathrm{trs}\rangle}) \\ + \frac{1}{4} K_{1,4}^{N_s,N_s} \times (I_{4,0}^{\langle \mathrm{s},\,\mathrm{trs}\rangle} + I_{0,4}^{\langle \mathrm{s},\,\mathrm{trs}\rangle}) - \frac{3}{2} K_{3,2}^{N_s,N_s} I_{2,2}^{\langle \mathrm{s},\,\mathrm{trs}\rangle} \end{array} \right\} \tag{6.59}$$

and ambiguities are resolved by

$$\begin{aligned} & \left[\frac{1}{2} K_{1,2}^{N_s,N_s} \tilde{C}_2^{N_s} \tilde{C}_3^{N_s} - K_{3,2}^{N_s,N_s} (\tilde{C}_2^{N_s})^2 \right] I_{0,0}^{\langle \mathrm{r}_2,\,\mathrm{s},\,\mathrm{trs}\rangle} \\ & + \left[\frac{5}{4} K_{3,2}^{N_s,N_s} \tilde{C}_2^{N_s} - \frac{1}{4} K_{1,2}^{N_s,N_s} \tilde{C}_3^{N_s} - \frac{1}{4} K_{1,4}^{N_s,N_s} \tilde{C}_4^{N_s} \right] \\ & \qquad \times (I_{2,0}^{\langle \mathrm{r}_2,\,\mathrm{s},\,\mathrm{trs}\rangle} + I_{0,2}^{\langle \mathrm{r}_2,\,\mathrm{s},\,\mathrm{trs}\rangle}) \\ & \qquad + \frac{1}{4} K_{1,4}^{N_s,N_s} (I_{4,0}^{\langle \mathrm{r}_2,\,\mathrm{s},\,\mathrm{trs}\rangle} + I_{0,4}^{\langle \mathrm{r}_2,\,\mathrm{s},\,\mathrm{trs}\rangle}) - \frac{3}{2} K_{3,2}^{N_s,N_s} I_{2,2}^{\langle \mathrm{r}_2,\,\mathrm{s},\,\mathrm{trs}\rangle} > 0. \end{aligned} \tag{6.60}$$

□

6.2.6 Reflection Invariants

The mirror reflection can be resolved by using the following constraint

$$I_{2,1}^{\langle \mathrm{l},\, \mathrm{r}_2,\, \mathrm{s},\, \mathrm{trs} \rangle} \geq 0 \tag{6.61}$$

where $I_{n,m}^{\langle \mathrm{l},\, \mathrm{r}_2,\, \mathrm{s},\, \mathrm{trs} \rangle}$ denotes the Tchebichef moment after the TRS, stretching, second rotation, and mirror reflection normalization.

6.3 Experimental Results

In this experiment a set of non-symmetric images and a set of symmetric images with 1-fold symmetric up to 4-fold symmetric are selected. Each pattern was deformed successively by the following transformations

$$\begin{pmatrix} a_1 & a_2 \\ b_1 & b_2 \end{pmatrix} = \begin{pmatrix} 1 & 0 \\ 0 & z \end{pmatrix} \begin{pmatrix} \cos\rho & \sin\rho \\ -sin\rho & cos\rho \end{pmatrix} \begin{pmatrix} \omega & 0 \\ 0 & \omega \end{pmatrix} \begin{pmatrix} \delta & 0 \\ 0 & \frac{1}{\delta} \end{pmatrix} \begin{pmatrix} \cos\alpha & \sin\alpha \\ -\sin\alpha & \cos\alpha \end{pmatrix} \tag{6.62}$$

where z denotes the reflective deformation with value ± 1. The coefficients ω and δ are parameters for uniform scale and stretch deformation respectively. Together they form non-uniform scaling. On the other hand α and ρ are the angles for first and second rotation deformation, respectively. Finally the deformed images are translated from the middle of the space by values of $\{-5, 0, 1\}$. Together they form the affine deformation. The parameter values are randomly selected to emulate various type of deformations. The deformed images are shown in Tables 6.1 and 6.2. In the experiment, for non-symmetric images and 1-fold symmetric image “B", the first second rotation algorithms is deployed. For 2-fold image symmetric image,“H" the second rotation algorithms given by (6.34) and (6.35) are used in the experiment.The company logo of Mitsubishi is 3-fold symmetrical and the third second rotation algorithm is used. Finally the “box" is a 4-fold symmetric image and the forth second rotation is deployed. The selected feature values of non-symmetric images and symmetric images are shown in Tables 6.3 and 6.4 , respectively. The result indicates that the propose normalization algorithms are able to accurately compute the affine invariant for the both types of images. Similar to normalization by AST and TRS, the odd order invariants with relatively small values are more vulnerable to discretization errors. This is mainly due to cancellation process of invariant transformation functions. The errors can be easily corrected by adding with the suitable

skew parameter values to the normalization process. Figure 6.1 denotes the canonical position of all the output images. It is generated by overlapping the output of all patterns of the same class. As shown in Figure 6.1 , no ambiguity has been detected on the output images. This indicates that all the images are accurately transformed to their standard form without ambiguities.

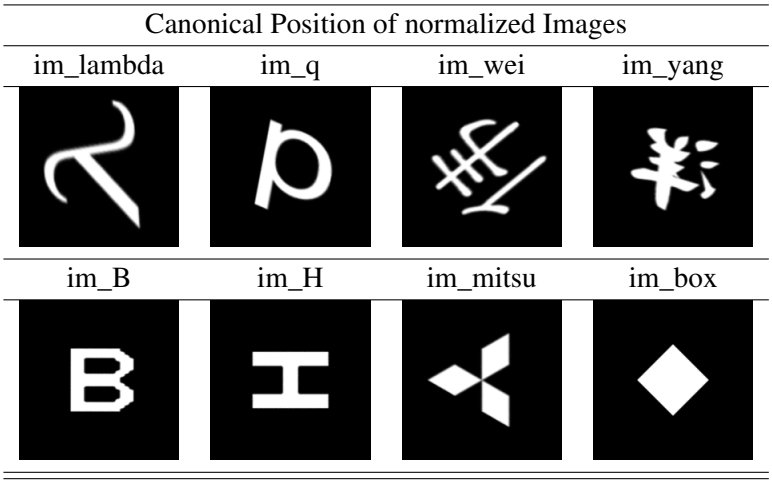

Figure 6.1: Canonical positions of normalized images.

6.4 Conclusion

In this chapter a new set of affine Tchebichef moment invariants has been proposed. The invariant algorithm consists of a set of recurrence relations for fast computation and the normalization parameters are determined from the discrete Tchebichef moments. The experiment results show that the proposed normalization scheme can accurately normalized images of both non-symmetric and symmetric patterns.

Table 6.1: Non-symmetric test images used in experiment of affine Transformation

(z,ω,δ) (α,ρ) (t_x,t_y)	Original	$(-1,0.8,0.7)$ $(226^o,21^o)$ $(-5,-5)$	$(1,0.8,0.8)$ $(189^o,160^o)$ $(5,5)$	$(-1,1.2,0.6)$ $(165^o,312^o)$ $(-5,0)$	$(1,1.2,1)$ $(345^o,144^o)$ $(0,5)$	$(-1,0.6,0.9)$ $(265^o,166^o)$ $(0,-5)$	$(1,1.1,1.5)$ $(112^o,299^o)$ $(0,0)$	$(-1,1.1,1.1)$ $(234^o,321^o)$ $(5,5)$	$(1,0.9,0.8)$ $(300^o,222^o)$ $(0,0)$	$(-1,1.1,0.7)$ $(0^o,111^o)$ $(-5,0)$
							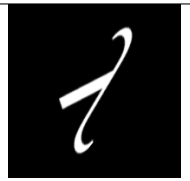			
Image	im_lbda-1	im_lbda-2	im_lbda-3	im_lbda-4	im_lbda-5	im_lbda-6	im_lbda-7	im_lbda-8	im_lbda-9	im_lbda-10
			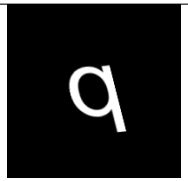	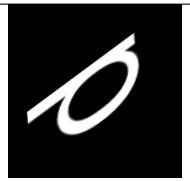		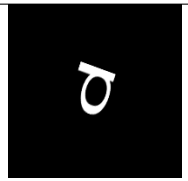			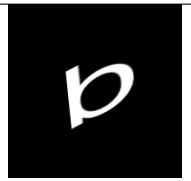	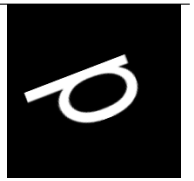
Image	im_q-1	im_q-2	im_q-3	im_q-4	im_q-5	im_q-6	im_q-7	im_q-8	im_q-9	im_q-10
							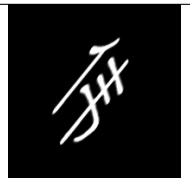			
Image	im_wei-1	im_wei-2	im_wei-3	im_wei-4	im_wei-5	im_wei-6	im_wei-7	im_wei-8	im_wei-9	im_wei-10
					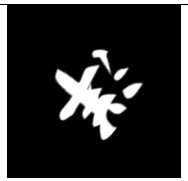					
Image	im_yang-1	im_yang-2	im_yang-3	im_yang-4	im_yang-5	im_yang-6	im_yang-7	im_yang-8	im_yang-9	im_yang-10

Table 6.2: Symmetric test images used in experiment of Affine Transformation

(z, ω, δ) (α, ρ) (t_x, t_y)	Original	$(-1, 0.8, 0.7)$ $(226^o, 21^o)$ $(-5, -5)$	$(1, 0.8, 0.8)$ $(189^o, 160^o)$ $(5, 5)$	$(-1, 1.2, 0.6)$ $(165^o, 312^o)$ $(-5, 0)$	$(1, 1.2, 1)$ $(345^o, 144^o)$ $(0, 5)$	$(-1, 0.6, 0.9)$ $(265^o, 166^o)$ $(0, -5)$	$(1, 1.1, 1.5)$ $(112^o, 299^o)$ $(0, 0)$	$(-1, 1.1, 1.1)$ $(234^o, 321^o)$ $(5, 5)$	$(1, 0.9, 0.8)$ $(300^o, 222^o)$ $(0, 0)$	$(-1, 1.1, 0.7)$ $(0^o, 111^o)$ $(-5, 0)$
	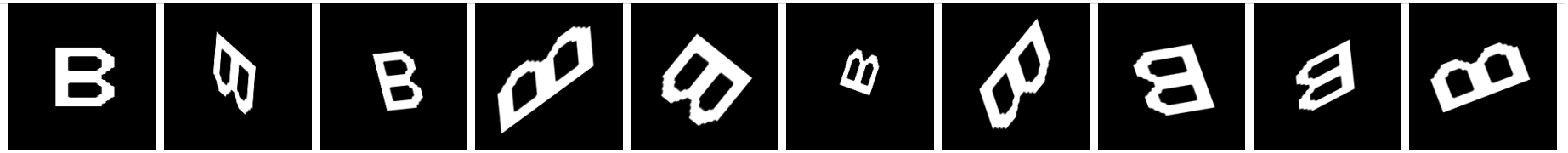									
Image	im_B-1	im_B-2	im_B-3	im_B-4	im_B-5	im_B-6	im_B-7	im_B-8	im_B-9	im_B-10
	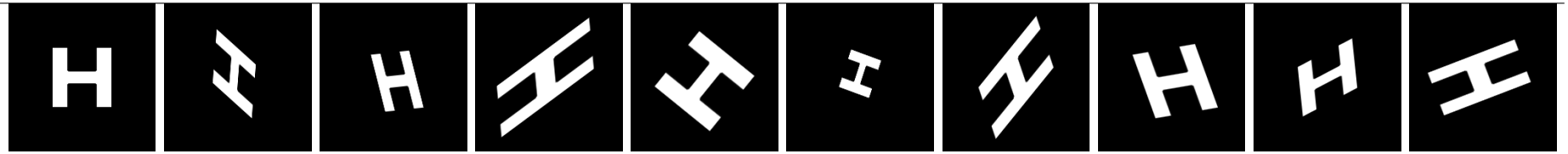									
Image	im_H-1	im_H-2	im_H-3	im_H-4	im_H-5	im_H-6	im_H-7	im_H-8	im_q-9	im_H-10
	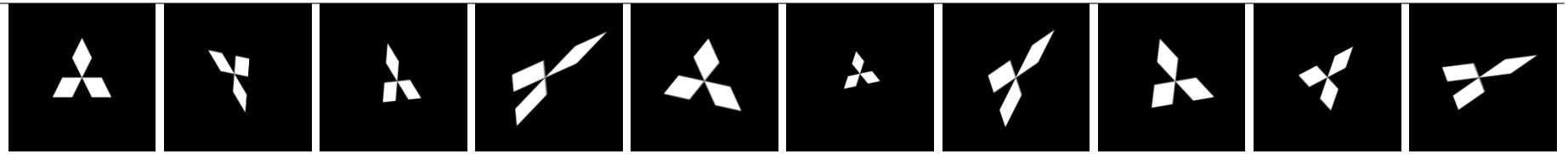									
Image	im_mitsu-1*	im_mitsu-2	im_mitsu-3	im_mitsu-4	im_mitsu-5	im_mitsu-6	im_mitsu-7	im_mitsu-8	im_mitsu-9	im_mitsu-10
	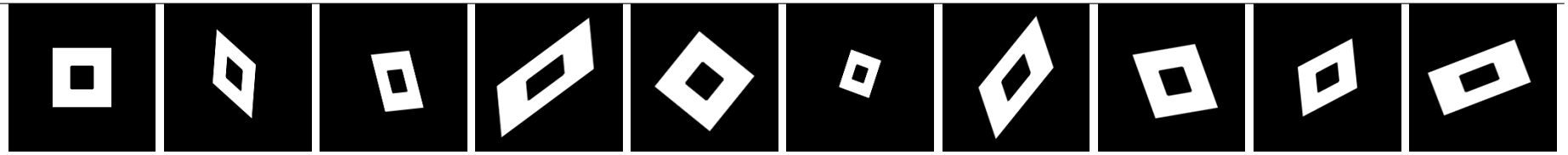									
Image	im_box-1	im_box-2	im_box-3	im_box-4	im_box-5	im_box-6	im_box-7	im_box-8	im_box-9	im_box-10

*Original images of "im_mitsu" is courtesy of Flusser et al. (2009)

Table 6.3: Selected orders of affine transformed Tchebichef moments for non-symmetric images

Images	$I_{2,0}^{\langle am \rangle}$	$I_{0,2}^{\langle am \rangle}$	$I_{3,0}^{\langle am \rangle}$	$I_{2,1}^{\langle am \rangle}$	$I_{1,2}^{\langle am \rangle}$	$I_{0,3}^{\langle am \rangle}$	$I_{4,0}^{\langle am \rangle}$	$I_{0,4}^{\langle am \rangle}$
im_lbda-1	−14.283	−14.283	−2.800	0.701	3.560	−0.798	2.976	4.872
im_lbda-2	−14.287	−14.287	−2.825	0.597	3.576	−0.680	2.994	4.865
im_lbda-3	−14.292	−14.292	−2.806	0.653	3.566	−0.744	2.990	4.876
im_lbda-4	−14.285	−14.285	−2.801	0.694	3.562	−0.790	2.977	4.871
im_lbda-5	−14.285	−14.285	−2.794	0.722	3.555	−0.822	2.975	4.873
im_lbda-6	−14.293	−14.293	−2.767	0.816	3.528	−0.929	2.984	4.889
im_lbda-7	−14.285	−14.285	−2.798	0.707	3.559	−0.805	2.977	4.873
im_lbda-8	−14.284	−14.284	−2.800	0.701	3.561	−0.798	2.977	4.872
im_lbda-9	−14.285	−14.285	−2.794	0.725	3.555	−0.825	2.977	4.873
im_lbda-10	−14.284	−14.284	−2.797	0.705	3.560	−0.802	2.975	4.874
RSD(%)	0.024	0.024	0.506	7.866	0.343	7.848	0.227	0.124
Average RSD(%) = 2.120								
im_q-1	−16.799	−16.799	0.959	0.572	−0.541	−0.652	6.663	6.973
im_q-2	−16.792	−16.792	0.982	0.554	−0.562	−0.631	6.637	6.956
im_q-3	−16.799	−16.799	0.962	0.572	−0.543	−0.651	6.662	6.973
im_q-4	−16.798	−16.798	0.964	0.568	−0.546	−0.647	6.658	6.971
im_q-5	−16.800	−16.800	0.962	0.569	−0.544	−0.648	6.662	6.974
im_q-6	−16.801	−16.801	0.957	0.577	−0.537	−0.657	6.668	6.977
im_q-7	−16.800	−16.800	0.962	0.569	−0.544	−0.648	6.661	6.973
im_q-8	−16.800	−16.800	0.958	0.573	−0.540	−0.652	6.663	6.974
im_q-9	−16.799	−16.799	0.963	0.570	−0.544	−0.649	6.661	6.972
im_q-10	−16.800	−16.800	0.960	0.572	−0.542	−0.651	6.663	6.974
RSD(%)	0.015	0.015	0.735	1.064	1.234	1.051	0.126	0.082
Average RSD(%) = 0.540								
im_wei-1	−15.874	−15.874	1.202	0.049	0.524	−0.056	7.110	6.191
im_wei-2	−15.882	−15.882	1.194	0.051	0.525	−0.058	7.117	6.202
im_wei-3	−15.874	−15.874	1.206	0.047	0.522	−0.054	7.110	6.190
im_wei-4	−15.873	−15.873	1.201	0.049	0.525	−0.056	7.107	6.187
im_wei-5	−15.875	−15.875	1.203	0.050	0.523	−0.056	7.111	6.191
im_wei-6	−15.873	−15.873	1.201	0.058	0.521	−0.066	7.103	6.186
im_wei-7	−15.877	−15.877	1.201	0.050	0.523	−0.057	7.113	6.195
im_wei-8	−15.876	−15.876	1.202	0.049	0.524	−0.056	7.111	6.193
im_wei-9	−15.872	−15.872	1.202	0.050	0.524	−0.057	7.106	6.185
im_wei-10	−15.875	−15.875	1.202	0.050	0.523	−0.057	7.111	6.191
RSD(%)	0.018	0.018	0.249	5.781	0.242	5.643	0.054	0.080
Average RSD(%) = 1.511								
im_yang-1	−18.384	−18.384	0.994	0.046	−0.036	−0.052	11.485	11.017
im_yang-2	−18.386	−18.386	0.996	0.047	−0.035	−0.053	11.489	11.025
im_yang-3	−18.384	−18.384	0.993	0.044	−0.036	−0.051	11.486	11.017
im_yang-4	−18.385	−18.385	0.993	0.045	−0.036	−0.052	11.487	11.018
im_yang-5	−18.385	−18.385	0.993	0.046	−0.036	−0.052	11.486	11.017
im_yang-6	−18.389	−18.389	0.992	0.041	−0.037	−0.047	11.497	11.028
im_yang-7	−18.385	−18.385	0.994	0.045	−0.036	−0.052	11.487	11.017
im_yang-8	−18.385	−18.385	0.993	0.046	−0.036	−0.052	11.487	11.018
im_yang-9	−18.385	−18.385	0.992	0.047	−0.036	−0.053	11.486	11.018
im_yang-10	−18.384	−18.384	0.994	0.046	−0.036	−0.052	11.485	11.016
RSD(%)	0.008	0.008	0.118	3.901	1.309	3.319	0.031	0.036
Average RSD(%) = 1.091								

Table 6.4: Selected orders of affine transformed Tchebichef moments for symmetric images

Images	$I_{2,0}^{\langle am \rangle}$	$I_{0,2}^{\langle am \rangle}$	$I_{3,0}^{\langle am \rangle}$	$I_{2,1}^{\langle am \rangle}$	$I_{1,2}^{\langle am \rangle}$	$I_{0,3}^{\langle am \rangle}$	$I_{4,0}^{\langle am \rangle}$	$I_{0,4}^{\langle am \rangle}$
im_B-1	−20.126	−20.126	0.000	0.000	0.000	0.000	15.702	15.702
im_B-2	−20.125	−20.125	0.000	0.000	0.000	0.000	15.700	15.700
im_B-3	−20.125	−20.125	0.000	0.000	0.000	0.000	15.700	15.700
im_B-4	−20.125	−20.125	0.000	0.000	0.000	0.000	15.700	15.700
im_B-5	−20.125	−20.125	0.000	0.000	0.000	0.000	15.700	15.700
im_B-6	−20.125	−20.125	0.000	0.000	0.000	0.000	15.700	15.700
im_B-7	−20.125	−20.125	0.000	0.000	0.000	0.000	15.700	15.700
im_B-8	−20.125	−20.125	0.000	0.000	0.000	0.000	15.700	15.700
im_B-9	−20.125	−20.125	0.000	0.000	0.000	0.000	15.700	15.700
im_B-10	−20.125	−20.125	0.000	0.000	0.000	0.000	15.700	15.700
RSD(%)	0.002	0.002	0.000	0.000	0.000	0.000	0.004	0.004
Average RSD(%) = 0.002								
im_H-1	−18.197	−18.197	0.000	0.000	0.000	0.000	10.684	9.848
im_H-2	−18.192	−18.192	0.000	0.000	0.000	0.000	10.670	9.834
im_H-3	−18.197	−18.197	0.000	0.000	0.000	0.000	10.684	9.849
im_H-4	−18.196	−18.196	0.000	0.000	0.000	0.000	10.681	9.846
im_H-5	−18.196	−18.196	0.000	0.000	0.000	0.000	10.682	9.846
im_H-6	−18.199	−18.199	0.000	0.000	0.000	0.000	10.689	9.854
im_H-7	−18.196	−18.196	0.000	0.000	0.000	0.000	10.682	9.847
im_H-8	−18.196	−18.196	0.000	0.000	0.000	0.000	10.682	9.847
im_H-9	−18.196	−18.196	0.000	0.000	0.000	0.000	10.682	9.847
im_H-10	−18.196	−18.196	0.000	0.000	0.000	0.000	10.681	9.845
RSD(%)	0.010	0.010	0.000	0.000	0.000	0.000	0.044	0.051
Average RSD(%) = 0.014								
im_mitsu-1	−17.664	−17.664	−1.717	0.004	1.498	0.014	9.593	9.582
im_mitsu-2	−17.668	−17.668	−1.710	0.004	1.495	0.012	9.597	9.588
im_mitsu-3	−17.666	−17.666	−1.715	0.004	1.496	0.013	9.597	9.585
im_mitsu-4	−17.664	−17.664	−1.716	0.004	1.498	0.013	9.592	9.581
im_mitsu-5	−17.664	−17.664	−1.716	0.004	1.498	0.012	9.593	9.580
im_mitsu-6	−17.665	−17.665	−1.712	0.004	1.499	0.013	9.592	9.588
im_mitsu-7	−17.663	−17.663	−1.717	0.004	1.498	0.013	9.591	9.579
im_mitsu-8	−17.663	−17.663	−1.717	0.004	1.498	0.013	9.591	9.578
im_mitsu-9	−17.663	−17.663	−1.716	0.004	1.498	0.013	9.592	9.580
im_mitsu-10	−17.663	−17.663	−1.716	0.004	1.498	0.013	9.592	9.580
RSD(%)	0.009	0.009	0.137	0.000	0.078	4.400	0.023	0.038
Average RSD(%) = 0.587								
im_box-1	−20.126	−20.126	0.000	0.000	0.000	0.000	15.702	15.702
im_box-2	−20.125	−20.125	0.000	0.000	0.000	0.000	15.700	15.700
im_box-3	−20.125	−20.125	0.000	0.000	0.000	0.000	15.700	15.700
im_box-4	−20.125	−20.125	0.000	0.000	0.000	0.000	15.700	15.700
im_box-5	−20.125	−20.125	0.000	0.000	0.000	0.000	15.700	15.700
im_box-6	−20.125	−20.125	0.000	0.000	0.000	0.000	15.700	15.700
im_box-7	−20.125	−20.125	0.000	0.000	0.000	0.000	15.700	15.700
im_box-8	−20.125	−20.125	0.000	0.000	0.000	0.000	15.700	15.700
im_box-9	−20.125	−20.125	0.000	0.000	0.000	0.000	15.700	15.700
im_box-10	−20.125	−20.125	0.000	0.000	0.000	0.000	15.700	15.700
RSD(%)	0.002	0.002	0.000	0.000	0.000	0.000	0.004	0.004
Average RSD(%) = 0.002								

CHAPTER 7

CONCLUSION AND FUTURE RESEARCH DIRECTIONS

7.1 Conclusions

Moment invariants are commonly used in image analysis to recognize patterns distorted by various spatial deformations. In this thesis, several invariant algorithms of discrete orthogonal moments have been studied. They are anisotropic scale and translation invariants, translation, rotation and scale invariants and affine invariants. New recurrence relation functions have been derived for fast computation of the invariant descriptors. These come together with new sets of normalization schemes to determine the normalization parameters from discrete domain so that the descriptors have better discriminative power and less sensitive to noise disturbance. Discrete Tchebichef moments are selected as the implementation platform for the invariant algorithms. This is mainly due to Tchebichef moments being global feature descriptors with unit weight function. The invariants can be accurately derived from original Tchebichef moments without any numerical approximation on the weight function itself.

In Chapter 2 a brief overview is given to moments and classification functions that have been used in this thesis.

In Chapter 3 two fast computational algorithms for the anisotropic scale and translation invariants of Zhu et al. (2007c) have been proposed. The first algorithm used an indirect approach from which the invariant descriptors are calculated indirectly from geometric moments. In the second algorithm, the features are directly computed from Tchebichef moments using the proposed recurrence relations.

Anisotropic scale and translation invariants can alternatively be achieved using image normalization approach. In Chapter 4 the existing algorithms have been reviewed (Goh et al., 2009; Liu et al., 2011) and they are found to be numerically inferior. Thus a new set of recurrence relations has been derived for fast computation of the invariants moments. This comes together with three new normalization schemes based on Tchebichef moments for determination of normalization parameters. The use of centre of symmetry

as centroid for the canonical image is crucial in preserving feature discriminative power. The experimental results showed that the new algorithms outperform existing methods from the aspect of numerical efficiency, robustness to noise and feature discriminative power.

In Chapter 5 the fast computational algorithms proposed in Chapter 4 are generalized further to solve the much more sophisticated problems - the affine Tchebichef transformation. This comes together with a new normalization scheme based on the Tchebichef moments. From that, a fast with high discriminative power TRS Tchebichef moments invariants have been derived.

In Chapter 6 new affine Tchebichef moment invariants that use the seven decomposition transformations of Flusser et al. (2009) have been proposed. For the proposed invariants, the initial seven decomposition transformations are combined and reduced to four transformations: TRS transformation, stretch transformation, second rotation transformation and reflective transformation. A new set of normalization schemes based on Tchebichef moments has been proposed to determine the normalization parameters. Four distinct normalization schemes have been derived for second rotation transformation to handle symmetric patterns with 1-fold symmetric up to 4-fold symmetric, respectively. With that the affine invariants are capable to accurately discriminate all non-symmetric patterns, as well as the symmetric patterns with 1-fold symmetry up to 4-fold symmetry.

7.2 Future Research Directions

There are many possibilities to extend current research project. Below are some ideas that are worth mentioning:

- **Chapters 3 to 6**

    1. The definition of moments invariants $I_{n,m}^{\langle \text{ast} \rangle}, I_{n,m}^{\langle \text{trs} \rangle}$, and $I_{n,m}^{\langle \text{am} \rangle}$ are based on the assumptions of canonical forms being in discrete domain and the invariants are derivable from the original moments. Despite ambiguities between the invariants of canonical form and the above assumption, the results of derivation is accurate for low order moment invariants. However insufficient study were conducted for higher order moment invariants. Therefore further study

on the moment invariants of higher orders would be helpful to understand the limitation and restriction in using the definition of the moment invariants.

2. Tchebichef moments as global features extractor, is bounded with the limitation of not being able to extract the local information in a particular region of an image. Krawtchouk and Hahn moments on the other hand having non-uniform weight kernel that can be used in extracting the local information. Therefore an extension of all the proposed invariant algorithms to other members of discrete orthogonal moments like Krawtchouk and Hahn moments would be very interesting and useful for the recognition system to extract local information of images which have been deformed by various type of spatial distortions.

3. One of the objectives of this thesis is to study the new normalization strategy and to generate moment invariant features with high discriminative power. Therefore further performance comparison on the proposed invariants with other family of moment invariants like Legendre moments and Zernkie moments would be interesting to confirm the capability of the discrete orthogonal moment invariants.

- **Chapter 6**

1. Derivation of the second rotation transformation for the symmetric images with 5-fold symmetry and above would be very useful. Study on determining the number of symmetrical fold of images using Tchebichef moments is important to automate the selection process of the second rotation algorithm. However a theoretical study on second rotation transformation using a single set of normalization constraints for all types of images would be the greatest breakthrough for the method.

2. Recently Tchebichef based affine invariants XSR and XYS have been proposed by Liu et al. (2011). However the algorithms are complicated and slow in numerical computation. Therefore fast computation and new normalization strategy for the moment invariants would be very helpful.

Appendices

APPENDIX A

ANISOTROPIC SCALE AND TRANSLATION INVARIANTS OF LIU ET. AL.

The Tchebichef moments

$$I_{n,m}^{\langle \text{ast-L}\rangle} = \sum_{k=0}^{n}\sum_{j=0}^{m}\sum_{r=0}^{k}\sum_{s=0}^{j}\tilde{a}_1^{k+1}\tilde{b}_1^{j+1}c_{n,k}^{N}c_{m,j}^{N}d_{k,r}^{N}d_{j,s}^{N}T_{r,s}^{\langle c\rangle} \quad n,m=0,1,\cdots,N-1. \tag{A.1}$$

is anisotropic scale and translation invariants, if the scale parameters $\tilde{a}_1$ and $\tilde{b}_1$ are determined by the constraint

$$I_{2,0}^{\langle \text{ast-L}\rangle} = \Omega_L = I_{0,2}^{\langle \text{ast-L}\rangle} \quad \text{where} \quad \Omega_L \in \Re$$

or from solutions of the following system equations

$$\begin{aligned}(c_{2,2}^{N}d_{2,0}^{N}T_{0,0}^{\langle c\rangle} + c_{2,2}^{N}d_{2,1}^{N}T_{1,0}^{\langle c\rangle} + T_{2,0}^{\langle c\rangle})\tilde{a}_1^3\tilde{b}_1 + (c_{2,1}^{N}d_{1,0}^{N}T_{0,0}^{\langle c\rangle} \\ + c_{2,1}^{N}d_{1,1}^{N}T_{1,0}^{\langle c\rangle})\tilde{a}_1^2\tilde{b}_1 + (c_{2,0}^{N}d_{0,0}^{N}T_{0,0}^{\langle c\rangle})\tilde{a}_1\tilde{b}_1 &= \Omega_L \qquad (A.2)\\ (c_{2,2}^{N}d_{2,0}^{N}T_{0,0}^{\langle c\rangle} + c_{2,2}^{N}d_{2,1}^{N}T_{0,1}^{\langle c\rangle} + T_{0,2}^{\langle c\rangle})\tilde{a}_1\tilde{b}_1^3 + (c_{2,1}^{N}d_{1,0}^{N}T_{0,0}^{\langle c\rangle} \\ + c_{2,1}^{N}d_{1,1}^{N}T_{0,1}^{\langle c\rangle})\tilde{a}_1\tilde{b}_1^2 + (c_{2,0}^{N}d_{0,0}^{N}T_{0,0}^{\langle c\rangle})\tilde{a}_1\tilde{b}_1 &= \Omega_L. \qquad (A.3)\end{aligned}$$

Proof. We review some formulations that will be used by the proof. From chapter 4, the image centroid has expressions

$$\bar{x} = \frac{c_{0,0}^{N}T_{1,0} - c_{1,0}^{N}T_{0,0}}{c_{1,1}^{N}T_{0,0}} \quad \text{and} \quad \bar{y} = \frac{c_{0,0}^{N}T_{0,1} - c_{1,0}^{N}T_{0,0}}{c_{1,1}^{N}T_{0,0}} \tag{A.4}$$

and

$$\sum_{k=m}^{n} c_{n,k}^{N}d_{k,m}^{N} = \delta_{n,m} \tag{A.5}$$

where

$$x^n = \sum_{j=0}^{n} d_{n,j}^{N}\tilde{t}_k^{N}(x) \tag{A.6}$$

$$t_n^{N}(x) = \sum_{k=0}^{n} c_{n,k}^{N}x^k, \quad x,n=0,1,\cdots N-1 \tag{A.7}$$

and $\delta_{n,m}$ denotes the Kronecker's delta that returns unity when $n = m$ and zero otherwise.

We will now solve the equations of $(A.2)$ and $(A.3)$.

For simplicity, let

$$I_{2,0}^{\langle \text{ast-L} \rangle} = A_1\tilde{a}_1^3\tilde{b}_1 + A_2\tilde{a}_1^2\tilde{b}_1 + A_3\tilde{a}_1\tilde{b}_1 \text{ and} \tag{A.8}$$

$$I_{0,2}^{\langle \text{ast-L} \rangle} = B_1\tilde{a}_1\tilde{b}_1^3 + B_2\tilde{a}_1\tilde{b}_1^2 + A_3\tilde{a}_1\tilde{b}_1 \tag{A.9}$$

where

$$A_1 = c_{2,2}^N d_{2,0}^N T_{0,0}^{\langle c \rangle} + c_{2,2}^N d_{2,1}^N T_{1,0}^{\langle c \rangle} + T_{2,0}^{\langle c \rangle} \tag{A.10}$$

$$A_2 = c_{2,1}^N d_{1,0}^N T_{0,0}^{\langle c \rangle} + c_{2,1}^N d_{1,1}^N T_{1,0}^{\langle c \rangle} \tag{A.11}$$

$$A_3 = c_{2,0}^N d_{0,0}^N T_{0,0}^{\langle c \rangle} \tag{A.12}$$

$$B_1 = c_{2,2}^N d_{2,0}^N T_{0,0}^{\langle c \rangle} + c_{2,2}^N d_{2,1}^N T_{0,1}^{\langle c \rangle} + T_{0,2}^{\langle c \rangle} \tag{A.13}$$

$$B_2 = c_{2,1}^N d_{1,0}^N T_{0,0}^{\langle c \rangle} + c_{2,1}^N d_{1,1}^N T_{0,1}^{\langle c \rangle} \tag{A.14}$$

The central transformed images having centroid at the origin. From $(A.4)$, we get

$$c_{0,0}^N T_{1,0}^{\langle c \rangle} - c_{1,0}^N T_{0,0}^{\langle c \rangle} = 0 \tag{A.15}$$

$$c_{0,0}^N T_{0,1} - c_{1,0}^N T_{0,0} = 0. \tag{A.16}$$

With the help from $(A.5)$,$(A.15)$ and $(A.16)$, we can deduce that $A_2 = B_2 = 0$. The expression $(A.8)$ and $(A.9)$ can thus be written as

$$I_{2,0}^{\langle \text{ast-L} \rangle} = A_1\tilde{a}_1^3\tilde{b}_1 + A_3\tilde{a}_1\tilde{b}_1, \text{ and} \tag{A.17}$$

$$I_{0,2}^{\langle \text{ast-L} \rangle} = B_1\tilde{a}_1^3\tilde{b}_1 + A_3\tilde{a}_1\tilde{b}_1. \tag{A.18}$$

From the given constraint $I_{2,0}^{\langle \text{ast-L} \rangle} = I_{0,2}^{\langle \text{ast-L} \rangle}$, we have

$$\tilde{a}_1 = \tilde{b}_1\sqrt{\frac{B_1}{A_1}}. \tag{A.19}$$

By using the constraint $I_{2,0}^{\langle \text{ast-L} \rangle} = \Omega_L = I_{0,2}^{\langle \text{ast-L} \rangle}$, $(A.19)$ is finally solved as

$$\tilde{a}_1^2 = \frac{-A_3 \pm \sqrt{A_3^2 + 4\Omega_L\sqrt{A_1B_1}}}{2A_1} \quad \text{and} \tag{A.20}$$

$$\tilde{b}_1^2 = \frac{-A_3 \pm \sqrt{A_3^2 + 4\Omega_L\sqrt{A_1B_1}}}{2B_1}. \tag{A.21}$$

□

APPENDIX B

DERIVATION OF SECOND ORDER ANISOTROPIC SCALE AND TRANSLATED TCHEBICHEF MOMENT INVARIANTS

We need to show that the second order AST moments $I_{2,0}^{\langle \text{ast} \rangle}$ *and* $I_{0,2}^{\langle \text{ast} \rangle}$ *have following expressions:*

$$\begin{aligned} I_{2,0}^{\langle \text{ast} \rangle} &= \left(\frac{N_0}{N_s}\right) a_1^3 b_1 \left\{ K_{1,1}^{N_s,N_0} K_{2,2}^{N_s,N_0} T_{2,0} + 2\left(\frac{N_0-1}{2} - \bar{x}\right) \tilde{A}_1^{N_s} K_{2,1}^{N_s,N_0} T_{1,0} + \right. \\ &\qquad \left. \left[\tilde{A}_1^{N_s} \tilde{A}_2^{N_s} \left(\frac{N_0-1}{2} - \bar{x}\right)^2 - K_{1,1}^{N_s,N_0} K_{2,2}^{N_s,N_0} \tilde{C}_2^{N_0} \right] T_{0,0} \right\} \\ &\quad + a_1 b_1 \left(\frac{N_0}{N_s}\right) \tilde{C}_2^{N_s} T_{0,0} \end{aligned} \tag{B.1}$$

and

$$\begin{aligned} I_{0,2}^{\langle \text{ast} \rangle} &= \left(\frac{N_0}{N_s}\right) a_1 b_1^3 \left\{ K_{1,1}^{N_s,N_0} K_{2,2}^{N_s,N_0} T_{0,2} + 2\left(\frac{N_0-1}{2} - \bar{y}\right) \tilde{A}_1^{N_s} K_{2,1}^{N_s,N_0} T_{0,1} + \right. \\ &\qquad \left. \left[\tilde{A}_1^{N_s} \tilde{A}_2^{N_s} \left(\frac{N_0-1}{2} - \bar{y}\right)^2 - K_{1,1}^{N_s,N_0} K_{2,2}^{N_s,N_0} \tilde{C}_2^{N_0} \right] T_{0,0} \right\} \\ &\quad + a_1 b_1 \left(\frac{N_0}{N_s}\right) \tilde{C}_2^{N_s} T_{0,0}. \end{aligned} \tag{B.2}$$

Suppose $f'(x',y') = f(x,y)$ denotes the AST transformed image f that

$$\begin{aligned} x' &= a_1 x - a_1 \bar{x} + \frac{N_s - 1}{2} \quad \text{and} \\ y' &= b_1 y - b_1 \bar{y} + \frac{N_s - 1}{2} \\ &\qquad (x,y) \in S_2(N_0), \text{ and } (x',y') \in S_2(N_s). \end{aligned} \tag{B.3}$$

In this case, the centroid of f' is on the middle of $S_2(N_s)$.

From Theorem 4.3.1, we have

$$I_{n,m}^{\langle \text{ast} \rangle} = |a_1 b_1| \sum_{k=0}^{n} \sum_{j=0}^{m} \lambda_{n,k}^{(1)} \lambda_{m,j}^{(2)} T_{k,j} \tag{B.4}$$

where

$$\lambda^{(1)}_{n,k}(a_1,-a_1\bar{x}+\frac{Ns-1}{2};N_0,N_s) = \lambda^{(1)}_{n-1,k-1}a_1K^{N_s,N_0}_{n,k}+\lambda^{(1)}_{n-1,k}a_1\tilde{A}^{N_s}_n\left[\frac{(N_0-1)}{2}-\bar{x}\right] -\lambda^{(1)}_{n-1,k+1}a_1K^{N_s,N_0}_{n,k+2}\tilde{C}^{N_0}_{k+2}+\lambda^{(1)}_{n-2,k}\tilde{C}^{N_s}_n \quad (B.5)$$

$$\lambda^{(2)}_{m,j}(b_1,-b_1\bar{y}+\frac{Ns-1}{2};N_0,N_s)) = \lambda^{(2)}_{m-1,j-1}b_1K^{N_s,N_0}_{m,j}+\lambda^{(2)}_{m-1,j}b_1\tilde{A}^{N_s}_m\left[\frac{(N_0-1)}{2}-\bar{y}\right] -\lambda^{(2)}_{m-1,j+1}b_1K^{N_s,N_0}_{m,j+2}\tilde{C}^{N_0}_{i+2}+\lambda^{(2)}_{m-2,i}\tilde{C}^{N_s}_m. \quad (B.6)$$

By using the recurrence relation we get

$$\lambda^{(1)}_{0,0} = \sqrt{\left(\frac{N_0}{N_s}\right)} \quad (B.7)$$

$$\lambda^{(1)}_{1,1} = a_1\sqrt{\left(\frac{N_0}{N_s}\right)}K^{N_s,N_0}_{1,1} \quad (B.8)$$

$$\lambda^{(1)}_{1,0} = a_1\tilde{A}^{N_s}_1\left[\frac{N_0-1}{2}-\bar{x}\right]\sqrt{\left(\frac{N_0}{N_s}\right)} \quad (B.9)$$

$$\lambda^{(1)}_{2,2} = a_1^2\sqrt{\left(\frac{N_0}{N_s}\right)}K^{N_s,N_0}_{1,1}K^{N_s,N_0}_{2,2} \quad (B.10)$$

$$\lambda^{(1)}_{2,1} = 2a_1^2\tilde{A}^{N_s}_2K^{N_s,N_0}_{1,1}\sqrt{\left(\frac{N_0}{N_s}\right)}\left[\frac{N_0-1}{2}-\bar{x}\right] \quad (B.11)$$

$$\lambda^{(1)}_{2,0} = a_1^2\tilde{A}^{N_s}_1\tilde{A}^{N_s}_2\sqrt{\left(\frac{N_0}{N_s}\right)}\left[\frac{N_0-1}{2}-\bar{x}\right]^2 -a_1^2K^{N_s,N_0}_{1,1}K^{N_s,N_0}_{2,2}\tilde{C}^{N_0}_2\sqrt{\left(\frac{N_0}{N_s}\right)}+\sqrt{\left(\frac{N_0}{N_s}\right)}\tilde{C}^{N_s}_2 \quad (B.12)$$

and

$$\lambda^{(2)}_{0,0} = \sqrt{\left(\frac{N_0}{N_s}\right)} \quad (B.13)$$

$$\lambda^{(2)}_{1,1} = b_1\sqrt{\left(\frac{N_0}{N_s}\right)}K^{N_s,N_0}_{1,1} \quad (B.14)$$

$$\lambda^{(2)}_{1,0} = b_1\tilde{A}^{N_s}_1\left[\frac{N_0-1}{2}-\bar{y}\right]\sqrt{\left(\frac{N_0}{N_s}\right)} \quad (B.15)$$

$$\lambda^{(2)}_{2,2} = b_1^2\sqrt{\left(\frac{N_0}{N_s}\right)}K^{N_s,N_0}_{1,1}K^{N_s,N_0}_{2,2} \quad (B.16)$$

$$\lambda^{(2)}_{2,1} = 2b_1^2\tilde{A}^{N_s}_2K^{N_s,N_0}_{1,1}\sqrt{\left(\frac{N_0}{N_s}\right)}\left[\frac{N_0-1}{2}-\bar{y}\right] \quad (B.17)$$

$$\lambda^{(2)}_{2,0} = b_1^2\tilde{A}^{N_s}_1\tilde{A}^{N_s}_2\sqrt{\left(\frac{N_0}{N_s}\right)}\left[\frac{N_0-1}{2}-\bar{y}\right]^2 -b_1^2K^{N_s,N_0}_{1,1}K^{N_s,N_0}_{2,2}\tilde{C}^{N_0}_2\sqrt{\left(\frac{N_0}{N_s}\right)}+\sqrt{\left(\frac{N_0}{N_s}\right)}\tilde{C}^{N_s}_2. \quad (B.18)$$

From $(B.10)$,$(B.11)$, $(B.12)$ and $(B.13)$ we have

$$\begin{aligned} I_{2,0}^{\langle \text{ast} \rangle} &= \left(\frac{N_0}{N_s}\right) a_1^3 b_1 \left\{ K_{1,1}^{N_s,N_0} K_{2,2}^{N_s,N_0} T_{2,0} + 2\left(\frac{N_0-1}{2} - \bar{x}\right) \tilde{A}_1^{N_s} K_{2,1}^{N_s,N_0} T_{1,0} \right. \\ &\qquad \left. + \left[\tilde{A}_1^{N_s} \tilde{A}_2^{N_s} \left(\frac{N_0-1}{2} - \bar{x}\right)^2 - K_{1,1}^{N_s,N_0} K_{2,2}^{N_s,N_0} \tilde{C}_2^{N_0} \right] T_{0,0} \right\} \\ &\quad + a_1 b_1 \left(\frac{N_0}{N_s}\right) \tilde{C}_2^{N_s} T_{0,0}. \end{aligned} \tag{B.19}$$

Similarly, from $(B.16)$,$(B.17)$, $(B.18)$ and $(B.7)$ we get

$$\begin{aligned} I_{0,2}^{\langle \text{ast} \rangle} &= \left(\frac{N_0}{N_s}\right) a_1 b_1^3 \left\{ K_{1,1}^{N_s,N_0} K_{2,2}^{N_s,N_0} T_{0,2} + 2\left(\frac{N_0-1}{2} - \bar{y}\right) \tilde{A}_1^{N_s} K_{2,1}^{N_s,N_0} T_{0,1} \right. \\ &\qquad \left. + \left[\tilde{A}_1^{N_s} \tilde{A}_2^{N_s} \left(\frac{N_0-1}{2} - \bar{y}\right)^2 - K_{1,1}^{N_s,N_0} K_{2,2}^{N_s,N_0} \tilde{C}_2^{N_0} \right] T_{0,0} \right\} \\ &\quad + a_1 b_1 \left(\frac{N_0}{N_s}\right) \tilde{C}_2^{N_s} T_{0,0}. \end{aligned} \tag{B.20}$$

APPENDIX C

TRANSLATION AND ROTATION TCHEBICHEF MOMENT INVARIANTS OF ZHANG ET. AL.

Translation and rotational invariants of Tchebichef moments by Zhang et.al. (2010) can be derived as follow

$$\begin{aligned} I_{n,m}^{\langle \text{tr-Z} \rangle} &= \sum_{k=0}^{n}\sum_{j=0}^{m}\sum_{s=0}^{k}\sum_{t=0}^{m}\sum_{u=0}^{s+t}\sum_{v=0}^{k+j-s-t}\binom{k}{s}\binom{j}{t}(-1)^t \\ &\quad \times(\cos\theta_z)^{j+s-t}(\sin\theta_z)^{k+t-s}c_{n,k}^{N}c_{m,j}^{N}d_{s+t,u}^{N}d_{j+k-s-t,v}^{N}T_{u,v}^{\langle \text{c} \rangle} \end{aligned} \tag{C.1}$$

where

$$\theta_z = \frac{1}{2}tan^{-1}\left(\frac{pT_{1,1}^{\langle \text{c} \rangle} - qT_{0,0}^{\langle \text{c} \rangle}}{T_{2,0}^{\langle \text{c} \rangle} - T_{0,2}^{\langle \text{c} \rangle}}\right) \qquad p = \frac{2c_{2,2}^{N}c_{0,0}^{N}}{(c_{1,1}^{N})^2} \quad q = \frac{2c_{2,2}^{N}(c_{1,0}^{N})^2}{c_{0,0}^{N}(c_{1,1}^{N})^2}. \tag{C.2}$$

and $T_{n,m}^{\langle \text{c} \rangle}$ denotes the Tchebichef central moment.

Here we want to show that the rotation invariants is equivalent to the constraint of

$$I_{1,1}^{\langle \text{tr-Z} \rangle} - \left(\frac{c_{1,0}^{N}}{c_{0,0}^{N}}\right)^2 I_{0,0}^{\langle \text{tr-Z} \rangle} = 0. \tag{C.3}$$

Proof. We review some of the equations required by the proof. From Chapter 5, the centroid has expressions

$$\bar{x} = \frac{c_{0,0}^{N}T_{1,0}^{\langle \text{c} \rangle} - c_{1,0}^{N}T_{0,0}^{\langle \text{c} \rangle}}{c_{1,1}^{N}T_{0,0}^{\langle \text{c} \rangle}} \quad \text{and} \quad \bar{y} = \frac{c_{0,0}^{N}T_{0,1}^{\langle \text{c} \rangle} - c_{1,0}^{N}T_{0,0}^{\langle \text{c} \rangle}}{c_{1,1}^{N}T_{0,0}^{\langle \text{c} \rangle}} \tag{C.4}$$

and

$$\sum_{k=m}^{n} c_{n,k}^{N}d_{k,m}^{N} = \delta_{n,m} \tag{C.5}$$

where

$$x^n = \sum_{j=0}^{n} d_{n,j}^{N}\tilde{t}_k^{N}(x) \tag{C.6}$$

$$t_n^{N}(x) = \sum_{k=0}^{n} c_{n,k}^{N}x^k, \tag{C.7}$$

$$x, n = 0, 1, \cdots N-1$$

and $\delta_{n,m}$ denotes the Kronecker's delta that return unity when $n = m$ and zero otherwise.

From $(C.1)$, we can deduce that

$$\begin{aligned} I_{1,1}^{\langle \text{tr-Z} \rangle} &= (c_{1,0}^N)^2 (d_{0,0}^N)^2 T_{0,0}^{\langle \text{c} \rangle} \\ &\quad + c_{1,0}^N c_{1,1}^N d_{0,0}^N \Big\{ \cos\theta_z [2 d_{1,0}^N T_{0,0}^{\langle \text{c} \rangle} + d_{1,1}^N T_{1,0}^{\langle \text{c} \rangle} + d_{1,1}^N T_{0,1}^{\langle \text{c} \rangle}] \\ &\qquad + \sin\theta_z [-d_{1,1}^N T_{1,0}^{\langle \text{c} \rangle} + d_{1,1}^N T_{0,1}^{\langle \text{c} \rangle}] \Big\} \\ &\quad + \frac{(c_{1,1}^N)^2}{2} d_{0,0}^N \sin(2\theta_z) \left\{ - \sum_{k=0}^{2} d_{2,k}^N T_{k,0}^{\langle \text{c} \rangle} + \sum_{j=0}^{2} d_{2,j}^N T_{0,j}^{\langle \text{c} \rangle} \right\} \\ &\quad + (c_{1,1}^N)^2 \cos(2\theta_z) \left\{ \sum_{k=0}^{1} \sum_{j=0}^{1} d_{1,k}^N d_{1,j}^N T_{k,j}^{\langle \text{c} \rangle} \right\}. \end{aligned} \tag{C.8}$$

As centroid of Tchebichef central moments is at the origin, from $(C.4)$, we get

$$c_{0,0}^N T_{1,0}^{\langle \text{c} \rangle} = c_{1,0}^N T_{0,0}^{\langle \text{c} \rangle} \tag{C.9}$$

$$c_{0,0}^N T_{0,1}^{\langle \text{c} \rangle} = c_{1,0}^N T_{0,0}^{\langle \text{c} \rangle}. \tag{C.10}$$

By using $(C.9)$, $(C.10)$ and $(C.5)$, the equation $(C.8)$ can be simplified as such

$$\begin{aligned} I_{1,1}^{\langle \text{tr-Z} \rangle} - \left(\frac{c_{1,0}^N}{c_{0,0}^N} \right)^2 I_{0,0}^{\langle \text{tr-Z} \rangle} &= \cos(2\theta_z) \left[T_{1,1}^{\langle \text{c} \rangle} - \left(\frac{c_{1,0}^N}{c_{0,0}^N} \right)^2 T_{0,0}^{\langle \text{c} \rangle} \right] \\ &\quad + \sin(2\theta_z) \frac{(c_{1,1}^N)^2}{2 c_{0,0}^N c_{2,2}^N} \left[T_{0,2}^{\langle \text{c} \rangle} - T_{2,0}^{\langle \text{c} \rangle} \right]. \end{aligned} \tag{C.11}$$

Therefore the theorem is proved. □

APPENDIX D

DERIVATION OF SECOND ORDER TRANSLATION, ROTATION AND SCALE TCHEBICHEF MOMENT INVARIANTS

From chapter 5, TRS-invariants have expression

$$I_{n,m}^{\langle \mathrm{trs} \rangle} = \omega^2 \sum_{k=0}^{n+m} \sum_{j=0}^{n+m-k} \lambda_{n,m,k,j}^{\langle \mathrm{trs} \rangle} T_{k,j} \qquad n,m \in \{0,1,\cdots,\min\{N_0-1,N_s-1\}\} \tag{D.1}$$

where

$$\lambda_{n,m,k,j}^{\langle \mathrm{trs} \rangle} = \lambda_{n,m,k,j} \left(\begin{array}{c} \omega\cos\theta, \quad \omega\sin\theta, \\ -\omega\bar{x}\cos\theta - \omega\bar{y}\sin\theta + \frac{N_s-1}{2}; \\ -\omega\sin\theta, \quad \omega\cos\theta, \\ \omega\bar{x}\sin\theta - \omega\bar{y}\cos\theta + \frac{N_s-1}{2} \end{array} \middle| N_0, N_s \right) \tag{D.2}$$

and the scale coefficients ω is determined by

$$\omega = \sqrt{\frac{\Omega_0 N_s^2}{T_{0,0} N_0}} \tag{D.3}$$

where Ω_0 is the ratio between the mass of canonical form and the space $N_s \times N_s$.

The recurrence relations of the TRS-invariant are

$$\begin{aligned} \lambda_{n,m,k,j}^{\langle \mathrm{trs} \rangle} = & -\lambda_{n-1,m,k+1,j}^{\langle \mathrm{trs} \rangle} \omega\cos\theta K_{n,k+2}^{N_s,N_0} \tilde{C}_{k+2}^{N_0} - \lambda_{n-1,m,k,j+1}^{\langle \mathrm{trs} \rangle} \omega\sin\theta K_{n,j+2}^{N_s,N_0} \tilde{C}_{j+2}^{N_0} \\ & + \lambda_{n-1,m,k,j}^{\langle \mathrm{trs} \rangle} \omega \tilde{A}_n^{N_s} \left[\cos\theta \left(\frac{N_0-1}{2} - \bar{x} \right) + \sin\theta \left(\frac{N_0-1}{2} - \bar{y} \right) \right] \\ & + \lambda_{n-1,m,k-1,j}^{\langle \mathrm{trs} \rangle} \omega\cos\theta K_{n,k}^{N_s,N_0} + \lambda_{n-1,m,k,j-1}^{\langle \mathrm{trs} \rangle} \omega\sin\theta K_{n,k}^{N_s,N_0} \\ & + \lambda_{n-2,m,k,j}^{\langle \mathrm{trs} \rangle} \tilde{C}_n^{N_s} \end{aligned} \tag{D.4}$$

and

$$\begin{aligned} \lambda_{n,m,k,j}^{\langle \mathrm{trs} \rangle} = & \lambda_{n,m-1,k+1,j}^{\langle \mathrm{trs} \rangle} \omega\sin\theta K_{m,k+2}^{N_s,N_0} \tilde{C}_{k+2}^{N_0} - \lambda_{n,m-1,k,j+1}^{\langle \mathrm{trs} \rangle} \omega\cos\theta K_{m,j+2}^{N_s,N_0} \tilde{C}_{j+2}^{N_0} \\ & + \lambda_{n,m-1,k,j}^{\langle \mathrm{trs} \rangle} \omega \tilde{A}_m^{N_s} \left[-\sin\theta \left(\frac{N_0-1}{2} - \bar{x} \right) + \cos\theta \left(\frac{N_0-1}{2} - \bar{y} \right) \right] \\ & - \lambda_{n,m-1,k-1,j}^{\langle \mathrm{trs} \rangle} \omega\sin\theta K_{m,k}^{N_s,N_0} + \lambda_{n,m-1,k,j-1}^{\langle \mathrm{trs} \rangle} \omega\cos\theta K_{m,j}^{N_s,N_0} \\ & + \lambda_{n,m-2,k,j}^{\langle \mathrm{trs} \rangle} \tilde{C}_m^{N_s}. \end{aligned} \tag{D.5}$$

We will now derive $\lambda^{\langle \mathrm{trs} \rangle}_{n,m,k,j}$ recursively.

For $(n,m) = (0,0)$,

$$\lambda^{\langle \mathrm{trs} \rangle}_{0,0,0,0} = \left(\frac{N_0}{N_s}\right) \tag{D.6}$$

and $(n,m) = (1,0)$,

$$\lambda^{\langle \mathrm{trs} \rangle}_{1,0,1,0} = \omega \cos\theta K^{N_s,N_0}_{1,1}\left(\frac{N_0}{N_s}\right) \tag{D.7}$$

$$\lambda^{\langle \mathrm{trs} \rangle}_{1,0,0,1} = \omega \sin\theta K^{N_s,N_0}_{1,1}\left(\frac{N_0}{N_s}\right) \tag{D.8}$$

$$\lambda^{\langle \mathrm{trs} \rangle}_{1,0,0,0} = \omega \tilde{A}^{N_s}_1\left(\frac{N_0}{N_s}\right)\left\{\cos\theta\left(\frac{N_0-1}{2}-\bar{x}\right)+\sin\theta\left(\frac{N_0-1}{2}-\bar{y}\right)\right\}. \tag{D.9}$$

For $(n,m) = (0,1)$,

$$\lambda^{\langle \mathrm{trs} \rangle}_{0,1,1,0} = -\omega \sin\theta K^{N_s,N_0}_{1,1}\left(\frac{N_0}{N_s}\right) \tag{D.10}$$

$$\lambda^{\langle \mathrm{trs} \rangle}_{0,1,0,1} = \omega \cos\theta K^{N_s,N_0}_{1,1}\left(\frac{N_0}{N_s}\right) \tag{D.11}$$

$$\lambda^{\langle \mathrm{trs} \rangle}_{0,1,0,0} = \omega \tilde{A}^{N_s}_1\left(\frac{N_0}{N_s}\right)\left\{-\sin\theta\left(\frac{N_0-1}{2}-\bar{x}\right)+\cos\theta\left(\frac{N_0-1}{2}-\bar{y}\right)\right\} \tag{D.12}$$

and $(n,m) = (1,1)$

$$\lambda^{\langle \mathrm{trs} \rangle}_{1,1,2,0} = -\frac{\omega^2}{2}\sin(2\theta)K^{N_s,N_0}_{1,1}K^{N_s,N_0}_{1,2}\left(\frac{N_0}{N_s}\right) \tag{D.13}$$

$$\lambda^{\langle \mathrm{trs} \rangle}_{1,1,0,2} = \frac{\omega^2}{2}\sin(2\theta)K^{N_s,N_0}_{1,1}K^{N_s,N_0}_{1,2}\left(\frac{N_0}{N_s}\right) \tag{D.14}$$

$$\lambda^{\langle \mathrm{trs} \rangle}_{1,1,1,1} = \omega^2\cos(2\theta)\left(K^{N_s,N_0}_{1,1}\right)^2\left(\frac{N_0}{N_s}\right) \tag{D.15}$$

$$\lambda^{\langle \mathrm{trs} \rangle}_{1,1,1,0} = \omega^2\tilde{A}^{N_s}_1 K^{N_s,N_0}_{1,1}\left(\frac{N_0}{N_s}\right)\left\{-\sin(2\theta)\left(\frac{N_0-1}{2}-\bar{x}\right)+\cos(2\theta)\left(\frac{N_0-1}{2}-\bar{y}\right)\right\} \tag{D.16}$$

$$\lambda^{\langle \mathrm{trs} \rangle}_{1,1,0,1} = \omega^2\tilde{A}^{N_s}_1 K^{N_s,N_0}_{1,1}\left(\frac{N_0}{N_s}\right)\left\{\cos(2\theta)\left(\frac{N_0-1}{2}-\bar{x}\right)+\sin(2\theta)\left(\frac{N_0-1}{2}-\bar{y}\right)\right\} \tag{D.17}$$

$$\lambda^{\langle \mathrm{trs} \rangle}_{1,1,0,0} = \omega^2\left(\tilde{A}^{N_s}_1\right)^2\left(\frac{N_0}{N_s}\right)\left\{\cos(2\theta)\left(\frac{N_0-1}{2}-\bar{x}\right)\left(\frac{N_0-1}{2}-\bar{y}\right)+\frac{1}{2}\sin(2\theta)\left[-\left(\frac{N_0-1}{2}-\bar{x}\right)^2+\left(\frac{N_0-1}{2}-\bar{y}\right)^2\right]\right\} \tag{D.18}$$

From $(D.13)$ to $(D.18)$, we thus get

$$
\begin{aligned}
I_{1,1}^{\langle \mathrm{trs} \rangle} &= \sum_{k=0}^{2} \sum_{j=0}^{2-k} \lambda_{1,1,k,j}^{\langle \mathrm{trs} \rangle} T_{k,j} \\
&= \left\{ \begin{array}{l} \frac{1}{2}\sin(2\theta)\left[-\left(\frac{N_0-1}{2}-\bar{x}\right)^2 + \left(\frac{N_0-1}{2}-\bar{y}\right)^2 \right] \\ +\cos(2\theta)\left(\frac{N_0-1}{2}-\bar{x}\right)\left(\frac{N_0-1}{2}-\bar{y}\right) \end{array} \right\} \times \omega^2 \left(\tilde{A}_1^{N_s}\right)^2 \left(\frac{N_0}{N_s}\right) T_{0,0} \\
&\quad + K_{1,1}^{N_s,N_0} \omega^2 \tilde{A}_1^{N_s} \left(\frac{N_0}{N_s}\right) \left\{ \begin{array}{l} -\sin(2\theta)\left(\frac{(N_0-1)}{2}-\bar{x}\right) \\ +\cos(2\theta)\left(\frac{(N_0-1)}{2}-\bar{y}\right) \end{array} \right\} T_{1,0} \\
&\quad + K_{1,1}^{N_s,N_0} \omega^2 \tilde{A}_1^{N_s} \left(\frac{N_0}{N_s}\right) \left\{ \begin{array}{l} \sin(2\theta)\left(\frac{(N_0-1)}{2}-\bar{y}\right) \\ +\cos(2\theta)\left(\frac{(N_0-1)}{2}-\bar{x}\right) \end{array} \right\} T_{0,1} \\
&\quad + \cos(2\theta)\left(\frac{N_0}{N_s}\right)\left(K_{1,1}^{N_s,N_0}\right)^2 \omega^2 T_{1,1} \\
&\quad - \frac{1}{2}\sin(2\theta) K_{1,1}^{N_s,N_0} K_{1,2}^{N_s,N_0} \omega^2 \left(\frac{N_0}{N_s}\right) T_{2,0} \\
&\quad + \frac{1}{2}\sin(2\theta) K_{1,1}^{N_s,N_0} K_{1,2}^{N_s,N_0} \omega^2 \left(\frac{N_0}{N_s}\right) T_{0,2}. \qquad \text{(D.19)}
\end{aligned}
$$

APPENDIX E

DERIVATION OF TCHEBICHEF MOMENTS FOR STRETCH NORMALIZATION

The stretch normalization of a TRS transformed image can be express as

$$x' = \delta x + \delta\bar{x} + \frac{N_s - 1}{2} \quad \text{and} \tag{E.1}$$

$$y' = \frac{1}{\delta}y + \frac{1}{\delta}\bar{y} + \frac{N_s - 1}{2} \tag{E.2}$$

where $\bar{x} = \bar{y} = \frac{N_s-1}{2}$.

From Theorem 4.3.1, the stretched and TRS normalized Tchebichef moment is

$$I_{n,m}^{\langle \text{s, trs} \rangle} = \sum_{k=0}^{n}\sum_{j=0}^{m} \lambda_{n,k}^{(1)}\lambda_{m,j}^{(2)} I_{k,j}^{\langle \text{trs} \rangle} \tag{E.3}$$

where

$$\begin{aligned} \lambda_{n,k}^{(1)}(\delta, -\delta\bar{x} + \frac{N_s-1}{2}; N_s, N_s) &= \lambda_{n-1,k-1}^{(1)}\delta K_{n,k}^{N_s,N_s} - \lambda_{n-1,k+1}^{(1)}\delta K_{n,k+2}^{N_s,N_s}\tilde{C}_{k+2}^{N_s} \\ &\quad + \lambda_{n-2,k}^{(1)}\tilde{C}_n^{N_s} \quad \text{and} \end{aligned} \tag{E.4}$$

$$\begin{aligned} \lambda_{m,j}^{(2)}(\frac{1}{\delta}, -\frac{1}{\delta}\bar{y} + \frac{N_s-1}{2}; N_s, N_s) &= \lambda_{m-1,j-1}^{(2)}\frac{1}{\delta}K_{m,j}^{N_s,N_s} - \lambda_{m-1,j+1}^{(2)}\frac{1}{\delta}K_{m,j+2}^{N_s,N_s}\tilde{C}_{j+2}^{N_s} \\ &\quad + \lambda_{m-2,j}^{(2)}\tilde{C}_m^{N_s}. \end{aligned} \tag{E.5}$$

By using $(E.4)$, we get

$$\lambda_{0,0}^{(1)} = 1 \tag{E.6}$$

$$\lambda_{1,1}^{(1)} = \delta \tag{E.7}$$

$$\lambda_{2,2}^{(1)} = \delta^2 \tag{E.8}$$

$$\lambda_{2,0}^{(1)} = \tilde{C}_2^{N_s}(1 - \delta^2) \tag{E.9}$$

$$\lambda_{1,0}^{(1)} = \lambda_{2,1}^{(1)} = 0. \tag{E.10}$$

From $(E.5)$, we get

$$\lambda_{0,0}^{(2)} = 1 \tag{E.11}$$

$$\lambda_{1,1}^{(2)} = \frac{1}{\delta} \tag{E.12}$$

$$\lambda_{2,2}^{(2)} = \left(\frac{1}{\delta}\right)^2 \tag{E.13}$$

$$\lambda_{2,0}^{(2)} = \tilde{C}_2^{N_s}\left[1-\left(\frac{1}{\delta}\right)^2\right] \tag{E.14}$$

$$\lambda_{1,0}^{(2)} = \lambda_{2,1}^{(2)} = 0. \tag{E.15}$$

By $(E.6)$ to $(E.10)$ and $(E.11)$ we get

$$I_{2,0}^{\langle \mathrm{s,\,trs}\rangle} = \delta^2 I_{2,0}^{\langle \mathrm{trs}\rangle} + \tilde{C}_2^{N_s}\left(1-\delta^2\right) I_{0,0}^{\langle \mathrm{trs}\rangle}. \tag{E.16}$$

Similarly, from $(E.6)$ and $(E.11)$ to $(E.15)$ we have

$$I_{0,2}^{\langle \mathrm{s,\,trs}\rangle} = \left(\frac{1}{\delta^2}\right) I_{0,2}^{\langle \mathrm{trs}\rangle} + \tilde{C}_2^{N_s}\left[1-\left(\frac{1}{\delta^2}\right)\right] I_{0,0}^{\langle \mathrm{trs}\rangle}. \tag{E.17}$$

APPENDIX F

DERIVATION OF TCHEBICHEF MOMENTS USED IN SECOND ROTATION TRANSFORMATION

In the proof of 2nd rotational invariants, the following moments are required:

$$I_{2,1}^{\langle \mathrm{r}_2,\,\mathrm{s},\,\mathrm{trs}\rangle}, I_{0,3}^{\langle \mathrm{r}_2,\,\mathrm{s},\,\mathrm{trs}\rangle}, I_{1,3}^{\langle \mathrm{r}_2,\,\mathrm{s},\,\mathrm{trs}\rangle}, \text{ and } I_{3,1}^{\langle \mathrm{r}_2,\,\mathrm{s},\,\mathrm{trs}\rangle} \tag{F.1}$$

From Theorem 5.3.1, the recurrence relation for the second rotation can be expressed as

$$I_{n,m}^{\langle \mathrm{r}_2,\,\mathrm{s},\,\mathrm{trs}\rangle} = \sum_{k=0}^{n+m} \sum_{j=0}^{n+m-k} \lambda_{n,m,k,j}^{\langle \mathrm{r}_2\rangle} I_{k,j}^{\langle \mathrm{s},\,\mathrm{trs}\rangle} \tag{F.2}$$

where the recurrence relation of coefficient $\lambda_{n,m,k,j}^{\langle \mathrm{r}_2\rangle}$ has two different expressions in directions of row and column, respectively.

$$\begin{aligned}
&\lambda_{n,m,k,j}^{\langle \mathrm{r}_2\rangle} \left(\begin{array}{c} \cos\theta_2, \sin\theta_2, \frac{(N_s-1)}{2}(1-\cos\theta_2-\sin\theta_2) \\ -\sin\theta_2, \cos\theta_2, \frac{(N_s-1)}{2}(1+\sin\theta_2-\cos\theta_2) \end{array} \middle| N_s, N_s \right) \\
&\quad = -\lambda_{n-1,m,k+1,j}^{\langle \mathrm{r}_2\rangle} \cos\theta_2 K_{n,k+2}^{N_s,N_s} \tilde{C}_{k+2}^{N_s} - \lambda_{n-1,m,k,j+1}^{\langle \mathrm{r}_2\rangle} \sin\theta_2 K_{n,j+2}^{N_s,N_s} \tilde{C}_{j+2}^{N_s} \\
&\qquad + \lambda_{n-1,m,k-1,j}^{\langle \mathrm{r}_2\rangle} \cos\theta_2 K_{n,k}^{N_s,N_s} + \lambda_{n-1,m,k,j-1}^{\langle \mathrm{r}_2\rangle} \sin\theta_2 K_{n,j}^{N_s,N_s} \\
&\qquad + \lambda_{n-2,m,k,j}^{\langle \mathrm{r}_2\rangle} \tilde{C}_n^{N_s}
\end{aligned} \tag{F.3}$$

and

$$\begin{aligned}
&\lambda_{n,m,k,j}^{\langle \mathrm{r}_2\rangle} \left(\begin{array}{c} \cos\theta_2, \sin\theta_2, \frac{(N_s-1)}{2}(1-\cos\theta_2-\sin\theta_2) \\ -\sin\theta_2, \cos\theta_2, \frac{(N_s-1)}{2}(1+\sin\theta_2-\cos\theta_2) \end{array} \middle| N_s, N_s \right) \\
&\quad = \lambda_{n,m-1,k+1,j}^{\langle \mathrm{r}_2\rangle} \sin\theta_2 K_{m,k+2}^{N_s,N_s} \tilde{C}_{k+2}^{N_s} - \lambda_{n,m-1,k,j+1}^{\langle \mathrm{r}_2\rangle} \cos\theta_2 K_{m,j+2}^{N_s,N_0} \tilde{C}_{j+2}^{N_s} \\
&\qquad - \lambda_{n,m-1,k-1,j}^{\langle \mathrm{r}_2\rangle} \sin\theta_2 K_{m,k}^{N_s,N_s} + \lambda_{n,m-1,k,j-1}^{\langle \mathrm{r}_2\rangle} \cos\theta_2 K_{m,j}^{N_s,N_s} \\
&\qquad + \lambda_{n,m-2,k,j}^{\langle \mathrm{r}_2\rangle} \tilde{C}_m^{N_s}.
\end{aligned} \tag{F.4}$$

From $(F.3)$ and $(F.4)$, we can deduce the following recursively

for $n+m \leq 1$,

$$\lambda^{\langle r_2 \rangle}_{0,0,0,0} = 1 \tag{F.5}$$

$$\lambda^{\langle r_2 \rangle}_{1,0,1,0} = \cos\theta_2 \tag{F.6}$$

$$\lambda^{\langle r_2 \rangle}_{1,0,0,1} = \sin\theta_2 \tag{F.7}$$

$$\lambda^{\langle r_2 \rangle}_{0,1,1,0} = -\sin\theta_2 \tag{F.8}$$

$$\lambda^{\langle r_2 \rangle}_{0,1,0,1} = \cos\theta_2 \tag{F.9}$$

$$\lambda^{\langle r_2 \rangle}_{1,0,0,0} = \lambda^{\langle r_2 \rangle}_{0,1,0,0} = 0. \tag{F.10}$$

For $n+m=2$, we have that

$$\lambda^{\langle r_2 \rangle}_{2,0,2,0} = \cos^2\theta_2 \tag{F.11}$$

$$\lambda^{\langle r_2 \rangle}_{2,0,1,1} = \sin(2\theta_2) K^{N_s,N_s}_{2,1} \tag{F.12}$$

$$\lambda^{\langle r_2 \rangle}_{2,0,0,2} = \sin^2\theta_2 \tag{F.13}$$

$$\lambda^{\langle r_2 \rangle}_{2,0,1,0} = \lambda^{\langle r_2 \rangle}_{2,0,0,1} = \lambda^{\langle r_2 \rangle}_{2,0,0,0} = 0. \tag{F.14}$$

$$\lambda^{\langle r_2 \rangle}_{1,1,2,0} = -\frac{1}{2}\sin(2\theta_2) K^{N_s,N_s}_{1,2} \tag{F.15}$$

$$\lambda^{\langle r_2 \rangle}_{1,1,1,1} = \cos(2\theta_2) \tag{F.16}$$

$$\lambda^{\langle r_2 \rangle}_{1,1,0,2} = \frac{1}{2}\sin(2\theta_2) K^{N_s,N_s}_{1,2} \tag{F.17}$$

$$\lambda^{\langle r_2 \rangle}_{1,1,1,0} = \lambda^{\langle r_2 \rangle}_{1,1,0,1} = \lambda^{\langle r_2 \rangle}_{1,1,0,0} = 0. \tag{F.18}$$

And

$$\lambda^{\langle r_2 \rangle}_{0,2,2,0} = \sin^2\theta_2 \tag{F.19}$$

$$\lambda^{\langle r_2 \rangle}_{0,2,1,1} = -\sin(2\theta_2) K^{N_s,N_s}_{2,1} \tag{F.20}$$

$$\lambda^{\langle r_2 \rangle}_{0,2,0,2} = \cos^2\theta_2 \tag{F.21}$$

$$\lambda^{\langle r_2 \rangle}_{0,2,1,0} = \lambda^{\langle r_2 \rangle}_{0,2,0,1} = \lambda^{\langle r_2 \rangle}_{0,2,0,0} = 0. \tag{F.22}$$

For $n=3, m=0$

$$\lambda^{\langle r_2\rangle}_{3,0,3,0} = \cos^3\theta_2 \tag{F.23}$$

$$\lambda^{\langle r_2\rangle}_{3,0,2,1} = \frac{3}{2}\sin(2\theta_2)\cos\theta_2 K^{N_s,N_s}_{3,1} \tag{F.24}$$

$$\lambda^{\langle r_2\rangle}_{3,0,1,2} = \frac{3}{2}\sin(2\theta_2)\sin\theta_2 K^{N_s,N_s}_{3,1} \tag{F.25}$$

$$\lambda^{\langle r_2\rangle}_{3,0,0,3} = \sin^3\theta_2 \tag{F.26}$$

$$\lambda^{\langle r_2\rangle}_{3,0,1,0} = \tilde{C}^{N_s}_3\cos\theta_2\sin^2\theta_2 - \sin(2\theta_2)\sin\theta_2 K^{N_s,N_s}_{3,1}\tilde{C}^{N_s}_2 \tag{F.27}$$

$$\lambda^{\langle r_2\rangle}_{3,0,0,1} = \tilde{C}^{N_s}_3\sin\theta_2\cos^2\theta_2 - \sin(2\theta_2)\cos\theta_2 K^{N_s,N_s}_{3,1}\tilde{C}^{N_s}_2 \tag{F.28}$$

$$\lambda^{\langle r_2\rangle}_{3,0,2,0} = \lambda^{\langle r_2\rangle}_{3,0,1,1} = \lambda^{\langle r_2\rangle}_{3,0,0,2} = \lambda^{\langle r_2\rangle}_{3,0,0,0} = 0. \tag{F.29}$$

For $n=2, m=1$,

$$\lambda^{\langle r_2\rangle}_{2,1,3,0} = -\frac{1}{2}\sin(2\theta_2)\cos\theta_2 K^{N_s,N_s}_{1,3} \tag{F.30}$$

$$\lambda^{\langle r_2\rangle}_{2,1,2,1} = \cos(2\theta_2)\cos\theta_2 - \frac{1}{2}\sin(2\theta_2)\sin\theta_2 \tag{F.31}$$

$$\lambda^{\langle r_2\rangle}_{2,1,1,2} = \cos(2\theta_2)\sin\theta_2 + \frac{1}{2}\sin(2\theta_2)\cos\theta_2 \tag{F.32}$$

$$\lambda^{\langle r_2\rangle}_{2,1,0,3} = \frac{1}{2}\sin(2\theta_2)\sin\theta_2 K^{N_s,N_s}_{1,3} \tag{F.33}$$

$$\lambda^{\langle r_2\rangle}_{2,1,1,0} = -\left[\cos(2\theta_2)\sin\theta_2 + \sin\theta_2\right]\tilde{C}^{N_s}_2 + \frac{1}{2}\sin(2\theta_2)\cos\theta_2 K^{N_s,N_s}_{1,3}\tilde{C}^{N_s}_3 \tag{F.34}$$

$$\lambda^{\langle r_2\rangle}_{2,1,0,1} = -\left[\cos(2\theta_2)\cos\theta_2 - \cos\theta_2\right]\tilde{C}^{N_s}_2 - \frac{1}{2}\sin(2\theta_2)\sin\theta_2 K^{N_s,N_s}_{1,3}\tilde{C}^{N_s}_3 \tag{F.35}$$

$$\lambda^{\langle r_2\rangle}_{2,1,2,0} = \lambda^{\langle r_2\rangle}_{2,1,1,1} = \lambda^{\langle r_2\rangle}_{2,1,0,2} = \lambda^{\langle r_2\rangle}_{2,1,0,0} = 0. \tag{F.36}$$

And $n=1, m=2$,

$$\lambda^{\langle r_2\rangle}_{1,2,3,0} = \frac{1}{2}\sin(2\theta_2)\sin\theta_2 K^{N_s,N_s}_{1,3} \tag{F.37}$$

$$\lambda^{\langle r_2\rangle}_{1,2,2,1} = -\cos(2\theta_2)\sin\theta_2 - \frac{1}{2}\sin(2\theta_2)\cos\theta_2 \tag{F.38}$$

$$\lambda^{\langle r_2\rangle}_{1,2,1,2} = \cos(2\theta_2)\cos\theta_2 - \frac{1}{2}\sin(2\theta_2)\sin\theta_2 \tag{F.39}$$

$$\lambda^{\langle r_2\rangle}_{1,2,0,3} = \frac{1}{2}\sin(2\theta_2)\cos\theta_2 K^{N_s,N_s}_{1,3} \tag{F.40}$$

$$\lambda^{\langle r_2\rangle}_{1,2,1,0} = -\left[\cos(2\theta_2)\cos\theta_2 - \cos\theta_2\right]\tilde{C}^{N_s}_2 - \frac{1}{2}\sin(2\theta_2)\sin\theta_2 K^{N_s,N_s}_{1,3}\tilde{C}^{N_s}_3 \tag{F.41}$$

$$\lambda^{\langle r_2\rangle}_{1,2,0,1} = \left[\cos(2\theta_2)\sin\theta_2 + \sin\theta_2\right]\tilde{C}^{N_s}_2 - \frac{1}{2}\sin(2\theta_2)\cos\theta_2 K^{N_s,N_s}_{1,3}\tilde{C}^{N_s}_3 \tag{F.42}$$

$$\lambda^{\langle r_2\rangle}_{1,2,2,0} = \lambda^{\langle r_2\rangle}_{1,2,1,1} = \lambda^{\langle r_2\rangle}_{1,2,0,2} = \lambda^{\langle r_2\rangle}_{1,2,0,0} = 0. \tag{F.43}$$

When $n=0, m=3$, we get

$$\lambda^{\langle r_2\rangle}_{0,3,3,0} = -\sin^3\theta_2 \tag{F.44}$$

$$\lambda^{\langle r_2\rangle}_{0,3,2,1} = \frac{3}{2}\sin(2\theta_2)\sin\theta_2 K^{N_s,N_s}_{3,1} \tag{F.45}$$

$$\lambda^{\langle r_2\rangle}_{0,3,1,2} = -\frac{3}{2}\sin(2\theta_2)\cos\theta_2 K^{N_s,N_s}_{3,1} \tag{F.46}$$

$$\lambda^{\langle r_2\rangle}_{0,3,0,3} = \cos^3\theta_2 \tag{F.47}$$

$$\lambda^{\langle r_2\rangle}_{0,3,1,0} = \sin(2\theta_2)\cos\theta_2\left(-\frac{1}{2}\tilde{C}^{N_s}_3 + K^{N_s,N_s}_{3,1}\tilde{C}^{N_s}_2\right) \tag{F.48}$$

$$\lambda^{\langle r_2\rangle}_{0,3,0,1} = \sin(2\theta_2)\sin\theta_2\left(\frac{1}{2}\tilde{C}^{N_s}_3 - K^{N_s,N_s}_{3,1}\tilde{C}^{N_s}_2\right) \tag{F.49}$$

$$\lambda^{\langle r_2\rangle}_{0,3,2,0} = \lambda^{\langle r_2\rangle}_{0,3,1,1} = \lambda^{\langle r_2\rangle}_{0,3,0,2} = \lambda^{\langle r_2\rangle}_{0,3,0,0} = 0. \tag{F.50}$$

For $n=3, m=1$,

$$\lambda^{\langle r_2\rangle}_{3,1,4,0} = -\cos^3\theta_2\sin\theta_2 K^{N_s,N_s}_{1,4} \tag{F.51}$$

$$\lambda^{\langle r_2\rangle}_{3,1,3,1} = \cos(3\theta_2)\cos\theta_2 \tag{F.52}$$

$$\lambda^{\langle r_2\rangle}_{3,1,2,2} = \frac{3}{4}\sin(4\theta_2)K^{N_s,N_s}_{3,2} \tag{F.53}$$

$$\lambda^{\langle r_2\rangle}_{3,1,1,3} = \sin(3\theta_2)\sin\theta_2 \tag{F.54}$$

$$\lambda^{\langle r_2\rangle}_{3,1,0,4} = \sin^3\theta_2\cos\theta_2 K^{N_s,N_s}_{1,4} \tag{F.55}$$

$$\begin{aligned}\lambda^{\langle r_2\rangle}_{3,1,2,0} = {} & \cos^3\theta_2\sin\theta_2 K^{N_s,N_s}_{1,4}\tilde{C}^{N_s}_4 - \tilde{C}^{N_s}_3 K^{N_s,N_s}_{1,2}\sin^3\theta_2\cos\theta_2 \\ & + K^{N_s,N_s}_{3,2}\tilde{C}^{N_s}_2\sin(2\theta_2)\left[-\frac{3}{2}\cos^2\theta_2 + \sin^2\theta_2\right]\end{aligned} \tag{F.56}$$

$$\begin{aligned}\lambda^{\langle r_2\rangle}_{3,1,0,2} = {} & -\sin^3\theta_2\cos\theta_2 K^{N_s,N_s}_{1,4}\tilde{C}^{N_s}_4 + \tilde{C}^{N_s}_3 K^{N_s,N_s}_{1,2}\sin\theta_2\cos^3\theta_2 \\ & + K^{N_s,N_s}_{3,2}\tilde{C}^{N_s}_2\sin(2\theta_2)\left[\frac{3}{2}\sin^2\theta_2 - \cos^2\theta_2\right]\end{aligned} \tag{F.57}$$

$$\lambda^{\langle r_2\rangle}_{3,1,0,0} = \sin(4\theta_2)\left\{-\frac{1}{4}K^{N_s,N_s}_{1,2}\tilde{C}^{N_s}_2\tilde{C}^{N_s}_3 + \frac{1}{2}K^{N_s,N_s}_{3,2}(\tilde{C}^{N_s}_2)^2\right\} \tag{F.58}$$

$$\lambda^{\langle r_2\rangle}_{3,1,3,0} = \lambda^{\langle r_2\rangle}_{3,1,2,1} = \lambda^{\langle r_2\rangle}_{3,1,1,2} = \lambda^{\langle r_2\rangle}_{3,1,0,3} = \lambda^{\langle r_2\rangle}_{3,1,1,1} = \lambda^{\langle r_2\rangle}_{3,1,1,0} = \lambda^{\langle r_2\rangle}_{3,1,0,1} = 0. \tag{F.59}$$

For $n=1, m=3$,

$$\lambda^{\langle \mathrm{r}_2\rangle}_{1,3,4,0} = -\sin^3\theta_2\cos\theta_2 K^{N_s,N_s}_{1,4} \tag{F.60}$$

$$\lambda^{\langle \mathrm{r}_2\rangle}_{1,3,3,1} = \sin(3\theta_2)\sin\theta_2 \tag{F.61}$$

$$\lambda^{\langle \mathrm{r}_2\rangle}_{1,3,2,2} = -\frac{3}{4}K^{N_s,N_s}_{3,2}\sin(4\theta_2) \tag{F.62}$$

$$\lambda^{\langle \mathrm{r}_2\rangle}_{1,3,1,3} = \cos(3\theta_2)\cos\theta_2 \tag{F.63}$$

$$\lambda^{\langle \mathrm{r}_2\rangle}_{1,3,0,4} = \cos^3\theta_2\sin\theta_2 K^{N_s,N_s}_{1,4} \tag{F.64}$$

$$\begin{aligned}\lambda^{\langle \mathrm{r}_2\rangle}_{1,3,2,0} &= \sin^3\theta_2\cos\theta_2 K^{N_s,N_s}_{1,4}\tilde{C}^{N_s}_4 - \frac{1}{2}\tilde{C}^{N_s}_3 K^{N_s,N_s}_{1,2}\sin(2\theta_2)\cos^2\theta_2 \\ &\quad + K^{N_s,N_s}_{3,2}\tilde{C}^{N_s}_2\sin(2\theta_2)\left[-\frac{3}{2}\sin^2\theta_2+\cos^2\theta_2\right]\end{aligned} \tag{F.65}$$

$$\begin{aligned}\lambda^{\langle \mathrm{r}_2\rangle}_{1,3,0,2} &= -\cos^3\theta_2\sin\theta_2 K^{N_s,N_s}_{1,4}\tilde{C}^{N_s}_4 + \frac{1}{2}\sin(2\theta_2)\sin^2\theta_2\tilde{C}^{N_s}_3 \\ &\quad + K^{N_s,N_s}_{3,2}\tilde{C}^{N_s}_2\sin(2\theta_2)\left[\frac{3}{2}\cos^2\theta_2-\sin^2\theta_2\right]\end{aligned} \tag{F.66}$$

$$\lambda^{\langle \mathrm{r}_2\rangle}_{1,3,0,0} = \sin(4\theta_2)\left\{\frac{1}{4}K^{N_s,N_s}_{1,2}\tilde{C}^{N_s}_2\tilde{C}^{N_s}_3 - \frac{1}{2}K^{N_s,N_s}_{3,2}(\tilde{C}^{N_s}_2)^2\right\} \tag{F.67}$$

$$\lambda^{\langle \mathrm{r}_2\rangle}_{1,3,3,0} = \lambda^{\langle \mathrm{r}_2\rangle}_{1,3,2,1} = \lambda^{\langle \mathrm{r}_2\rangle}_{1,3,1,2} = \lambda^{\langle \mathrm{r}_2\rangle}_{1,3,0,3} = \lambda^{\langle \mathrm{r}_2\rangle}_{1,3,1,1} = \lambda^{\langle \mathrm{r}_2\rangle}_{1,3,1,0} = \lambda^{\langle \mathrm{r}_2\rangle}_{1,3,0,1} = 0. \tag{F.68}$$

From $(F.30-F.36)$, we have

$$\begin{aligned}I^{\langle \mathrm{r}_2,\,\mathrm{s},\,\mathrm{trs}\rangle}_{2,1} &= -\frac{1}{2}\sin(2\theta_2)\cos\theta_2 K^{N_s,N_s}_{1,3} I^{\langle \mathrm{s},\,\mathrm{trs}\rangle}_{3,0} \\ &\quad + \frac{1}{2}\sin(2\theta_2)\sin\theta_2 K^{N_s,N_s}_{1,3} I^{\langle \mathrm{s},\,\mathrm{trs}\rangle}_{0,3} \\ &\quad + \left\{\cos(2\theta_2)\cos\theta_2 - \frac{1}{2}\sin(2\theta_2)\sin\theta_2\right\} I^{\langle \mathrm{s},\,\mathrm{trs}\rangle}_{2,1} \\ &\quad + \left\{\cos(2\theta_2)\sin\theta_2 + \frac{1}{2}\sin(2\theta_2)\cos\theta_2\right\} I^{\langle \mathrm{s},\,\mathrm{trs}\rangle}_{1,2} \\ &\quad + \Big\{-[\cos(2\theta_2)\sin\theta_2+\sin\theta_2]\tilde{C}^{N_s}_2 \\ &\qquad + \frac{1}{2}\sin(2\theta_2)\cos\theta_2 K^{N_s,N_s}_{1,3}\tilde{C}^{N_s}_3\Big\} I^{\langle \mathrm{s},\,\mathrm{trs}\rangle}_{1,0} \\ &\quad - \Big\{[\cos(2\theta_2)\cos\theta_2-\cos\theta_2]\tilde{C}^{N_s}_2 \\ &\qquad + \frac{1}{2}\sin(2\theta_2)\sin\theta_2 K^{N_s,N_s}_{1,3}\tilde{C}^{N_s}_3\Big\} I^{\langle \mathrm{s},\,\mathrm{trs}\rangle}_{0,1}\end{aligned} \tag{F.69}$$

and from $(F.44-F.50)$ we get

$$\begin{aligned} I_{0,3}^{\langle \mathrm{r}_2,\,\mathrm{s},\,\mathrm{trs}\rangle} &= -\sin^3\theta_2 I_{3,0}^{\langle \mathrm{s},\,\mathrm{trs}\rangle} + \cos^3\theta_2 I_{0,3}^{\langle \mathrm{s},\,\mathrm{trs}\rangle} \\ &\quad + \frac{3}{2}\sin(2\theta_2)\sin\theta_2 K_{3,1}^{N_s,N_s} I_{2,1}^{\langle \mathrm{s},\,\mathrm{trs}\rangle} \\ &\quad - \frac{3}{2}\sin(2\theta_2)\cos\theta_2 K_{3,1}^{N_s,N_s} I_{1,2}^{\langle \mathrm{s},\,\mathrm{trs}\rangle} \\ &\quad + \left\{ \sin(2\theta_2)\cos\theta_2 \left[-\frac{1}{2}\tilde{C}_3^{N_s} + K_{3,1}^{N_s,N_s}\tilde{C}_2^{N_s} \right] \right\} I_{1,0}^{\langle \mathrm{s},\,\mathrm{trs}\rangle} \\ &\quad + \left\{ \sin(2\theta_2)\sin\theta_2 \left[\frac{1}{2}\tilde{C}_3^{N_s} - K_{3,1}^{N_s,N_s}\tilde{C}_2^{N_s} \right] \right\} I_{0,1}^{\langle \mathrm{s},\,\mathrm{trs}\rangle}. \end{aligned} \tag{F.70}$$

As $I_{1,0}^{\langle \mathrm{s},\,\mathrm{trs}\rangle} = I_{0,1}^{\langle \mathrm{s},\,\mathrm{trs}\rangle} = 0$, the expressions of $I_{2,1}^{\langle \mathrm{s},\,\mathrm{trs}\rangle}$ and $I_{0,3}^{\langle \mathrm{s},\,\mathrm{trs}\rangle}$ can be further simplified. We thus get

$$\begin{aligned} I_{2,1}^{\langle \mathrm{r}_2,\,\mathrm{s},\,\mathrm{trs}\rangle} &= -\frac{1}{2}\sin(2\theta_2)\cos\theta_2 K_{1,3}^{N_s,N_s} I_{3,0}^{\langle \mathrm{s},\,\mathrm{trs}\rangle} \\ &\quad + \frac{1}{2}\sin(2\theta_2)\sin\theta_2 K_{1,3}^{N_s,N_s} I_{0,3}^{\langle \mathrm{s},\,\mathrm{trs}\rangle} \\ &\quad + \left\{ \cos(2\theta_2)\cos\theta_2 - \frac{1}{2}\sin(2\theta_2)\sin\theta_2 \right\} I_{2,1}^{\langle \mathrm{s},\,\mathrm{trs}\rangle} \\ &\quad + \left\{ \cos(2\theta_2)\sin\theta_2 + \frac{1}{2}\sin(2\theta_2)\cos\theta_2 \right\} I_{1,2}^{\langle \mathrm{s},\,\mathrm{trs}\rangle} \end{aligned} \tag{F.71}$$

and

$$\begin{aligned} I_{0,3}^{\langle \mathrm{r}_2,\,\mathrm{s},\,\mathrm{trs}\rangle} &= -\sin^3\theta_2 I_{3,0}^{\langle \mathrm{s},\,\mathrm{trs}\rangle} + \cos^3\theta_2 I_{0,3}^{\langle \mathrm{s},\,\mathrm{trs}\rangle} \\ &\quad + \frac{3}{2}\sin(2\theta_2)\sin\theta_2 K_{3,1}^{N_s,N_s} I_{2,1}^{\langle \mathrm{s},\,\mathrm{trs}\rangle} \\ &\quad - \frac{3}{2}\sin(2\theta_2)\cos\theta_2 K_{3,1}^{N_s,N_s} I_{1,2}^{\langle \mathrm{s},\,\mathrm{trs}\rangle}. \end{aligned} \tag{F.72}$$

Similarly, by using $(F.51-F.59)$ and $(F.60-F.68)$, we get

$$\begin{aligned} I_{3,1}^{\langle \mathrm{r}_2,\,\mathrm{s},\,\mathrm{trs}\rangle} &= -\cos^3\theta_2\sin\theta_2 K_{1,4}^{N_s,N_s} I_{4,0}^{\langle \mathrm{s},\,\mathrm{trs}\rangle} + \sin^3\theta_2\cos\theta_2 K_{1,4}^{N_s,N_s} I_{0,4}^{\langle \mathrm{s},\,\mathrm{trs}\rangle} \\ &\quad + \cos(3\theta_2)\cos\theta_2 I_{3,1}^{\langle \mathrm{s},\,\mathrm{trs}\rangle} + \sin(3\theta_2)\sin\theta_2 I_{1,3}^{\langle \mathrm{s},\,\mathrm{trs}\rangle} \\ &\quad + \frac{3}{4}\sin(4\theta_2) K_{3,2}^{N_s,N_s} I_{2,2}^{\langle \mathrm{s},\,\mathrm{trs}\rangle} \\ &\quad + \Big\{ \cos^3\theta_2\sin\theta_2 K_{1,4}^{N_s,N_s}\tilde{C}_4^{N_s} - \tilde{C}_3^{N_s} K_{1,2}^{N_s,N_s}\sin^3\theta_2\cos\theta_2 \\ &\qquad + K_{3,2}^{N_s,N_s}\tilde{C}_2^{N_s}\sin(2\theta_2)\left[-\frac{3}{2}\cos^2\theta_2 + \sin^2\theta_2 \right] \Big\} I_{2,0}^{\langle \mathrm{s},\,\mathrm{trs}\rangle} \\ &\quad + \Big\{ -\sin^3\theta_2\cos\theta_2 K_{1,4}^{N_s,N_s}\tilde{C}_4^{N_s} + \tilde{C}_3^{N_s} K_{1,2}^{N_s,N_s}\sin\theta_2\cos^3\theta_2 \\ &\qquad + K_{3,2}^{N_s,N_s}\tilde{C}_2^{N_s}\sin(2\theta_2)\left[\frac{3}{2}\sin^2\theta_2 - \cos^2\theta_2 \right] \Big\} I_{0,2}^{\langle \mathrm{s},\,\mathrm{trs}\rangle} \\ &\quad + \sin(4\theta_2)\left\{ -\frac{1}{4} K_{1,2}^{N_s,N_s}\tilde{C}_2^{N_s}\tilde{C}_3^{N_s} + \frac{1}{2} K_{3,2}^{N_s,N_s}(\tilde{C}_2^{N_s})^2 \right\} I_{0,0}^{\langle \mathrm{s},\,\mathrm{trs}\rangle} \end{aligned} \tag{F.73}$$

and

$$
\begin{aligned}
I_{1,3}^{\langle \mathrm{r}_2,\,\mathrm{s},\,\mathrm{trs}\rangle} \;=\;& -\sin^3\theta_2\cos\theta_2 K_{1,4}^{N_s,N_s} I_{4,0}^{\langle \mathrm{s},\,\mathrm{trs}\rangle} + \cos^3\theta_2\sin\theta_2 K_{1,4}^{N_s,N_s} I_{0,4}^{\langle \mathrm{s},\,\mathrm{trs}\rangle} \\
& + \sin(3\theta_2)\sin\theta_2 I_{3,1}^{\langle \mathrm{s},\,\mathrm{trs}\rangle} + \cos(3\theta_2)\cos\theta_2 I_{1,3}^{\langle \mathrm{s},\,\mathrm{trs}\rangle} \\
& - \frac{3}{4} K_{3,2}^{N_s,N_s}\sin(4\theta_2) I_{2,2}^{\langle \mathrm{s},\,\mathrm{trs}\rangle} \\
& + \left\{ \sin^3\theta_2\cos\theta_2 K_{1,4}^{N_s,N_s}\tilde{C}_4^{N_s} - \frac{1}{2}\tilde{C}_3^{N_s} K_{1,2}^{N_s,N_s}\sin(2\theta_2)\cos^2\theta_2 \right. \\
& \qquad \left. + K_{3,2}^{N_s,N_s}\tilde{C}_2^{N_s}\sin(2\theta_2)\left[-\frac{3}{2}\sin^2\theta_2 + \cos^2\theta_2 \right] \right\} I_{2,0}^{\langle \mathrm{s},\,\mathrm{trs}\rangle} \\
& + \left\{ -\cos^3\theta_2\sin\theta_2 K_{1,4}^{N_s,N_s}\tilde{C}_4^{N_s} + \frac{1}{2}\sin(2\theta_2)\sin^2\theta_2 K_{1,2}^{N_s,N_s}\tilde{C}_3^{N_s} \right. \\
& \qquad \left. + K_{3,2}^{N_s,N_s}\tilde{C}_2^{N_s}\sin(2\theta_2)\left[\frac{3}{2}\cos^2\theta_2 - \sin^2\theta_2 \right] \right\} I_{0,2}^{\langle \mathrm{s},\,\mathrm{trs}\rangle} \\
& + \sin(4\theta_2)\left\{ \frac{1}{4} K_{1,2}^{N_s,N_s}\tilde{C}_2^{N_s}\tilde{C}_3^{N_s} - \frac{1}{2} K_{3,2}^{N_s,N_s}(\tilde{C}_2^{N_s})^2 \right\} I_{0,0}^{\langle \mathrm{s},\,\mathrm{trs}\rangle}. \qquad \text{(F.74)}
\end{aligned}
$$

REFERENCES

Abu-Mostafa, Y., & Psaltis, D. (1985). Image normalization by complex moments. *IEEE Transaction Pattern Analisys and Machine Intelligence*, *7*(1), 46–55.

Andrews, G., Askey, R., & Roy, R. (2004). *Special functions*. Cambridge university press.

Arfken, G. (1985). Gram-schmidt orthogonalization. *Mathematical Methods for Physicists*, *3*, 516–520.

Belkasim, S. O. (1991). Pattern recognition with moment invariants – a comparative study and new results. *Pattern Recognition*, *24*(12), 1117–1138.

Boser, B. E., Guyon, I., & V., V. (1992). A training algorithm for optimal margin classifier. In *Proceedings of the fifth annual workshop on computational learning theory* (pp. 144–152). ACM Press.

Chang, C.-C., & Lin, C.-J. (2011). LIBSVM: A library for support vector machines. *ACM Transactions on Intelligent Systems and Technology*, *2*, 27:1–27:27. (Software available at `http://www.csie.ntu.edu.tw/~cjlin/libsvm`)

Chebyshev, P. (1864). Sur l'interpolation. *Zapiski Akademii Nauk 4 Oeuvres*, *1*, 539-560.

Chebyshev, P. (1907). Sur l'interpolation des valeurs équidistants. *Markoff, A.; Sonin, N., Oeuvres de P. L. Tchebychef*, *2*, 219-242. (Reprinted by Chelsea)

Chong, C.-W., Raveendran, P., & Mukundan, R. (2004). Translation and scale invariants of Legendre moments. *Pattern recognition*, *37*, 119-129.

Comtet, L. (1974). *Advanced combinatorics: the art of finite and infinite expansions*. D. Reidel.

Cortes, C., & Vapnik, V. (1995). Support-vector networks. *Machine learning*, *20*(3), 273–297.

Dudani, S. A., Breeding, K. J., & McGhee, R. B. (1977, jan.). Aircraft identification by moment invariants. *Computers, IEEE Transactions on*, *C-26*(1), 39 -46.

Erdelyi, A., Magnus, W., Oberhettinger, F. G., & Tricomi, F. G. (1953). *Higher transcendental functions* (Vol. 2). McGraw-Hill.

Flusser, J. (2000). On the independence of rotation moment invariants. *Pattern Recognition*, *33*(9), 1405–1410.

Flusser, J. (2002). On the inverse problem of rotation moment invariants. *Pattern Recognition*, *35*(12), 3015.

Flusser, J. (2007). Moment invariants in image analysis. In (pp. 878–883). World Academy of Science, Engineering and Technology.

Flusser, J., & Suk, T. (1993). Pattern recognition by affine moment invariants. *Pattern Recognition*, *26*(1), 167 - 174.

Flusser, J., & Suk, T. (1994a). Affine moment invariants: a new tool for character recognition. *Pattern Recognition Letters*, *15*(4), 433 - 436.

Flusser, J., & Suk, T. (1994b, mar). A moment-based approach to registration of images with affine geometric distortion. *Geoscience and Remote Sensing, IEEE Transactions on*, *32*(2), 382 -387. doi: 10.1109/36.295052

Flusser, J., Suk, T., & Zitová, B. (2009). *Moments and moment invariants in pattern recognition*. John Wiley and Son.

Goh, H.-A., Chong, C.-W., Rosli, B., Fazli, S. A., & Sim, K.-S. (2009). Translation and scale invariants of Hahn moments. *International Journal of Image and Graphics*, *9*(2), 271-285.

Goshtasby, A. (1985, may). Template matching in rotated images. *Pattern Analysis and Machine Intelligence, IEEE Transactions on*, *PAMI-7*(3), 338 -344. doi: 10.1109/TPAMI.1985.4767663

Gram, J. (1883). Ueber die entwickelung reeller functionen in reihen mittelst der methode der kleinsten quadrate. *Journal für die reine und angewandte Mathematik*, 41–73.

Hahn, W. (1949). Über orthogonalpolynome, die q-differenzengleichungen genügen. *Mathematische Nachrichten*, *2*(1-2), 4–34.

Hilbert, D., & Sturmfels, B. (1993). *Theory of algebraic invariants*. Cambridge Univ Pr.

Hsu, H.-S., & Tsai, W.-H. (1993). Moment preserving edge detection and its application to image data compression. *Optical engineering*, *32*(7), 1596–1608.

Hu, M.-K. (1962). Visual pattern recognition by moment invariants. *IRE Transactions on Information Theory*, *8*(2), 179–187.

Johnson, R., & Wichern, D. (2002). *Applied multivariate statistical analysis* (Vol. 5). Prentice hall Upper Saddle River, NJ.

Khotanzad, A., & Hong, Y. (1990, may). Invariant image recognition by zernike moments. *Pattern Analysis and Machine Intelligence, IEEE Transactions on*, *12*(5), 489 -497. doi: 10.1109/34.55109

Khotanzad, A., & Yaw, H. (1990). Invariant image recognition by Zernike moments. *IEEE Transactions on Pattern Analysis and Machine Intelligence*, *12*(5), 489–497.

Kimia, B. (n.d.). *Large database of closed binary shapes collected by the lems vision group at brown university.* (Images available at `http://www.lems.brown.edu/~dmc/`)

Koekoek, R., & Swarttouw, R. F. (1998). *The askey-scheme of hypergeometric orthogonal polynomials and its q-analogue* (Report 98–17). faculty of Technical mathematics and Informatics, Delft University of Technology.

Koepf, W. (1998). *Hypergeometric summation*. Vieweg Braunschweig/Wiesbaden.

Krawtchouk, M. (1929a). On interpolation by means of orthogonal polynomials. *Memoirs Agricultural Inst. Kyiv*, *4*, 21–28.

Krawtchouk, M. (1929b). Sur une généralisation des polynomes d'hermite. *Comptes Rendus de l'Académie des Sciences*, *189*, 620–622.

Li, Y. (1992). Reforming the theory of invariant moments for pattern recognition. *Pattern Recognition*, *25*(7), 723 - 730.

Liao, S., & Lu, Q. (1997, aug). A study of moment functions and its use in chinese character recognition. In *Document analysis and recognition, 1997., proceedings of the fourth international conference on* (Vol. 2, p. 572 -575 vol.2). doi: 10.1109/ICDAR.1997.620566

Liu, Q., Zhu, H., & Li, Q. (2011). Image recognition by affine Tchebichef moment invariants. *Artificial Intelligence and Computational Intelligence Lecture Notes in Computer Science*, *7004/2011*, 472–480.

McLachlan, G., & Wiley, J. (1992). *Discriminant analysis and statistical pattern recognition* (Vol. 5). Wiley Online Library.

Mukundan, R. (2004). Some computation aspect of discrete orthogonal moments. *IEEE Transactions on Image Processing*, *13*(8), 1055–1059.

Mukundan, R., Ong, S. H., & Lee, P. A. (2001). Image analysis by Tchebichef moments. *IEEE Transactions on Image Processing*, *10*(9), 1357–1364.

Mukundan, R., & Ramakrishnan, K. R. (1998). *Moment functions in image analysis – theory and applications*. World Scientific.

Nikiforov, A., Suslov, S., & Uvarov, V. (1991). *Classical orthogonal polynomials of a discrete variable* (Vol. 19). Springer-Verlag Berlin.

Palaniappan, R., Raveendran, P., & Omatu, S. (2000). New invariant moments for non-uniformly scaled images. *Pattern Analysis and Applications*, *3*(2), 78–87.

Pan, F., & Keane, M. (1994). A new set of moment invariants for handwritten numeral recognition. In *International Conference on Image Processing* (pp. 154–158).

Pei, S.-C., & Lin, C.-N. (1995). Image normalization for pattern recognition. *Image and Vision Computing*, *13*(10), 711–723.

Prokop, R., & Reeves, A. P. (1992). A survey of moment based techniques for unocclued object representation. *Graphical Models and Image Processing-CVGIP*, *54*(5), 438–460.

Reiss, T. (1991, aug). The revised fundamental theorem of moment invariants. *Pattern Analysis and Machine Intelligence, IEEE Transactions on*, *13*(8), 830 -834.

Rothe, I., Susse, H., & Voss, K. (1996, apr). The method of normalization to determine invariants. *Pattern Analysis and Machine Intelligence, IEEE Transactions on*, *18*(4), 366–376.

Shen, D., & Ip, H. (1997, may). Generalized affine invariant image normalization. *Pattern Analysis and Machine Intelligence, IEEE Transactions on*, *19*(5), 431–440.

Szegö, G. (1939). *Orthogonal polynomials* (Vol. 23). Amer Mathematical Society.

Teague, M. R. (1980, Aug). Image analysis via the general theory of moments∗. *J. Opt. Soc. Am.*, *70*(8), 920–930.

Teh, C.-H., & Chin, R. (1988). On image analysis by the methods of moments. *IEEE Transactions on Pattern Analysis and Machine Intelligence*, *10*(4), 496–513.

Vapnik, V. (1995). *The nature of statistical learning theory*. Springer.

Webb, A., Copsey, K., & Cawley, G. (2011). *Statistical pattern recognition*. Wiley.

Wong, R. Y., & Hall, E. L. (1978). Scene matching with invariant moments. *Computer Graphics and Image Processing*, *8*(1), 16 - 24.

Wong, W.-H., Siu, W.-C., & Lam, K.-M. (1995). Generation of moment invariants and their uses for character recognition. *Pattern Recognition Letters*, *16*(2), 115 - 123.

Yap, P. T. (2006). *Moments-based pattern analysis: theory and applications*. Unpublished doctoral dissertation, University of Malaya.

Yap, P.-T., Raveendran, P., & Ong, S.-H. (2003). Image analysis by Krawtchouk moments. *IEEE Transactions on Image Processing*, *12*(11), 1367–1377.

Yap, P.-T., Raveendran, P., & Ong, S.-H. (2007). Image analysis by Hahn moments. *IEEE Transactions on Pattern Analysis and Machine Intelligence*, *29*(11), 2057–2062.

Zhang, H., Dai, X., Sun, P., Zhu, H., & Shu, H. (2010). Symmetric image recognition by Tchebichef moment invariants. In *Proceedings of 2010 IEEE 17th International Conference on Image Processing* (pp. 2273–2276). Hong Kong, China.

Zhang, H., Guo, J., Chen, G., & Li, C. (2009). HCL2000—-A large-scale handwritten Chinese character database for handwritten character recognition. In *2009, 10th international conference on document analysis and recognition* (pp. 287–290).

Zhang, H., Shu, H., Coatrieux, G., Zhu, J., Wu, Q. J., Zhang, Y., ... Luo, L. (2011). Affine Legendre moment invariants for image watermarking robust to geometric distortions. *IEEE Transactions on Image Processing*, *20*(8), 2189–2199.

Zhang, Y., Wen, C., Zhang, Y., & Soh, Y. C. (2003). On the choice of consistent canonical form during moment normalization. *Pattern Recognition Letters*, *24*(16), 3205–3215.

Zhu, H., Shu, H., Liang, J., Luo, L., & Coatrieux, J.-L. (2007a). Image analysis by discrete orthogonal racah moments. *Signal Processing*, *87*(4), 687 - 708.

Zhu, H., Shu, H., Zhou, J., Luo, L., & Coatrieux, J. (2007b). Image analysis by discrete orthogonal dual hahn moments. *Pattern Recognition Letters*, *28*(13), 1688 - 1704.

Zhu, H., Xia, T., Luo, L., & Coatrieux, J. (2007c). Translation and scale invariants of Tchebichef moments. *Pattern Recognition*, *40*(9), 2530–2542.

Zvolanek, B. (1981, January). Autonomous ship classification by moment invariants. In W. H. Carter (Ed.), *Society of photo-optical instrumentation engineers (spie) conference series* (Vol. 292, p. 241).